

**DEVELOPMENT OF MAGNETIC GREEN ADSORBENTS
USING BIO-WASTE MATERIALS FOR THE REMOVAL
OF POLLUTANTS FROM AQUEOUS SOLUTIONS**

Thesis Submitted for the Award of the Degree of

DOCTOR OF PHILOSOPHY
in
Environmental Sciences

By
RIMZIM

Registration Number: 12021185

Supervised By
Dr. Harminder Singh (11839)
Department of Chemistry (Professor)
Lovely Professional University



L OVELY
P ROFESSIONAL
U NIVERSITY

Transforming Education Transforming India

LOVELY PROFESSIONAL UNIVERSITY, PUNJAB
2024

DECLARATION

I, hereby declared that the presented work in the thesis entitled “**Development of magnetic green adsorbents using bio-waste materials for the removal of pollutants from aqueous solutions**” in fulfilment of degree of **Doctor of Philosophy (Ph.D.)** is outcome of research work carried out by me under the supervision of Dr. Harminder Singh, working as Professor in the School of Chemical Engineering and Physical Sciences, Lovely Professional University, Punjab, India. In keeping with general practice of reporting scientific observations, due acknowledgements have been made whenever work described here has been based on findings of other investigator. This work has not been submitted in part or full to any other University or Institute for the award of any degree.

(Signature of Scholar)

Name of the scholar: Rimzim

Registration No.: 12021185

Department of Chemistry

School of Chemical Engineering and Physical Sciences

Lovely Professional University,

Punjab, India

CERTIFICATE

This is to certify that the work reported in the Ph. D. thesis entitled “**Development of magnetic green adsorbents using bio-waste materials for the removal of pollutants from aqueous solutions**” submitted in fulfillment of the requirement for the award of degree of **Doctor of Philosophy (Ph.D.)** in the Department of Chemistry, School of Chemical Engineering and Physical Sciences is a research work carried out by **RIMZIM** (12021185), is bonafide record of her original work carried out under my supervision and that no part of thesis has been submitted for any other degree, diploma or equivalent course.

(Signature of Supervisor)

Name of supervisor: Dr. Harminder Singh (Professor)

School of Chemical Engineering and Physical Sciences

Lovely Professional University, Phagwara

Punjab, India

ACKNOWLEDGEMENT

I am deeply grateful to almighty God and my heavenly grandparents **Sh. Gandharb Singh, Smt. Satya Devi** and **Sh. Raghubir Singh** for their immense blessings. I am thankful to my grandmother **Smt. Sudesh Rani** for her inseparable love and prayers.

I wish to express my sincere appreciation and gratitude to my research advisor, **Dr. Harminder Singh** (Professor), Lovely Professional University, Phagwara (Punjab) for their constant guidance, support and encouragement throughout this work.

My parents **Mr. Ravi Singh** and **Mrs. Nandni Jasrotia** deserve special thanks and gratitude for their constant motivation and encouragement. I would like to express deep appreciation to my family as they all are the greatest blessing in my life. I would also like to thank my seniors, research fellows and Lab Technician at Lovely Professional University for their cooperation and helpfulness during this work. Last, but not the least, a special gratitude to my brother, **Mr. Pushap Jasrotia** and my sister-in-law, **Mrs. Shivani**. This work could not have been a success without their incessant moral support.

ABSTRACT

Water serves as the basis of life on Earth, vital for all living organisms and a critical asset for human society. Ensuring access to clean and affordable water stands among the fundamental objectives, yet it remains a tough global challenge. The issue of environmental contamination especially regarding water pollution has long been a matter of public concern. Addressing this issue demands the removal of pollutants from different water sources to enhance their quality. Among the pollutants persisting in polluted water are heavy metals, inorganic compounds and organic dyes which entered into the environment through untreated sewage, hazardous industrial discharges, the disposal of effluents from various industrial and the agricultural runoff into water bodies. Presently, numerous developing nations confront the persistent issue of water contamination. Various methods including physico-chemical and bioremedial measures have been applied to remove different pollutants from wastewater. Among various techniques, the adsorption method stands out as a promising physical approach for the treatment of wastewater containing organic and inorganic contaminants because of certain advantages like cost-effectiveness, ease of handling and good efficiency. Adsorbents are classified into two categories: natural and synthetic. Natural adsorbents are economically viable, abundantly available and exhibit considerable potential for removing both inorganic and organic pollutants from wastewater. However, traditional adsorbents have demonstrated limited effectiveness in removing hazardous contaminants from wastewater due to their low adsorption capacities. Consequently, various synthetic adsorbents have been studied to address this limitation. Over the past two decades, synthetic adsorbents have been extensively synthesized from a variety of industrial and agricultural waste materials to effectively remove diverse pollutants from contaminated water sources.

In recent times, there has been a growing interest in the application of nano materials and their composites for wastewater treatment. These materials possess distinctive size, shape and physiochemical properties that facilitate the removal of impurities from water. Amongst several nano-materials, magnetic nano ferrites along with their synthesised composites have garnered significant attention in wastewater treatment. Nano ferrites exhibit remarkable magnetic properties, allowing easy removal by applying an external magnetic field from water after its treatment. However, despite their effectiveness as adsorbents, nano ferrites are prone to short-term performance issues and low stability in an aqueous solution. To address these drawbacks, magnetic ferrites are being modified

with different materials which has emerged as a crucial strategy to enhance their stability against oxidization and aggregation. Moreover, the modification of surface increases the possibility of surface functionalization, thereby improving their capacity of adsorption as well as selectivity towards target pollutant. Among the various types of surfactants, polymers etc. bio-waste modified spinel ferrites have gained significance owing to their unique properties like non-toxicity, cost-effectiveness and higher adsorption capacity for treating wastewater. Consequently, in the present study, bio-wastes such as pine cone, walnut shell and pistachio shell have been employed to alter the surface properties of nano ferrites. These modified ferrites were then utilized to adsorb different dyes and Cu(II) metal ion from waste water. The review of literature suggests that among the various synthesis methods, the low temperature combustion method stands out as a simple, time efficient and cost effective approach for synthesizing nano metal ferrites. So, in this research study, magnetic ferrites have been synthesized using low combustion method and their composites have been prepared using low cost bio-waste materials viz. pine cone, walnut shell and pistachio shell under ambient environmental conditions.

The surface characteristics of the magnetic ferrites and their bio-waste based composites were assessed using Fourier Transform Infrared (FTIR) spectroscopy while their crystallite size was examined by X-ray Diffraction (XRD). The morphological structure was determined using Scanning Electron Microscopy (SEM) and elemental composition was determined by Energy Dispersive Spectroscopy (EDS). The surface area was analysed by the Brunauer-Emmett-Teller (BET) technique. The thermal stability of material was evaluated through Thermogravimetric Analysis (TGA) while the pH of point zero charge (pH_{pzc}) was calculated to assess the pH at which there is net zero charge on the surface of the material. The FTIR spectra of various metal ferrites and their bio-waste based composites indicated successful attachment of the bio-wastes onto the surfaces of metal ferrites. X-ray Diffraction spectra confirmed the phase purity and spinel character of the prepared metal ferrites which was also found in the metal ferrite bio-waste composites despite their surface modification. The average crystallite size of metal ferrites varied from 20 to 40 nm, whereas for the bio-waste composites, it increased from 30 to 60 nm. SEM analysis revealed that the pure metal ferrites exhibit granular structure and varied particle size while the bio-wastes showed a rough, flaky structure. The composites exhibit uneven surface with ferrites attached on the surface. EDS analysis revealed the elemental composition of the metal ferrites before and after surface

modification, showing a rise in the carbon content and a decline in other elemental constituents in the metal ferrite bio-waste composites compared to the simple metal ferrites. BET analysis revealed that the specific surface area of pure metal ferrites ranged from 0.4 to 2 m²/g, while for the metal ferrite bio-waste composites, it increased from 1 to 4 m²/g, confirming the attachment of the bio-wastes onto the surfaces of the metal ferrites. TGA analysis revealed the thermal stability of different bio-waste composites. pH point zero charge analysis showed that the calculated pH_{pzc} values for the bio-waste based metal ferrites composites ranged from 5.5 to 7.5.

The adsorption behavior of various magnetic ferrite bio-waste composites was studied for inorganic metal ions and organic dyes using batch adsorption method. Preliminary studies were conducted to determine the most suitable magnetic ferrite bio-waste composites, which were then selected for further analysis of their adsorption behavior towards selected dyes in single, binary, ternary systems and metal ions. Therefore, the adsorption studies demonstrated the specificity of different magnetic composites towards particular types of dyes and Cu(II) metal ion in aqueous solution. Analysis of the adsorption data obtained from kinetic and thermodynamic equilibrium studies revealed that the magnetic bio-waste composites serve as effective materials for removing various cationic dyes from different dye systems and Cu(II) metal ion. Additionally, the adsorption kinetic studies affirmed that the Pseudo second order model fitted best for the removal of cationic dyes (in single, binary, ternary systems) and Cu(II) metal ions by using various magnetic ferrite bio-waste composites followed the. These findings indicated chemical nature of adsorption process for the adsorption of various cationic dyes and Cu(II) metal ion. The adsorption behavior of different dyes and Cu(II) ion was studied by changing the pH values between 3 and 11 and adsorbent dosage from 0.1 - 0.5 g. Optimal removal percentages were observed at pH 6-7 for dyes and pH 7 for Cu(II) metal ion. Furthermore, the adsorption behavior of prepared composites was assessed at varying concentrations ranging from 50 to 250 mg/L (single dye system) and 20 to 100 mg/L (binary and ternary dye system). It was observed that adsorption capacity (Q_e) of cationic dyes and Cu(II) ion increased as the concentration of adsorbate increased in single, binary and ternary system. The effect of concentration was determined at three distinct temperatures which were 25°C, 30°C and 35°C. Results from the temperature study revealed the endothermic nature of adsorption process. Different isotherm models including Langmuir, Freundlich, Temkin and Dubinin-Radushkevich (D-R) model were employed to analyse the

adsorption equilibrium behavior of different magnetic composites in both single as well as multi-component systems. The findings indicated that among the different isotherm models, the equilibrium data for various dyes was best described by the Langmuir model which suggests that the surface of various magnetic ferrite bio-waste composites contain uniform active sites and Cu(II) ion fitted best with Freundlich model. The cationic dyes form a monolayer on the surface of the magnetic composites. Regenerating nano ferrites based bio-waste composites post-adsorption is crucial in assessing the performance of the material. The effectiveness of the adsorbent after recycling process is the primary factor in determining its cost efficiency. Hence, the regeneration capabilities of various metal ferrite bio-waste composites were individually studied in different systems over five to six successive cycles. The calculated data clearly demonstrates that even after five to six adsorption-desorption cycles, the magnetic ferrite bio-waste composites still maintained a good regeneration efficiency. These findings highlighted the favourable reusability of the metal ferrite bio-waste composites, yielding notable outcomes. In summary, the study suggests that magnetic bio-waste composites are environmentally friendly, highly selective and cost-effective in nature. They could serve as viable alternatives for removing various dyes and metal ions from wastewater.

TABLE OF CONTENTS

TITLE	PAGE
Declaration	i
Certificate	ii
Acknowledgement	iii
Abstract	iv-vii
Table of Contents	viii-xiii
List of Figures	xiv-xix
List of Tables	xx-xxii
Frequently used Acronyms and their expanded forms	xxiii-xxiv

S. No.	CONTENT	PAGE
CHAPTER 1: INTRODUCTION		
1.1.	General Introduction	1
1.2.	Target Pollutants	2
1.2.1.	Dyes	2
1.2.1.1.	Effect of Dyes	3
1.2.2.	Heavy Metals	4
1.2.2.1.	Effect of Heavy Metals	4
1.3.	Methods for Wastewater Treatment	6
1.4.	Adsorption	7
1.5.	Types of Adsorbent	7
CHAPTER 2: REVIEW OF LITERATURE		
2.1.	Nanomaterials in Adsorption	9
2.1.1.	Nano Ferrite: A Magnetic Material	10
2.1.2.	Synthesis Method and Adsorption Behavior of Metal Ferrite	11
2.1.2.1.	Synthesis Method	11
2.1.2.2.	Adsorption Behavior of Metal Ferrite	13
2.2.	Surface Modification of Metal Ferrites	14
2.2.1.	Deposition of Metal and their Oxide	14

S. No.	CONTENT	PAGE
2.2.2.	Surfactant Treatment/Coating	15
2.2.3.	Polymer Treatment/Coating	16
2.3.	Adsorption Behaviour	18
2.4.	Regeneration	24
2.5.	Need for the Study	26
2.6.	Objectives of the Research Work	26
CHAPTER 3: MATERIALS AND METHODS		
3.1.	Materials Used	28
3.2.	Experimental Method	28
3.2.1.	Synthesis of Metal Ferrite Nanoparticles using Combustion Method	28
3.3.	Surface Modification of Spinel Metal Ferrites with Bio-Waste	29
3.3.1.	Surface Modification with Pine Cone/Walnut Shell/Pistachio Shell	29
3.4.	Preliminary Adsorption Studies	30
3.4.1.	With Dyes	31
3.4.2.	With Metal Ions	33
3.5.	Characterization of Metal Ferrites and their Composites	34
3.5.1.	Fourier Transform Infrared (FTIR) Analysis	34
3.5.2.	X-Ray Diffraction (XRD) Analysis	35
3.5.3.	Scanning Electron Microscope (SEM) Analysis	35
3.5.4.	Energy Dispersive Spectra (EDS) Analysis	36
3.5.5.	Brunauer-Emmett-Teller (BET) Analysis	36
3.5.6.	Thermogravimetric Analysis (TGA)	36
3.5.7.	pH of Point Zero Charge (pH_{pzc}) Analysis	37
3.6.	Batch Adsorption Studies	37
3.7.	Single, Binary and Ternary Dye System	38
3.7.1.	Single Dye System	38
3.7.2.	Binary Dye System	38
3.7.3.	Ternary Dye System	39

S. No.	CONTENT	PAGE
3.8.	Metal Ion System	39
3.8.1.	Solution Preparation for Heavy Metal Ion	40
3.9.	Regeneration Study of the Adsorbent	40
3.10.	Adsorption Kinetics	41
3.10.1.	Pseudo First Order Model	41
3.10.2.	Pseudo Second Order Model	42
3.10.3.	Elovich Model	42
3.10.4.	Weber-Morris Model	43
3.11.	Adsorption Isotherms	43
3.11.1.	Langmuir Isotherm	43
3.11.2.	Freundlich Isotherm	44
3.11.3.	Temkin Isotherm	44
3.11.4.	Dubinin-Radushkevich (D-R) Isotherm	45
3.11.5.	Adsorption Energy (E)	45
3.11.6.	Separation Factor	46
3.12.	Adsorption Thermodynamics	46
CHAPTER 4: RESULTS AND DISCUSSION		
<u>PART-I</u>		
(Dyes Adsorption using bio-waste metal ferrite composite)		
4.1.	Zinc Ferrite Pine Cone (ZFPC) Composite	48
4.1.1.	Characterization and Morphology	48
4.1.1.1.	Fourier Transform Infrared Spectroscopy	48
4.1.1.2.	X-Ray Diffraction	50
4.1.1.3.	Field Emission Scanning Electron Microscope	51
4.1.1.4.	Energy Dispersive Spectra	51
4.1.1.5.	Thermogravimetric Analysis	53
4.1.1.6.	Brunauer-Emmett-Teller Analysis	53
4.1.1.7.	pH of Point Zero Charge Analysis	54
4.1.2.	Adsorption Study in Single and Ternary Dye System	55
4.1.2.1.	Effect of Contact Time	55
4.1.2.2.	Adsorption Kinetics	57

S. No.	CONTENT	PAGE
4.1.2.3.	Effect of pH	60
4.1.2.4.	Effect of Adsorbent Dosage	60
4.1.2.5.	Effect of Concentration and Temperature	62
4.1.2.6.	Adsorption Isotherms	63
4.1.2.7.	Adsorption Thermodynamics	68
4.1.3.	Regeneration of Adsorbent	70
4.2.	Nickel Ferrite Pine Cone (NFPC) Composite	72
4.2.1.	Characterization and Morphology	72
4.2.1.1.	Fourier Transform Infrared Spectroscopy	72
4.2.1.2.	X-Ray Diffraction	73
4.2.1.3.	Field Emission Scanning Electron Microscope	73
4.2.1.4.	Energy Dispersive Spectra	75
4.2.1.5.	Thermogravimetric Analysis	76
4.2.1.6.	Brunauer-Emmett-Teller Analysis	77
4.2.1.7.	pH of Point Zero Charge Analysis	77
4.2.2.	Adsorption Study in Single and Binary Dye System	78
4.2.2.1.	Effect of Contact Time	78
4.2.2.2.	Adsorption Kinetics	80
4.2.2.3.	Effect of pH	82
4.2.2.4.	Effect of Adsorbent Dosage	83
4.2.2.5.	Effect of Concentration and Temperature	84
4.2.2.6.	Adsorption Isotherms	86
4.2.2.7.	Adsorption Thermodynamics	89
4.2.3.	Regeneration of Adsorbent	91
4.3.	Walnut Shell Zinc Ferrite (WSZF) Composite	93
4.3.1.	Characterization and Morphology	93
4.3.1.1.	Fourier Transform Infrared Spectroscopy	93
4.3.1.2.	X-Ray Diffraction	94
4.3.1.3.	Field Emission Scanning Electron Microscope	95
4.3.1.4.	Energy Dispersive Spectra	96
4.3.1.5.	Thermogravimetric Analysis	97

S. No.	CONTENT	PAGE
4.3.1.6.	Brunauer-Emmett-Teller Analysis	98
4.3.1.7.	pH of Point Zero Charge Analysis	98
4.3.2.	Adsorption Study in Single and Binary Dye System	99
4.3.2.1.	Effect of Contact Time	99
4.3.2.2.	Adsorption Kinetics	101
4.3.2.3.	Effect of pH	104
4.3.2.4.	Effect of Adsorbent Dosage	104
4.3.2.5.	Effect of Concentration and Temperature	105
4.3.2.6.	Adsorption Isotherms	107
4.3.2.7.	Adsorption Thermodynamics	110
4.3.3.	Regeneration of Adsorbent	112
4.4.	Walnut Shell Cobalt Ferrite (WScoF) Composite	114
4.4.1.	Characterization and Morphology	114
4.4.1.1.	Fourier Transform Infrared Spectroscopy	114
4.4.1.2.	X-Ray Diffraction	115
4.4.1.3.	Field Emission Scanning Electron Microscopy	115
4.4.1.4.	Energy Dispersive Spectra	117
4.4.1.5.	Thermogravimetric Analysis	118
4.4.1.6.	Brunauer-Emmett-Teller Analysis	119
4.4.1.7.	pH of Point Zero Charge Analysis	119
4.4.2.	Adsorption Study in Single and Ternary Dye System	120
4.4.2.1.	Effect of Contact Time	120
4.4.2.2.	Adsorption Kinetics	121
4.4.2.3.	Effect of pH	124
4.4.2.4.	Effect of Adsorbent Dosage	125
4.4.2.5.	Effect of Concentration and Temperature	126
4.4.2.6.	Adsorption Isotherms	128
4.4.2.7.	Adsorption Thermodynamics	132
4.4.3.	Regeneration of Adsorbent	134

S. No.	CONTENT	PAGE
<u>PART-II</u>		
(Metal ion adsorption using bio-waste metal ferrite composite)		
4.5.	Nickel Ferrite Pistachio Shell (NFPS) Composite	136
4.5.1.	Characterization and Morphology	136
4.5.1.1.	Fourier Transform Infrared Spectroscopy	136
4.5.1.2.	X-Ray Diffraction	137
4.5.1.3.	Field Emission Scanning Electron Microscope	137
4.5.1.4.	Energy Dispersive Spectra	139
4.5.1.5.	Thermogravimetric Analysis	140
4.5.1.6.	pH of Point Zero Charge Analysis	141
4.5.2.	Adsorption Study of Metal Ion	142
4.5.2.1.	Effect of Contact Time	142
4.5.2.2.	Adsorption Kinetics	143
4.5.2.3.	Effect of pH	145
4.5.2.4.	Effect of Adsorbent Dosage	146
4.5.2.5.	Effect of Concentration and Temperature	147
4.5.2.6.	Adsorption Isotherms	148
4.5.2.7.	Adsorption Thermodynamics	151
4.5.3.	Regeneration of Adsorbent	152
CHAPTER 5: SUMMARY AND CONCLUSION		
5.1.	Summary and Conclusion	154
	Reference	159
	List of Publications	184
	Publications Proof	186
	Conference Certificates	193

LIST OF FIGURES

FIGURE NO.	TITLE OF FIGURE	PAGE
1.1.	Sustainable Development Goal 6	2
1.2.	A pictorial representation showing different types of adsorbents	8
2.1.	Magnetic separation of adsorbent after wastewater treatment	10
2.2.	Different materials used for surface modification of spinel ferrite	17
2.3.	Schematic representation showing various cycles of regeneration process	25
3.1.	Synthesis of bio-waste based composites	30
<u>PART-I</u>		
(Dyes Adsorption using bio-waste metal ferrite composite)		
4.1.	Zinc Ferrite Pine Cone (ZFPC) Composite	
4.1.1.	FTIR spectra of pine cone, zinc ferrite and zinc ferrite pine cone composite	49
4.1.2.	XRD spectra of zinc ferrite and zinc ferrite pine cone composite	50
4.1.3.	SEM image (a) Zinc ferrite (b) Zinc ferrite pine cone composite	51
4.1.4.	EDS image (a) Zinc ferrite (b) Zinc ferrite pine cone composite	52
4.1.5.	TGA curve of zinc ferrite pine cone composite	53
4.1.6.	pH _{pzc} of zinc ferrite pine cone composite	54
4.1.7.	Effect of contact time for single dye system	56
4.1.8.	Effect of contact time for ternary dye system	56
4.1.9.	Lagergren pseudo first order and pseudo second order kinetics for single and ternary dye system	57
4.1.10.	Elovich model for single and ternary dye system	58
4.1.11.	Intra particle diffusion model for single and ternary dye system	59

FIGURE NO.	TITLE OF FIGURE	PAGE
4.1.12.	Effect of pH for single dye system	60
4.1.13.	Effect of adsorbent dosage for single dye system	61
4.1.14.	Effect of adsorbent dosage for ternary dye system	61
4.1.15.	Effect of concentration for single dye system	62
4.1.16.	Effect of concentration for ternary dye system	63
4.1.17. (a)	Langmuir adsorption isotherm for single and ternary dye system	64
4.1.17. (b)	Freundlich adsorption isotherm for single and ternary dye system	65
4.1.17. (c)	Temkin adsorption isotherm for single and ternary dye system	65
4.1.17. (d)	D-R adsorption isotherm for single and ternary dye system	66
4.1.18.	Adsorption thermodynamic plot for CV, MG and MB in single dye system	68
4.1.19.	Adsorption thermodynamic plot for CV, MG and MB in ternary dye system	69
4.2.	Nickel Ferrite Pine Cone (NFPC) Composite	
4.2.1.	FTIR of spectra pine cone, nickel ferrite and nickel ferrite pine cone composite	72
4.2.2.	XRD spectra of nickel ferrite and nickel ferrite pine cone composite	74
4.2.3.	SEM image (a) Nickel ferrite (b) Nickel ferrite pine cone composite	74
4.2.4.	EDS image (a) Nickel ferrite (b) Nickel ferrite pine cone composite	75
4.2.5.	TGA curve of nickel ferrite pine cone composite	76
4.2.6.	pH _{zpc} of nickel ferrite pine cone composite	78
4.2.7.	Effect of contact time for single and binary dye system	79
4.2.8.	Lagergren pseudo first order and pseudo second order kinetics for single and binary dye system	80
4.2.9.	Elovich model for single and binary dye system	81

FIGURE NO.	TITLE OF FIGURE	PAGE
4.2.10.	Intra particle diffusion model for single and binary dye system	82
4.2.11.	Effect of pH for single dye system	83
4.2.12.	Effect of adsorbent dosage for single and binary dye system	84
4.2.13.	Effect of concentration for single dye system	85
4.2.14.	Effect of concentration for binary dye system	85
4.2.15. (a)	Langmuir adsorption isotherm for single and binary dye system	86
4.2.15. (b)	Freundlich adsorption isotherm for single and binary dye system	87
4.2.15. (c)	Temkin adsorption isotherm for single and binary dye system	87
4.2.15. (d)	D-R adsorption isotherm for single and binary dye system	88
4.2.16.	Adsorption thermodynamic plot for BG and MB in single dye system	90
4.2.17.	Adsorption thermodynamic plot for BG and MB in binary dye system	90
4.3.	Walnut Shell Zinc Ferrite (WSZF) Composite	
4.3.1.	FTIR spectra of walnut shell, zinc ferrite and walnut shell zinc ferrite composite	93
4.3.2.	XRD spectra of zinc ferrite and walnut shell zinc ferrite composite	94
4.3.3.	SEM image (a)Walnut shell (b) Zinc ferrite (c) Walnut shell zinc ferrite composite	95
4.3.4.	EDS image (a) Zinc ferrite (b) Walnut shell zinc ferrite composite	96
4.3.5.	TGA curve of walnut shell zinc ferrite composite	97
4.3.6.	pH _{zpc} of walnut shell zinc ferrite composite	99
4.3.7.	Effect of contact time for single and binary dye system	100

FIGURE NO.	TITLE OF FIGURE	PAGE
4.3.8.	Lagergren pseudo first order and pseudo second order kinetics for single and binary dye system	101
4.3.9.	Elovich model for single and binary dye system	102
4.3.10.	Intra particle diffusion model for single and binary dye system	103
4.3.11.	Effect of pH for single dye system	104
4.3.12.	Effect of adsorbent dosage for single and binary dye system	105
4.3.13.	Effect of concentration for single dye system	106
4.3.14.	Effect of concentration for binary dye system	106
4.3.15. (a)	Langmuir adsorption isotherm for single and binary dye system	108
4.3.15. (b)	Freundlich adsorption isotherm for single and binary dye system	108
4.3.15. (c)	Temkin adsorption isotherm for single and binary dye system	109
4.3.15. (d)	D-R adsorption isotherm for single and binary dye system	109
4.3.16.	Adsorption thermodynamic plot for MG and MB in single dye system	111
4.3.17.	Adsorption thermodynamic plot for MG and MB in binary dye system	111
4.4.	Walnut Shell Cobalt Ferrite (WScoF) Composite	
4.4.1.	FTIR spectra of walnut shell, cobalt ferrite and walnut shell cobalt ferrite composite	114
4.4.2.	XRD spectra of cobalt ferrite and walnut shell cobalt ferrite composite	116
4.4.3.	SEM image (a) Walnut shell (b) Cobalt ferrite (c) Walnut shell cobalt ferrite composite	116
4.4.4.	EDS image (a) Cobalt ferrite (b) Walnut shell cobalt ferrite composite	117
4.4.5.	TGA curve of walnut shell cobalt ferrite composite	118

FIGURE NO.	TITLE OF FIGURE	PAGE
4.4.6.	pH _{Zpc} of walnut shell cobalt ferrite composite	120
4.4.7.	Effect of contact time for single and ternary dye system	121
4.4.8.	Lagergren pseudo first order and pseudo second order kinetics for single and ternary dye system	122
4.4.9.	Elovich model for single and ternary dye system	122
4.4.10.	Intra particle diffusion model for single and ternary dye system	124
4.4.11.	Effect of pH for single dye system	124
4.4.12.	Effect of adsorbent dosage for single and ternary dye system	125
4.4.13.	Effect of concentration for single dye system	127
4.4.14.	Effect of concentration for ternary dye system	127
4.4.15. (a)	Langmuir adsorption isotherm for single and ternary dye system	128
4.4.15. (b)	Freundlich adsorption isotherm for single and ternary dye system	129
4.4.15. (c)	Temkin adsorption isotherm for single and ternary dye system	129
4.4.15. (d)	D-R adsorption isotherm for single and ternary dye system	130
4.4.16.	Adsorption thermodynamic plot for CV, BG and MB in single dye system	132
4.4.17.	Adsorption thermodynamic plot for CV, BG and MB in ternary dye system	132

PART-II

(Metal ion adsorption using bio-waste metal ferrite composite)

4.5.	Nickel Ferrite Pistachio Shell (NFPS) Composite	
4.5.1.	FTIR spectra of pistachio shell, nickel ferrite and nickel ferrite pistachio shell composite	136
4.5.2.	XRD spectra of nickel ferrite and nickel ferrite pistachio shell composite	138

FIGURE NO.	TITLE OF FIGURE	PAGE
4.5.3.	SEM image (a) Pistachio shell (b) Nickel ferrite (c) Nickel ferrite pistachio shell composite	138
4.5.4.	EDS image (a) Nickel ferrite (b) Nickel ferrite pistachio shell composite	139
4.5.5.	TGA curve of nickel ferrite pistachio shell composite	140
4.5.6.	pH _{zpc} of nickel ferrite pistachio shell composite	141
4.5.7.	Effect of contact time for the removal of Cu(II) ions	141
4.5.8.	Lagergren pseudo first order and pseudo second order kinetic model for Cu(II) ions	143
4.5.9.	Elovich model for Cu(II) ions	144
4.5.10.	Weber-Morris model for Cu(II) ions	145
4.5.11.	Effect of pH for the removal of Cu(II) ion	146
4.5.12.	Effect of adsorbent dosage for the removal of Cu(II) ion	146
4.5.13.	Effect of concentration for the removal of Cu(II) ion	147
4.5.14. (a)	Langmuir isotherm for the removal of Cu(II) ion	149
4.5.14. (b)	Freundlich isotherm for the removal of Cu(II) ion	149
4.5.14. (c)	Temkin isotherm for the removal of Cu(II) ion	150
4.5.14. (d)	D-R isotherm for the removal of Cu(II) ion	150
4.5.15.	Adsorption thermodynamic plot for the removal of Cu(II) ion	152

LIST OF TABLES

TABLE NO.	LIST OF TABLES	PAGE
1.1.	Different methods used for wastewater treatment along with advantages and disadvantages	6
2.1.	Different methods of ferrite preparation along with advantages and disadvantages	12
2.2.	Various method for the synthesis of ferrite with adsorption capacities	13
2.3.	Information of different metal ferrite composites employed to remove pollutants	18
2.4.	Adsorption behaviour of bio-wastes used for the removal of different pollutants	19
2.5.	Adsorption behaviour of bio-waste based metal ferrite composites used for the removal of different pollutants	21
2.6.	Different desorbing agents used for the regeneration of adsorbents	24
3.1.	List of different composite prepared	30
3.2.	Preliminary results showing percentage removal of various dyes	31
3.3.	Preliminary results showing percentage removal of heavy metals	34
<u>PART-I</u>		
(Dyes Adsorption using bio-waste metal ferrite composite)		
4.1.	Zinc Ferrite Pine Cone (ZFPC) Composite	
4.1.1.	Elemental composition of zinc ferrite and zinc ferrite pine cone composite	52
4.1.2.	Calculated values of different kinetic constants for single and ternary dye system	58
4.1.3.	Adsorption isotherm constants for single and ternary dye system	67
4.1.4.	Thermodynamic parameters in single and ternary dye system	69

TABLE NO.	LIST OF TABLES	PAGE
4.1.5.	Regeneration efficiency of zinc ferrite pine cone composite for single and ternary dye system	71
4.2.	Nickel Ferrite Pine Cone (NFPC) Composite	
4.2.1.	Elemental composition of nickel ferrite and nickel ferrite pine cone composite	76
4.2.2.	Calculated values of different kinetic constants for single and binary dye system	81
4.2.3.	Calculated values of adsorption isotherm constants for single and binary dye system	89
4.2.4.	Calculated values of thermodynamic parameters in single and binary dye system	91
4.2.5.	Regeneration efficiency of nickel ferrite pine cone composite for single and binary dye system	92
4.3.	Walnut Shell Zinc Ferrite (WSZF) Composite	
4.3.1.	Elemental composition of zinc ferrite and walnut shell zinc ferrite composite	97
4.3.2.	Calculated values of different kinetic constants for single and binary dye system	102
4.3.3.	Calculated values of adsorption isotherm constants for single and binary dye system	110
4.3.4.	Calculated values of thermodynamic parameters in single and binary dye system	112
4.3.5.	Regeneration efficiency of walnut shell zinc ferrite composite for single and binary dye system	113
4.4.	Walnut Shell Cobalt Ferrite (WScoF) Composite	
4.4.1.	Elemental composition of cobalt ferrite and walnut shell cobalt ferrite composite	118
4.4.2.	Calculated values of different kinetic constants for single and ternary dye system	123
4.4.3.	Calculated values of adsorption isotherm constants for single and ternary dye system	131

TABLE NO.	LIST OF TABLES	PAGE
4.4.4.	Calculated values of thermodynamic parameters in single and ternary dye system	133
4.4.5.	Regeneration efficiency of walnut shell cobalt ferrite composite in single and ternary dye system	134
<u>PART-II</u>		
(Metal ion adsorption using bio-waste metal ferrite composite)		
4.5.	Nickel Ferrite Pistachio Shell (NFPS) Composite	
4.5.1.	Elemental composition of nickel ferrite and nickel ferrite pistachio shell composite	140
4.5.2.	Calculated values of different kinetic constants for Cu(II) ion	144
4.5.3.	Calculated values of adsorption isotherm constants for the removal of Cu(II) ion	151
4.5.4.	Calculated values of thermodynamic parameters used for the removal of Cu(II) ion	152
4.5.5.	Regeneration efficiency of nickel ferrite pistachio shell composite for the removal of Cu(II) ion	153

FREQUENTLY USED ACRONYMS AND THEIR EXPANDED FORMS

ABBREVIATIONS	EXPANDED FORMS
SDS	Sodium dodecyl sulphate
CTAB	Cetyl-tri methyl ammonium bromide
ODH	Oxalyldihydrazide
FTIR	Fourier Transform Infra-Red
XRD	X- Ray Diffraction
SEM	Scanning Electron Microscope
EDS	Energy Dispersive Spectra
TGA	Thermogravimetric and Differential Thermal Analysis
BET	Brunauer-Emmett-Teller
pH _{zpc}	pH of zero point charge
rpm	Rotation per minute
UV-VIS	Ultra Violet-Visible
CoF	Cobalt Ferrite
ZF	Zinc Ferrite
NF	Nickel Ferrite
CuF	Copper Ferrite
ZFPC	Zinc Ferrite Pine Cone
NFPC	Nickel Ferrite Pine Cone
CoFPC	Cobalt Ferrite Pine Cone
CuFPC	Copper Ferrite Pine Cone
WSZF	Walnut Shell Zinc Ferrite
WSNF	Walnut Shell Nickel Ferrite
WScoF	Walnut Shell Cobalt Ferrite
WSCuF	Walnut Shell Copper Ferrite
NFPS	Nickel Ferrite Pistachio Shell
ZFPS	Zinc Ferrite Pistachio Shell
CoFPS	Cobalt Ferrite Pistachio Shell
CuFPS	Copper Ferrite Pistachio Shell
CR	Congo Red
CV	Crystal violet

ABBREVIATIONS	EXPANDED FORMS
MB	Methylene Blue
MG	Malachite Green
BG	Brilliant Green

CHAPTER-1

INTRODUCTION



1.1. General Introduction

Improved standard of living, world's continuous rising population demand more natural resources. With the increase in demands on global scale, the problems of environment are also increasing. Among all the natural resources, water is the vital component which is responsible for the proper functioning of the ecosystem.¹ About 71% of Earth's surface is covered with water which comprises of 97% salty water, 2% water available which is in frozen form and the remaining 1% water which is utilized for various purposes such as household chores, drinking, industrial applications etc.² Water pollution worldwide emerge as the biggest problem of this century, so United Nations (2015) in their 17 Sustainable Development Goals (SDGs) also highlighted the issue in their Sustainable Development Goal number 6 which states **“Clean water and sanitation for all”** by the year **2030**. Safe water access is essential for economic growth as well as productivity.³ Water pollution is one of the problem which contributes majorly to the environmental pollution.⁴ Access to reliable clean water becomes a global challenge of 21st century.⁵ According to the Sustainable Development Goal 6 established by the United Nations, “reaching universal coverage by 2030 will necessitate a significant boost in current worldwide advancement rates: a six-fold increase for drinking water, a fivefold increase for sanitation and an eightfold increase for hygiene”.⁶ In accordance with Goal 6's target 6.2, “By 2030, achieve universal and equitable access to safe and affordable drinking water for all. By 2030, achieve access to adequate and equitable sanitation and hygiene for all and end open defecation, paying special attention to the needs of women and girls and those in vulnerable situations”. As per target 6.3, “By 2030, improve water quality by reducing pollution, eliminating dumping and minimizing release of hazardous chemicals and materials, halving the proportion of untreated wastewater and substantially increasing recycling and safe reuse globally”.^{7,8} The main problem recognized is untreated water discharged from various sources such as agriculture, industries, municipal etc. to water bodies which affects the quality of water and harm the aquatic organisms and ultimately results in water pollution.⁹ Therefore, in much affected areas, it is much important to implement basic technologies for the treatment of waste water. Recycling, reduce and reuse of water are vital in reduction of wastewater pollution as well as in the contamination of fresh water resources.¹⁰



Figure 1.1: Sustainable Development Goal 6

From all the sources, the discharge of industrial waste water in natural water bodies pose serious threats to the life existing on earth.¹¹ Various industries such as metal refining, automobile, textile, pharmaceuticals, cosmetic, paint manufacturing etc. contribute various type of pollutants to the water bodies.¹²⁻¹⁵ The pollutants are majorly categorized into organic pollutants and inorganic pollutants. As a consequence, water pollution caused by both organic and inorganic contaminants has emerged as the most substantial environmental concern that endangers human existence on a global scale.^{16,17} Different pollutants include heavy metals¹⁸⁻²⁰, dyes^{21,22}, antibiotics, metalloids^{23,24}, Surfactants^{17,18}, insecticides, herbicides¹⁸, pesticides^{18,25} etc. have been discharged without their prior treatment. From the above mentioned pollutants, dyes and heavy metals are of great concern because of having mutagenic and carcinogenic properties.^{13,17,26}

1.2. Target Pollutants

Dyes and heavy metals are non-biodegradable compounds which cannot be eliminated at the time of wastewater treatment in effluent treatment plants and are of great concern because water is the basic necessity and it should be free from all types of contaminants.^{27,28} Untreated disposal of heavy metals and dyes cause environmental pollution and become a major concern worldwide by threatening human health as well as ecosystem.²⁹ Dyes and heavy metals emerge as major source of environmental pollution which ultimately affects the ecosystem and human health.^{22,30}

1.2.1. Dyes

Many industries use dyes as coloring agents such as pharmaceutical, cosmetic, paint, textile, plastic etc. In various industries, the dyes produced annually are more than 7×10^5 tons.³¹ In the year 1956, artificial dyes are firstly invented. Before 1956, different

plant parts such as roots, leaves, bark, lichens, wood etc. were used as natural dyes. Due to some limitations such as low fastness of colour to fabrics, easily fade of colour on exposure to light and washings, less colour range etc., natural dyes were replaced with synthetic dyes.³² But after 1956, synthetic dyes were used for the coloring of different materials derived from petrochemicals which provides fast colour and have wide range.³² Chromophores and auxochromes are two compounds basically which are mainly responsible for the composition of synthetic dyes where, the dye color is produced because of chromophore and color intensity is attained due to auxochrome.³³ Dyes are harmful for aquatic life, plants, animals, human beings etc.^{22,34} Dyes may show acute or chronic effects on the exposed organisms which depends upon the concentration of dye and exposure time.³⁵ In humans, these dyes if inhaled or ingested may cause serious health issues like skin problems, nervous system disorder, kidney failure, liver damage etc.³⁶ Due to mutagenic and carcinogenic dye characteristics effluent from various textile plants should be taken in view and require proper treatment before discharge into the environment.³⁷

1.2.1.1. Effect of Dyes

The presence of dyes in wastewater can have numerous adverse effects on the entire ecosystem:^{22,34,38}

- **Environmental Pollution:** Dyes can give water bodies unnatural colors, affecting aquatic ecosystems and disrupting the balance of aquatic life. Some dyes are toxic to aquatic organisms, leading to a decline in biodiversity.
- **Water quality degradation:** Dyes can reduce the transparency of water, limiting sunlight penetration and hindering photosynthesis in aquatic plants. This can lead to the depletion of oxygen in water, causing harm to fish and other aquatic organisms.
- **Health risks:** Certain dyes and their breakdown products are carcinogenic or have toxic effects on humans. When present in drinking water sources, they pose health risks such as skin irritation, respiratory issues, and even long-term health complications like cancer.
- **Bioaccumulation:** Dyes can accumulate in aquatic organisms through food chain, leading to bio magnification. This means that higher-level predators may consume

contaminated prey and accumulate higher concentrations of dye compounds, increasing the risk of toxicity.

Overall, the existence of dyes in the wastewater poses significant environmental and health risks, highlighting the importance of effective dye removal techniques and stricter regulations to minimize their impact on water quality and ecosystems.

1.2.2. Heavy Metals

Heavy metals basically are the metallic elements with high atomic mass and density. These elements occur naturally in the Earth's crust but human activities like industrial processes, metal refining, mining and agricultural practices can lead to their increased release into the environment.¹ Some common heavy metals are arsenic, lead, copper, nickel, mercury, chromium and cadmium.^{18,39,40} Exposure to these metals may lead to damage of liver, kidney, central nervous system etc.^{41,42} Heavy metals may reach human body through dermal exposure, inhalation or may be through oral ingestion.³ But the main passage for the entry of these elements into human body is through two main channels i.e.; water and food.⁴³ These may become fatal and pose serious threats to life if the intake will exceed permissible limits which are provided by World Health Organization (WHO).⁴⁴ Additionally, heavy metals can persist in environment for long periods, posing risks to ecosystems and wildlife. For clean environment and good human health, it is much important to eliminate harmful heavy metals from water bodies.⁴⁵ Because of their persistence and toxicity, they are regulated pollutants in many countries and efforts are made to monitor and control their release into the environment. Treatment technologies such as filtration, precipitation, and adsorption are often employed to remove heavy metals and mitigate their environmental impact.^{15,46}

1.2.2.1. Effect of Heavy Metals

The effects of heavy metals can differ based on the particular metal, its concentration, and the exposure duration. Generally, heavy metals can cause various adverse effects as discussed below:^{34,46,47}

A. Human health effects:

- Toxicity: Heavy metals including lead, mercury, cadmium, copper and arsenic are toxic to humans, even at low concentrations. Chronic exposure to these metals can

lead to different health problems including kidney damage, neurological disorders, respiratory issues, cardiovascular diseases and various types of cancer.

- Developmental and reproductive effects: Prenatal exposure to certain heavy metals can affect fetal development and lead to birth defects. Heavy metals may also impact reproductive health and fertility in both men and women.
- Accumulation: These can accumulate in body particularly in organs like liver, brain and kidneys. This accumulation can result in long-term health complications.

B. Environmental Effects:

- Ecological toxicity: Heavy metals can have toxic effects on plants, animals, and microorganisms in ecosystems. They can disrupt biochemical processes, inhibit growth and reproduction, and even lead to mortality in sensitive species.
- Bioaccumulation and Bio magnification: Heavy metals may bioaccumulate in tissues of living organisms, meaning that concentrations increase up the food chain. Predators at the top of the food chain may accumulate high levels of heavy metals, leading to bio magnification and increased risk of toxicity.
- Disruption of Ecosystems: Elevated concentrations of heavy metals can disrupt the balance of ecosystems by affecting nutrient cycling, species composition, and overall biodiversity.

C. Environmental Contamination:

- Soil and water pollution: Heavy metals can contaminate soil and water sources which poses risk to agricultural productivity as well as drinking water quality. They can persist in environment for longer periods, leaching into groundwater sources and spreading through surface water bodies.
- Contaminated sites: Industrial activities such as mining, smelting, and manufacturing can create contaminated sites known as "brownfields" or "superfund sites," where heavy metal pollution poses risk to human health and the environment.

Overall, the effects of heavy metals underscore the importance of monitoring and regulating their release into the environment, implementing pollution prevention measures and employing remediation strategies to mitigate their impact on human health and ecosystems.

1.3. Methods for Wastewater Treatment

Pollutants present in industrial effluents can be removed by various physical, chemical and biological methods.^{15,48,49} The treatments for polluted water is a three step procedure which includes primary treatment, secondary treatment and tertiary treatment.⁴⁹ Over the last ten years, an extensive range of methods have been employed to treat organic and inorganic contaminants in wastewater.^{16,50,51} These include chemical oxidation, precipitation, coagulation/flocculation, enzymes, fungi, reverse osmosis, evaporation, algae, photo degradation, membrane filtration, adsorption, ion exchange etc.^{36,52–54} which can be applied as per the nature of the target pollutant. Table 1.1. outlines the different treatment technologies along with their respective advantages as well as disadvantages.

Table 1.1: Different methods used for wastewater treatment along with advantages and disadvantages:^{17,30,49,55}

TREATMENT METHOD	APPLICATION	ADVANTAGE	DISADVANTAGE
Ion Exchange	Hydrometallurgy, metals finishing	Produce good quality treated material Less time consuming Low waste generation	High maintenance cost Rapid clogging and more saturation of reactors
Membrane Filtration	Pharmaceutical industry, chemical industry	Less consumption of Chemical Less waste generation	Flow rates are limited High operational and maintenance cost Fouling of membrane
Adsorption	Wastewater treatment	Simple Low cost Easy operation Target pollutants of wide variety	Efficiency depends on type of material Waste management Require adsorbent's regeneration
Coagulation/Flocculation	Purification of water, textile industry	Characteristic feature of sludge settling Economically good Process simplicity	More sludge generation and formation of bigger particles

TREATMENT METHOD	APPLICATION	ADVANTAGE	DISADVANTAGE
Photo catalysis	Water splitting, disinfection and cleaning	More degradation rate Energy production	Handling issues Exposure to UV light may cause harm as it is carcinogenic
Biological Methods	Industrial and municipal wastewater/ Effluents	Economically feasible High BOD removal	Require optimum favorable environment Need more maintenance and management Slow process

1.4. Adsorption

Numerous studies in the literature suggest that, among all the treatment methods, adsorption seems to be the best method employed for removing different pollutants from wastewater.^{56,57} Adsorption basically is a phenomenon whereby the molecules of liquid phase got attached to the surface of solid phase. Adsorption is a widely used method as it has certain advantages which includes low operational cost, high efficiency, less time consuming, more productive, recyclable ability, convenient, simple in operation etc.^{28,58,59} Adsorption is a separation technique wherein fluid, liquid or gas molecules known as adsorbate adhere to the exterior and interior surfaces of a solid object termed as adsorbent.^{50,60}

1.5. Types of Adsorbent

Various adsorbents can be utilized for removing pollutants from aqueous solution.

Adsorbents are majorly categorized into two different types which are:^{50,61-64}

- Conventional adsorbents
- Non-Conventional adsorbents

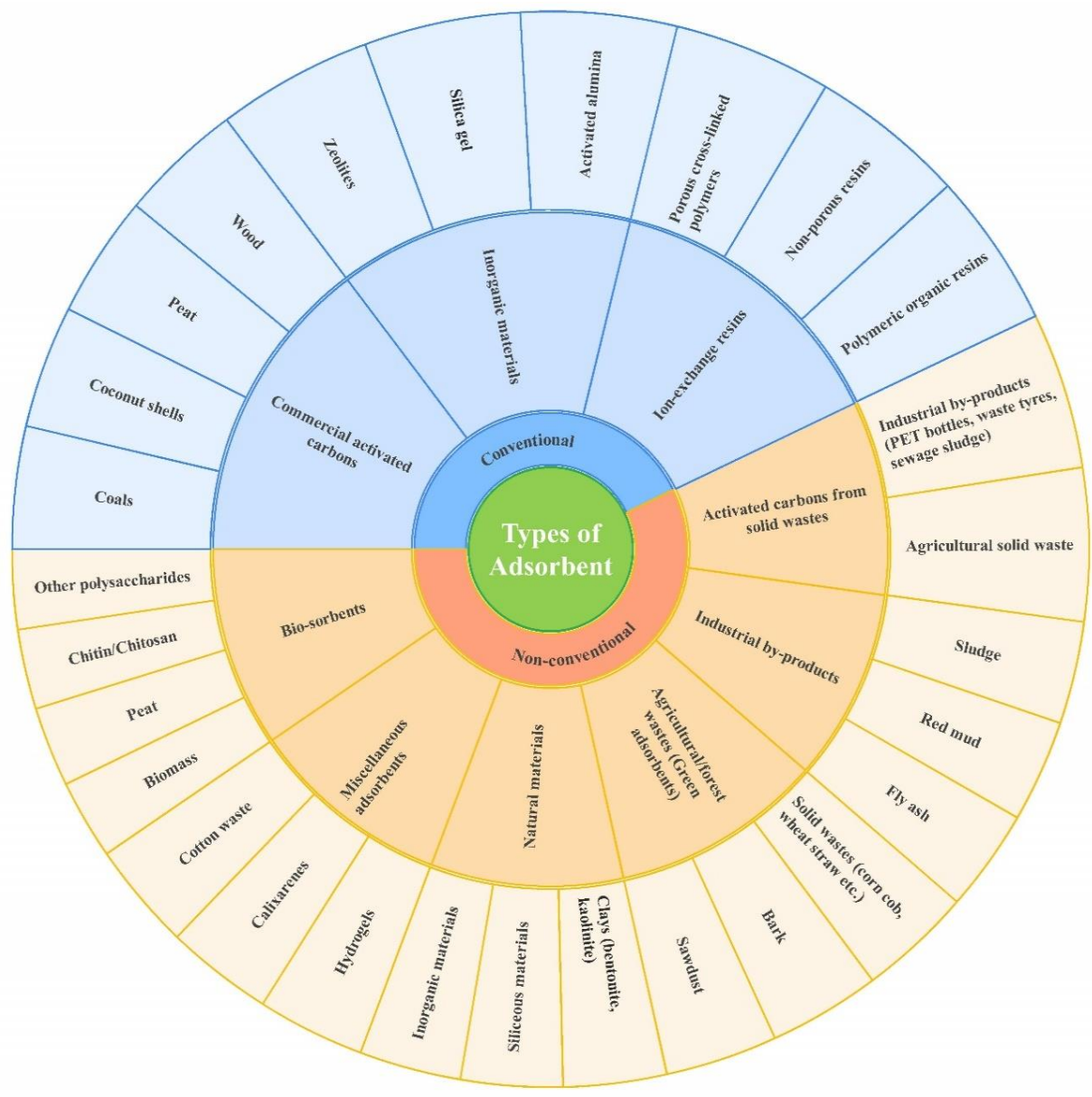


Figure 1.2: A pictorial representation showing different types of adsorbents

CHAPTER-2
REVIEW OF LITERATURE



The present research study focuses on the surface modification of magnetic metal ferrites and their application as an adsorbent for the purpose of eliminating various types of dyes and Cu(II) metal ion from aqueous solution. This chapter offers comprehensive literature review focusing on nanomaterials such as metal ferrites and their composites.

2.1. Nanomaterials in Adsorption

According to recent innovations, nanotechnology provide tremendous opportunities in establishing sustainable and cost-effective systems for water supply.⁵ Nanotechnology relates to the materials having physical dimensions 100 nm or less.²⁵ Nanotechnology gives potential opportunity for purifying water at a low cost and shows great operational effectiveness in removing pollutants and reusability. Nanomaterials have been successfully employed in a variety of fields such as medicinal science, catalysis, material science, space science etc. and are now widely preferred in wastewater treatment as these have shown significant results with good adsorption efficiency.^{5,23,65,66} Experts have found that nanotechnology is a better option for treating wastewater because it also has certain distinctive characteristics such as nano size, broad surface area, high reactivity, robust solution mobility, mechanically strong, pore volume, high selectivity, dispersibility, easily modifiable etc. Several heavy metals including Pb, Mo as well as other contaminants (organic and inorganic) and many harmful microorganisms have been successfully eliminated by utilizing different nanomaterials.^{67,68} Nanomaterials may be in the form of nano tubes, nano rods, nano wires and nano particles.⁶⁹ Various nano materials such as graphene, carbon nano tubes, quantum dots, nano porous materials, metal organic framework nano sheets (MOFs), core shell nanoparticles etc. have been used in several applications including the treatment of wastewater.⁷⁰

Significant research in the field of wastewater treatment is conducted by using nano materials and concluded that nanomaterials show efficient results in removing different types of waste from effluent.¹⁰ Nano materials have specific properties such as high surface area, versatile surface modifications etc. which make them suitable to remove variety of contaminants easily and effectively.^{65,71}

From last decade, magnetic nanoparticles have gained much attention by researchers in the wastewater treatment field. Numerous nanomaterials had been used for the removal of inorganic and organic pollutants from the waste water out of which magnetic nano

ferrites are of great interest. Magnetic materials are of three types mainly i.e.; diamagnetic, ferromagnetic and paramagnetic.^{24,72}

2.1.1. Nano Ferrite: A Magnetic Material

Waste water treatment employ several types of nano materials such as meso-porous components, nano metal oxides, nano ferrites because of unique physiochemical properties.^{70,73-76} Among all these categories, nano ferrites and their composites have gained considerable significance in waste water treatment because of having remarkable magnetic character which allows easy separation of ferrites using magnetic force. Ferrites basically comprises of iron oxide and are ceramic materials having certain advantages like tunable properties, high magnetization and electrical resistance which makes them suitable for effectively removing various pollutants from aqueous solution.⁷⁷⁻⁷⁹ These materials also exhibit magnetic properties which have an added advantage of easy separation of the adsorbent from wastewater after adsorption process. Figure 2.1 illustrates the magnetic separation of adsorbent from wastewater after treatment. Due to cost effectiveness and suitability for different industrial applications, the interest of using ferrites for conducting various research studies is increasing rapidly.⁷² Certain other advantaged such as strong adsorption capacity, reusability and easy separability after their use makes magnetic nano ferrites more feasible for waste water treatment.

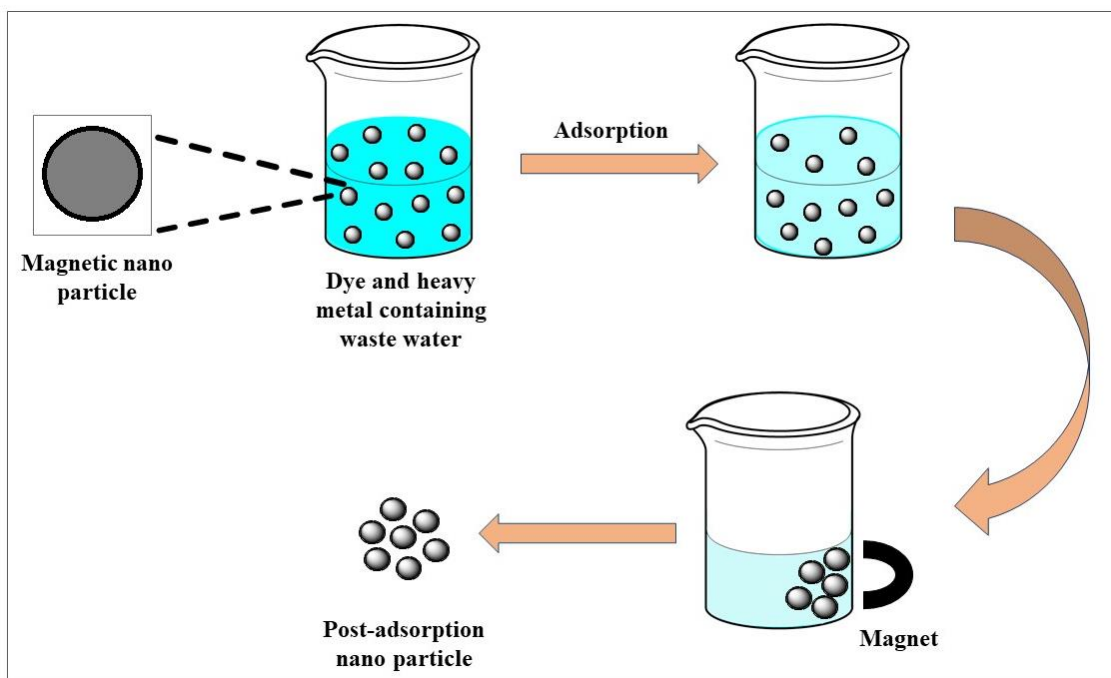


Figure 2.1: Magnetic separation of adsorbent after wastewater treatment

Ferrites are also widely used these days by researchers in distinct fields such as pigments, mobile communication, magnetic biosensors, catalysis, pollution control etc.⁷⁷ Ferrites are ceramic, non- conductive ferromagnetic metal compounds. These possess remarkable physical as well as chemical properties. Large surface area, porous surface, magnetized nature etc. makes ferrites suitable for the process of adsorption.⁷⁷⁻⁷⁹ There are three main types of ferrites which are as:⁷²

1. Spinel
2. Garnet
3. Hexagonal

Due to excellent potential applications, physiochemical properties and simple composition in comparison to other ferrites⁷⁴, spinel ferrites have gained enormous interest globally in the field of wastewater treatment.⁸⁰ Spinel ferrites are basically metal oxides with general formula AB_2O_4 .⁷⁷

Where, A- Divalent metal ion such as Zn^{2+} , Mg^{2+} , Cu^{2+} , Ni^{2+} , Co^{2+} etc.

B- Fe

O- Oxygen

Spinel ferrites are widely used because of having flexibility, variability, good efficiency, chemical stability, thermal stability etc. Spinel ferrites exhibit unique properties which are useful in the field of waste water treatment.^{74,77,81}

2.1.2. Synthesis Method and Adsorption Behavior of Metal Ferrite

2.1.2.1. Synthesis Method

Magnetic nano ferrites can be synthesized by different methods such as co-precipitation, hydrothermal, sol-gel method, combustion, ultra-spray pyrolysis, refluxing, microwave thermal, wet-chemical method etc. which can be used to obtain magnetic nano ferrites having different structural and morphological properties. Some important methods of ferrite synthesis are shown in table 2.1 along with their benefits and drawbacks.⁵⁹

Table 2.1: Different methods of ferrite preparation along with advantages and disadvantages

Method of Ferrite Preparation	Advantages	Disadvantages
Hydrothermal	<ul style="list-style-type: none"> • Direct formation of powder from solution • Control of particle size • Resulting powder exhibits high reactive nature 	<ul style="list-style-type: none"> • Prior information about solubility is required • Slurry formed showed high corrosive nature
Microwave Thermal	<ul style="list-style-type: none"> • Cost effective • Rapid synthesis process • Crystalline in structure 	<ul style="list-style-type: none"> • Exaggerated growth • Presence of impurities
Sol-Gel	<ul style="list-style-type: none"> • Morphology control and small particle size • Better homogeneity 	<ul style="list-style-type: none"> • Expensive procedure • Requires close monitoring
Combustion	<ul style="list-style-type: none"> • Requires low temperature • Cost effective • Good stoichiometry control 	<ul style="list-style-type: none"> • More chances of impurity • Fast reaction possibility which needs extra protection
Co-precipitation	<ul style="list-style-type: none"> • Nano particles formed are of uniform size • Reduction in reaction temperature • Reacting materials homogeneous mixing 	<ul style="list-style-type: none"> • Chances of impurity formation • More time consuming • Reacting materials solubility affects precipitation rate
Wet chemical	<ul style="list-style-type: none"> • Uniform particle size • Required low temperature 	<ul style="list-style-type: none"> • Low yield • More possibility of impurities

2.1.2.2. Adsorption Behavior of Metal Ferrite

The literature review of different ferrites prepared by using various methods along with the various parameters is shown in the table 2.2.

Table 2.2: Various method for the synthesis of ferrite with adsorption capacities

S. No.	Magnetic Material	Method	Adsorbate	Adsorption		
				Capacity (mg/g)	Year	Reference
1.	MnFe ₂ O ₄	Co-precipitation method	Methyl blue	148.04	2014	82
2.	CaFe ₂ O ₄	Sol-gel technique	Congo Red	40.93	2015	83
3.	MnFe ₂ O ₄	Co-precipitation method	Zn(II)	454.5	2020	84
4.	CoFe ₂ O ₄	Co-precipitation method	Zn(II)	384.6	2020	84
5.	CoFe ₂ O ₄	Microwave mediated	Eriochrome Black T (EBT)	82.6	2020	85
		hydrothermal method	Bromophenol Blue (BRB)	25.6		
6.	Magnesium-Zinc Ferrite	Sol-gel auto combustion method	Cr(VI)	30.49	2021	86
7.	Cobalt Ferrite Nanoparticles (CFN)	Co-precipitation method	Lead	275	2022	27
			Zinc	390		
			Congo Red	831		
			Malachite Green	161		
8.	ZnFe ₂ O ₄	Hydrothermal method	Auramine O (AO)	201.29	2022	29
			Methylene Blue (MB)	256.76		
			Cd(II)	152.48		

S. No.	Magnetic Material	Method	Adsorbate	Adsorption		
				Capacity (mg/g)	Year	Reference
9.	NiFe ₂ O ₄	Co-precipitation method	Thiazole yellow G (TYG)	63.04	2023	76
			Alizarin yellow R (AYR)	55.71		
10.	CoFe ₂ O ₄	Co-precipitation method	Thiazole yellow G (TYG)	67.05	2023	76
			Alizarin yellow R (AYR)	60.19		

2.2. Surface Modification of Metal Ferrites

Although magnetic nano ferrites have various advantages but sometimes show certain limitations which affects their removal efficiency. So to enhance efficiency, stability, shelf life etc., magnetic nano ferrites can be modified with various organic and inorganic materials.⁸⁷ Surface modifications can be done by using metal oxides^{88,89}, surfactants^{87,90}, polymers^{18,91} etc. The modification on the surface of magnetic nano ferrites results in the addition of specific functionalization groups onto the material's surface. This process enhances the adsorption efficiency and improves selectivity towards removal of target pollutants from wastewater.⁵⁹

2.2.1. Deposition of Metal and their Oxide

The doping of ferrites with metals and their oxides to form new adsorbents plays a crucial role in wastewater treatment by facilitating the removal of various pollutants. The process of adsorption comprises the attachment of different molecules on the surface of the metal oxide particles resulting in the reduction of pollutant concentration in the water. Metals and metal oxides possess a high surface area and specific surface properties that make them effective adsorbents.⁹² They can adsorb an variety of pollutants from wastewater through physical and chemical interactions.

Deposition of metals and metal oxides onto various substrates such as activated carbon or silica, agricultural wastes, bio-wastes etc. allows for the modification of the adsorbent's surface properties. This modification enhances its affinity for specific pollutants improving its overall performance in wastewater treatment. Metal and metal oxide based adsorbents are often capable of being regenerated and reused making them economically viable for wastewater treatment^{5,93} This reduces the cost linked with disposing of used adsorbents, thus enhances the sustainability of the treatment process. The environmental impact of metal and metal oxide-based adsorbents should be considered especially in terms of potential leaching of metals into the treated water. The development of environmentally friendly adsorbents and strategies to mitigate any negative effects is an ongoing area of research. Liu et al. prepared magnetic $\text{Ni}_{0.5}\text{Zn}_{0.5}\text{Fe}_2\text{O}_4$ using sol combustion method and followed the process of calcination. The prepared material was utilized for the removal of dye Congo Red. It has been observed that CR adsorption increased with nickel doped zinc ferrite when compared with pure zinc ferrite.⁹⁴ Abbas et al. synthesized $\text{Ni}_{0.5}\text{Zn}_{0.5}\text{Fe}_2\text{O}_4$ (Nickel doped zinc ferrite) nanocomposite and further used for removal of W(VI), Cr(VI), V(V) and Mo(VI) ions.⁹⁵

2.2.2. Surfactant Treatment/Coating

Surfactants, or surface-active agents, can play a significant role as adsorbents in wastewater treatment. Surfactants have amphiphilic properties, which means they have both hydrophobic (water-repelling) and hydrophilic (water-attracting) regions. This unique characteristic allows surfactants to interact with a wide range of pollutants in water. Surfactants can adsorb hydrophobic organic compounds, such as oils, greases, and certain organic pollutants, onto their hydrophobic tails. This adsorption helps in removal of hydrophobic contaminants from the waste water improving water quality. Some surfactants have been found efficient in adsorbing metal ions and dyes from wastewater. The hydrophilic head group of surfactants can interact with metal ions, dyes etc. leading to their removal through adsorption onto the surfactant micelles or surfaces. These can enhance the adsorption capacity of certain materials.^{96,97} For example, modified ferrites impregnated with surfactants may exhibit improved adsorption performance due to the synergistic effects of surfactant interactions with pollutants. The biodegradability of many surfactants is an important consideration in wastewater treatment. Biodegradable

surfactants are preferred to minimize any adverse environmental impacts associated with their use.⁹⁸ In conclusion, surfactants play a versatile role in wastewater treatment by adsorbing a variety of contaminants, thereby enhancing the overall efficacy of the treatment processes. Their unique amphiphilic properties make them valuable in addressing challenges related to the elimination of hydrophobic and hydrophilic pollutants from the aqueous solution.

Singh et al. modified the surface of CoFe_2O_4 nanoparticles with sodium dodecyl sulfate and studied the removal of Crystal violet. The results obtained indicated that SDS modified CoFe_2O_4 nanoparticles showed good adsorption efficiency for removing cationic dyes.⁹⁹ Zhang et al. synthesized SDS modified ZnFe_2O_4 nanoparticles for removing Methylene blue.¹⁰⁰ Adel et al. synthesized MgFe_2O_4 -CTAB NPs and applied to remove indigo carmine dye from wastewater.¹⁰¹

2.2.3. Polymer Treatment/Coating

Polymers are macromolecules, which are extremely large molecules formed by the fusion of numerous smaller molecules. Before they are transformed into polymers, these smaller components are referred to as monomers. Indeed, the term "polymer" originates in Greek and translates to "many members".^{102,103} One of the most innovative materials being used for effective wastewater treatment is nanomaterials and polymers. These entities possess distinct functional features that can be modified to accommodate the needs of an extensive array of wastewater treatment technologies. Polymer nanocomposites are a novel category of materials that exhibit enhanced performance as a result of combining the advantageous characteristics of nanomaterials and polymers. Clearly, a thorough understanding of the fundamental properties and scientific principles that strengthen these types of functional materials is essential for their evident development.¹⁰⁴ Polymer coatings on surface of adsorbent materials increases their effective surface area. This enhanced surface area offers additional active spots on the adsorbent's surface, hence improving the overall adsorption capacity. Surface modification alters the chemical as well as physical properties of material making it more effective in adsorbing specific contaminants from wastewater. Blending polymer coatings with other substances such as carbon-based adsorbents or metal oxides can augment overall adsorption capacity as well as the efficiency of prepared material. Polymer-coated adsorbents can often be

regenerated and also reused which makes them cost-efficient and environmentally friendly.¹⁰⁵ The coatings may prevent irreversible interactions with pollutants allowing for repeated use of the adsorbent. In summary, polymer coating plays a versatile role in improving adsorption capabilities of materials used for water treatment. Through surface modification and the introduction of specific functionalities, polymer-coated adsorbents can be tailored for improved selectivity, stability and efficiency in removal of pollutants from wastewater.^{41,104,106}

Pandey et al. highlighted the use of recent advancements in polymer nanocomposites for water purification. Their properties with respect to metal ions, pigments and microorganisms in water were examined, as well as the diverse techniques used in their preparation and characterization.¹⁰⁷ Noamani et al. discussed about the application of carbon-based polymer nano membranes for the treatment of oily wastewater.¹⁰⁸

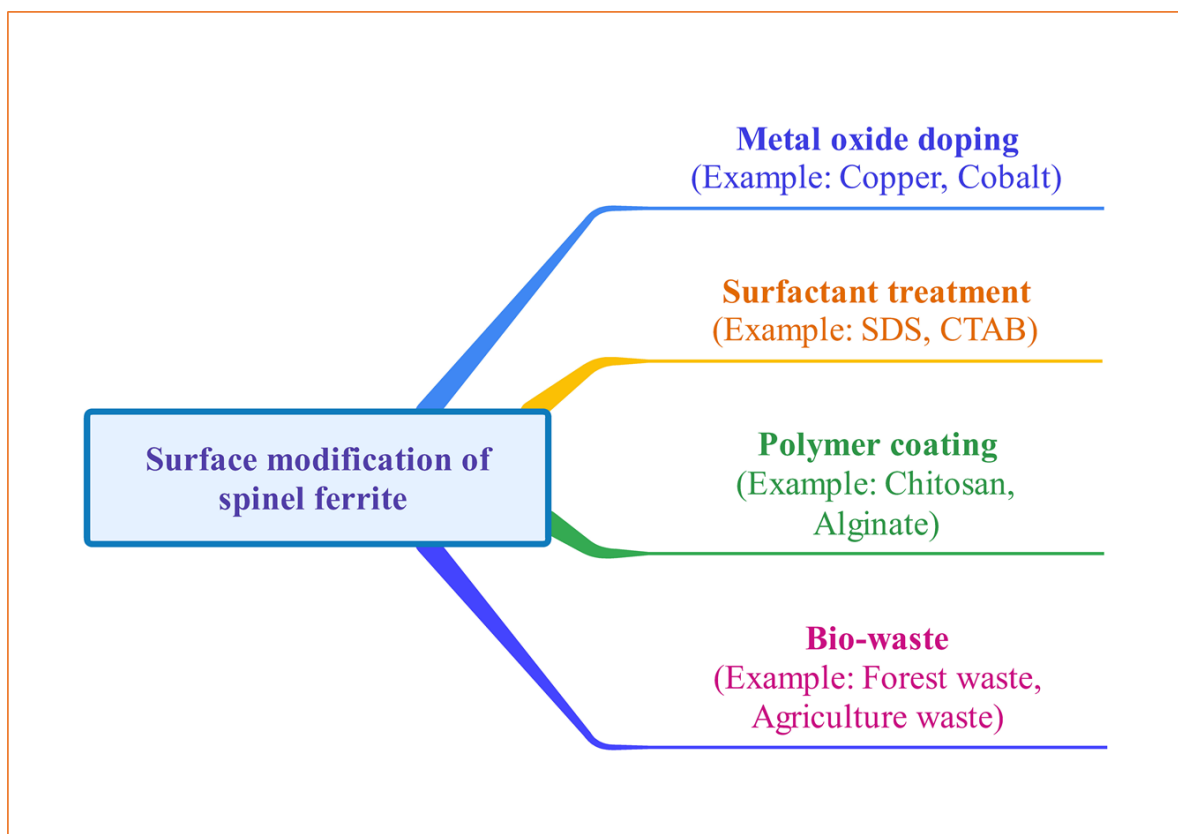


Figure 2.2: Different materials used for surface modification of spinel ferrite

Table 2.3: Information of different metal ferrite composites employed to remove pollutants

Adsorbent	Doping/Coating Agent	Target pollutant	Adsorption Capacity (mg/g)	Reference
Mn_{1-x}Co_xFe₂O₄	Cobalt	Cr (VI)	*	109
Ni_{0.5}Zn_{0.5}Fe₂O₄	Nickel-Zinc	Congo Red	204.8	94
NiFe₂O₄-CTAB	CTAB	Direct Red 31	142.86	110
		Direct Red 81	90.909	
		Direct Red 80	50	
SDS-MNPs	SDS	Crystal Violet	166.6	111
ZnFe₂O₄-SDS	SDS	Crystal Violet	188.3	112
NiFe₂O₄-CTAB	CTAB	Brilliant Green	250	87
CS/CoFe₂O₄	Chitosan	Cadmium (II)	26.347	113
CS/NiFe₂O₄	Chitosan	Cadmium (II)	25.553	113

2.3. Adsorption Behavior

The rapid decline in potable water availability convinced the researchers of the world to find and investigate new and innovative methods for the treatment of wastewater. For this, invasive plants and bio-waste which are unwanted otherwise can be used as sorbents as such or after some treatment for the ecofriendly remediation of wastewater.¹¹⁴ Bio-wastes having low costs are preferred because of ecofriendly nature, easy availability, economical value etc.¹¹⁵ Bio-wastes alone were used for removing various target pollutants from the wastewater according to literature survey as represented in table 2.4. However, researchers are focusing more on bio-waste (agricultural wastes, forest waste etc.) in composition with ferrite nano particles using green synthesis to make synthesized material easily separable, more efficient, stable etc. and makes the compound more cost-effective as well as reliable. The use of bio-waste based spinel ferrites in the treatment of waste water is a less exposed area which needs to be strengthened as it leads to less generation of waste and cleaning of the environment.^{74,116} Table 2.5 showed various bio-wastes in combination with spinel ferrite nanoparticles composite used for removing dyes and metal ions from wastewater.

Table 2.4: Adsorption behaviour of bio-wastes used for the removal of different pollutants

S. No.	Bio-waste	Modified agent	Adsorbate	Langmuir Adsorption Capacity (mg/g)	Year	Reference
1.	Walnut shell	Citric acid	Zn(II)	28.58	2018	47
2.	Sugarcane bagasse soot	CO ₂ (Obtained activated carbon at 900°C)	Methylene blue	331	2017	73
3.	Sugar palm dregs	*	Methylene blue	23.866	2021	117
4.	Plantago ovata seeds	*	Malachite green Rose Bengal	86.23 81.23	2013	118
5.	Pine tree leaves	*	Methylene Blue	126.58	2012	119
6.	Pine cone biomass	*	Methylene Blue	109.89	2011	120
7.	Pine bark	*	Congo red		2019	121
8.	Neem sawdust Carbon	Carbonization (at 500°C)	Congo red	29.107	2010	122
9.	Araucaria angustifolia bark	*	Gentian violet dye	305.3	2018	123
10.	Pine cone	Phosphoric acid	Congo red	500	2014	124
11.	Cashew Nut shell	Carbonized(at 700°C), KOH, Nitrogen flow	Methylene Blue	68.72	2011	125
12.	Lemon grass ash	Muffle furnace(at 500°C)	Methylene Blue	413.22	2014	126
13.	Citrus limetta	Sulphuric Acid, NaOH	Methylene Blue	500	2017	127

S. No.	Bio-waste	Modified agent	Adsorbate	Langmuir Adsorption Capacity (mg/g)	Year	Reference
14.	Coir pith (Activated carbon)	Carbonization(at 700°C)	Congo red	6.72	2002	128
15.	Citrullus Lanatus Rind	*	Crystal violet	11.99	2012	129
16.	Mahogany sawdust (Activated carbon) Rice Husk (Activated carbon)	Carbonisation, steam activation	Acid Yellow 36	183.8 86.9	2003	130

* indicates that data is not given

Table 2.5: Adsorption behaviour of bio-waste based metal ferrite composites used for the removal of different pollutants

S. No.	Bio-waste	Modified agent	Magnetic material	Composite prepared	Adsorbate	Parameter studied	Langmuir Adsorption Capacity (mg/g)	Removal Efficiency (%)	Year	Reference
1.	Citrus limetta leaves (Activated Carbon)	Pulverized, activated (at 700°C)	CuFe ₂ O ₄	AC/CuFe ₂ O ₄	Methyl violet 2B	pH, Adsorbent dose, Temperature, Dye concentration, Contact time	80.65	97.85	2021	131
2.	Papaya Seeds(Porous Carbon)	Sulphuric Acid, Carbonization	CoFe ₂ O ₄	CoFe ₂ O ₄ @PC	Phosphate, Nitrate	Agitating time, adsorbent dosage, solution pH, co-existing ions	92.34 78.98	*	2020	132
3.	Wild plant based bio char (WPC)	Pyrolysis, nitrogen flow, carbonization	MnFe ₂ O ₄	MnFe@WPC	Cu(II)	Solution pH, adsorbent dosage, concentration, time, temperature	30.96	*	2021	133

S. No.	Bio-waste	Modified agent	Magnetic material	Composite prepared	Adsorbate	Parameter studied	Langmuir Adsorption Capacity (mg/g)	Removal Efficiency (%)	Year	Reference
4.	Banana Peel (Activated Carbon)	Burned(30°C), NaCl	MgFe ₂ O ₄	BPAC/ MgFe ₂ O ₄	Methylene blue	pH, Contact time, concentration	51.4	99.26	2020	134
5.	Coconut Shell (Activated Carbon)	Pyrolysis(700°C), Nitrogen flow	CoFe ₂ O ₄	CAC/ CoFe ₂ O ₄	Rhodamine B	Contact time, adsorbent dosage, dye concentration	107.48	92.34	2020	135
6.	Moringa oleifera seeds	Carbonisation (400°C), nitrogen flow, Sulphuric acid treatment	MnFe ₂ O ₄	MnFe ₂ O ₄ @MOAC	Reactive Blue 4, Indigo Carmine, Acid Blue 158	Contact time, adsorbent dosage, solution pH, initial concentration	32.45, 33.53, 35.27	86.35, 90.45, 92.65	2021	136
7.	Capra Aegagrus Hircus Dung (Activated Carbon)	H ₂ SO ₄ , Carbonized (at 500°C)	CoFe ₂ O ₄	(GDAC-CFMC)	Direct Brown 2, Reactive Red 152	Initial dye concentration, contact time,	66.66, 32.26	98.6, 99.3	2017	137

S. No.	Bio-waste	Modified agent	Magnetic material	Composite prepared	Adsorbate	Parameter studied	Langmuir Adsorption Capacity (mg/g)	Removal Efficiency (%)	Year	Reference
						adsorbent dosage, pH, temperature				
8.	Phoenix dactylifera stones(Activated Carbon)	Carbonization, sodium hydroxide	CoFe ₂ O ₄	AC/CoFe ₂ O ₄	Cr(VI)	pH, adsorbent dose, contact time, initial concentration	70.42	98.38	2018	138
9.	Muskmelon peel(Activated Carbon)	Sulphuric acid, carbonization	ZnFe ₂ O ₄	AC/ZnFe ₂ O ₄	Phosphate and nitrate ions	Shaking time, solution pH, temperature, interfering ions	91.80, 75.58	*	2020	139
10.	Apocynaceae leaf waste(Activated Carbon)	Phosphoric acid, pyrolysis (absence of air)	CoFe ₂ O ₄	ALW/CoFe ₂ O ₄	Reactive red 141	pH, adsorbent dosage, concentration, temperature	83.33	94.12	2019	140

2.4. Regeneration

The adsorbent's regeneration and reusability significantly reduces the operational expenses of water treatments. This enables the elimination of pollutants from the adsorbent's surface. Stability, recyclability as well as reusability are crucial factors in the practical application of material on commercial scale.¹⁴¹ For the regeneration of adsorbents, various approaches have been employed. In literature studies, different desorption agents have already been reported that remove loaded contaminants from adsorbent's surface. Selection of the desorption agent is influenced by a number of parameters like concentration, temperature and pH. Specifically, the value of pH is an important parameter which determines the effectiveness of inorganic and organic chemical pollutants desorption from the surface of an adsorbent. Table 2.6 shows different desorbing agents that have been utilised for removing various dyes and metal ions from the different adsorbent surfaces.^{59,66}

Table 2.6: Different desorbing agents used for the regeneration of adsorbents

Adsorbent	Adsorbate	Desorbing Agent	Concentration of desorbing agent	Reference
CoFN-Alg	BG	HCl	0.1N	142
	MB			
CoFN-Alg	CR	NaOH	0.5M	142
CoFe ₂ O ₄	Thiazole yellow G (TYG)	NaOH	0.1M	76
	Alizarin yellow R (AYR)			
CaFe ₂ O ₄	CR	Ethanol/Na ₃ PO ₄	(1:1)	83
CoFe ₂ O ₄	Eriochrome Black T	Methanol	(1:1)	85
	(EBT)			
	Bromophenol Blue (BRB)			
ZFN-Alg	Pb(II)	HCl	0.1N	42
	Cu(II)			
MgFe ₂ O ₄	Mn ²⁺	MgCl ₂	10 ⁻³ M	143
	Co ²⁺			
	Ni ²⁺			
	Cu ²⁺			

Adsorbent	Adsorbate	Desorbing Agent	Concentration of desorbing agent	Reference
GAC/MnFe ₂ O ₄	As(III)	NaOH	0.05M	144
	As(V)			
DMSA@Fe ₃ O ₄ MNRs	Pb(II)	HCl	0.01M	145
PTFAC	CR	Distilled water	*	33
	RhB			
MZF-BC ₅₀	Pb ²⁺	HCl	0.2M	146
CoFe ₂ O ₄ @PC	Phosphate	NaOH	0.1M	132
	Nitrate			
CpMA	Cu(II)	HCl	0.30M	147

Regeneration is a cyclic process in which the used adsorbent is taken after the adsorption procedure and reused again. By following the appropriate procedure, the regenerability of the used adsorbent can be calculated. Figure 2.3 shows the schematic representation of various cycles of regeneration process.

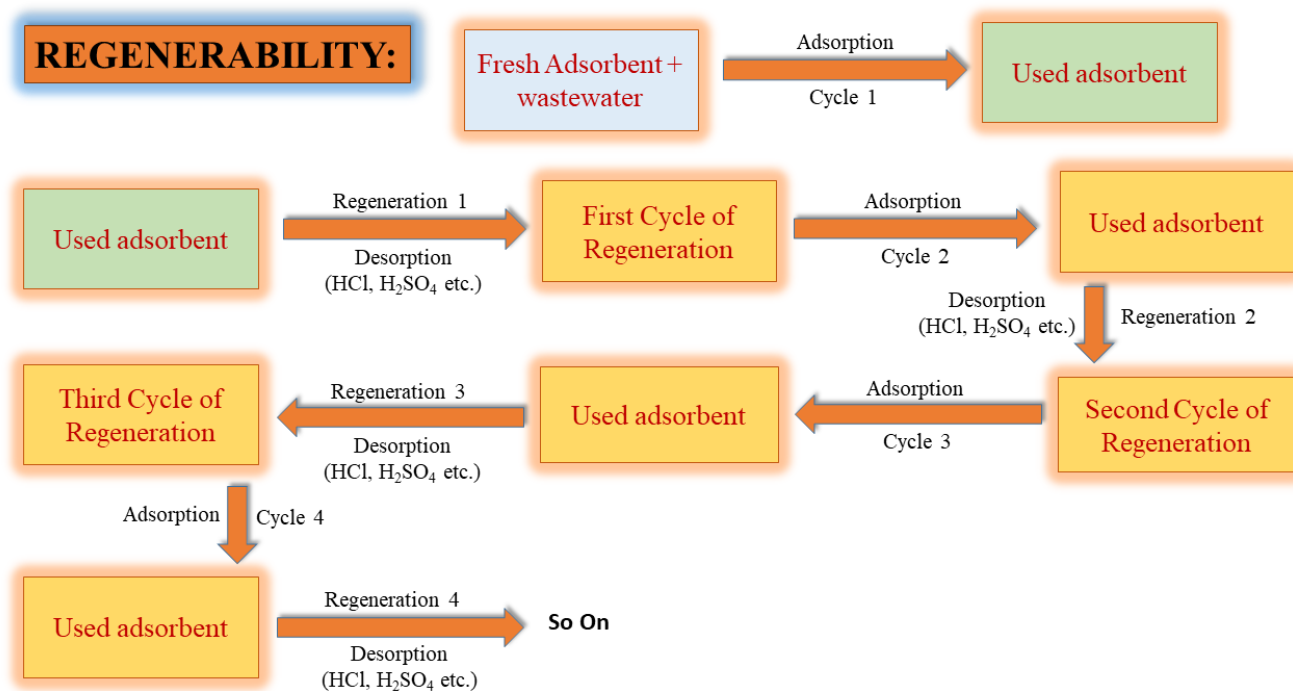


Figure 2.3: Schematic representation showing various cycles of regeneration process

2.5. Need for the Study

The global demand for clean water keeps increasing on a regular basis. According to research studies, the adsorption technique provides a strong potential for waste water treatment with remarkable outcomes. This approach is extensively adopted in treating wastewater owing to its cost effectiveness, simplicity and minimal space requirements than alternative methods. Adsorbents of different varieties have already been used to treat waste water. Among the different adsorbents, nano materials in form of metal ferrites are being used for treating the waste water and became a rapidly growing area.

On the basis of literature survey, the combustion method among others is regarded to be the simplest, cost efficient and least time consuming method for the nano metal ferrites synthesis. The usage of ferrites both individually and with surface treatments using other metals, polymers and surfactants has proven that these materials with magnetic properties are effective alternative adsorbents that possess good adsorption abilities. As a result, there is a need for further study using spinel nano metal ferrite bio-waste based composites for pollutant removal from waste water. As per literature study, less number of studies on the adsorption behaviour of bio-waste based nano ferrites composites have yet been reported. It suggests that modifying the surface of magnetic nano ferrites using bio-wastes is still a less explored field which needs to be strengthened. A survey of the literature also shows that pine cone, walnut shell and pistachio shell bio-wastes have significant adsorption capacity for removing various kinds of contaminants from waste water. There has been less work reported for spinel metal ferrites in combination with bio-wastes such as pine cone, walnut shell and pistachio shell to develop effective adsorbents. Therefore, further research in this area needs to be done. Adsorbent's regeneration following the process of adsorption is a cost-effective approach for which limited research articles have been published. As a result, the current research study aims at the synthesis of spinel metal ferrites and modification of their surface with different bio-wastes in order to develop magnetic bio-waste composites which have greater adsorption capacity and selectivity towards certain dyes and heavy metals. Bio-waste based ferrite nano particles in adsorption is an innovative area of research which is environmentally sustainable as well as economical in nature.

2.6. Objectives of the Research Work

From the above review of literature, it has been identified that bio-wastes act as good

adsorbents as they show strong adsorption capacity for removing both dyes and metal ions but still some work in this field is unexplored that could yield even better adsorption outcomes. As green synthesis is highlighted more from last one decade due to the increased level of pollution, so there is a need to treat waste water by using bio-wastes along with spinel ferrite nano particles and will try to explore further in this field. The regeneration study was performed to know about the efficiency and cost effectiveness of the material. The prepared composite has been regenerated after the adsorption procedure and then reused again for adsorption.

The proposed objectives for the current research study is as follows:

1. To synthesize different transition metal ferrites by low temperature combustion method.
2. To develop and characterize bio-waste based spinel ferrite composites.
3. To test adsorption potential of developed composites for the removal of dyes/heavy metals.
4. To analyse the adsorption behaviour in single and multiple adsorbate system.
5. To study regeneration potential of synthesized composites and to reuse the adsorbent.

CHAPTER-3

MATERIALS AND METHODS



3.1. Materials Used

All the chemical reagents utilized were of an analytical grade and utilized in their original state without any additional purification. Zinc Chloride, Cobalt Chloride, Nickel Sulphate, Cupric Chloride, Ferric Chloride, Diethyl Oxalate, Hydrazine Hydride, Sodium Hydroxide, Glutaraldehyde, Crystal Violet, Methylene Blue, Brilliant Green, Malachite Green, Congo Red, Hydrochloric Acid, Cupric Sulphate, Hydroxylamine Hydrochloride, Sodium Citrate etc. were taken from Loba Chemie Reagent Co. Ltd. Disodium Bathocuproine Disulfonate was purchased from Central Drug House (P) Ltd. All other apparatus and the glassware used for the experimental study underwent cleaning with distilled water to eliminate all the dirt and impurities.

3.2. Experimental Method

3.2.1. Synthesis of Metal Ferrite Nanoparticles using Combustion Method

Different spinel metal ferrites such as CuFe_2O_4 , NiFe_2O_4 , CoFe_2O_4 and ZnFe_2O_4 were synthesized using the low temperature combustion approach. For spinel metal ferrites, the standard formula is MFe_2O_4 , where 'M' may represent Cu, Co, Ni or Zn etc. According to the stoichiometric equation of spinel metal ferrite, the intended product should have a ratio of 1:2:4. To accomplish this, stoichiometric aqueous solutions of the required metal salt and iron salt have been mixed in separate beakers in a ratio of 1:2 using distilled water in a saturated condition. Oxalyldihydrazide (ODH) works as reaction fuel and is used to initiate the reaction in solution mixture. Oxalyldihydrazide was prepared by slowly combining diethyl oxalate and hydrazine hydrate in a w/w ratio of 1:2 with continuous stirring at an ambient room temperature. Following the completion of the mixing process, the white powder obtained was permitted to air dry at ambient temperature.^{58,142} The saturated solution of particular metal salt and iron salt had been mixed together in a glass beaker and then the prepared ODH was gradually added into the above prepared mixture with vigorous stirring. The resultant solution was concentrated by heating it on water bath at temperature 70°C for the duration of two hours. Subsequently, the concentrated solution was subjected to annealing at temperature 600°C using a muffle furnace for three hours to complete the process. The ultimate product acquired was designated as ferrite of the desired metal.

3.3. Surface Modification of Spinel Metal Ferrites with Bio-Waste

Surface modification of several spinel ferrites have been achieved using various bio-wastes such as pine cone (PC), walnut shell (WS) and pistachio shell (PS). The subsequent sections provide a discussion of the surface modification.

3.3.1. Surface Modification with Pine Cone/Walnut Shell/Pistachio Shell

The pine cones were gathered from the Shivalik hills region of district Kathua (Jammu and Kashmir) while the walnut and pistachio shells were sourced from local markets of Jalandhar (Punjab). The bio-wastes were cleaned with tap water for removing dirt, then rinsed using distilled water. Subsequently, dried in hot air oven at 50°C to remove moisture, then crushed and sifted to achieve uniform size of the particle.

The pine cone/walnut shell/pistachio shell powder was mixed with distilled water to produce a 2% homogenous solution of pine cone/walnut shell/pistachio shell powder which was then stirred at 300 rpm (revolutions per minute) for approximately one hour using mechanical stirrer. To each aforementioned 2% solution, 2 g of metal ferrite in 10 mL of DW was added and the mixture was agitated for about an hour. To create homogenous bio-composite, the above mentioned mixture solution was combined with 0.5M NaOH solution along with 10% Glutaraldehyde as the crosslinking agent and stirred for 30 minutes. The composite is then reduced to a consistent size by stirring it with a glass rod. The final solution of the bio-composite was stored overnight. Subsequently, the bio-composite was separated using filtration and the resulting filtrate was then subjected to several washes with distilled water before being dried at temperature 50°C to get the desired product. The schematic representation of the composite synthesis using various ferrite and bio-wastes is presented as figure 3.1.

The obtained magnetic composite had been designated as metal ferrite pine cone composite, metal ferrite walnut shell composite and metal ferrite pistachio shell composite. The composites prepared in this study using above mentioned method are presented in table 3.1.

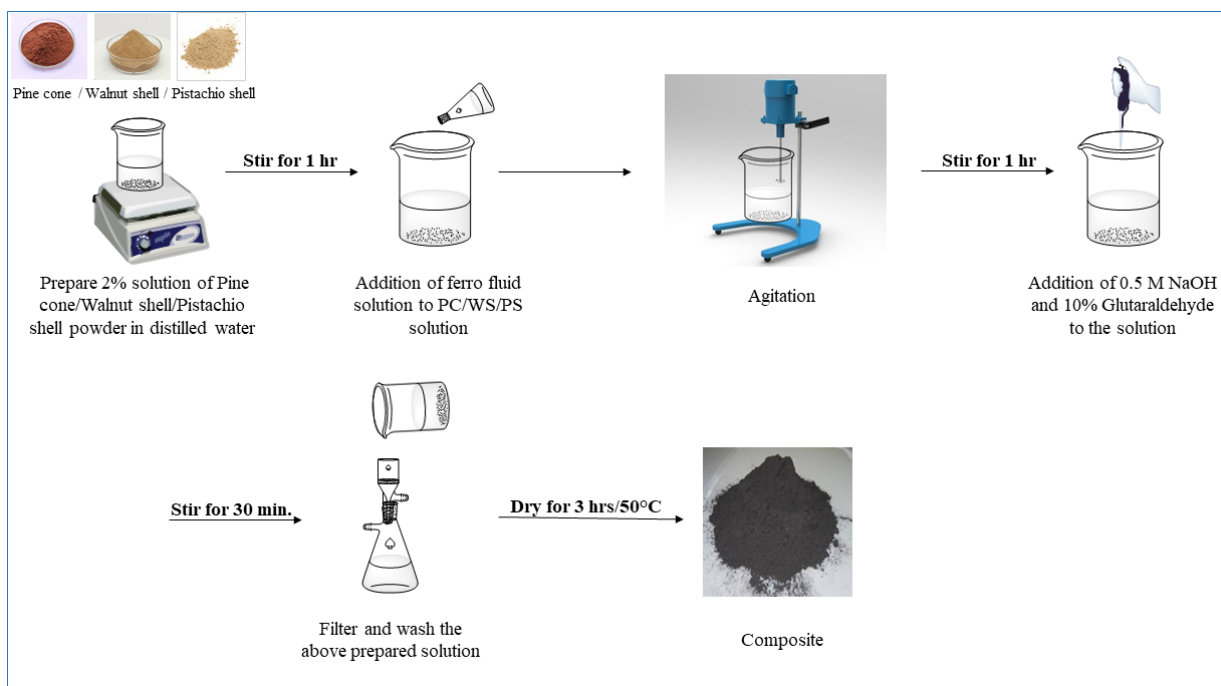


Figure 3.1: Synthesis of bio-waste based composites

Table 3.1: List of different composite prepared

Bio-waste	Composites Prepared			
Pine cone	Zinc ferrite pine cone (ZFPC)	Cobalt ferrite pine cone (CoFPC)	Nickel ferrite pine cone (NFPC)	Copper ferrite pine cone (CuFPC)
Walnut shell	Walnut shell zinc ferrite (WSZF)	Walnut shell cobalt ferrite (WSCoF)	Walnut shell nickel ferrite (WSNF)	Walnut shell copper ferrite (WSCuF)
Pistachio shell	Zinc ferrite pistachio shell (ZFPS)	Cobalt ferrite pistachio shell (CoFPS)	Nickel ferrite pistachio shell (NFPS)	Copper ferrite pistachio shell (CuFPS)

3.4. Preliminary Adsorption Studies

Based on preliminary studies, it is feasible to assess the selective properties of various metal ferrite composites. Different materials such as bio-waste based and chemically treated bio-waste based metal ferrite composites were examined. However, the outcomes from chemically treated bio-waste based composites didn't notably differ in terms of removal efficiencies compared to those from raw bio-waste based composites. Therefore, for subsequent experimentation, raw bio-waste based metal ferrite composites were chosen because they result in low resource and energy consumption, aligning with the

principles of green synthesis. The selectivity of different metal ferrite bio-waste based composites was evaluated using different dyes and metal ions. A comprehensive description of the preliminary adsorption studies is provided in the section 3.4.1 and 3.4.2.

3.4.1. With Dyes

A variety of dyes (anionic and cationic) in aqueous solutions were used for studying the adsorption characteristics of metal ferrite pine cone and metal ferrite walnut shell composites. Research on the adsorption performance of the aforementioned metal ferrites along with their bio-waste based composites was conducted using a variety of dyes including crystal violet (CV), brilliant green (BG), malachite green (MG), methylene blue (MB) and congo red (CR). Research on adsorption behavior of the different dyes had been conducted using the batch adsorption method. In preliminary experiments, 0.1g of metal ferrite composite was mixed with 50 mL of adsorbate with a known concentration and shaken at 200 rpm for a set time period. The samples were then taken out and the adsorbent was separated by using a magnet. UV-VIS spectrophotometer (SHIMADZU-1900I) was used to assess the decreased dye concentration. For dyes CV, MB, CR, BG and MG, the maximum wavelengths (λ_{max}) utilized were 590 nm, 664 nm, 497 nm, 625 nm and 617 nm respectively. Table 3.2 shows the findings of preliminary research study using metal ferrites and their bio-waste based composites for dye removal.

Table 3.2: Preliminary results showing percentage removal of various dyes

S. No.	Adsorbent	Percentage removal				
		Crystal Violet	Methylene Blue	Brilliant Green	Malachite Green	Congo Red
Bio-Waste						
1.	Pine cone	62.1	49.6	52.4	60.6	42.8
2.	Walnut Shell	59.6	49.8	50.4	54.8	46.7
Zinc ferrite and their composites						
1.	Zinc ferrite	47.2	41.6	45.9	54.8	30.1
2.	Zinc ferrite pine cone (Composite)	84.5	80.1	64.9	89.4	20.1

S. No.	Adsorbent	Percentage removal				
		Crystal Violet	Methylene Blue	Brilliant Green	Malachite Green	Congo Red
3.	Walnut shell zinc ferrite (Composite)	72.6	81.8	75.4	90.2	19.8
Nickel ferrite and their composites						
1.	Nickel ferrite	34.2	28.6	31.9	38.4	36.5
2.	Nickel ferrite pine cone (Composite)	69.8	78.6	82.7	77.4	23.1
3.	Walnut shell nickel ferrite (Composite)	60.5	52.6	56.7	60.1	17
Cobalt ferrite and their composites						
1.	Cobalt ferrite	50.1	32.4	35.2	42.4	30.4
2.	Cobalt ferrite pine cone (Composite)	64.1	53.2	55.6	61.9	24.4
3.	Walnut shell cobalt ferrite (Composite)	89.4	85.8	90.4	82.8	20.8
Copper ferrite and their composites						
1.	Copper ferrite	40.4	32.6	35.8	41	33.7
2.	Copper ferrite pine cone (Composite)	30.2	22.6	33.8	31.4	14.6
3.	Walnut shell copper ferrite (Composite)	22.4	19.8	26.7	30.9	20.4

In comparison to uncoated metal ferrite, it was noted that zinc ferrite pine cone (ZFPC), nickel ferrite pine cone (NFPC), walnut shell zinc ferrite (WSZF) and walnut shell cobalt ferrite (WScOF) composites exhibited a higher percentage of removal for cationic dye crystal violet (CV), methylene blue (MB), brilliant green (BG) and malachite green (MG) during the process of adsorption. The percentage removal was noticed to be decreased while using various composites for the removal of congo red (CR) which is an anionic dye.

Both pine cone and walnut shell bio-waste have reactive functional groups present in their structures. These include hydroxyl, carboxylic acids as well as other favorable groups which facilitate the efficient removal of cationic dyes. The existence of anionic functional groups on bio-waste based metal ferrite composites surface results in a negative charge. Thus functional groups provide specificity towards particular type of pollutants. Consequently, a surface with a negative charge easily attracts cationic dyes and results in higher percentage removal. However, a reduction in the percent removal of anionic CR dye was observed because both the adsorbent and the molecules of anionic dye had similar charges on their surface. This suggests that the composites prepared for this research work showed more selectivity towards the cationic species.

These findings led to the selection of ZFPC, NFPC, WSZF and WScOF composite for further adsorption investigations of cationic dyes CV, MB, BG and MG from dye containing wastewater. The adsorption experiments indicated that the percent removal of various dyes using pure metal ferrite was much lower as compared to the bio-waste based ferrite composites. The adsorption behavior of dye CV, BG, MB and MG was investigated using different composites.

3.4.2. With Metal Ions

Ni(II) and Cu(II) was investigated using bio-waste, pure metal ferrites and with metal ferrite bio-waste composite. The preliminary examination of heavy metals was conducted by employing the same method used for dyes. The concentration of metal ions in the samples was assessed using a UV-VIS Spectrophotometer (SHIMADZU-1900I). Different metal ferrite composites such as zinc ferrite pistachio shell (ZFPS), nickel ferrite pistachio shell (NFPS), copper ferrite pistachio shell (CuFPS) and cobalt ferrite pistachio shell (CoFPS) were prepared and used for the removal of Ni(II) and Cu(II) metal ion from the aqueous solutions. The composites CuFPS and CoFPS showed very less removal

effectiveness followed by ZFPS for both the heavy metal ions whereas NFPS showed good removal for Cu(II) ion. Therefore, NFPS composite was shortlisted as efficient adsorbent for removing Cu(II) from metal ion containing wastewater and used further for adsorption studies. Table 3.3 presents the percentage removal of different heavy metal ions.

Table 3.3: Preliminary results showing percentage removal of heavy metals

S. NO.	Adsorbent	Percentage Removal	
		Ni(II)	Cu(II)
Bio-waste			
1.	Pistachio shell	35.4	48.9
Nickel Ferrite and their composites			
1.	Nickel Ferrite	7.9	24.2
2.	Nickel Ferrite Pistachio Shell (Composite)	38.1	68.4

3.5. Characterization of Metal Ferrites and their Composites

The morphological behaviour and surface characterization of various magnetic ferrites and their corresponding bio-waste composites has been studied using number of techniques.

3.5.1. Fourier Transform Infrared (FTIR) Analysis

Fourier Transform Infrared (FTIR) Spectroscopy is a significant analytical technique utilized to recognize and characterize functional groups of a wide range of materials by examining their interaction with IR (Infrared) radiation. The surface of metal ferrites and prepared composites were characterized using a Perkin-Elmer Spectrum 2 FT-IR spectrophotometer and Bruker (Model: Tensor 27) within the range of 4000-400 cm^{-1} .¹⁴⁸⁻¹⁵⁰ FTIR functions based on the concept that molecules selectively absorb distinct frequencies of infrared light, inducing vibrational transitions between different energy states. These vibrational transitions are characteristic of the chemical bonding in a molecule.

3.5.2. X-Ray Diffraction (XRD) Analysis

X-ray diffraction (XRD) is a method of analysis utilized for determining the crystal structure of material. It relies on the principle of X-ray scattering by crystal lattice planes. X-ray diffractometer (Bruker D8 Advance) was used to investigate the crystallite structure of the material.^{20,151} The basic principle of XRD is based on Bragg's law, which outlines the relation between the angle of X-ray incidence, the X-ray wavelength and the separation between atomic planes within a crystal lattice. When X-rays interact with a crystal, they undergo diffraction due to the orderly arrangement of atomic planes inside the crystal lattice. The resulting diffraction pattern provides information about the crystal structure. X-ray diffraction is widely applied in various scientific fields including materials science, chemistry, geology and biology. It provides detailed information about the atomic arrangement within crystalline materials making it an essential tool for structural characterization.

The formula for calculating average crystallite size was calculated by using Scherrer formula which is as follows-^{76,143}

$$D = \frac{0.89\lambda}{\beta \cos\theta} \quad (3.1)$$

where, 'D' is crystallite size, 'λ' is the X-Ray wavelength, 'θ' is diffraction angle and 'β' is broadening peak.

3.5.3. Scanning Electron Microscope (SEM) Analysis

A Scanning Electron Microscope (SEM) is a tool utilized for high-resolution imaging and examination of surfaces at both the micro and nanoscale levels. The scanning electron microscope (JEOL JSM-7610F Plus) and Carl Zeiss, Germany (Model: Merlin Compact) was utilized to analyze the composite's size and morphological structure. The basic principle of SEM includes the interaction of electrons with a sample to create detailed images and gather information about its topography, composition, and other characteristics.^{149,152,153} In summary, SEM analysis involves focusing an electron beam on a conductive or coated sample, capturing the signals generated by the interaction and using detectors to produce high-resolution images and gather information about the sample's surface characteristics.

3.5.4. Energy Dispersive Spectra (EDS) Analysis

Energy Dispersive Spectroscopy (EDS) is used to determine elemental composition of materials using model EDS: OXFORD EDS LN2 free. It is often coupled with electron microscopes, such as scanning electron microscopes (SEM) or transmission electron microscopes (TEM) to provide details regarding the chemical composition of the sample.^{42,84,149} EDS relies on the principle that when electrons with high-energy interact with a material, they can knock inner shell electrons from atoms. Subsequently, outer shell electrons fall into the vacancies left by the ejected inner shell electrons, and X-rays are emitted during this process. The energy of these characteristic X-rays correlates directly with the energy differences between the involved electron shells and is specific to elements present in the sample. EDS is a valuable tool in various other fields where detailed information about the elemental composition of samples is essential.

3.5.5. Brunauer-Emmett-Teller (BET) Analysis

The Brunauer-Emmett-Teller (BET) is an analytical technique utilized to determine the surface area of the porous materials. The method relies on the physical adsorption of molecules of gas onto the surface of a solid material. BET was studied using BET analyser Quantachrome® ASiQwin™ [Version 5.21] and Nova series [M/s. Anton Paar]. The BET theory is grounded in the multilayer adsorption of gas molecules onto a solid surface. It assumes that gas molecules form layers on the surface of material and the surface area can be determined by analyzing the adsorption isotherm, which relates the amount of adsorbed gas to the relative pressure. The BET analysis provides valuable information about the specific surface area distribution of the porous materials, aiding in the characterization of catalysts, adsorbents, and other substances where surface properties are crucial.^{27,153}

3.5.6. Thermogravimetric Analysis (TGA)

Thermogravimetric Analysis (TGA) is a method employed to examine alterations in the mass of a sample in response to temperature (or time) variations, under controlled atmospheric conditions. Thermogravimetric analyzer Perkin Elmer TGA 4000 was utilized to determine the material's thermal stability.^{133,154,155} TGA is based on the principle that changes in the mass of a sample can occur due to various processes, such as decomposition, oxidation, reduction, dehydration or volatilization. By monitoring the fluctuations in the mass of a sample as it undergoes heating or cooling within a controlled

environment, valuable information about its thermal stability, composition, and reaction kinetics can be obtained. TGA is widely used in different fields to investigate the thermal behavior of material and determine decomposition temperature.

3.5.7. pH of Point Zero Charge (pH_{pzc}) Analysis

The pH of point zero charge (pH_{pzc}) is a property of a solid surface and it refers to the pH level where the surface charge becomes neutral meaning that the surface is neither positively nor negatively charged^{143,156}. The pH_{pzc} is a key aspect in considering the performance of materials in aqueous solutions particularly in fields such as colloid chemistry, surface science and environmental science. It relies on the principle that the charge on a solid surface is effected by the dissociation of functional groups present on the surface. In the context of point zero charge of the material, the pH of surrounding solution determines the charge on the surface of adsorbent. At the zero-point charge, the concentration of protons (H⁺ ions) in solution is such that it exactly compensates the charge on the surface, resulting in a neutral surface charge. The pH of point zero charge was determined using solid addition method. The solid samples (0.1 g) were suspended in solution containing 50 mL 0.1M KNO₃ which were taken in 250 mL conical flasks with varying pH values ranging from 3-11. The solution's pH was adjusted by adding either HCl or NaOH. The solution was placed in orbital shaker for 24 hours at 30°C. The difference between the pH values was calculated using following equation.

$$\Delta\text{pH} = \text{pH}_i - \text{pH}_f \quad (3.2)$$

A graph was plotted between initial pH and ΔpH .

Then pH_{zpc} can be determined graphically by finding the intersection of the surface charge curve at the pH axis.^{157,158}

3.6. Batch Adsorption Studies

Dyes such as CV, MB, BG and MG in the single, binary, ternary dye system and Cu(II) metal ion were studied using batch adsorption method to determine the adsorption potential of selected composites as discussed in section 3.4.1 and 3.4.2. The reduced concentration of the adsorbate had been determined using UV-VIS spectrophotometer (SHIMADZU-1900I).

The effect of contact time, adsorbent dose, pH, concentration and the temperature was studied using metal ferrite bio-waste composites. The process described in the preliminary studies was utilized for the adsorption studies and the parameters such as equilibrium time of 3 hours, adsorbent dosage 0.1-0.5 g, pH range 3-11, dye concentration 50-250 mg/L (for single system) and 20-100 mg/L (for binary and ternary system), temperature 25°C, 30°C and 35°C were kept constant during the entire study.

3.7. Single, Binary and Ternary Dye System

The stock solutions for dyes CV, BG, MG and MB were made by adding 1 g of dye in 1L of DW which gave 1000 mg/L solution for each dye. This solution was further diluted with DW to get working solutions of desired concentration. For conducting adsorption studies in single as well as multiple dye system, a defined quantity of metal ferrite composite was added to 250 mL conical flasks that held a given volume (50 mL) of adsorbate at a known concentration and were shaken in a thermostatic shaker at speed 200 rpm for a predetermined period of time. The samples were removed and the adsorbent was separated using a bar magnet after the completion of experimentation. By determining the absorbance of solution using UV-VIS Spectrophotometer, the remaining amount of dye was determined. λ_{\max} values 590 nm, 624 nm, 617 and 664 nm were used to determine the dye concentration of CV, BG, MG and MB respectively.

3.7.1. Single Dye System

The equations used for calculating 'Q_e' adsorption capacity (mg/g) and percentage removal are given as:^{121,153,159}

$$Q_e = \frac{(C_o - C_e)}{m} \times V \quad (3.3)$$

$$\text{Removal percent} = \frac{(C_o - C_e)}{C_o} \times 100 \quad (3.4)$$

where, C_o and C_e are the concentration of dye at initial state and equilibrium state, respectively (mg/L), 'V' is the volume of dye solution (L) and 'm' is the mass of adsorbent (g).

3.7.2. Binary Dye System

For calculating the concentrations of components A and B in the binary system of dyes, the following equations had been used:^{158,160,161}

$$C_A = (K_{B2}d_1 - K_{B1}d_2)/(K_{A1}K_{B2} - K_{A2}K_{B1}) \quad (3.5)$$

$$C_B = (K_{A1}d_2 - K_{A2}d_1)/(K_{A1}K_{B2} - K_{A2}K_{B1}) \quad (3.6)$$

Where, the calibration constants of A and B in a binary dye solution at wave lengths 1 and 2 are K_{A1} , K_{B1} , K_{A2} , and K_{B2} . The OD (optical densities) of a dye mixture at positions 1 and 2 are d_1 and d_2 , respectively. Pure components A and B have absorption calibration constants K_{A1} and K_{B1} at the maximal wavelengths of component A. Similar to this, K_{A2} and K_{B2} are calibration constants of absorption for pure components A and B in the optimum wavelength of component B.

3.7.3. Ternary Dye System

Equations for determining the concentrations of components A, B and C in a ternary system of dyes are as follows:^{83,142,162}

$$C_A = (d_1X + d_2Y + d_3Z)/(K_{A1}X + K_{A2}Y + K_{A3}Z) \quad (3.7)$$

$$[X = K_{B3}K_{C2} - K_{B2}K_{C3}; Y = K_{B1}K_{C3} - K_{B3}K_{C1}; Z = K_{B2}K_{C1} - K_{B1}K_{C2}]$$

$$C_B = (d_1X' + d_2Y' + d_3Z')/(K_{B1}X' + K_{B2}Y' + K_{B3}Z') \quad (3.8)$$

$$[X' = K_{A2}K_{C3} - K_{A3}K_{C2}; Y' = K_{A3}K_{C1} - K_{A1}K_{C3}; Z' = K_{A1}K_{C2} - K_{A2}K_{C1}]$$

$$C_C = (d_1X'' + d_2Y'' + d_3Z'')/(K_{C1}X'' + K_{C2}Y'' + K_{C3}Z'') \quad (3.9)$$

$$[X'' = K_{A2}K_{B3} - K_{A3}K_{B2}; Y'' = K_{A3}K_{B1} - K_{A1}K_{B3}; Z'' = K_{A1}K_{B2} - K_{A2}K_{B1}]$$

where, K_{A1} , K_{A2} , K_{A3} , K_{B1} , K_{B2} , K_{B3} , K_{C1} , K_{C2} , K_{C3} denotes calibration constants of components A, B, C at different wavelengths i.e.; λ_1 , λ_2 and λ_3 respectively. At different wavelength, the optical density of dye mixture is written as d_1 , d_2 and d_3 . The adsorption coefficients for pure substances A, B and C at their respective maximum wavelength λ_1 for Component A are K_{A1} , K_{B1} and K_{C1} . K_{A2} , K_{B2} , K_{C2} and K_{A3} , K_{B3} , K_{C3} are coefficient of adsorption for pure dyes A, B and C at a wavelength λ_2 and λ_3 for components B and C, respectively.

3.8. Metal Ion System

For conducting adsorption experiments of heavy metal ion, the same procedure like dye adsorption was followed first. After the removal of samples from orbital shaker, the adsorbent was separated using a magnet followed by the standard procedure (given

below) used for the estimation of heavy metal ion by UV-VIS method. By determining the absorbance of solution using UV-VIS Spectrophotometer, the reduced concentration of metal ion samples was determined.¹⁶³

3.8.1. Solution Preparation for Heavy Metal Ion

A 1000 mg L⁻¹ solution of Cu(II) was prepared and DW was used to dilute the stock solution in order to prepare all working solutions. Comprehensive details regarding the procedure are provided in the subsequent section.¹⁶³

Estimation of Cu(II) Ions

A solution with a concentration 1000 mg/L of Cu(II) ions was obtained by dissolving 3.93 g of CuSO₄.5H₂O in 1L of DW. This resulted in the preparation of a stock solution of Cu(II). For the determination of Cu(II) concentration, the subsequent methodology has been implemented.

➤ Reagents Used

- 1:1 hydrochloric acid.
- Hydroxylamine hydrochloride solution: 50g NH₂OH.HCl were dissolved in 450 mL distilled water.
- Sodium citrate solution: 300g Na₃C₆H₅O₂.2H₂O were dissolved in distilled water and further distilled water was added to bring the total volume up to 1000 mL.
- Disodium bathocuproine disulfonate solution: 1g of C₆H₄N₂(CH₃)₂(C₆H₄)₂(SO₃Na)₂ was dissolved in DW and the final volume was made up to 1000 mL.

➤ Procedure

1 mL aliquot of the sample was diluted to 10 mL with distilled water. From this solution, 1 mL had been taken in 50 mL measuring flask. To this solution, 1mL of 1:1 HCl solution was added which was further followed by 4 mL NH₂OH.HCl solution, addition of 4 mL Na₃C₆H₅O₂.2H₂O solution and 4 mL C₆H₄N₂(CH₃)₂(C₆H₄)₂(SO₃Na)₂ solution respectively. The absorbance of solution was noted at 484 nm.

3.9. Regeneration Study of the Adsorbent

The adsorbent was separated from the dye solution and was collected after completion of adsorption process with Cu(II) and various dyes in single, binary and ternary dye system. The 250 mL Erlenmeyer flask containing dye saturated adsorbent having 50 mL

desorbing solution was placed in an orbital shaker and had been shaken at 110 rpm for a specific period of time. For dyes and metal ions, 0.1N HCl solution had been used as a desorbing agent. An adsorbent that had been regenerated was separated by filtration, dried and then utilised for the subsequent adsorption cycle. The adsorbent's regeneration efficiency was determined using the following equation:^{83,85,164–166}

$$\text{Regeneration efficiency (\%)} = \frac{\text{Amount of dye adsorbed in (n+1)th cycle}}{\text{Amount of dye adsorbed in nth cycle}} \times 100 \quad (3.10)$$

3.10. Adsorption Kinetics

The behaviour of adsorption exhibits time dependent nature. Therefore kinetic behaviour is quite important in understanding the nature of adsorption. The adsorption kinetic behaviour of synthesised magnetic bio-waste composites with Cu(II) metal ion and different cationic dyes in the single, binary and ternary systems had been studied using several kinetic models. These include the Lagergren pseudo first order model, pseudo second order model, the Elovich model and Weber Morris model.^{155,156} The kinetic models were fitted with the data acquired from adsorption experiments in order to determine the impact of contact time and to identify the optimal kinetic model.

3.10.1. Lagergren Pseudo First Order Model

The Lagergren pseudo first order model is an extension of traditional pseudo-first-order kinetic model, specifically applied to describe the kinetics of adsorption processes. This model is named after Swedish chemist Sven Erik Lagergren, who developed it in the early 20th century. The Lagergren model introduces an exponential term to account for the probability of adsorption, presuming that the rate of adsorption is proportionate to the number of unoccupied sites on the adsorbent's surface. The Lagergren pseudo first order model is commonly applied in the study of adsorption kinetics, especially for the adsorption of solutes or gases onto the solid surfaces. It serves to analyse data obtained from adsorption isotherms and provides insights into the rate at which adsorption occurs. The linearized equation of Lagergren pseudo-first-order kinetic model is as follows:^{117,167–169}

$$\log(Q_e - Q_t) = \log Q_{e1} - \frac{k_1}{2.303} t \quad (3.11)$$

where, Q_{e1} and Q_t represent the total amount of pollutant that has been adsorbed on adsorbent at equilibrium state and at time 't' (mg/g), k_1 is the Lagergren pseudo first order

rate constant (per min.). The values of various constant were determined using intercept of the plot $\log (Q_e - Q_t)$ vs t .

3.10.2. Pseudo Second Order Model

The pseudo-second-order model is another extensively used approach to characterize the kinetics of different chemical and physical processes, particularly in the context of adsorption onto solid surfaces. The pseudo-second-order model is commonly applied in studying the adsorption kinetics, especially for the adsorption of gases or solutes onto solid surfaces. This model aids in analysing experimental data derived from adsorption isotherms, offering insights into the rate of adsorption. It suggests that the rate-determining step involves chemisorption, where the adsorbate establishes a chemical bond with adsorbent surface. The linear equation of pseudo second order model is:^{84,149,170-172}

$$\frac{t}{Q_t} = \frac{1}{K_2 Q_e^2} + \frac{t}{Q_e} \quad (3.12)$$

where, Q_{e2} and Q_t represent the amount of adsorbate that is adsorbed per gram of adsorbent at the equilibrium state and at time 't' (mg/g), h is equal to $k_2 Q_e^2$, and k_2 is pseudo second order kinetics rate constant (mg/min). The linear relationship between t and Q_t is represented by the graph, which is utilised to determine Q_e and K_2 .

3.10.3. Elovich Model

Elovich kinetic model is commonly used to define the kinetics of chemisorption. It was introduced by I. Elovich in 1962. The Elovich equation is often applied to study the adsorption of gases or solutes onto solid surfaces. This model posits that the sites available for adsorption on the surface are energetically heterogeneous and that the adsorption process involves a distribution of activation energies. According to this model, the rate of adsorption reduces exponentially with time, indicating gradual occupation of adsorption sites.^{167,168,173} The linear formula of Elovich model is represented as:

$$Q_t = \frac{1}{\beta} \ln(\alpha\beta) + \frac{1}{\beta} \ln(t) \quad (3.13)$$

In the given context, α represents the rate of adsorption at initial stage (mg/min) while β signifies the activation energy for chemisorption (g/mg) and is associated with the extent of surface coverage.

A linear relationship is observed from the graph of Q_t versus $\ln t$, where the intercept is $1/\beta \ln(\alpha\beta)$ and the slope is $1/\beta$. The main limitation of the aforementioned model is the inability to ascertain the diffusion characteristics of both the adsorbate as well as adsorbent.

3.10.4. Weber-Morris Model

The Weber-Morris intra-particle diffusion model is often employed to study the adsorption kinetics of solutes onto solid surfaces, particularly when the rate-limiting step is intra-particle diffusion. The linear form of Weber-Morris model is expressed as:^{117,118,125,130,153,173}

$$Q_t = K_{int} t^{0.5} \quad (3.14)$$

where, Q_t is amount of adsorbate adsorbed at time 't', K_{int} is the intra-particle diffusion rate constant and t is the time.

The model suggests that if intra-particle diffusion is rate-limiting step, then the graph of Q_t versus $t^{0.5}$ should form a linear pattern starting from the origin. However, in many cases, the experimental data does not perfectly fit this model and additional steps or mechanisms may contribute to the overall adsorption process.

3.11. Adsorption Isotherms

Adsorption isotherms describe the relation between the quantity of adsorbate adsorbed per unit weight of the adsorbent and the concentration of the adsorbate in the solution at equilibrium at constant temperature. These isotherms are vital in understanding the behavior of adsorption process.^{174,175} For the present study, experimental data is typically fitted to different isotherm models including Langmuir, Freundlich, Temkin and Dubinin-Radushkevich (D-R) model to determine adsorption behavior.

3.11.1. Langmuir Isotherm

The Langmuir model of isotherm stands as a fundamental model in describing the adsorption of a gas or solute onto a solid surface. It was proposed by Irving Langmuir in 1916. The Langmuir isotherm assumes monolayer adsorption on a homogeneous surface. The Langmuir isotherm assumes no interaction between adsorbate molecules once they are adsorbed onto the surface. Each molecule acts independently.

The linear representation of the Langmuir isotherm equation is as follows:^{73,123,170}

$$\frac{1}{Q_e} = \frac{1}{Q} + \frac{1}{bQC_e} \quad (3.15)$$

where, Q_e represents the quantity of adsorbate adsorbed per unit mass of adsorbent at equilibrium, b denotes the Langmuir constant associated with adsorption energy (L/mg), Q signifies the maximum adsorption capacity (theoretical monolayer coverage) in mg/g and C_e indicates the equilibrium concentration of the adsorbate in the fluid phase. The relationship between $1/Q_e$ and $1/C_e$ is represented by a straight line with a slope of $1/bQ$ and an intercept of $1/Q$.

3.11.2. Freundlich Isotherm

The Freundlich isotherm model is an empirical equation which describes the adsorption of a solute onto solid surface. Herbert Freundlich proposed this model in the year 1906 and is generally used to describe heterogeneous surfaces and multilayer adsorption.

The Freundlich equation in linear form is represented as:^{86,149,176}

$$\log Q_e = \log K_f + \frac{1}{n} \log C_e \quad (3.16)$$

where, K_f represents the Freundlich equilibrium constant, measured in mg/g, 'n' indicates the Freundlich exponent, which has no units. The Freundlich constant K_f and exponent $1/n$ is calculated based on the intercept and slope of graph, respectively. A straight line is obtained by plotting $\log Q_e$ against the $\log C_e$.

3.11.3. Temkin Isotherm

The Temkin model of isotherm is another empirical equation employed to elucidate the adsorption of solutes onto a solid surface. It was proposed by M.I. Temkin and V. Pyzhev in 1940. The Temkin isotherm takes into account the interactions between the adsorbate molecules and assumes a linear reduction in the heat of adsorption as the coverage increases.

The linear equation of Temkin isotherm is given as:^{118,125,170,171}

$$Q_e = B \ln(A) + B \ln(C_e) \quad (3.17)$$

where, B is equal to RT/b_T , b_T is Temkin constant and indicates heat of adsorption, R represents the gas constant which is $8.314 \text{ JK}^{-1}\text{mol}^{-1}$, A denotes equilibrium binding constant which corresponds to the maximal binding energy (L/g) and T represents the

temperature in Kelvin. A positive value of b_T indicates that adsorption process is of exothermic nature whereas, a negative value indicates an endothermic nature.

3.11.4. Dubinin-Radushkevich (D-R) Isotherm

The Dubinin-Radushkevich (D-R) model is employed to explain the adsorption of gases on heterogeneous surfaces. It is particularly applicable to physical adsorption processes on microporous materials. Primarily designed for physical adsorption, where gas molecules are adsorbed onto a solid surface through weak van der Waal forces. It assumes a homogeneous distribution of pore sizes within the microporous material.

The linear representation of D-R isotherm is follows:^{122,173,177,178}

$$\ln Q_e = \ln Q_m + \beta \varepsilon^2 \quad (3.18)$$

$$\varepsilon = RT \ln(1 + 1/C_e) \quad (3.19)$$

where, Q_m represents the D-R monolayer capacity in mg/g and β is constant associated with adsorption energy. R represents the universal gas constant, which is measured in joules per kelvin per mole ($\text{JK}^{-1}\text{mol}^{-1}$) while T refers to the absolute temperature (Kelvin).

The D-R isotherm is often used to estimate the mean adsorption energy (E) of the adsorbate on the heterogeneous surface. This mean energy is indicative of the average energy required for an adsorbate molecule to move from bulk solution to the adsorption site on the solid surface.

3.11.5. Adsorption Energy (E)

Adsorption energy (E) refers to the energy released or absorbed as molecules of a substance (adsorbate) attach to the surface of another substance (adsorbent). In simple words, the energy associated with the adsorption process indicating the strength of the interaction between adsorbate molecules and the adsorbent surface.^{158,162}

The Adsorption Energy (E) is calculated using the equation:

$$E = \frac{1}{\sqrt{2K}} \quad (3.20)$$

where, K is the D-R isotherm constant associated to adsorption free energy ($\text{mol}^2\text{J}^{-2}$). The calculated adsorption energy value showed the adsorption type. Adsorption is classified physical if the calculated value is below 40 KJ/mol, otherwise if it equals or exceeds 40 KJ/mol, it is classified as chemical.

3.11.6. Separation Factor

Separation factor 'R_L' is also one parameter which is applied to know about nature of the adsorption process in Langmuir isotherm which is calculated using following equation:^{83,119}

$$R_L = \frac{1}{1+bc_0} \quad (3.21)$$

where, C₀ is adsorbate's highest initial concentration

Value of R _L factor	Adsorption
R_L > 1	Unfavourable
R_L = 1	Linear
0 < R_L < 1	Favourable
R_L = 0	Irreversible

3.12. Adsorption Thermodynamics

Adsorption thermodynamics involves the study of the energy changes, entropy changes, and other thermodynamic parameters associated with the adsorption process. Thermodynamics provides insights into the spontaneity, stability and feasibility of adsorption reactions. Enthalpy, Entropy change and Gibbs free energy are the key parameter in understanding adsorption thermodynamics.^{76,175,179–181} Here are some general aspects of adsorption thermodynamics:

a. Gibbs free energy (ΔG°):

- Gibbs free energy is the key thermodynamic parameter that governs the spontaneity of process. For adsorption, the Gibbs free energy change (ΔG°) is crucial.
- Negative value of ΔG° indicate spontaneous adsorption process.

b. Enthalpy (ΔH°):

- Enthalpy change (ΔH°) represents the heat released or absorbed during adsorption.

c. Entropy (ΔS°):

- Entropy change (ΔS°) is associated with the disorder or randomness of the system. It reflects changes in the molecular arrangement upon adsorption.

The Van't Hoff equation is used to compute ΔG° which is expressed as:

$$\Delta G^\circ = -RT \ln K_d \quad (3.22)$$

General equation for calculating adsorption equilibrium constant is:

$$K_d = \frac{C_o - C_e}{C_e} \quad (3.23)$$

According to the equation of Gibb's Helmholtz,

$$\Delta G^\circ = \Delta H^\circ - T \Delta S^\circ \quad (3.24)$$

From equations (3.23) and (3.24), we get

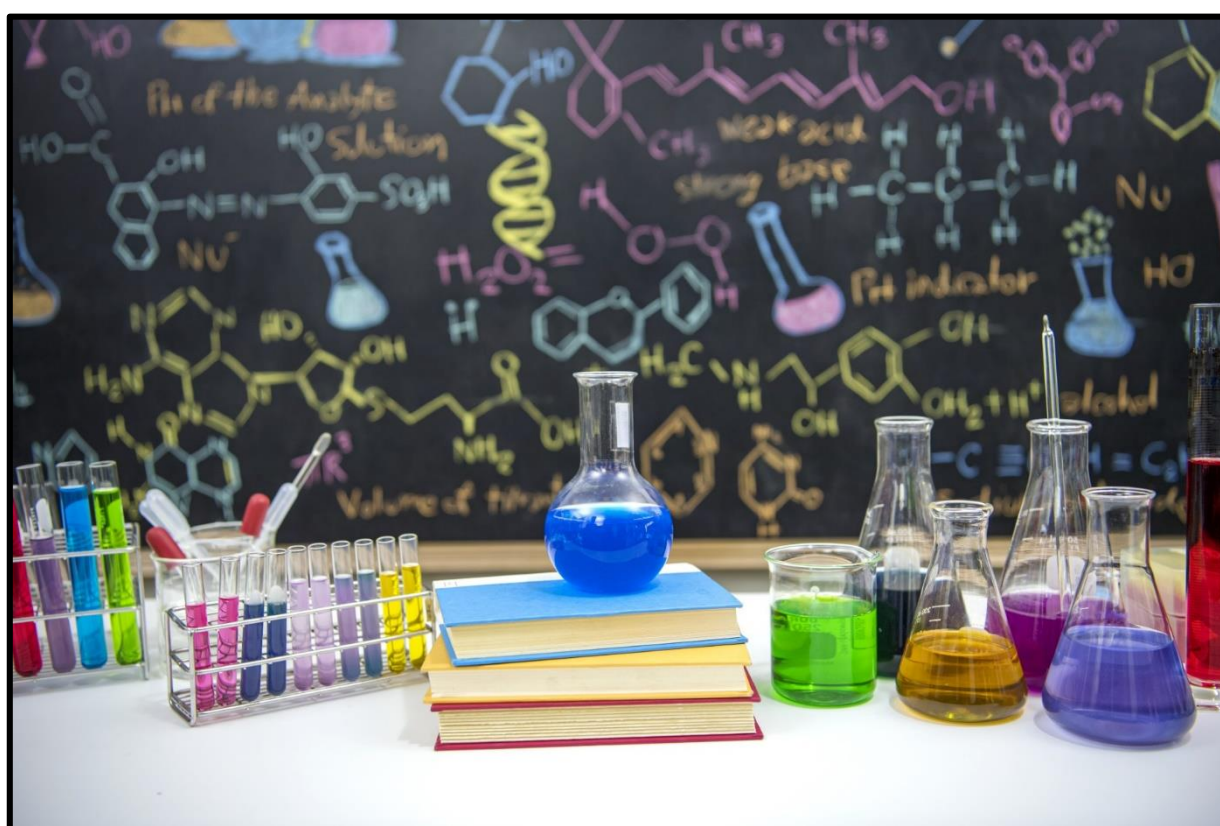
$$\ln K_d = \frac{\Delta S^\circ}{R} - \frac{\Delta H^\circ}{RT} \quad (3.25)$$

where, K_d signifies the dimensionless distribution equilibrium constant, R is the universal gas constant with value 8.314 Joule per kelvin per mole ($\text{JK}^{-1}\text{mol}^{-1}$) and T denotes the absolute temperature measured in Kelvin. The variables C_o and C_e denote the initial and equilibrium concentrations of the adsorbate (mg/L).

The value of ΔH° and ΔS° can be derived by analyzing the slope and intercepts of the linear graph of $\ln K_d$ versus $1/T$.

CHAPTER-4

RESULTS AND DISCUSSION



The findings of preliminary studies lead to the selection of several metal ferrite bio-waste composites for conducting extensive adsorption experiments with a variety of dyes in different dye systems which are single, binary and ternary for dyes as well as with Cu(II) metal ion. The results are divided into two sections, one for the study of dyes and other for the study of metal ion adsorption using metal ferrite bio-waste composites selected as described in the preliminary studies. In addition, each portion has been subdivided in order to provide detailed information of the adsorbents in terms of their characterization, parameters' effect on the percent removal of respective adsorbate and application of various kinetic, isotherm and thermodynamic models. The adsorption studies, adsorbent characterization and major findings are thoroughly addressed.

PART-I

(Dyes Adsorption using bio-waste metal ferrite composite)

Composites such as zinc ferrite pine cone (ZFPC), nickel ferrite pine cone (NFPC), walnut shell zinc ferrite (WSZF) and walnut shell cobalt ferrite (WScOF) had been selected as efficient adsorbents for removing different cationic dyes (CV, MG MB and BG) from single, binary and ternary dye system. The subsequent sections describe the comprehensive findings of surface characterization, morphological analysis and adsorption experiments conducted on selected metal ferrite bio-waste composites.

4.1. Zinc Ferrite Pine Cone (ZFPC) Composite

4.1.1. Characterization and Morphology

4.1.1.1. Fourier Transform Infrared Spectroscopy

The Fourier Transform Infrared spectrum of pine cone (PC), zinc ferrite (ZF) and zinc ferrite pine cone (ZFPC) is shown in figure 4.1.1. Two different adsorption peaks can be found below 600 cm^{-1} in the spectrum of ZF and ZFPC composite which correspond to the metal oxygen (M-O) band at two distinct sites.⁵⁸ The M-O band at the tetrahedral site is represented by the peak observed between 500 and 600 cm^{-1} while the M-O band at the octahedral site is represented by the peak noted between 450 and 400 cm^{-1} .¹⁵⁷ These peaks indicate spinel character of the ferrite and ferrite based composite used for the experimental study.

Peak found at 3281.60 cm^{-1} in PC corresponds to the O-H stretching. The spectral band seen at 2929.44 cm^{-1} indicates CH_n vibration due to the C-CH and C- CH_2 bonds.¹²⁰ A peak at 2361.46 cm^{-1} was observed due to the interference of CO_2 in the sample. The C=O and C=C vibrations corresponds to the peak seen at 1607.02 cm^{-1} . Another peak found at 1440.46 cm^{-1} is associated with a small alkane C-H absorption band.¹⁶⁸ Peak at 1261.79 cm^{-1} in the PC could be caused by the vibration of carboxylic acid C-O. Peak at 1024.08 cm^{-1} and 775.25 cm^{-1} observed might be caused by -C-C- and the stretching of -CN respectively.¹²⁰ The prepared ZFPC showed characteristic peaks of both the materials i.e.; PC and ZF with slight shifts as shown in figure 4.1.1 which confirmed the successful formation of ZFPC composite.

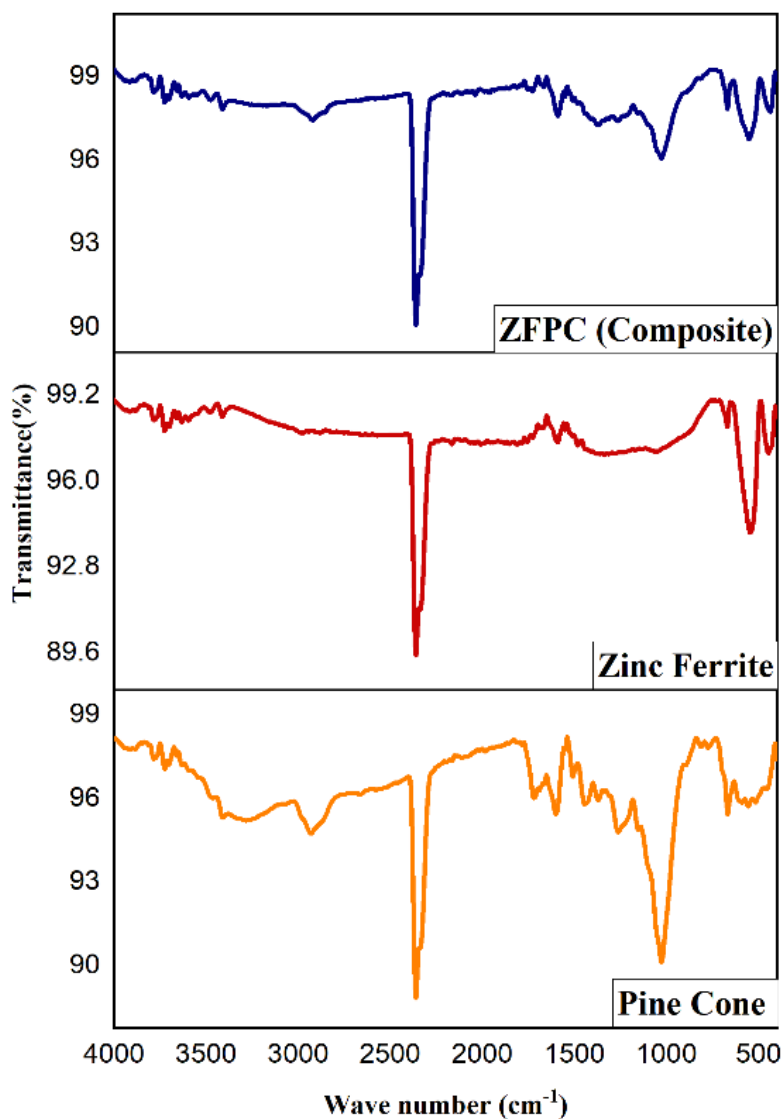


Figure 4.1.1: FTIR spectra of pine cone, zinc ferrite and zinc ferrite pine cone composite

4.1.1.2. X-Ray Diffraction

The X-ray diffraction pattern of ZF and ZFPC are presented in figure 4.1.2. The XRD pattern of ZF exhibited distinct peaks at $2\theta \sim 29.9^\circ, 35.2^\circ, 36.9^\circ, 42.8^\circ, 53.1^\circ, 56.6^\circ, 62.2^\circ, 70.5^\circ$ and 73.6° . These peaks correspond to the Miller indices patterns (220), (311), (222), (400), (422), (511), (440), (620) and (533) respectively. The lattice exhibited cubic spinel structure. The crystallinity and higher phase purity of ZF are shown by the peaks. To the contrary, the composite's X-ray diffraction pattern shows slightly different diffraction peaks. It was verified that the composite exhibits the identical pattern of Bragg's reflection.¹⁸² The findings demonstrated that the composite has a crystalline arrangement and maintains its spinel properties despite surface modifications.¹⁵⁷ The average size of the crystallites calculated as per Scherrer formula (equation 3.1) for pure ZF was 38.6 nm whereas the average size calculated for ZFPC composite was 54.9 nm. The hkl plane values are indexed from JCPDS file 01-071-5150.

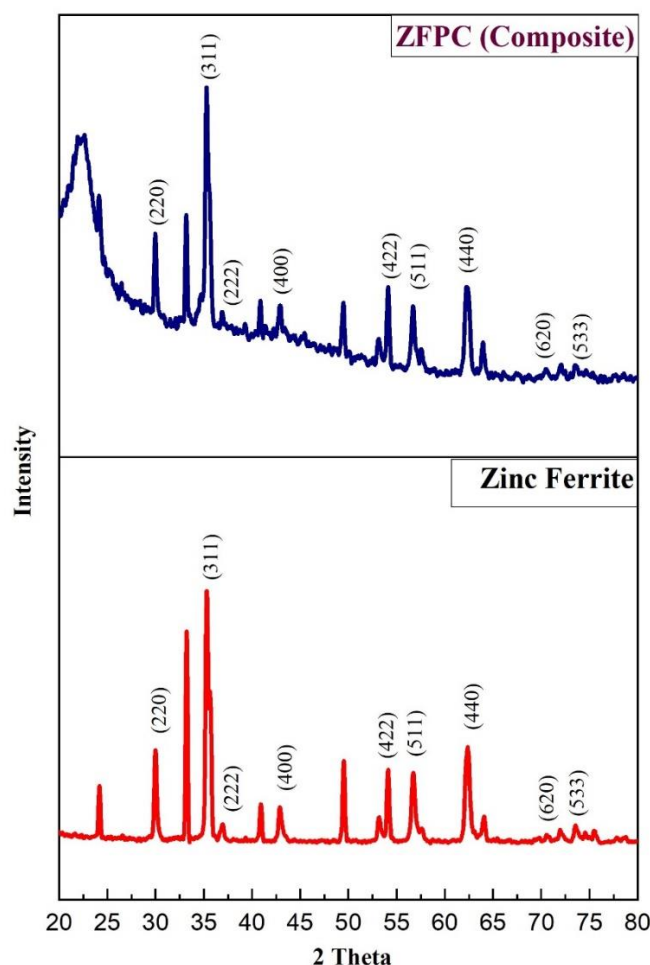


Figure 4.1.2: XRD spectra of zinc ferrite and zinc ferrite pine cone composite

4.1.1.3. Field Emission Scanning Electron Microscope

The surface morphology of the materials is illustrated in figure 4.1.3, which consists of FE-SEM images of ZF and ZFPC. ZF exhibit a non-uniform shape with a granular structure and have varied particle size. The largest particle size determined for zinc ferrite was 2.92 μm while the smallest size was 0.16 μm . Based on the calculations, the average size calculated for zinc ferrite was found to be 1.37 μm . ZFPC showed similar morphology and uneven surface with ferrites attached on the surface. The prepared composite yielded an average particle size of 1.52 μm having largest particle size 3.39 μm and the smallest 0.25 μm . Based on the calculations shown above, it has been found that the size of prepared ZFPC composite has larger particle size than that of pure ZF.¹⁵⁸ This finding provides evidence that the spinel zinc ferrite have successfully been modified with pine cone.

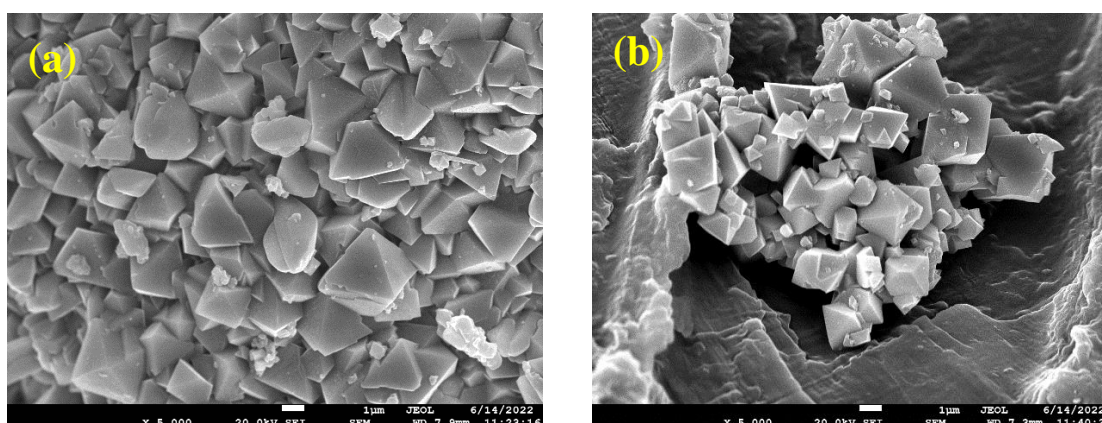


Figure 4.1.3: SEM image (a) Zinc ferrite (b) Zinc ferrite pine cone composite

4.1.1.4. Energy Dispersive Spectra

Energy Dispersive Spectra of ZF and ZFPC composite are shown in figure 4.1.4 along with the peaks that indicate the elemental composition present in each of these materials. The atomic and weight percentages of the various elemental components present in the ZF and ZFPC that were synthesized using magnetic nano particles are presented in table 4.1.1. It is evident that ZFPC composite contains a higher percentage of carbon in comparison to pure ZF which demonstrates successful modification of ZF with PC to form a magnetic composite.^{84,183}

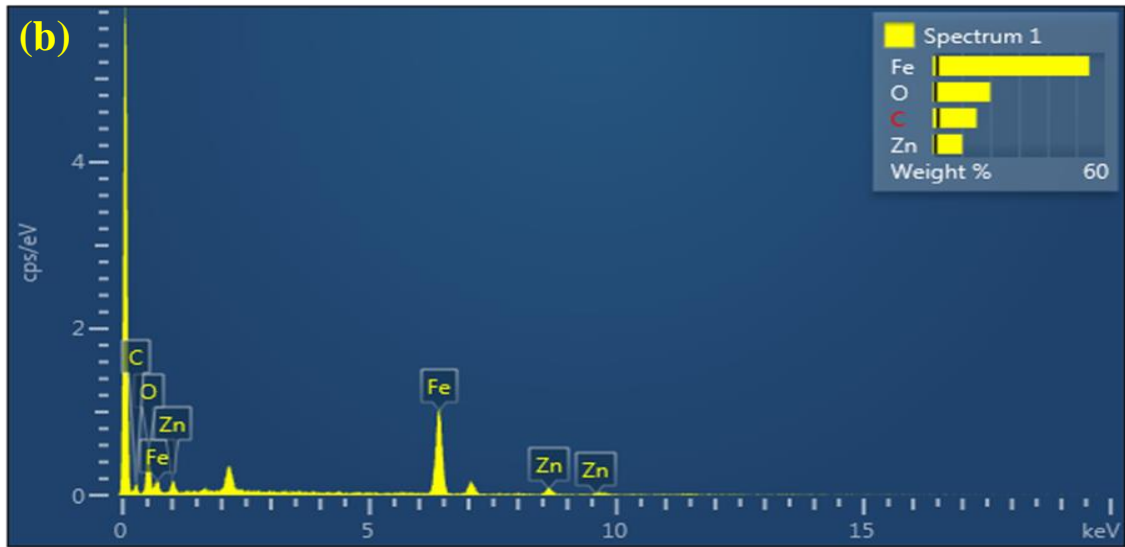
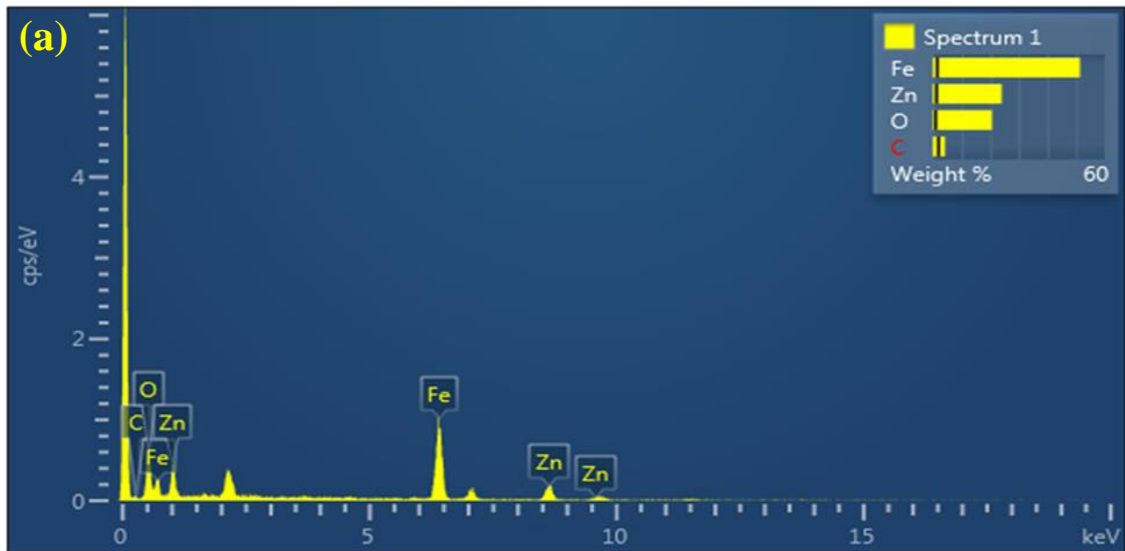


Figure 4.1.4: EDS image (a) Zinc ferrite (b) Zinc ferrite pine cone composite

Table 4.1.1: Elemental composition of zinc ferrite and zinc ferrite pine cone composite

Element	Zinc Ferrite		Zinc Ferrite Pine Cone composite	
	Weight %	Atomic %	Weight %	Atomic %
C	4.13	11.81	15.14	34.59
O	20.54	44.06	19.99	34.28
Fe	51.31	31.53	54.63	26.84
Zn	24.02	12.61	10.23	4.29
Total	100.00	100.00	100.00	100.00

4.1.1.5. Thermogravimetric Analysis

The TGA graph of ZFPC composite is presented in figure 4.1.5. The thermogravimetric analysis was conducted to investigate the thermal stability of composite. The TGA analysis was conducted in an air environment with temperature ranging from 28-600°C and a heat rate of 10°C/min. It is apparent from the graph that a loss in weight of 8.3% was observed from approximately 30.5°C to 92.05°C. This decrease in weight may be attributed to the evaporation of entrapped moisture in the sample. At around 150°C to 355.8°C, an abrupt weight loss of about 25.9% was observed which might be due to the breakdown of organic matter. As the temperature rose, another steady weight loss of 12.6% was noticed from 355.8°C to 595.9°C. After that, there observed no further loss which demonstrated the complete decomposition of organic matter with in the composite. Based on the above observations, it has been calculated that 0.420 grams of PC has been attached in 1 gram of ZFPC (Composite).^{58,155}

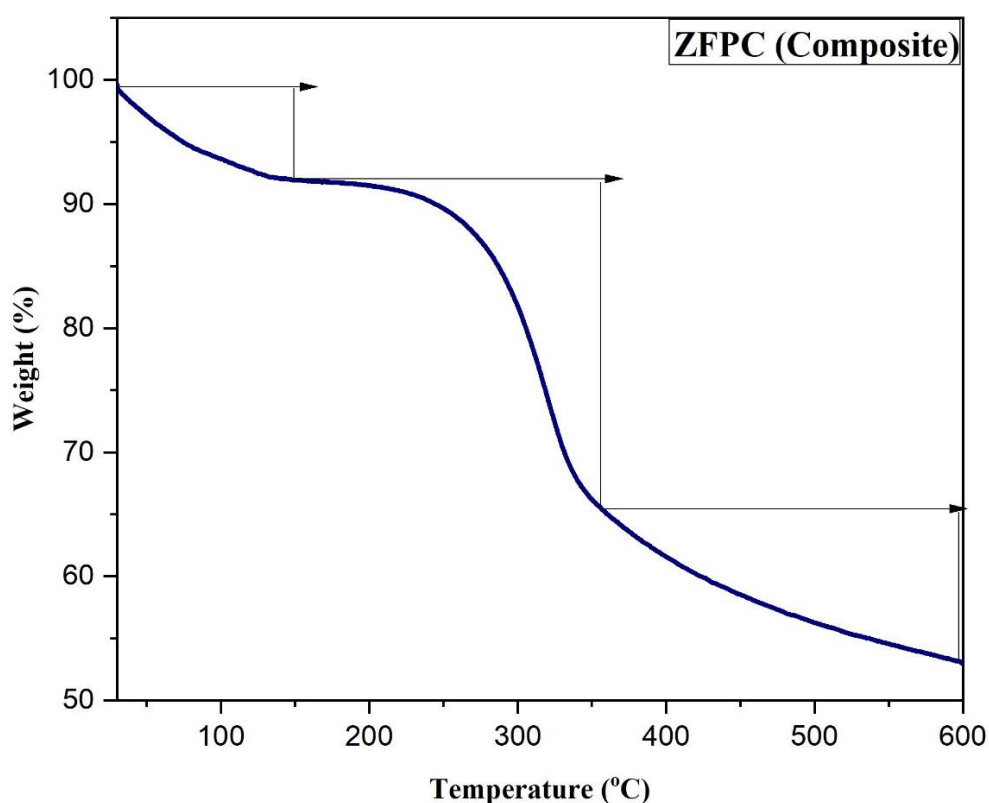


Figure 4.1.5: TGA curve of zinc ferrite pine cone composite

4.1.1.6. Brunauer-Emmett-Teller Analysis

A method known as BET was utilized to investigate the specific surface area distribution. The outcomes of BET analysis conducted on the prepared composite as well as pure

ferrite provides unambiguous evidence that the surface area of pure ferrite is less as compared to composite. The specific surface area of pure ZF obtained was $0.749 \text{ m}^2/\text{g}$ while the surface area obtained for ZFPC was $1.463 \text{ m}^2/\text{g}$. This happened because the particle size increased when the surface of ZF was modified with PC as compared to pure ZF. On surface modification, porosity increased at the surface of composite which caused an increase in the specific surface area.^{161,184}

4.1.1.7. pH of Point Zero Charge Analysis

For determining the pH_{zpc} of ZFPC composite, the solid addition method was utilized. To carry out the experiment, nine 250 mL Erlenmeyer flasks were taken and 50 mL of a 0.1M KNO_3 solution was added to each flask. Using Hydrochloric acid (0.1N) and Sodium hydroxide (0.1M), the pH of the prepared solution was adjusted within a range between 3-11 (the initial pH). 0.1 g of the ZFPC was added to each glass flask. These flasks were kept in thermostatic shaker at 30°C for a period of twenty-four hours. The flasks were taken out from the shaker after 24 hours and the contents of flasks were filtered in different beakers. The final pH of the solution present in each beaker was noted and calculations were performed using equation 3.2.^{121,156}

Using the above calculated values, a plot was obtained between initial pH (on x-axis) and ΔpH i.e.; the difference between the initial pH and final pH (on y-axis) as illustrated in figure 4.1.6. From the graph, the pH_{zpc} value of ZFPC calculated was 7.50. Thus, it states that the surface of the composite will be positively charged below pH 7.50 and a negatively charged above pH 7.50.^{185,186}

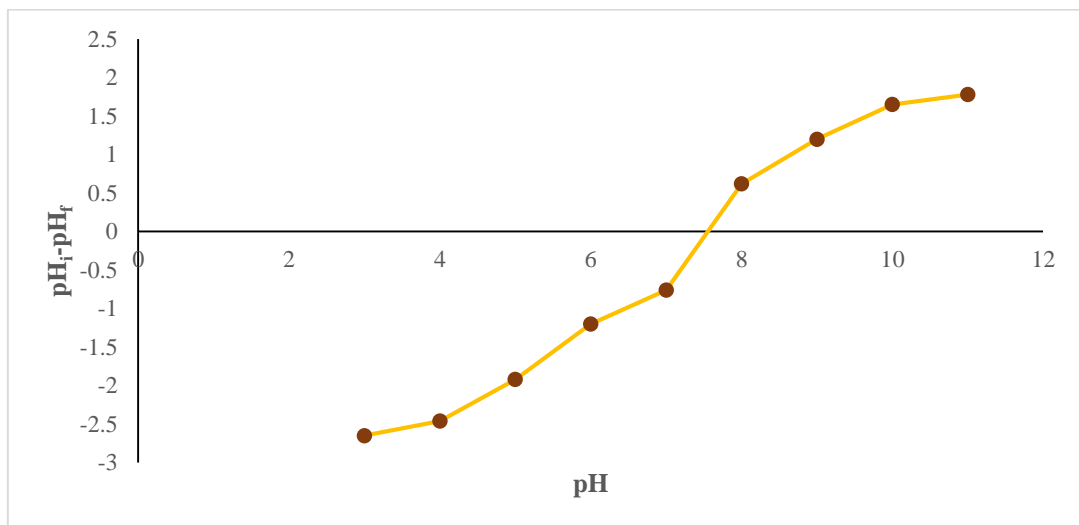


Figure 4.1.6: pH_{zpc} of zinc ferrite pine cone composite

4.1.2. Adsorption Study in Single and Ternary Dye System

Adsorption behavior of ZFPC composite was determined using batch process for various dyes.^{27,187} The ZFPC composite exhibits specific selectivity towards various dyes in aqueous solution as evidenced by pilot-scale studies described in chapter 3. The composite's adsorption characteristics were examined with several dyes including CV, MG, BG and MB. Among these, the dye BG exhibited lower adsorption efficiency. As a result, ZFPC composite was further explored for CV, MG, and MB dyes only in single as well as ternary dye system. Different adsorption factors including contact time, initial solution pH, adsorbent dosage, initial dye concentration and temperature were examined.

4.1.2.1. Effect of Contact Time

For analysing the effect of contact time on ZFPC composite in both single as well as ternary dye systems, a known concentration of single and ternary dye (50 mg/L and 20 mg/L, respectively) was poured in an Erlenmeyer flask (100 mL) with the addition of adsorbent dose (0.1 g) and a specified dye solution volume (50 mL). The flasks were then kept in a thermostatic orbital shaker for 3 hours. The flasks had been removed at predetermined intervals and the residual dye concentration was determined using UV-VIS Spectrophotometer. Effect of contact time on CV, MG and MB in single as well as ternary dye systems are shown in figure 4.1.7 and 4.1.8 respectively. From the graph, it is evident that the removal percentage of dye was extremely rapid during the initial phase of the process but with increasing time, it became more stable and eventually reached equilibrium. This may be due to the fact that during the initial phase, greater number of unoccupied adsorption sites available on the surface of ZFPC and molecules of dye got attached to those vacant sites. However, over time, these empty sites became occupied, the adsorption rate slowed down and after some time residual concentration became constant with respect to time. This stage was referred to as the equilibrium stage where rate adsorption becomes equal to rate of desorption.^{31,76,175,188} For single dye system, the rate of adsorption was initially rapid, facilitated by the abundance of active sites but after sometime, the removal dyes decelerated and ultimately reached equilibrium at 120 minutes. The maximum removal percentages achieved for CV, MG and MB were 81.5%, 90.0% and 67.9%, respectively. Similarly, for ternary dye system, the adsorption proceeded quickly in the initial phase and the equilibrium was attained at around 110 minutes. The maximum removal percentages for CV, MG and MB in the ternary system were calculated as 58.7%, 64.4% and 41.7% respectively.

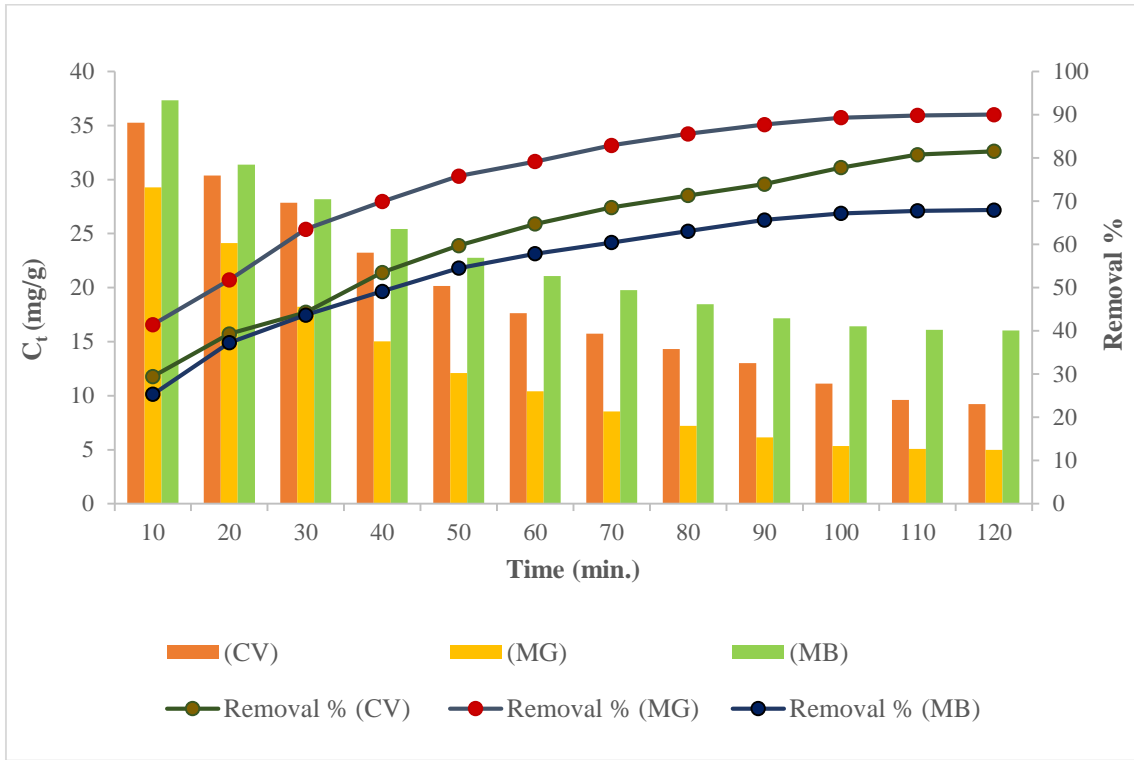


Figure 4.1.7: Effect of contact time for single dye system

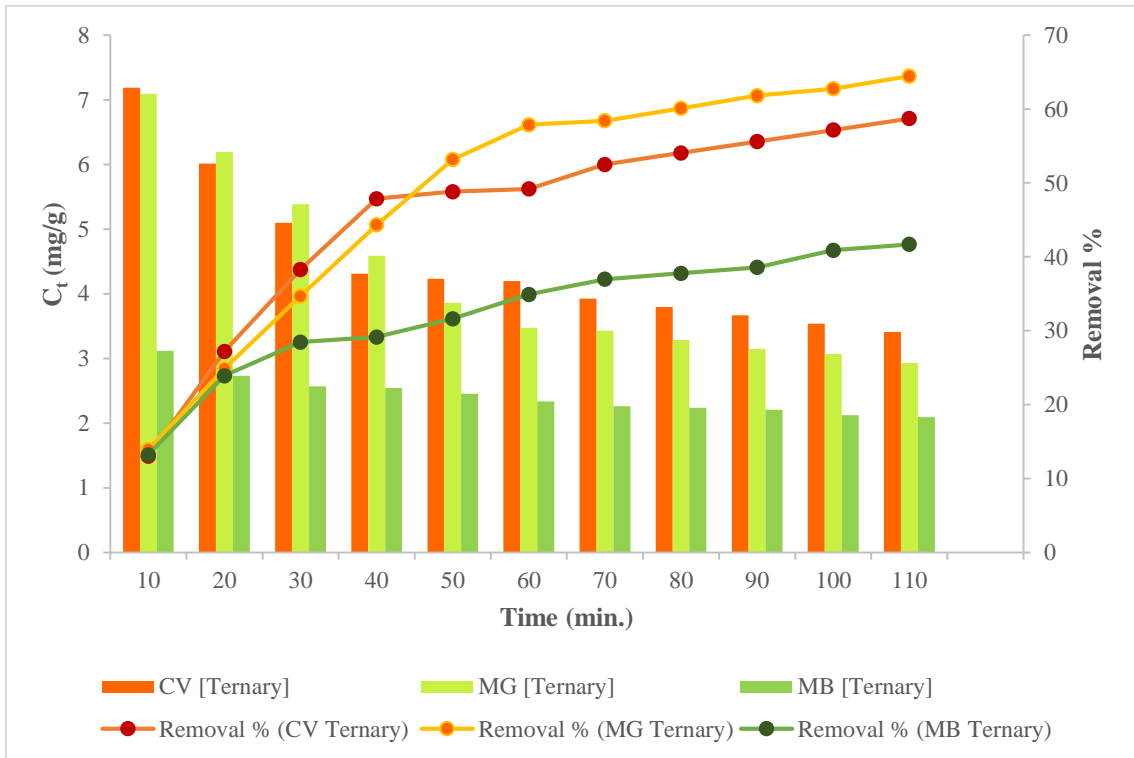


Figure 4.1.8: Effect of contact time for ternary dye system

4.1.2.2. Adsorption Kinetics

Several models including the Lagergren pseudo first order model, Pseudo second order model, Elovich model and Intra particle diffusion model were applied in order to study the kinetic behavior of the prepared composite (ZFPC) for both single as well as ternary dye system.^{93,167,168,173,189} The time study data was graphically represented by utilizing the kinetic models. The plot with respect to Lagergren pseudo first order and pseudo second order model is shown in figure 4.1.9 for both the single and ternary dye system while figure 4.1.10 represents plot of Elovich model. Table 4.1.2 displays calculated values of different constants linked to kinetic models using the plots. The degree of model suitability can be assessed by examining the regression coefficient (R^2) value. A higher R^2 value approaching 1 indicates a better fit of the model. Therefore, the pseudo second order kinetic model exhibited the best fit followed by Elovich model and pseudo first order model indicating that the process of adsorption in the experimental study was chemical in nature.

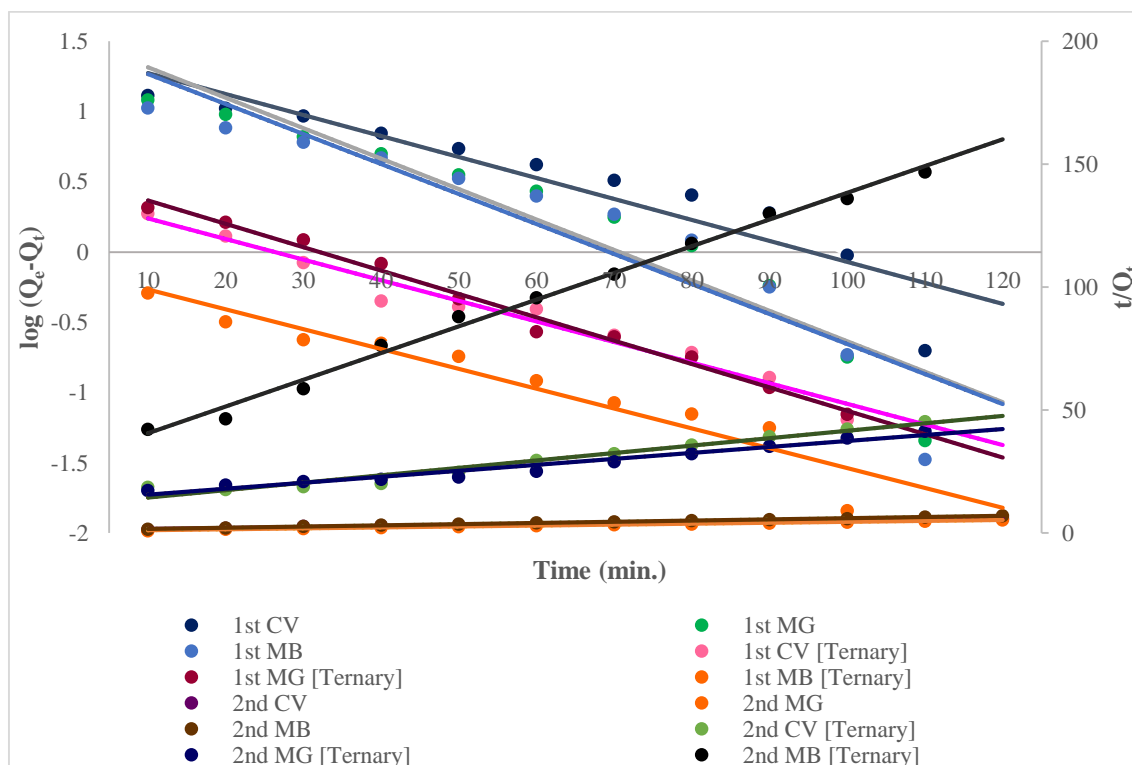


Figure 4.1.9: Lagergren pseudo first order and pseudo second order kinetics for single and ternary dye system

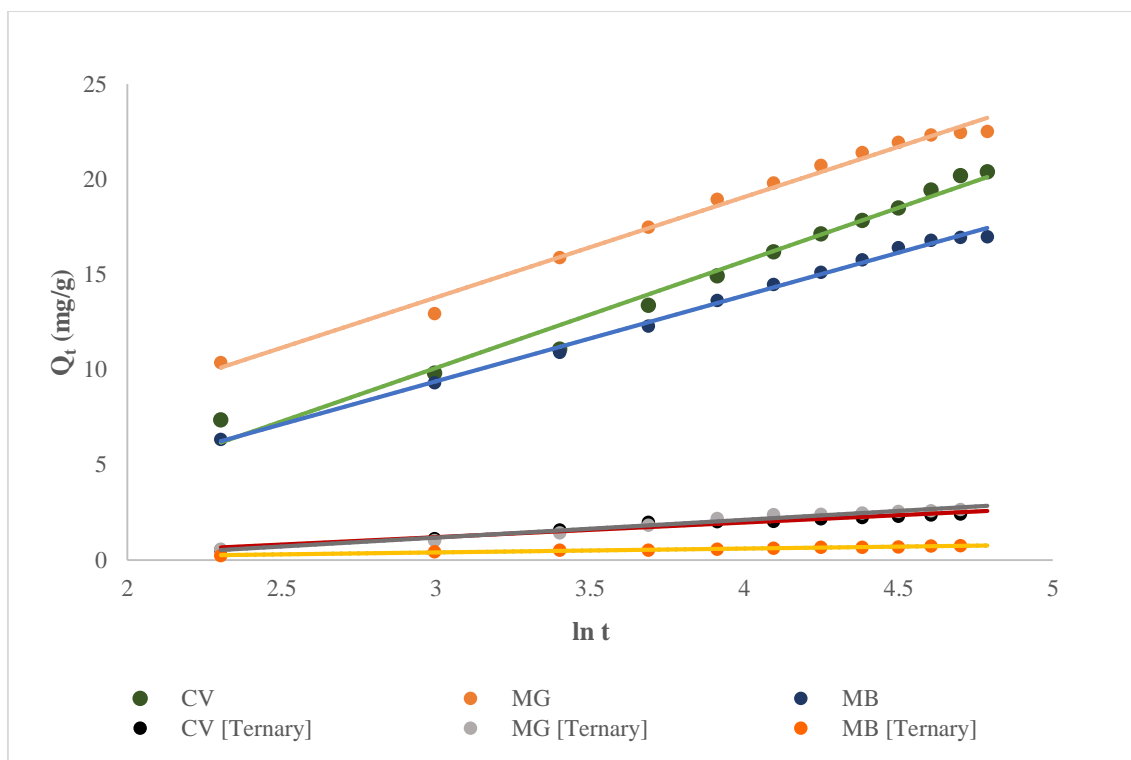


Figure 4.1.10: Elovich model for single and ternary dye system

Table 4.1.2: Calculated values of different kinetic constants for single and ternary dye system

KINETIC MODEL	SYSTEM						
	Parameter	Single	Single	Single	Ternary	Ternary	Ternary
		CV	MG	MB	CV	MG	MB
Lagergren Pseudo first order	Q_{e1}	26.466	33.955	30.248	2.428	3.407	0.748
	K_1	0.344	0.498	0.492	0.337	0.383	0.325
	R^2	0.868	0.907	0.872	0.969	0.989	0.915
Pseudo second order	Q_{e2}	2.584	2.623	2.076	0.332	0.413	0.092
	h	0.756	1.404	0.817	0.087	0.076	0.034
	K_2	5.046	9.662	3.524	0.009	0.013	0.001
	R^2	0.988	0.998	0.998	0.988	0.993	0.994
Elovich model	α	1.686	3.592	1.797	0.182	0.164	0.073
	β	0.178	0.189	0.222	1.295	1.068	4.924
	R^2	0.981	0.989	0.995	0.965	0.975	0.986

Weber-Morris intraparticle diffusion model was employed to study mechanism of adsorption for different dyes using ZFPC. The plot between Q_t and $t^{0.5}$ is represented in figure 4.1.11 and K_{int} i.e.; the intra-particle diffusion rate constant and the rate limiting step^{112,171} are calculated from the slope of line if it passes through origin. This rate-limiting step states that a straight line must intersect the origin point. However, graph indicates that the plot is non-linear and the line does not pass through origin. This suggested that in addition to intra-particle diffusion, there might be other factors that influence the adsorption rate in single and ternary system. As can be seen from figure 4.1.11, the slope was steep at the beginning of the process which suggested that the dye was absorbed quickly in the case of a single dye system. After a certain period of time, the slope flattened out and eventually reached equilibrium. However, this trend was absent in the ternary dye system. The decrease of adsorption in ternary dye systems was attributed to the antagonistic effect of dyes. Different forces like electrostatic interaction and π - π interactions existed among the molecules of CV, MG and MB and form stronger bond. Therefore, compared to a single dye system, the amount of different dyes removed was significantly lower in the ternary dye system.¹⁴²

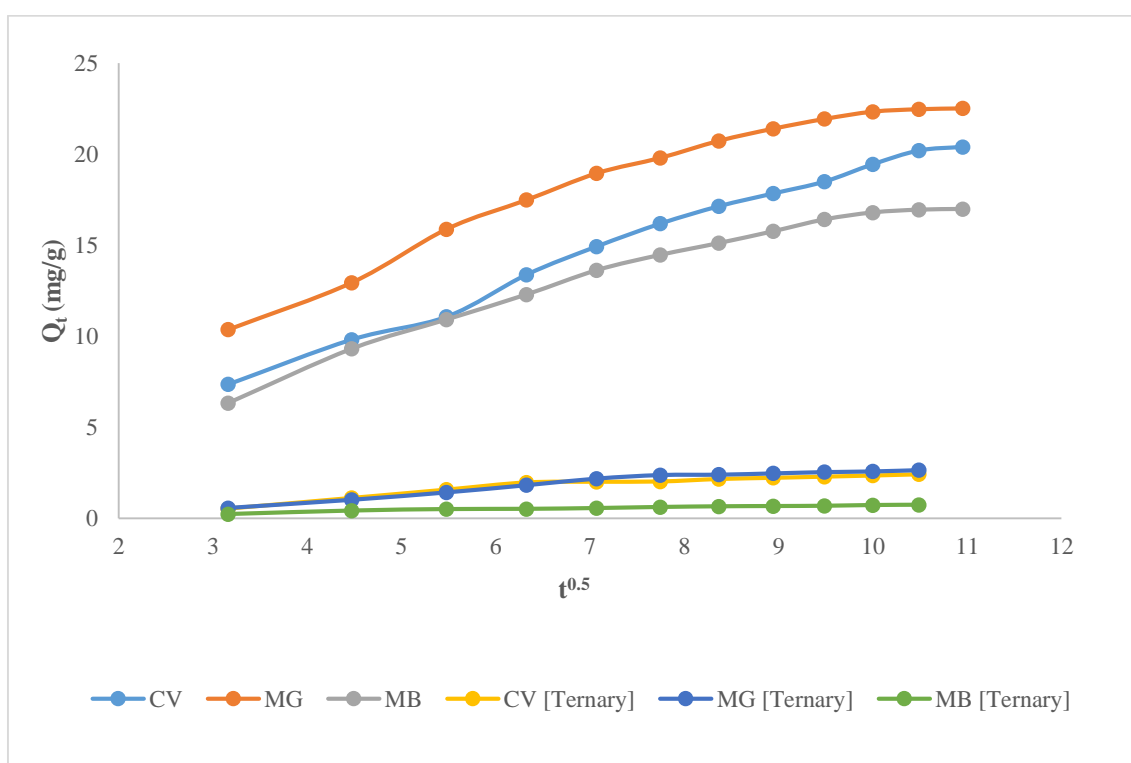


Figure 4.1.11: Intra particle diffusion model for single and ternary dye system

4.1.2.3. Effect of pH

The pH governs the surface charge of the adsorbent, which in turn affects the performance of the adsorbent under different pH conditions. The influence of pH was studied to determine the adsorption behavior of prepared ZFPC composite with different dyes CV, MG and MB in single dye system at pH values ranging from 3 to 11. Erlenmeyer flasks containing the prepared solution with an initial concentration of the dye 50 mg/L and an adsorbent dose 0.1 g were placed in an orbital shaker for a period of 3 hours at 25°C. The effect of pH on the removal of various dyes (CV, MG and MB) in a single dye system is illustrated in figure 4.1.12. From the figure, it was observed that the dye removal effectiveness increased with increasing pH of solution and reached maximum at 6 then further decreased. So, the pH 6 has been determined as optimal for the removal of dyes. According to the results, the maximum percentage of CV, MG and MB removed is 78.2%, 82.5% and 67.9% respectively.^{121,190}

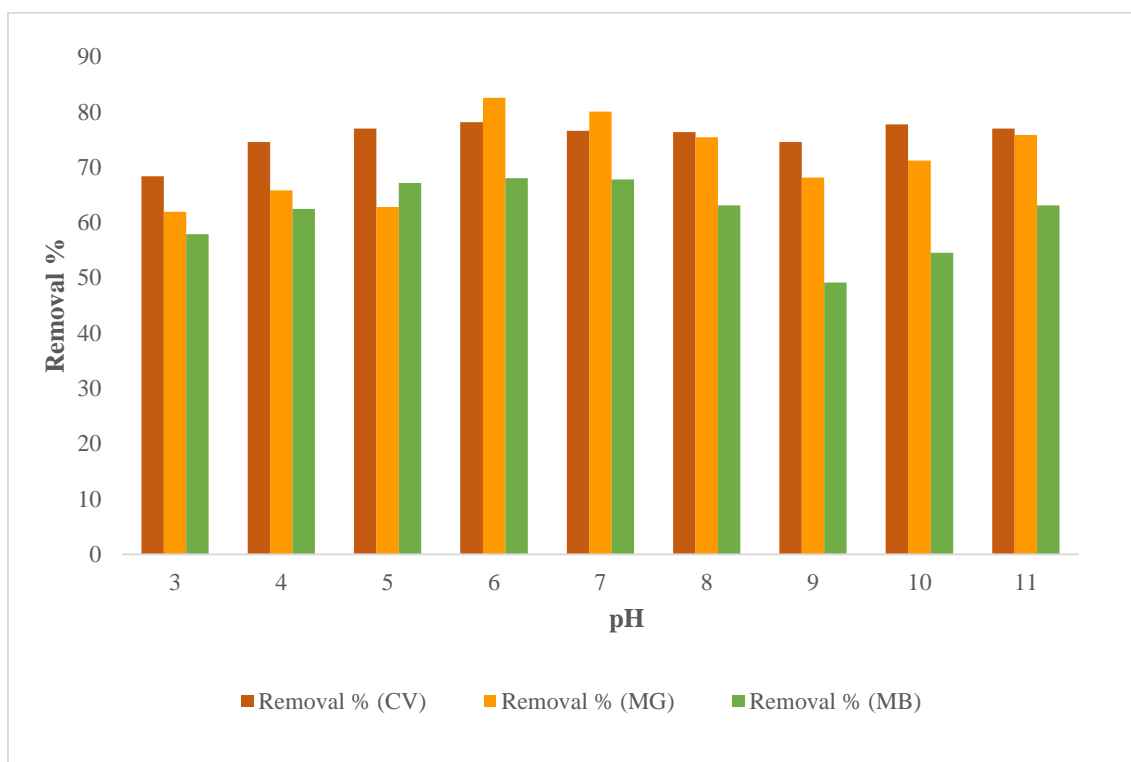


Figure 4.1.12: Effect of pH for single dye system

4.1.2.4. Effect of Adsorbent Dosage

To examine the effect of adsorbent dosage, the dosage of prepared ZFPC composite was varied from 0.1 g - 0.5 g for single and ternary dye systems. The data in figure 4.1.13 and 4.1.14 illustrates that as the dosage of the ZFPC composite increased, the

percentage removal of dye also increased in single as well as ternary system^{110,191}. This trend of increasing dye removal in both the dye systems was seen as a result of increased availability of unoccupied sites on the surface of ZFPC with increased amount of adsorbent. However, the quantity of adsorbate adsorbed per gram of adsorbent (Q_e) declined as the amount of adsorbent increased. This decline was due to the presence of more active sites on the adsorbent's surface, which remained unoccupied with the increase in adsorbent amount.^{142,192}

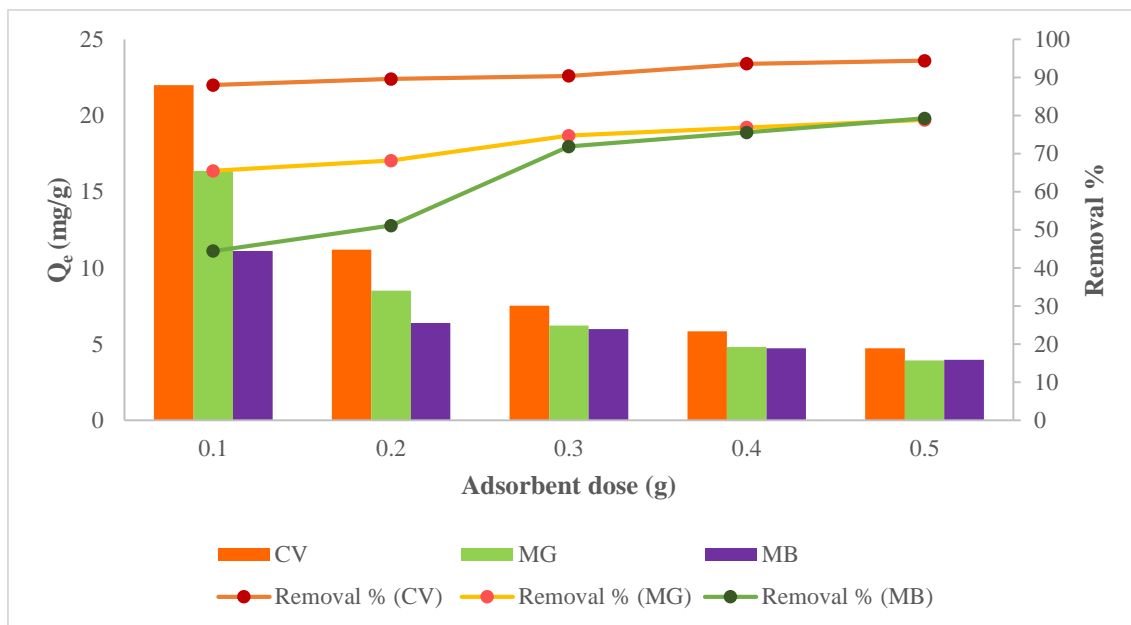


Figure 4.1.13: Effect of adsorbent dosage for single dye system

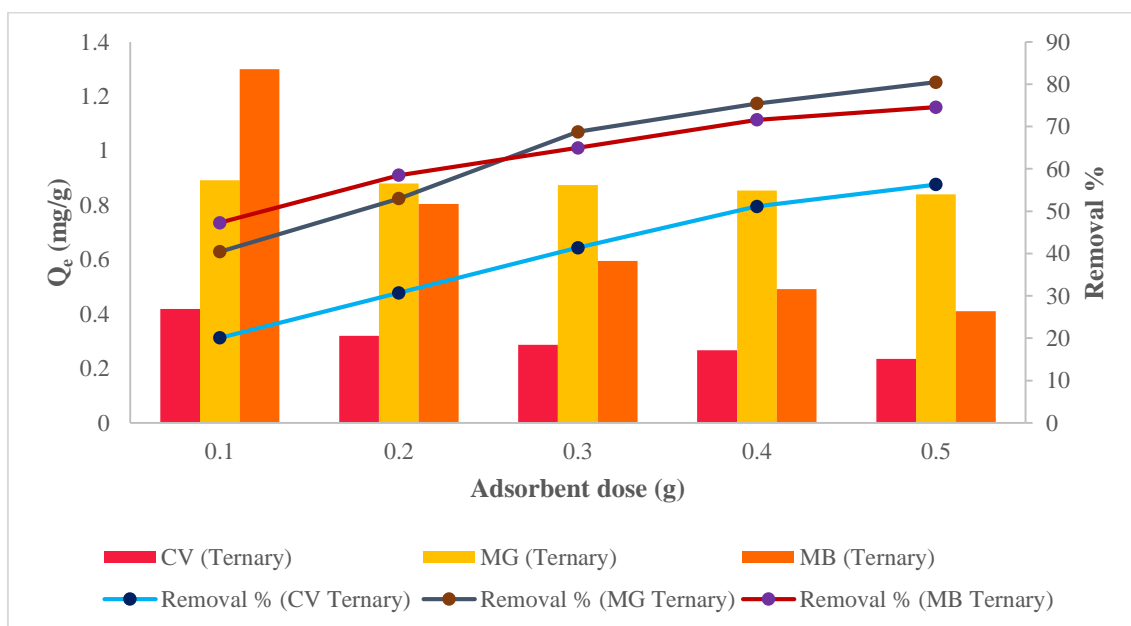


Figure 4.1.14: Effect of adsorbent dosage for ternary dye system

4.1.2.5. Effect of Concentration and Temperature

The effect of concentration for both dye systems was examined with initial dye concentration ranged from 50-250 mg/L for the single dye system and 20-100 mg/L for ternary dye system. In addition to the concentration, the effect of temperature was also investigated at temperature: 25°C, 30°C and 35°C. The concentration and temperature effect on the dyes are depicted in figure 4.1.15 and 4.1.16 for single dye as well as ternary dye system respectively. An increase in the initial dye concentration (C_o) resulted in the increase in the amount of dye adsorbed per unit weight of the adsorbent (Q_e) for the dyes used in this study in single as well as ternary dye systems. This rise in adsorption capacity occurred because the bond strength between dye molecules and the adsorbent strengthened as the quantity of dye molecules increased for a set amount of adsorbent, leading to more frequent collisions. The percent removal of dye however, dropped as the concentration of dye was increased in both the dye systems. This could be due to constant number of available active sites present on the adsorbent's surface in comparison to the increasing concentration of dye molecules. Additionally, it was observed that as the temperature increases, the adsorption capacity of different dyes also increased, which indicated that adsorption process was endothermic in nature for this study.^{157,168,190}

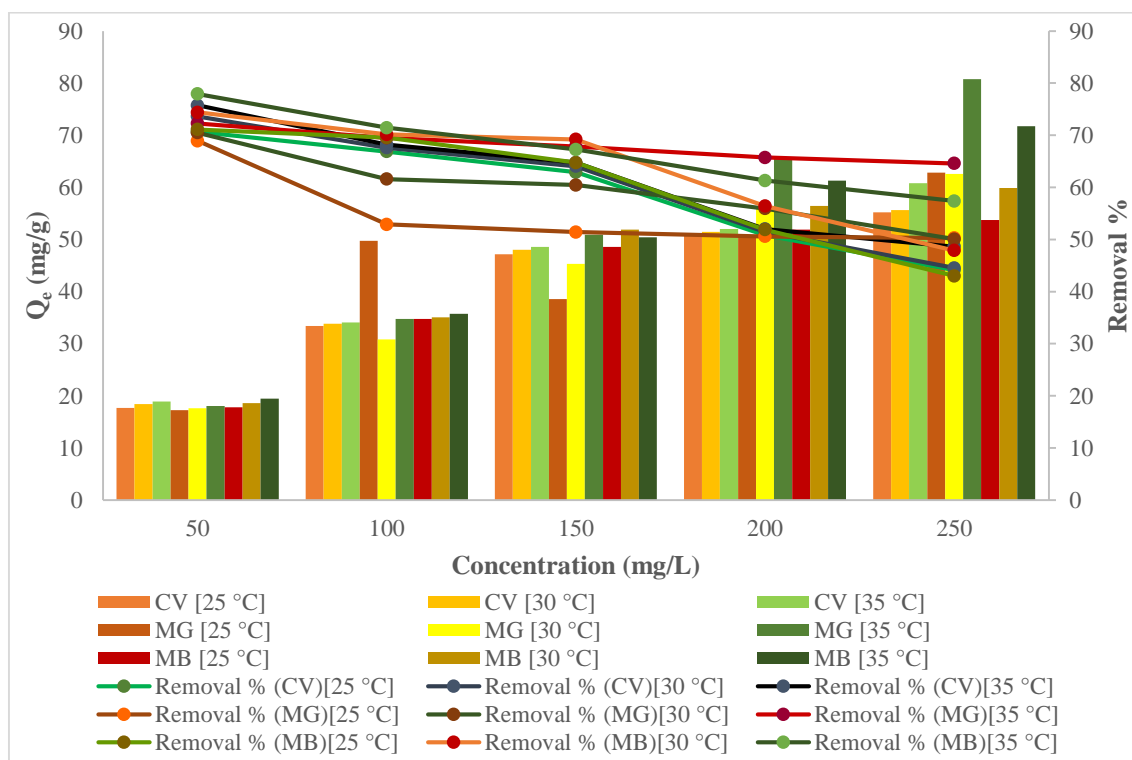


Figure 4.1.15: Effect of concentration for single dye system

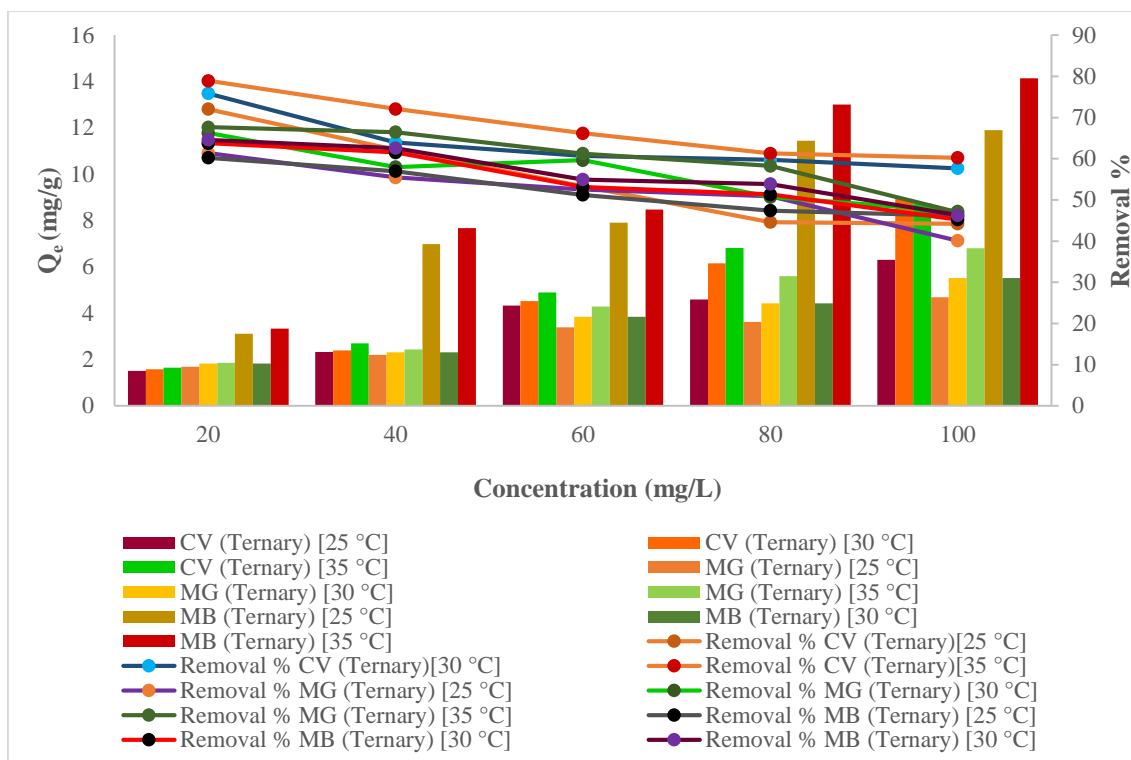


Figure 4.1.16: Effect of concentration for ternary dye system

The increase in the adsorption may be attributed to the increase in the number of collisions due to increased kinetic energy between dye molecules and ZFPC as well as enlargement of pores present on the surface of the adsorbent which lead to increase in the surface area thus helping in more adsorption.^{42,157}

When different dyes are present in the solution, they exhibit antagonistic effect which causes decreased adsorption. Moreover, multiple dye systems offer opportunity of mutual interaction among the dye molecules which is another reason for decrease in the adsorption of dyes in multiple dye systems.

4.1.2.6. Adsorption Isotherms

For dyes CV, MG and MB, various models of adsorption isotherms such as the Langmuir^{93,188}, Freundlich^{172,173,193}, Temkin^{122,170,177} and the Dubinin-Raduskevich (D-R) model^{112,173,177} were utilized to investigate the equilibrium state in different dye systems at varied temperatures (25°C, 30°C and 35°C) with ZFPC composite. Various adsorption isotherms were employed for both the systems at three distinct temperatures and varying concentrations, as depicted in figures 4.1.17 (a-d). From the plots of different isotherms, the values of isotherm constants were calculated for both the dye system which are presented in table 4.1.3. Among the different adsorption isotherms, the Langmuir model

demonstrated the highest R^2 (correlation coefficient) value, indicating the best fit with the experimental data. The results suggested that the surface of ZFPC composite possesses uniform active sites and different dyes form monolayer on the surface of composite. The Langmuir adsorption capacities for CV, MG and MB were determined to be 76.33, 200 and 94.33 mg/g, respectively for single dye system and 9.46, 20.45 and 27.93 mg/g, respectively for ternary dye system.

Furthermore, one of the parameter associated with Langmuir isotherm employed to describe the nature of adsorption is the separation factor (R_L). Table 4.1.3 shows that the calculated R_L factor values for the dyes used in this study for single and ternary system ranged from 0 to 1 which indicated that the adsorption process is favourable for dyes adsorption in both the dye systems using ZFPC composite.^{119,158}

An additional factor, the adsorbent's Adsorption Energy (E) related to D-R isotherm was calculated to determine the type of adsorption process. The adsorption is considered physical when $E < 8$ KJ/mol and chemical if it exceeds this value. It is evident from table 4.1.3 that in this case $E > 100$ KJ/mol. The obtained values of adsorption energy for both single as well as ternary dye system exceeded 100 KJ/mol which suggested that the adsorption process in this experimental study followed chemisorption.⁵⁸

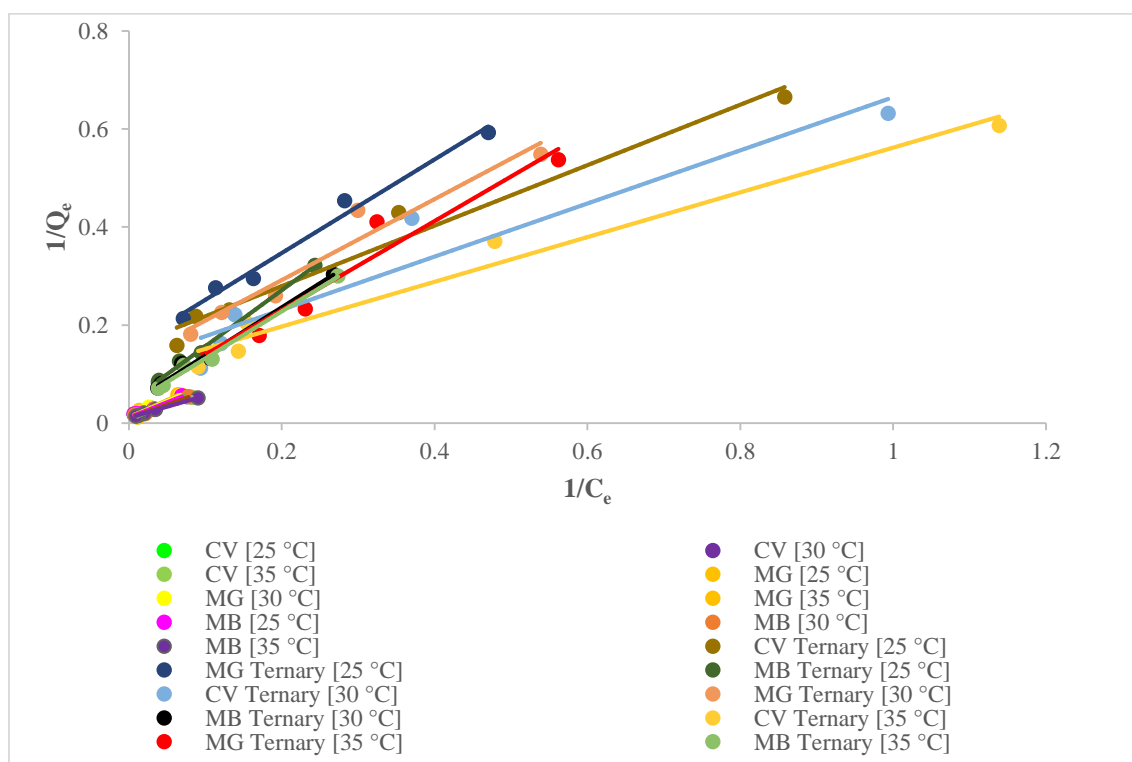


Figure 4.1.17 (a): Langmuir adsorption isotherms for single and ternary dye system

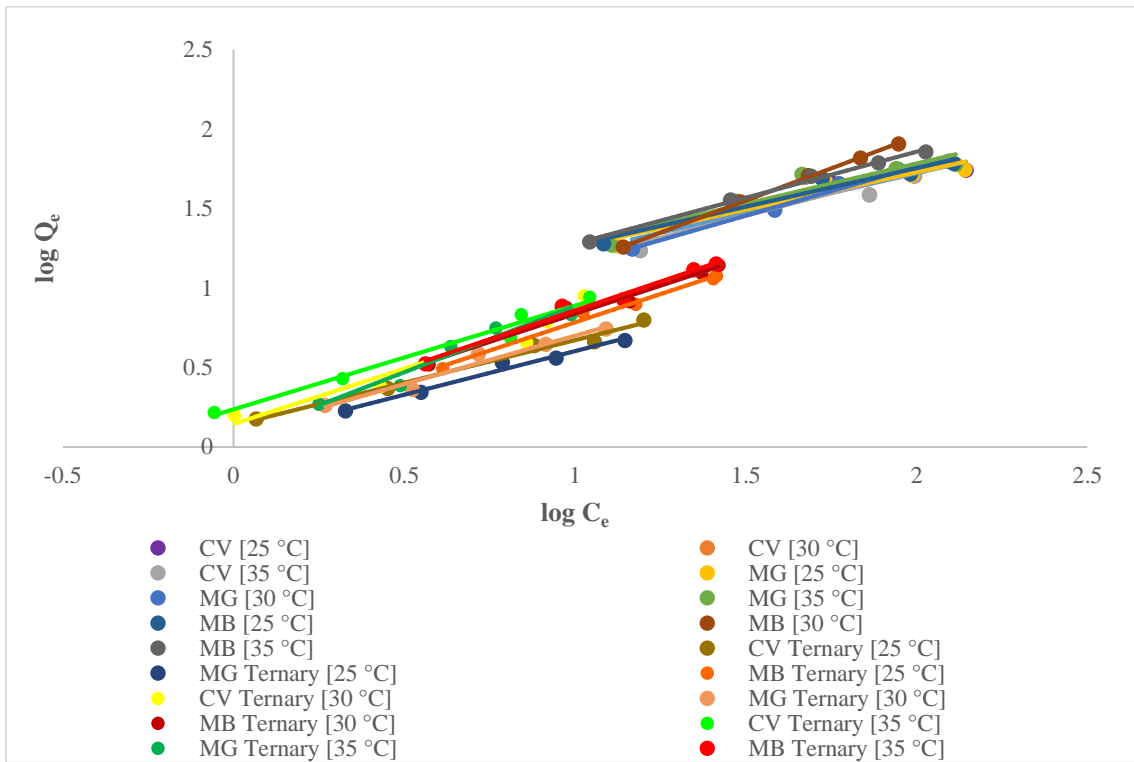


Figure 4.1.17 (b): Freundlich adsorption isotherms for single and ternary dye system

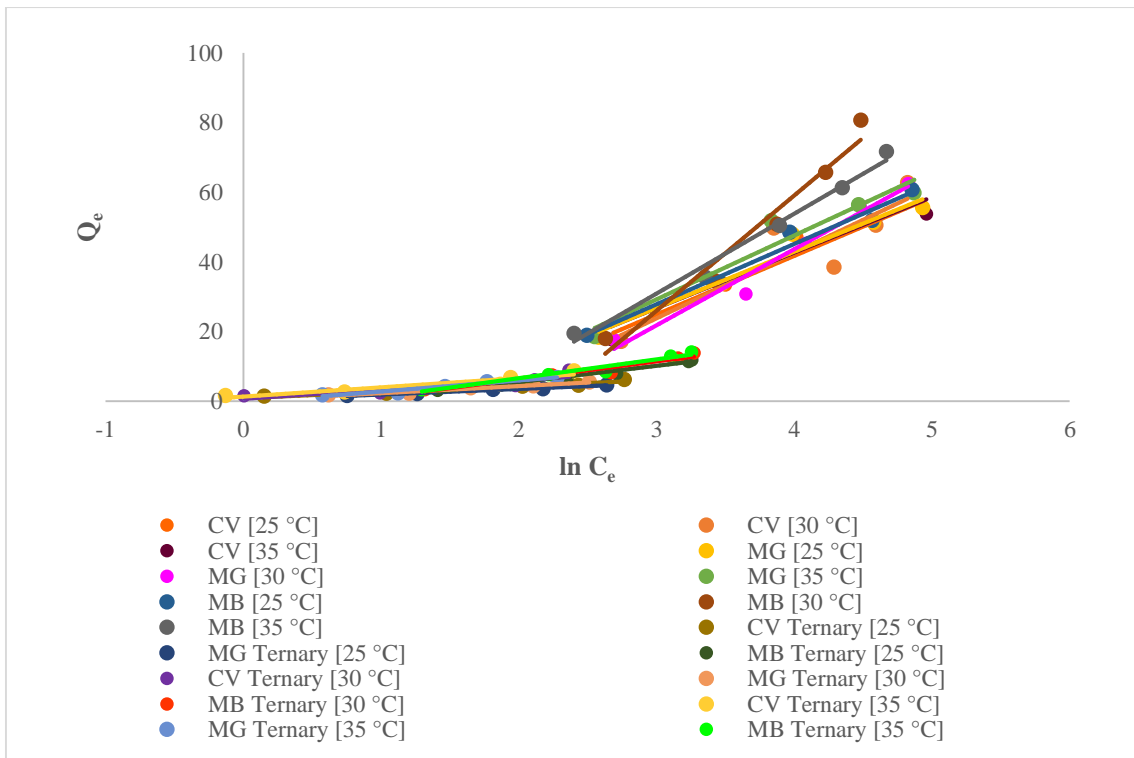


Figure 4.1.17 (c): Temkin adsorption isotherms for single and ternary dye system

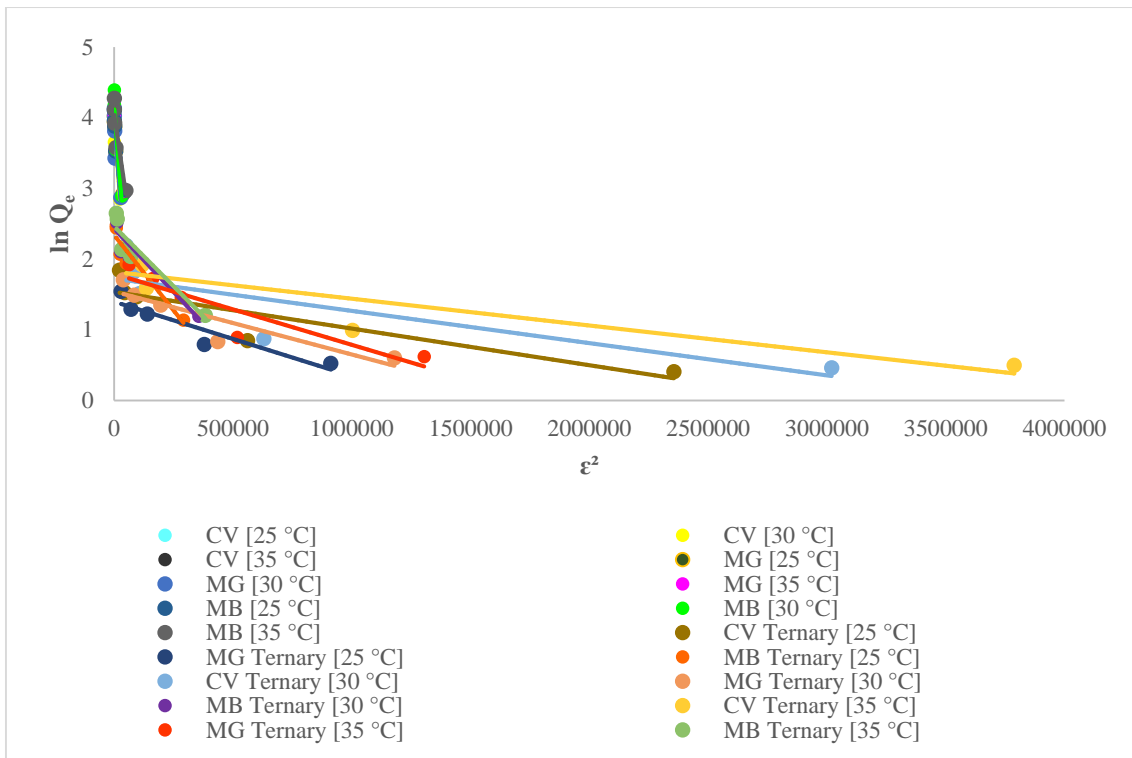


Figure 4.1.17 (d): D-R adsorption isotherms for single and ternary dye system

The obtained values of adsorption energy for both the dye system exceeded 100 KJ/mol which suggested that the adsorption process in this experimental study followed chemisorption.⁵⁸

Table 4.1.3: Adsorption isotherm constants for single and ternary dye system

System		Single CV			Single MG			Single MB			Ternary CV			Ternary MG			Ternary MB		
Isotherm Model	Constant	25°C	30°C	35°C	25°C	30°C	35°C	25°C	30°C	35°C	25°C	30°C	35°C	25°C	30°C	35°C	25°C	30°C	35°C
Langmuir	Q	84.034	76.924	76.335	89.285	89.285	200	86.956	94.339	94.339	6.397	8.130	9.461	6.410	7.917	20.450	23.753	25.445	27.933
	b	0.018	0.025	0.027	0.015	0.016	0.008	0.018	0.019	0.024	0.254	0.235	0.232	0.163	0.153	0.054	0.036	0.040	0.037
	R²	0.988	0.993	0.995	0.944	0.986	0.999	0.972	0.985	0.996	0.972	0.950	0.978	0.985	0.968	0.954	0.996	0.989	0.992
	R_L	0.182	0.137	0.129	0.211	0.200	0.334	0.182	0.174	0.143	0.037	0.041	0.042	0.057	0.062	0.156	0.217	0.200	0.213
Freundlich	K_f	5.260	6.120	6.086	4.040	3.365	2.186	4.040	5.90	5.030	1.368	1.397	1.725	1.134	1.230	1.130	1.190	1.348	1.359
	1/n	0.5003	0.4708	0.485	0.565	0.618	0.807	0.565	0.506	0.577	0.535	0.694	0.652	0.547	0.610	0.831	0.708	0.708	0.725
	R²	0.913	0.912	0.955	0.848	0.990	0.999	0.849	0.894	0.994	0.988	0.938	0.975	0.980	0.964	0.944	0.988	0.978	0.983
Temkin	b_T	149.833	156.235	145.263	133.920	115.293	76.117	158.109	137.224	109.766	1461.050	939.347	953.824	1586.862	1254.553	798.966	539.755	487.988	465.250
	A	0.220	0.263	0.247	0.176	0.135	0.110	0.266	0.245	0.192	1.692	1.306	1.672	1.265	1.180	0.895	0.440	0.460	0.460
	R²	0.962	0.960	0.975	0.810	0.973	0.962	0.920	0.936	0.986	0.938	0.786	0.885	0.978	0.963	0.949	0.975	0.946	0.955
D-R	Q_m	50.390	50.170	51.270	52.625	51.187	63.637	51.574	54.785	57.513	4.645	5.608	6.168	4.036	4.665	5.983	10.383	11.345	11.737
	K	4×10 ⁻⁵	3×10 ⁻⁵	3×10 ⁻⁵	5×10 ⁻⁵	4×10 ⁻⁵	4×10 ⁻⁵	4×10 ⁻⁵	3×10 ⁻⁵	2×10 ⁻⁵	5×10 ⁻⁷	5×10 ⁻⁷	4×10 ⁻⁷	1×10 ⁻⁶	9×10 ⁻⁷	1×10 ⁻⁶	4×10 ⁻⁶	4×10 ⁻⁶	3×10 ⁻⁶
	R²	0.944	0.925	0.887	0.892	0.830	0.856	0.971	0.927	0.853	0.798	0.687	0.785	0.875	0.819	0.825	0.905	0.880	0.885
	E	111.80	129.10	129.10	100.00	111.80	111.80	111.80	111.80	129.10	158.11	1000	1000	1118.03	707.11	745.36	707.11	353.55	353.55

4.1.2.7. Adsorption Thermodynamics

The adsorption characteristics of CV, MG and MB were examined in both single as well as ternary dye system at varying temperatures (25°C, 30°C and 35°C). The adsorption of dye increased with increasing temperature suggesting that the process of adsorption was endothermic in nature. Thermodynamic equations given in section 3.12 (chapter 3) were utilized to determine number of thermodynamic parameters related to adsorption including the change in entropy (ΔS°), the change in enthalpy (ΔH°) and the change in free energy (ΔG°). The slope and intercepts of linear plot of $\ln K_d$ versus $1/T$ were used to calculate the values of ΔH° , ΔS° and ΔG° (Figure 4.1.18 for single dye system and figure 4.1.19 for ternary dye systems, respectively). Table 4.1.4 presents the computed values for various thermodynamics parameters. The calculated ΔH° values were positive, which showed the endothermic nature of adsorption process. In a similar manner, the values of ΔS° were also positive suggested an increased level of randomization on the surface of the adsorbent, spontaneity of the process was indicated by the negative value of ΔG° .^{76,99,136}

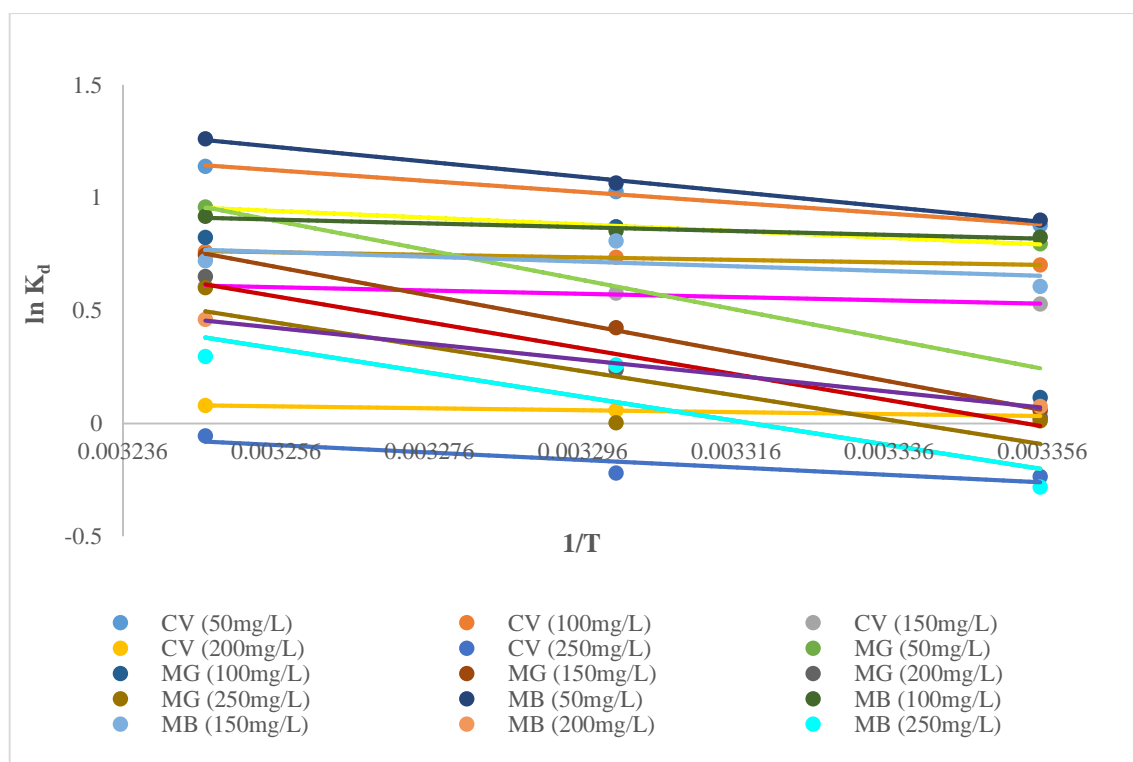


Figure 4.1.18: Adsorption thermodynamic plots for CV, MG and MB in single dye system

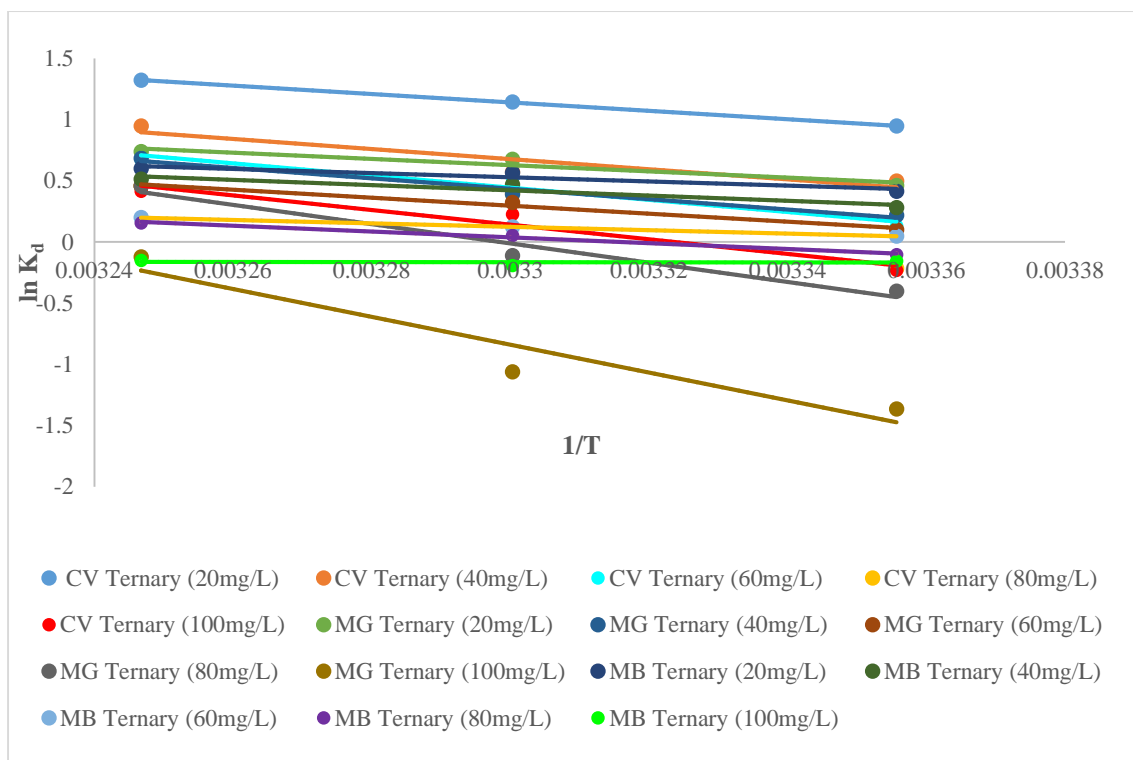


Figure 4.1.19: Adsorption thermodynamic plots for CV, MG and MB in ternary dye system

Table 4.1.4: Thermodynamic parameters in single and ternary dye system

System	Concentration (mg/L)	ΔH° (KJ/mol)	ΔS° (KJ/mol/K)	ΔG° [25°C] (KJ/mol)	ΔG° [30°C] (KJ/mol)	ΔG° [35°C] (KJ/mol)
Single CV	50	19.918	0.075	-2.175	-2.585	-2.915
	100	4.600	0.022	-1.739	-1.854	-1.950
	150	6.025	0.025	-1.310	-1.455	-1.555
	200	3.583	0.013	-0.082	-0.145	-0.205
	250	13.702	0.044	0.583	0.555	0.140
Single MG	50	12.378	0.048	-1.973	-2.195	-2.454
	100	54.374	0.185	-0.286	-1.188	-2.110
	150	52.692	0.177	-0.140	-1.066	-1.912
	200	47.792	0.160	-0.059	-0.600	-1.667
	250	44.770	0.150	-0.026	-0.005	-1.538
Single MB	50	27.498	0.100	-2.232	-2.684	-3.230
	100	7.063	0.031	-2.044	-2.152	-2.350
	150	8.690	0.034	-1.505	-2.037	-1.843
	200	29.385	0.100	-0.186	-0.650	-1.179

System	Concentration (mg/L)	ΔH° (KJ/mol)	ΔS° (KJ/mol/K)	ΔG° [25°C] (KJ/mol)	ΔG° [30°C] (KJ/mol)	ΔG° [35°C] (KJ/mol)
Ternary CV	250	44.354	0.147	0.697	0.215	-0.760
	20	28.555	0.104	-2.347	-2.885	-3.385
	40	34.347	0.118	-1.232	-1.442	-2.430
	60	41.263	0.140	-0.325	-1.305	-1.717
	80	49.510	0.165	0.536	-0.995	-1.176
	100	49.509	0.165	0.576	-0.573	-1.062
Ternary MG	20	21.146	0.075	-1.144	-1.702	-1.890
	40	35.396	0.120	-0.543	-0.984	-1.750
	60	27.275	0.093	-0.250	-0.812	-1.173
	80	65.453	0.215	0.995	0.280	-0.854
	100	94.680	0.305	3.383	2.670	0.311
Ternary MB	20	14.288	0.052	-1.027	-1.425	-1.540
	40	17.802	0.063	-0.695	-1.180	-1.315
	60	11.507	0.040	-0.120	-0.315	-0.510
	80	19.713	0.065	0.255	-0.135	0.383
	100	0.467	0.001	0.386	0.483	-0.397

4.1.3. Regeneration of Adsorbent

Adsorbent regeneration is crucial for assessing its performance after the adsorption studies. The effectiveness of the adsorbent after recycling process is the primary factor in determining its cost efficiency. Following the analysis of adsorption capacities for various dyes (CV, MG and MB) onto the ZFPC composite, the regeneration process was carried out by using HCl (0.1N) as desorbing agent for both the dye systems (single and ternary dye). The composite's regeneration efficiency was calculated for a maximum of five cycles. The results of study indicate that the ZFPC composite exhibit effective reusability and may serve as an economically feasible adsorbent for removing cationic dyes. The regeneration efficiency of the prepared composite is presented in table 4.1.5 for single and ternary dye system. The data clearly shows that even after five adsorption-desorption cycles, the ZFPC composite still maintained a good regeneration efficiency in both the dye systems. For single dye system, the regeneration efficiency calculated for CV, MG and MB was 90.1%, 87.2% and 89.9% respectively whereas, for ternary dye system, the efficiency found was 86.9%, 87.1% and

84.4% for CV, MG and MB respectively. These findings suggest that the ZFPC composite exhibits excellent reusability and can serve as a cost-effective adsorbent.^{59,165}

Table 4.1.5: Regeneration efficiency of zinc ferrite pine cone composite for single and ternary dye system

Regeneration cycle	Single dye (50 mg/L)			Ternary dye (20 mg/L)		
	CV (%)	MG (%)	MB (%)	CV (%)	MG (%)	MB (%)
1	100	100	100	100	100	100
2	98.6	98.2	99.1	96.6	96.9	95.8
3	96.0	95.3	96.4	92.2	93.0	92.7
4	93.4	91.4	92.8	89.1	90.4	89.0
5	90.1	87.2	89.9	86.9	87.1	84.4

4.2. Nickel Ferrite Pine Cone (NFPC) Composite

4.2.1. Characterization and Morphology

4.2.1.1. Fourier Transform Infrared Spectroscopy

The Fourier Transform Infrared spectrum of pine cone (PC), nickel ferrite (NF) and nickel ferrite pine cone (NFPC) is shown in figure 4.2.1. The spectrum of NF and NFPC composite exhibit two different adsorption peaks located below 600 cm^{-1} . These characteristic peaks indicate spinel character of ferrite and ferrite based composite. The characteristic peaks are attributed to the metal oxygen (M-O) band at two different locations [21]. The tetrahedral site's M-O band is denoted by the peak which is observed at a wavenumber ranging from $500\text{ to }600\text{ cm}^{-1}$. On the other hand, the octahedral site's M-O band is identified at a wavenumber ranging from $450\text{ to }400\text{ cm}^{-1}$.¹⁵⁷

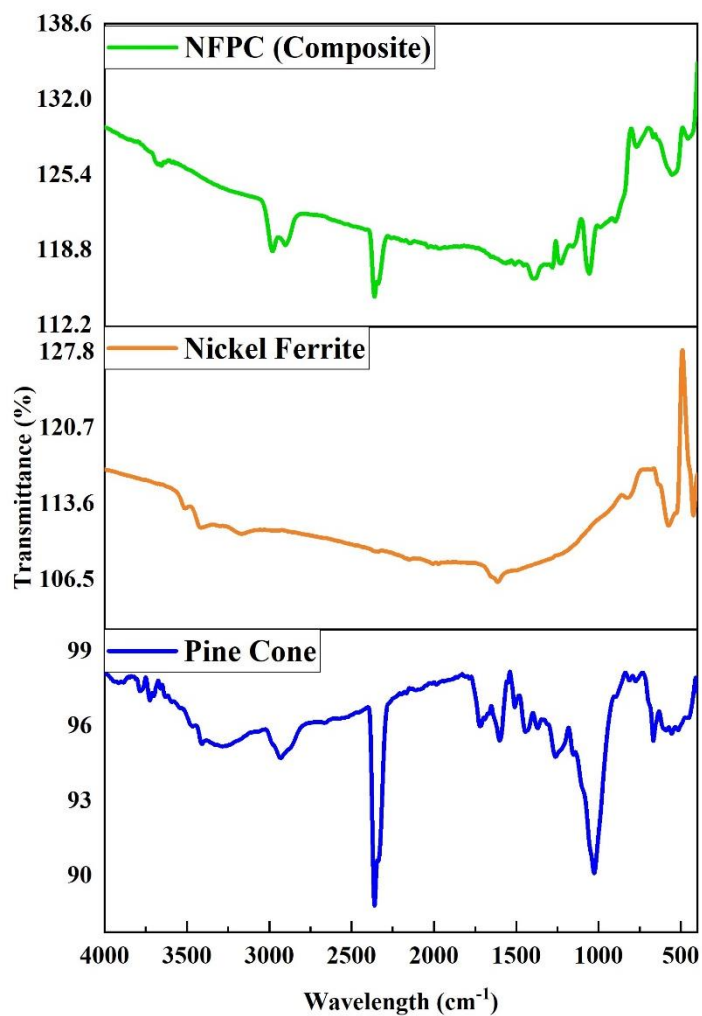


Figure 4.2.1: FTIR of spectra pine cone, nickel ferrite and nickel ferrite pine cone composite

In the spectra of pine cone, peak observed at approximately 3412.04 cm^{-1} corresponds to O-H group. The spectral band CH_n vibration which is caused by C-CH and C- CH_2 bonds is indicated by a peak at approximately 2925.41 cm^{-1} . A peak found at 2366.55 cm^{-1} may occur due to the presence of carbon dioxide. The peak at 1605.02 cm^{-1} observed in the pine cone sample corresponds to the C=O and C=C vibrations. Another peak, found at 1440.46 cm^{-1} corresponds to a minor alkane C-H adsorption band. The peak observed at 1261.79 cm^{-1} in the pine cone might have been formed by the vibration of a carboxylic acid C-O bond. Peak at 1024.08 cm^{-1} in the pine cone sample may be attributed to the stretching of -C-C bond.¹⁹⁴ The NFPC that was prepared exhibited characteristic peaks of both materials which are PC and NF with slight shifts, as illustrated in figure 4.2.1. These shifts confirmed the successful formation of the NFPC composite.

4.2.1.2. X-Ray Diffraction

The X-ray diffraction pattern of NF and NFPC composite are shown in figure 4.2.2. The XRD pattern of NF showed distinct peaks at $2\theta \sim 30.2^\circ, 36.4^\circ, 37.5^\circ, 43.1^\circ, 53.4^\circ, 57.9^\circ, 62.1^\circ, 71.32^\circ, 73.8^\circ$ and 79° . The peaks identified in the above order are indicative of the following Miller indices: (220), (311), (222), (400), (422), (511), (440), (620), (533) and (444) respectively. The peaks illustrate the greater phase purity and crystallinity of nickel ferrite. The X-ray diffraction pattern of NFPC composite, on the contrary, reveals almost similar peaks with a slight difference and the composite follows the same Bragg's reflection pattern [119]. The findings indicated that the composite possesses crystalline structure and retains its spinel character despite undergoing surface modifications.¹⁵⁷ The average size of crystallite calculated using the Scherrer formula (equation 3.1) was 35.4 nm for pure NF and 49.6 nm for the NFPC composite.

4.2.1.3. Field Emission Scanning Electron Microscope

FESEM images of the NF and NFPC is given in figure 4.2.3 which provide and insight to the surface morphology of these materials. NF ferrite showed varied particle size as well as an uneven shape whereas, the NFPC composite showed similar morphology with uneven surface where the particles of ferrites were attached. The largest particle size determined for NF was $1.51\text{ }\mu\text{m}$ while the smallest size observed was $0.10\text{ }\mu\text{m}$. Based on the calculations, average size calculated for nickel ferrite was obtained to be $0.91\text{ }\mu\text{m}$. The prepared composite yielded an average particle size of $2.89\text{ }\mu\text{m}$ with the largest particle size $2.08\text{ }\mu\text{m}$ and the smallest $0.28\text{ }\mu\text{m}$. Based on the above calculations, it was found that the size of NFPC composite was greater

as compared to pure NF. This finding provides evidence that spinel nickel ferrite has successfully been modified with pine cone.^{87,195}

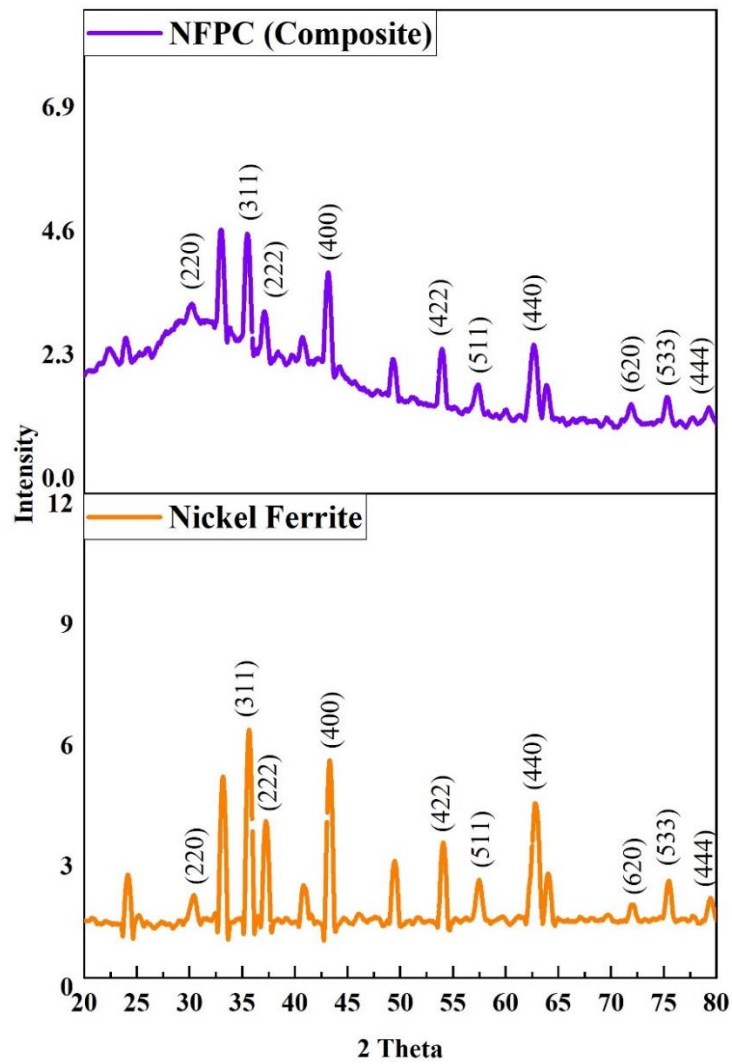


Figure 4.2.2: XRD spectra of nickel ferrite and nickel ferrite pine cone composite

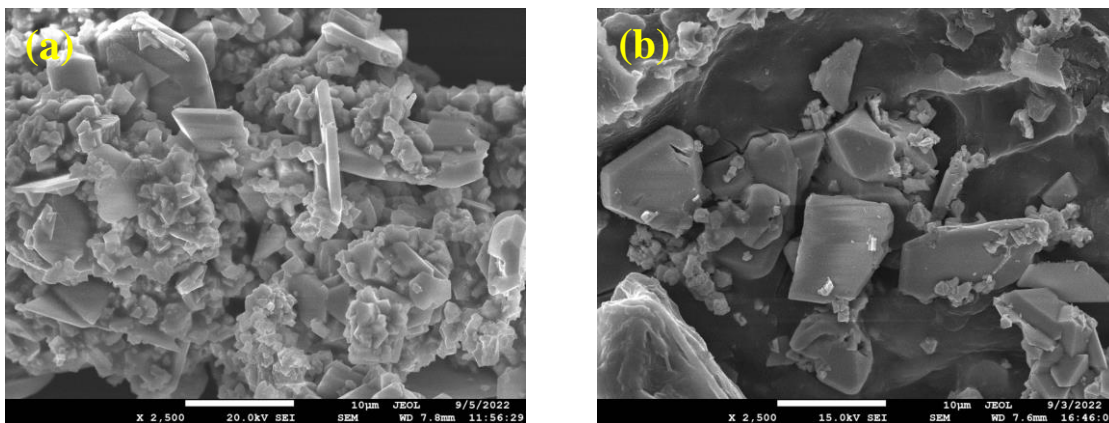


Figure 4.2.3: SEM image (a) Nickel ferrite (b) Nickel ferrite pine cone composite

4.2.1.4. Energy Dispersive Spectra

The Energy Dispersive spectra of NF and NFPC composite are shown in figure 4.2.4 along with the peaks representing the elemental composition of each compound. The atomic and weight percentages of the different elemental components present in the compounds are shown in table 4.2.1. The elemental composition clearly indicates that the proportion of carbon in the NFPC composite increased consistently in comparison to pure NF which serves as an evidence that the modification of nickel ferrite with pine cone can effectively result in the formation of a magnetic composite.⁸⁷

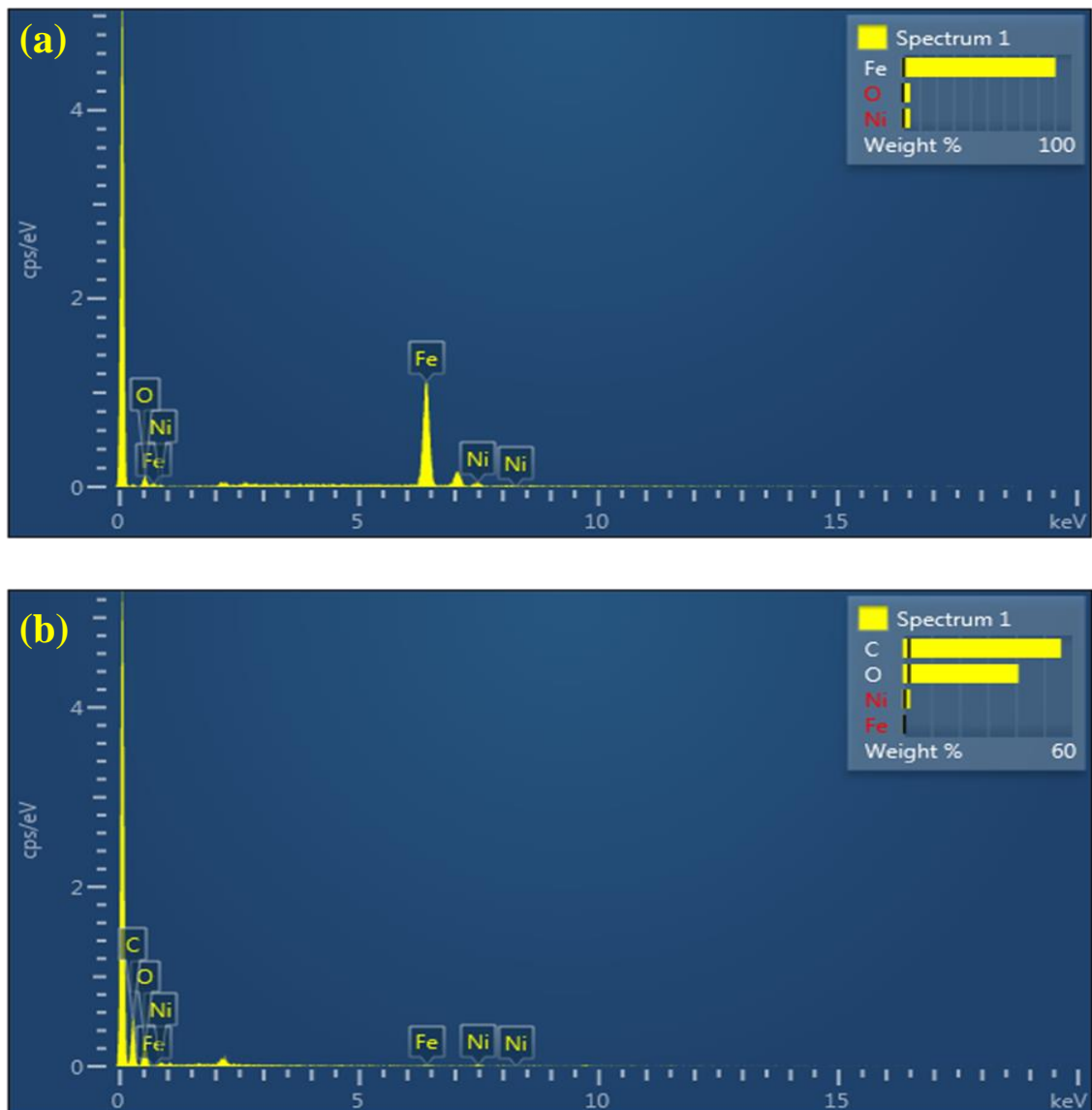


Figure 4.2.4: EDS image (a) Nickel ferrite (b) Nickel ferrite pine cone composite

Table 4.2.1: Elemental composition of nickel ferrite and nickel ferrite pine cone composite

Element	Nickel Ferrite		Nickel Ferrite Pine Cone composite	
	Weight %	Atomic %	Weight %	Atomic %
C			44.95	57.08
O	4.70	14.72	42.22	32.03
Fe	90.61	81.28	10.75	9.09
Ni	4.69	4.00	2.08	1.80
Total	100.00	100.00	100.00	100.00

4.2.1.5. Thermogravimetric Analysis

The thermogravimetric analysis graph of NFPC composite is presented in figure 4.2.5. The TGA was conducted to examine the thermal stability of composite material. The analysis was performed in an air atmosphere with conditions; temperature range:28-600°C and heat rate: 10°C/min.

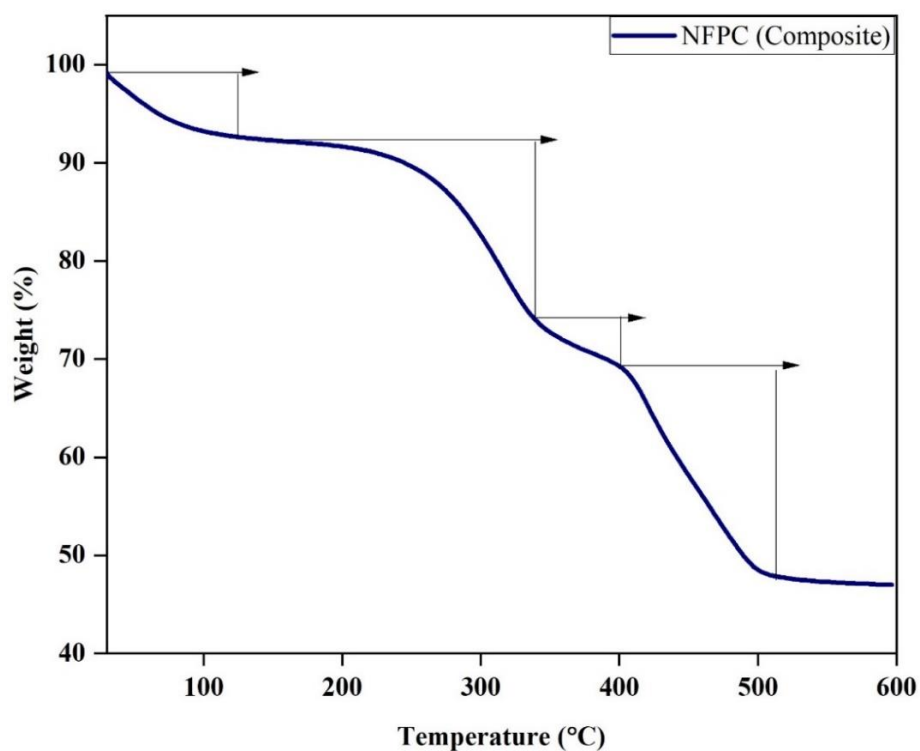


Figure 4.2.5: TGA curve of nickel ferrite pine cone composite

As shown in graph, an approximate weight reduction of 7.1% was detected at 32.9 °C to 101.6 °C. The reduced weight observed in the sample can be attributed to the evaporation of entrapped moisture in the sample. An additional weight loss of 19.4% and 5% was observed with an increase in temperature at approximately 101.6°C to 343.7°C and 343.7°C to 407.7°C respectively which could be due to the decomposition of organic matter. Further, at approximately 407.7°C to 501.75°C, an abrupt weight loss of 20.1% was again observed which indicated that the organic matter present in the composite had undergone complete decomposition, as no further weight loss was detected thereafter. On the basis of above observations, it has been calculated that 0.479 grams of PC has been attached with 1 gram of NFPC composite.¹⁹⁶

4.2.1.6. Brunauer-Emmett-Teller Analysis

The specific surface area of material was studied through BET analysis. The results of the BET analysis performed on NF and NFPC composite showed that the surface area calculated for NF is less than NFPC. The specific surface area of NF and NFPC composite was 0.443 m²/g and 1.823 m²/g respectively. The data clearly demonstrates that NF confronted a decrease in its specific surface area. This happened because the size of particles increased when the surface of the nickel ferrite had been modified with pine cone as compared to pure nickel ferrite. On surface modification, the porosity on the surface of composite increased which caused an increase in specific surface area.^{153,197}

4.2.1.7. pH of Point Zero Charge Analysis

The solid addition method was employed for studying the pH_{zpc} of NFPC. For conducting the experiment, 50 mL of distilled water based 0.1M KNO₃ solution had been added to each of nine 250 mL Erlenmeyer flasks. By adding NaOH (0.1M) and HCl (0.1N), the pH of prepared solution was adjusted to a range between 3 to 11, which corresponds to the initial pH of the solution. To each glass flask, 0.1 g composite was added. The flasks were placed a shaker for a period of 24 hours. After this, the glass flasks were removed and the content of each flask were filtered in separate beakers. The final pH value of solution present in beakers was noted and the calculations were performed using the equation 3.2 (Chapter-3).¹⁹⁶

Using the above calculations, a graph was plotted between initial pH (on x-axis) and Δ pH i.e.; the difference between the initial pH and final pH (on y-axis) as depicted in figure 4.2.6. From the graph, the pH_{zpc} value of NFPC composite was determined to be 7. It therefore states that

the surface of composite will have positive charge below pH 7 and a negative charge above pH 7.^{185,186}

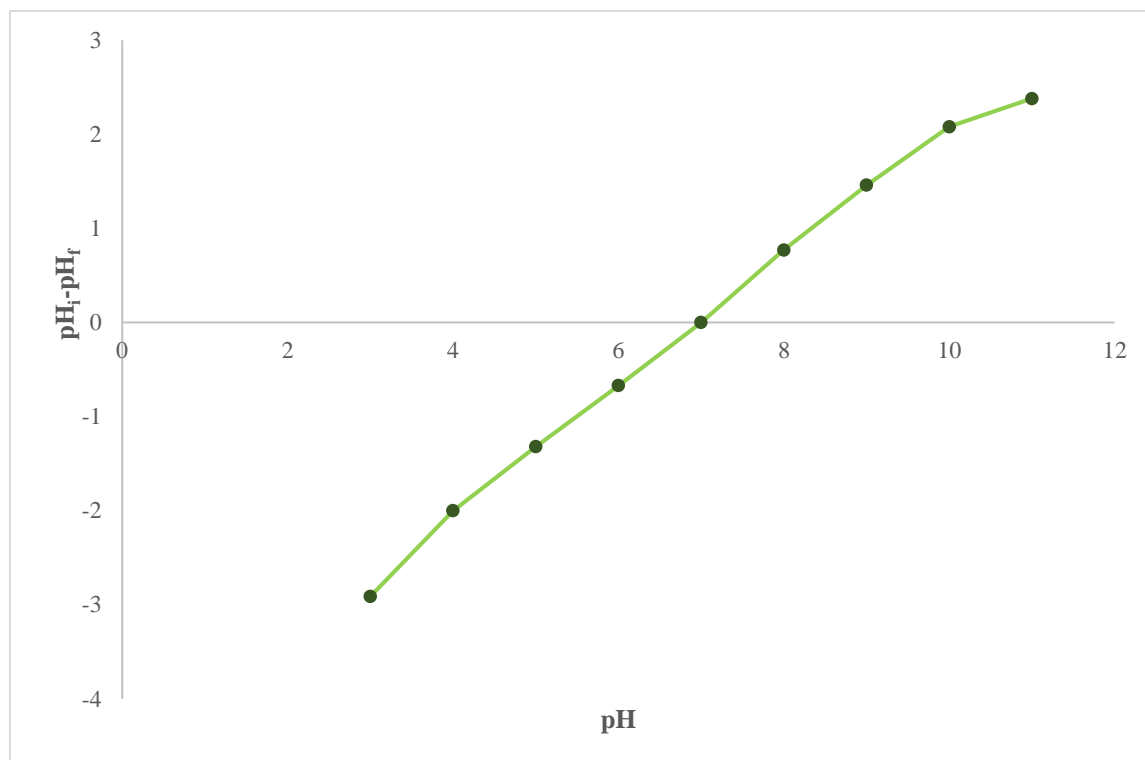


Figure 4.2.6: pH_{zpc} of nickel ferrite pine cone composite

4.2.2. Adsorption Study in Single and Binary Dye System

The batch adsorption method was employed to study the adsorption characteristics of the NFPC composite. The NFPC composite exhibits dye selectivity towards different dyes in an aqueous solution as demonstrated by pilot-scale studies described in chapter 3. Different dye systems which includes single and binary were studied to assess the selectivity of NFPC composite towards cationic dyes. The prepared composite's adsorption performance was examined with several dyes but the dyes BG and MB exhibit good removal efficiency among all. Therefore, BG and MB were utilized to examine the adsorption characteristics of NFPC in both single as well as binary dye systems. Different adsorption parameters like contact time, dosage of adsorbent, pH, temperature and adsorbate concentration were thoroughly studied.

4.2.2.1. Effect of Contact Time

To study the effect of contact time on NFPC composite in single and binary dye system, a known concentration of single and binary dye (50 mg/L and 20 mg/L, respectively) was added to an Erlenmeyer flask (100 mL) along with 0.1g adsorbent dose and a specified volume of dye solution (50 mL). These flasks were then placed in a thermostatic shaker for 3 hours. After

regular intervals, the glass flasks were taken out and the remaining concentration was assessed using a UV- VIS Spectrophotometer. The contact time effect on BG and MB dyes in single as well as binary dye system is shown in figure 4.2.7. The graph demonstrates that percentage of BG and MB removal was rapid during the initial phase but as the time increases, it stabilized and ultimately attained equilibrium. This may be due to the fact that initially, there were numerous available adsorption sites on the surface of NFPC, which facilitates the rapid adsorption of dye molecules. However, as time passed, these sites gradually became occupied, resulting in deceleration of the adsorption rate until it balanced with the rate of desorption, indicating the attainment of equilibrium.^{87,157} In single dye system, the rate of adsorption was initially high due to availability of abundant active sites but eventually slowed down and reached equilibrium at 110 and 120 minutes for MB and BG respectively. The maximum removal percentages obtained for BG and MB were 94% and 81.3%, respectively. Similarly, in binary dye system, the adsorption proceeded rapidly in initial phase and the equilibrium was attained at around 100 minutes. The maximum removal percentages for BG and MB dye in the ternary system were calculated as 79.7% and 62% respectively.

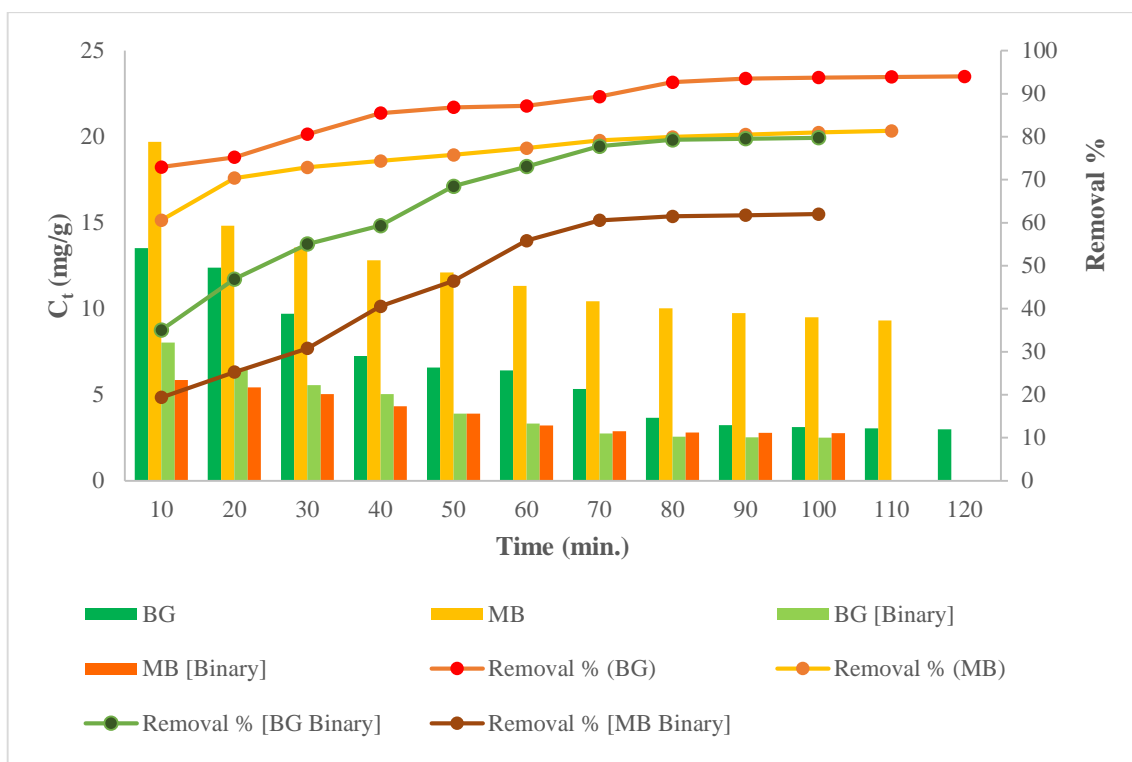


Figure 4.2.7: Effect of contact time for single and binary dye system

4.2.2.2. Adsorption Kinetics

Adsorption Kinetics were studied to determine the characteristics of the adsorption process. Adsorption kinetics study of NFPC composite for single as well as binary dye systems were examined by employing various models including the Lagergren pseudo-first order model, pseudo-second order model and the Elovich model.^{47,198} The time study data was represented graphically using these models of kinetics. The plot of Lagergren pseudo-first order and pseudo-second order model for the single and binary dye system is shown in figure 4.2.8, while the plot of Elovich model is represented in figure 4.2.9. Table 4.2.2 represents the calculated values of different constants associated with kinetic models. The degree of suitability of the model can be assessed by analysing the regression coefficient (R^2) value. A higher R^2 value approaching 1 suggests best fit to the data. So, the pseudo-second order model exhibited the most favourable among the three, followed by Elovich model and pseudo first order model suggesting the chemical nature of adsorption process.¹⁵⁷

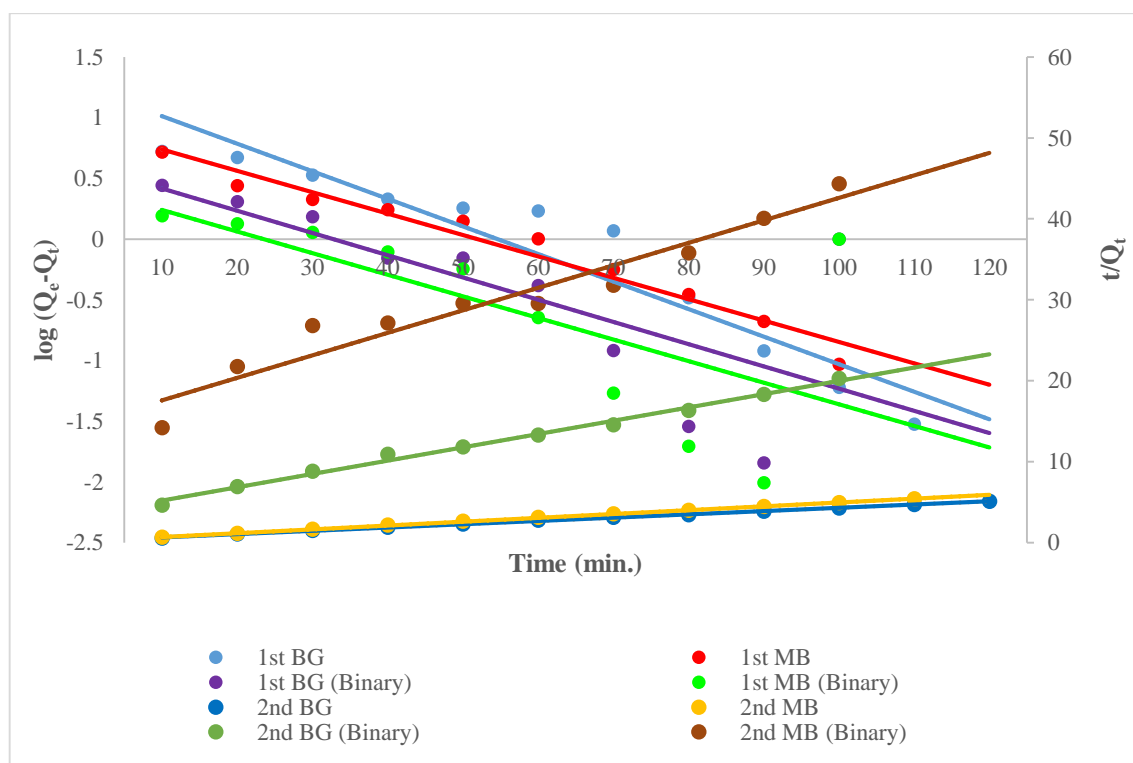


Figure 4.2.8: Lagergren pseudo first order and pseudo second order kinetics for single and binary dye system

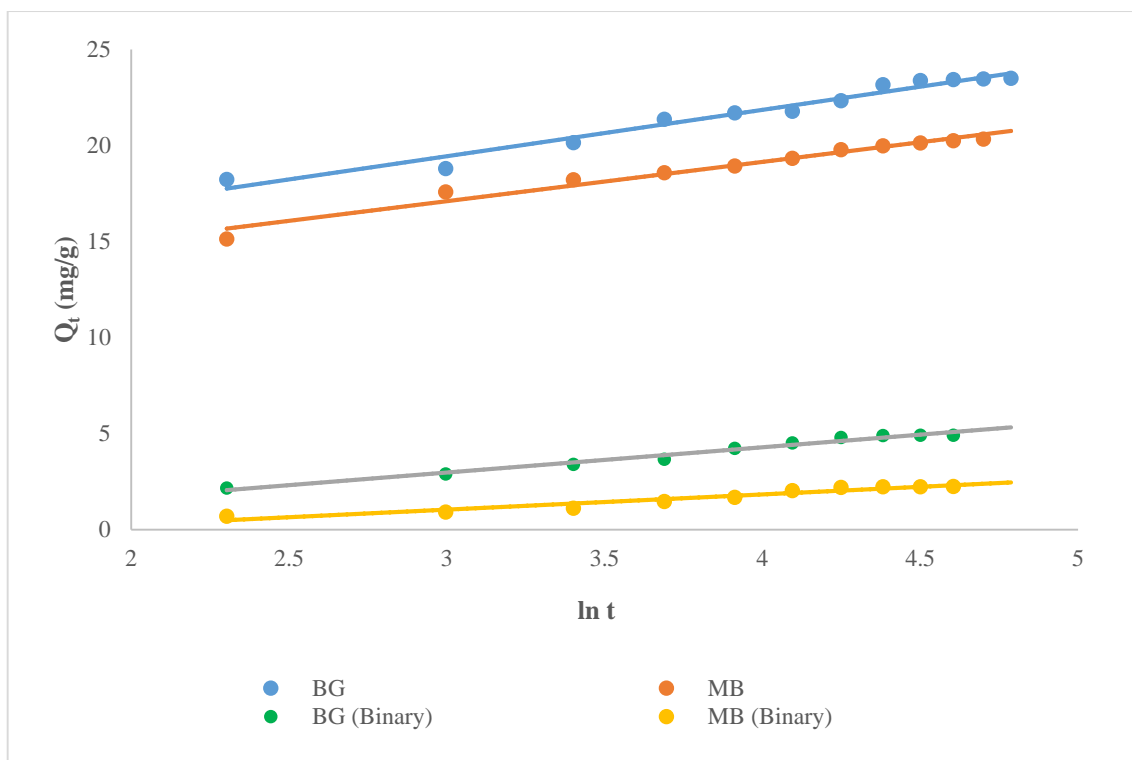


Figure 4.2.9: Elovich model for single and binary dye system

Table 4.2.2: Calculated values of different kinetic constants for single and binary dye system

KINETIC MODEL	SYSTEM				
	Parameter	Single BG	Single MB	Binary BG	Binary MB
Lagergren Pseudo first order	Q_{e1}	17.318	8.215	3.973	2.610
	K_1	0.523	0.406	0.421	0.409
	R^2	0.912	0.965	0.503	0.436
Pseudo second order	Q_{e2}	2.467	2.115	0.609	0.359
	h	4.115	4.428	0.281	0.067
	K_2	0.675	0.990	0.758	0.521
	R^2	0.998	0.999	0.993	0.935
Elovich model	α	384.206	439.670	0.629	0.146
	β	0.415	0.489	0.760	1.259
	R^2	0.967	0.969	0.981	0.940

The Weber-Morris model of intraparticle diffusion was employed to study the adsorption mechanism of different dyes using NFPC. The correlation between Q_t and $t^{0.5}$ signifies the diffusion characteristics of the adsorbent which is represented in figure 4.2.10, while K_{int}

denotes the rate constant for intra-particle diffusion and the rate limiting step. The rate-limiting step states that the line passing through the origin must be straight. However, the graph reveals the non-linearity and the line do not pass from origin which suggests that in addition to intra-particle diffusion there might be other aspects that influence the rate of adsorption in both the dye system. As shown in figure 4.2.10, the slope was steep in the beginning indicated the rapid dye adsorption for single dye system. After a specified duration of time, the slope flattened out and ultimately reached equilibrium. However, this trend was absent in binary dye system. The decline in adsorption capacity may be attributed to the dye's antagonistic effect. Various forces which includes π - π interactions and electrostatic interaction and existed among BG and MB dye molecules. Different dye molecules in binary dye system form strong bonds with one another as a consequence of these interactions, which in turn slows down the absorption rate. Therefore, percentage of dyes removed in binary dye system was significantly lower when compared to single dye system.^{142,196}

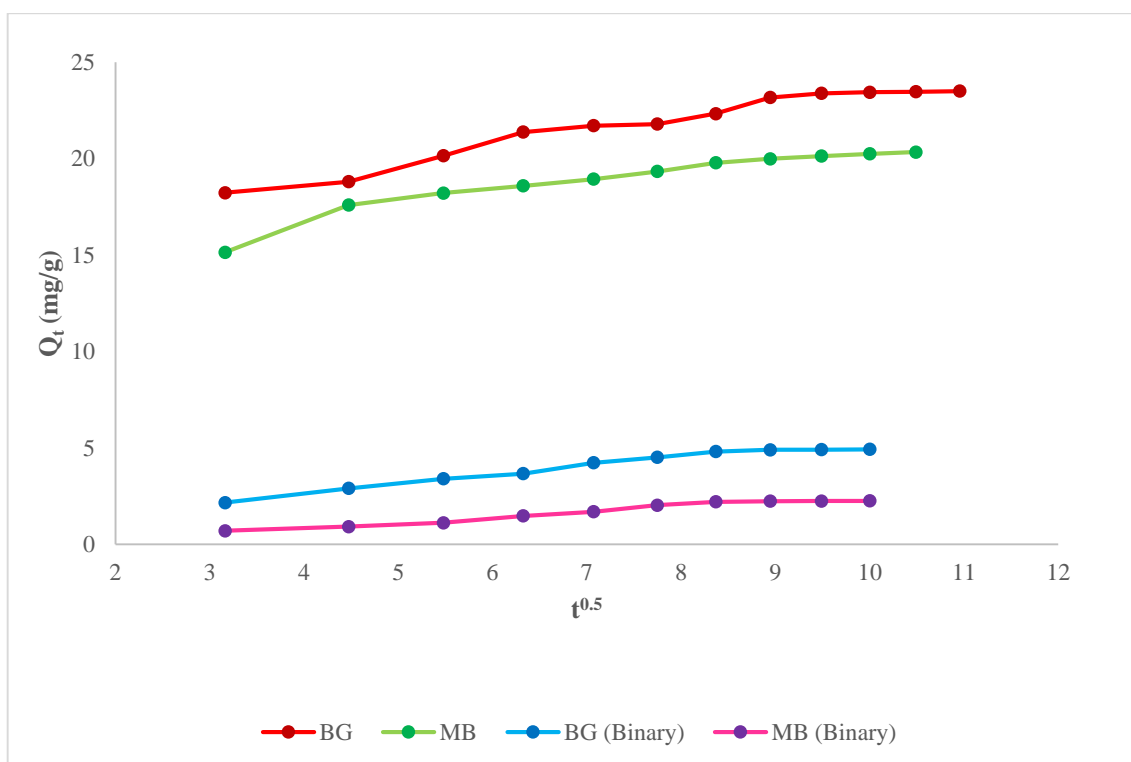


Figure 4.2.10: Intra particle diffusion model for single and binary dye system

4.2.2.3. Effect of pH

In adsorption process, the solution's pH plays a significant role by altering the surface charge of adsorbent, thereby influencing the removal efficacy. The effect of pH was studied to determine the behaviour of adsorption for NFPC composite with different dyes MB and BG in

single system at pH values ranging between 3 to 11. Erlenmeyer flasks containing the prepared dye solution with an initial dye concentration 50 mg/L and an adsorbent dose 0.1 g were placed in a thermostatic shaker for the time duration of three hours at 25°C. Figure 4.2.11 shows the pH effect on the removal of BG and MB dyes in single system. The graph indicates that with increasing pH, the dye removal efficiency increased and reached at pH 7 then further declined. According to findings, pH 7 comes out to be the most effective for the elimination of dyes for this experimental study. The calculated maximum removal percentages were 91.83% for BG and 78.54% for MB.

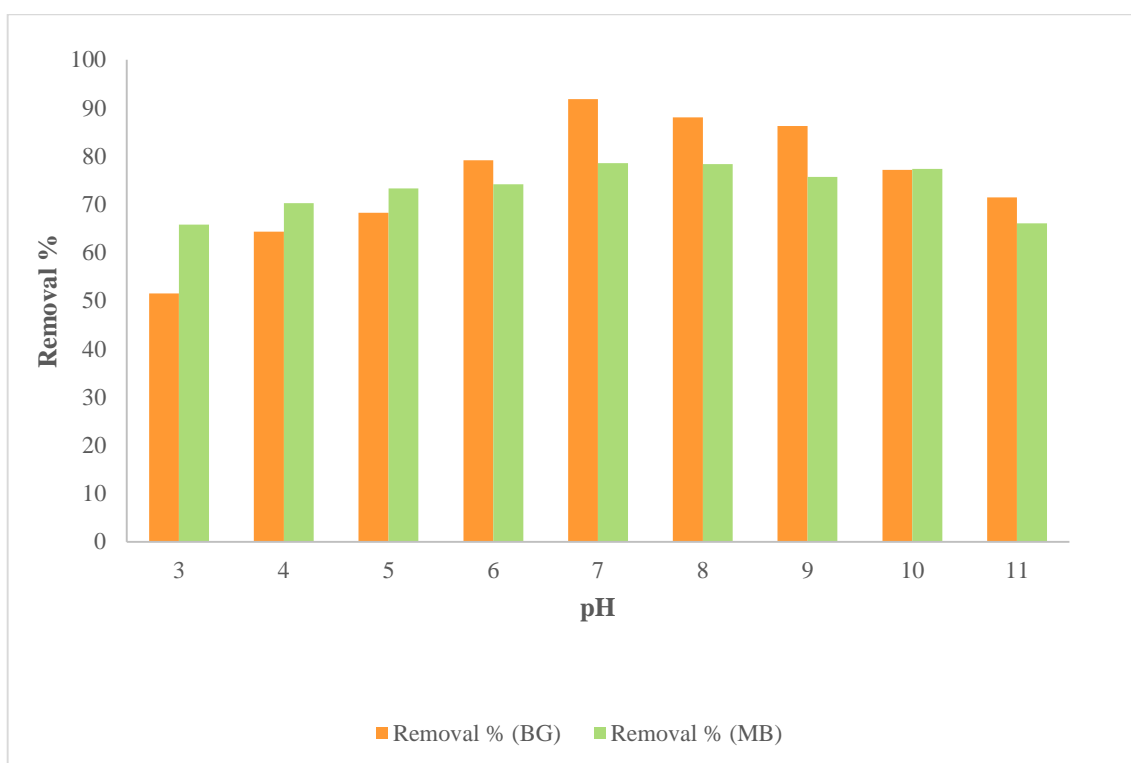


Figure 4.2.11: Effect of pH for single dye system

4.2.2.4. Effect of Adsorbent Dosage

For studying the adsorbent dosage effect, the dosage of prepared NFPC composite was adjusted from 0.1 g - 0.5 g for both single dye as well as binary dye system. The data in figure 4.2.12 illustrates that the efficiency of dye removal increased with increasing dosage of NFPC composite in single and ternary dye system. The enhanced dye removal pattern observed in both the dye systems could be due to the increased availability of unoccupied sites on the composite's surface with an increased adsorbent amount. However, with increased adsorbent amount, the quantity of adsorbate adsorbed per gram of the adsorbent (Q_e) decreased. This

decrease was observed due to more active sites on adsorbent's surface that remained unoccupied with an increase in amount of adsorbent.^{157,158}

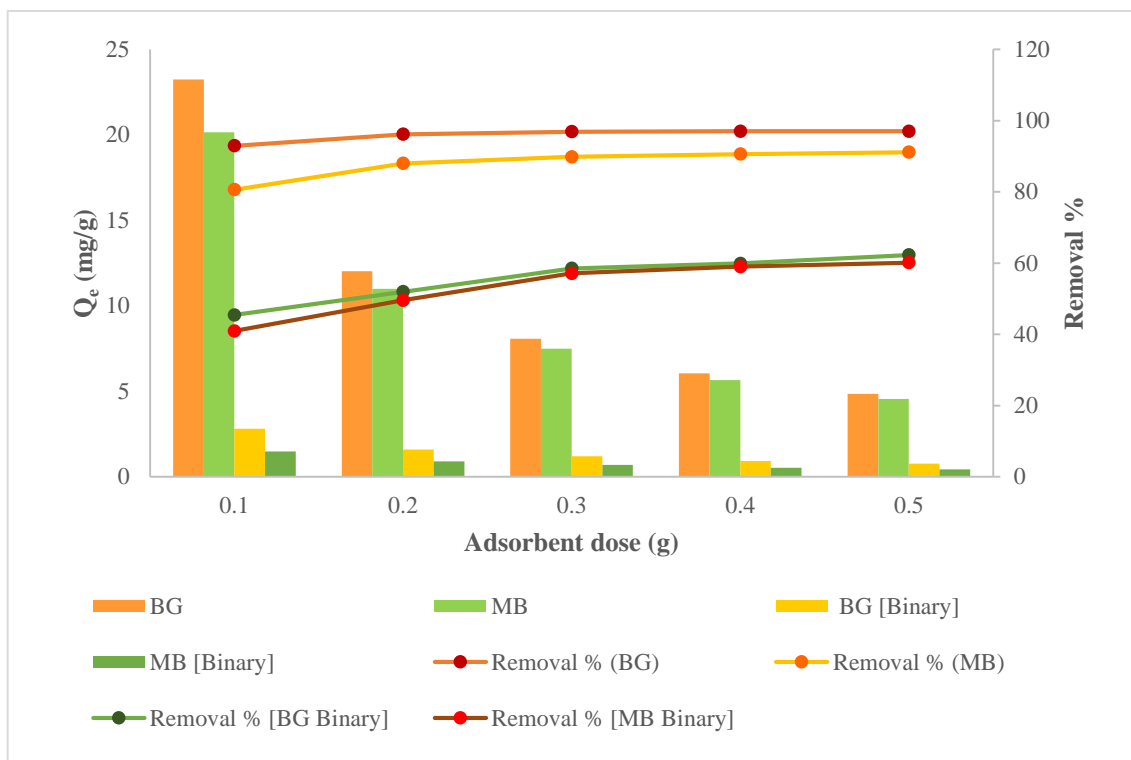


Figure 4.2.12: Effect of adsorbent dosage for single and binary dye system

4.2.2.5. Effect of Concentration and Temperature

The effect of concentration for single and binary dye system was studied with initial dye concentrations ranging from 50 to 250 mg/L for the single dye system and 20 to 100 mg/L for the binary dye system. Additionally, the effect of temperature was studied at temperature 25°C, 30°C and 35°C. Figure 4.2.13 and 4.2.14, illustrates the effect of concentration for dyes at various temperatures in single and binary dye system respectively. It was observed that adsorption capacity of BG and MB in both the dye systems increased as the concentration of dye increased. The rise in adsorption capacity (Q_e) occurred because the contact between dye molecules and adsorbent became stronger when the quantity of dyes increased for a given amount of adsorbent. This eventually led to a greater number of collisions between the adsorbent and the dye molecules. However, it was found that removal percent of dye decreased with increasing concentration in single and binary dye systems.⁵⁸ This may be because of constant number of accessible active sites present on the adsorbent's surface in comparison to the increasing dye concentration. Additionally, it was noted that dye's adsorption capacity increased with increase in temperature, suggesting an endothermic nature of the process.

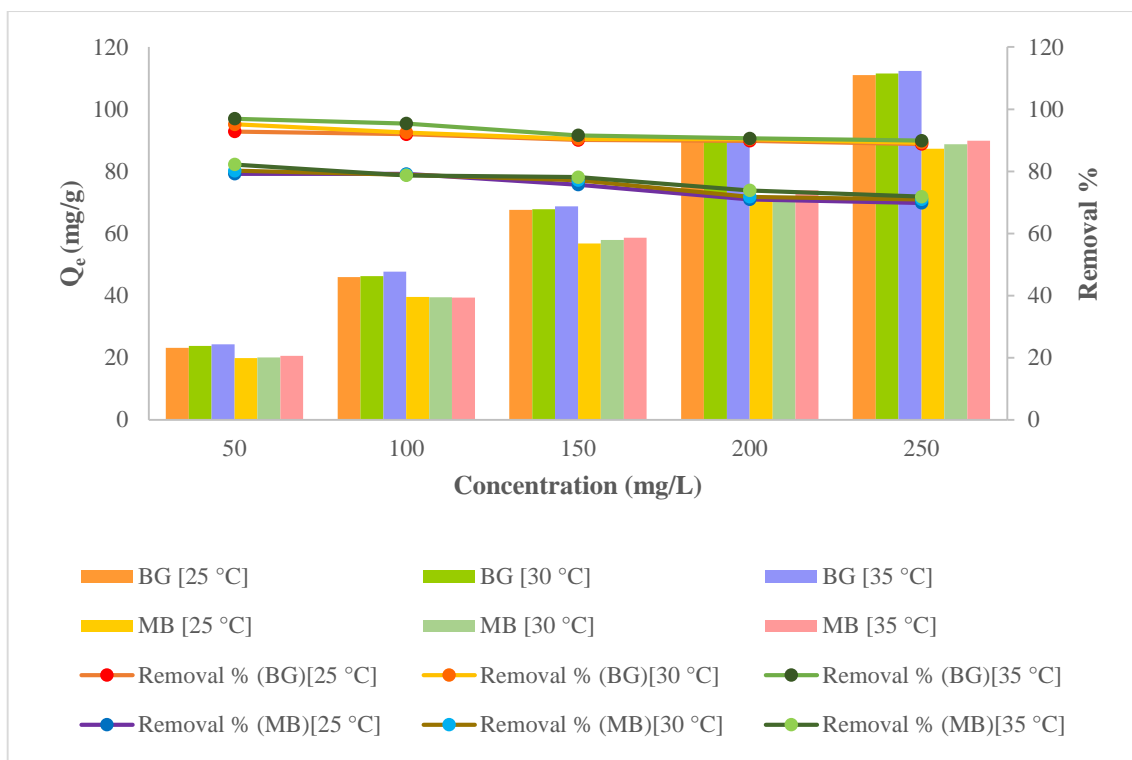


Figure 4.2.13: Effect of concentration for single dye system

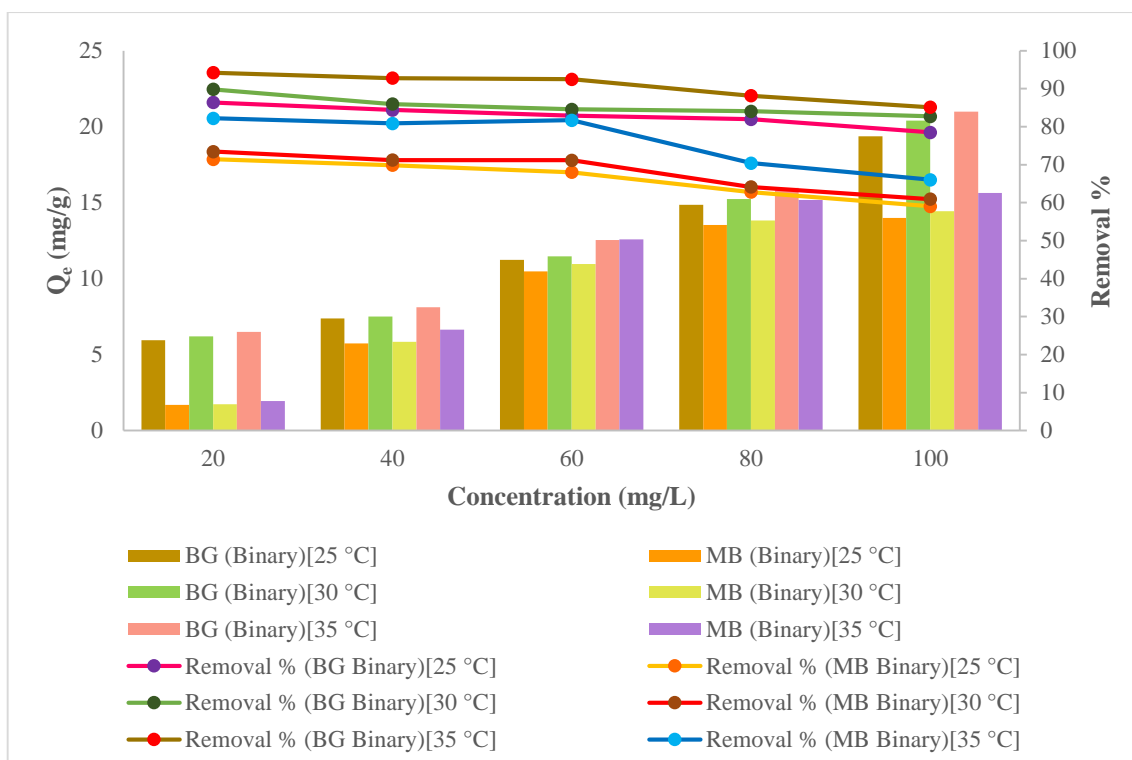


Figure 4.2.14: Effect of concentration for binary dye system

With increasing the adsorption capacity increase could be attributed to the enhanced interaction between the adsorbate and adsorbent molecules which lead to enlargement of certain pores

present in the sample, resulting in greater surface area for adsorption of different dye molecules. As a result, the increase in temperature, leads to an increase in kinetic energy, which results in more effective collisions.^{58,158,196}

The percentage removal of each dye was lower in the binary dye system than in the single dye system because they exhibit antagonistic effect. Moreover, multiple dye systems offer opportunity of mutual interaction among the dye molecules which is another reason for decrease in the adsorption of dyes in multiple dye systems

4.2.2.6. Adsorption Isotherms

Different models of isotherms including the Langmuir model, the Freundlich model, the Temkin model and the Dubinin-Raduskevich (D-R) model were applied to study the equilibrium state of adsorption for dyes BG and MB in single as well as binary dye systems at different temperatures i.e.; 25°C, 30°C and 35°C with NFPC composite.^{58,158} The figure 4.2.15 (a-d) illustrates the plots of different adsorption isotherms for both the dye systems which were studied at different temperatures and varying concentrations. From the plots of isotherms, the values of various constants for both the dye systems (single and binary dye system) were calculated which are shown in table 4.2.3.

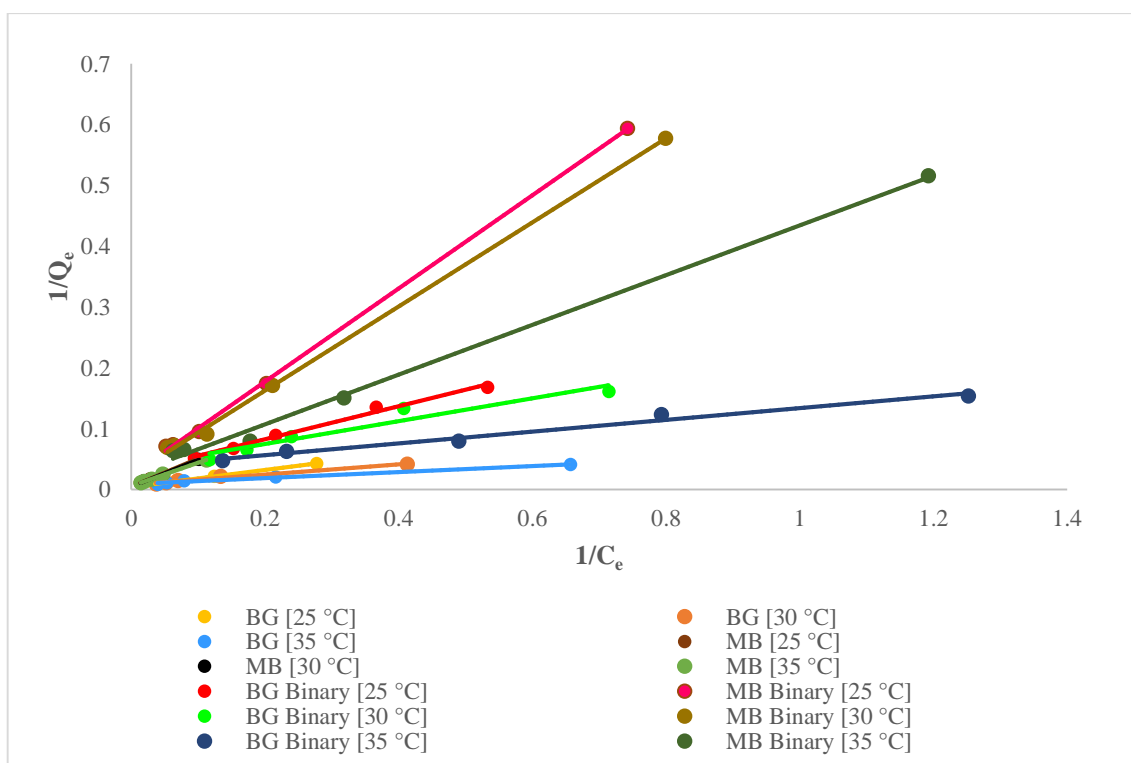


Figure 4.2.15 (a): Langmuir adsorption isotherm for single and binary dye system

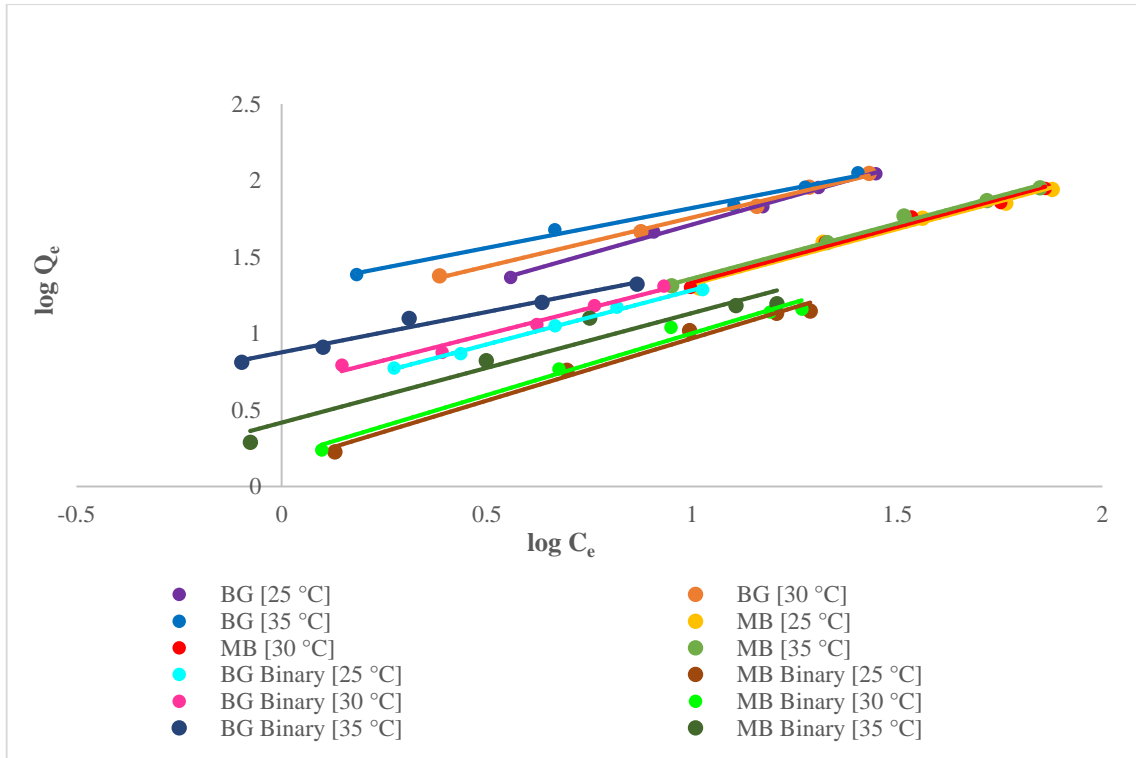


Figure 4.2.15 (b): Freundlich adsorption isotherm for single and binary dye system

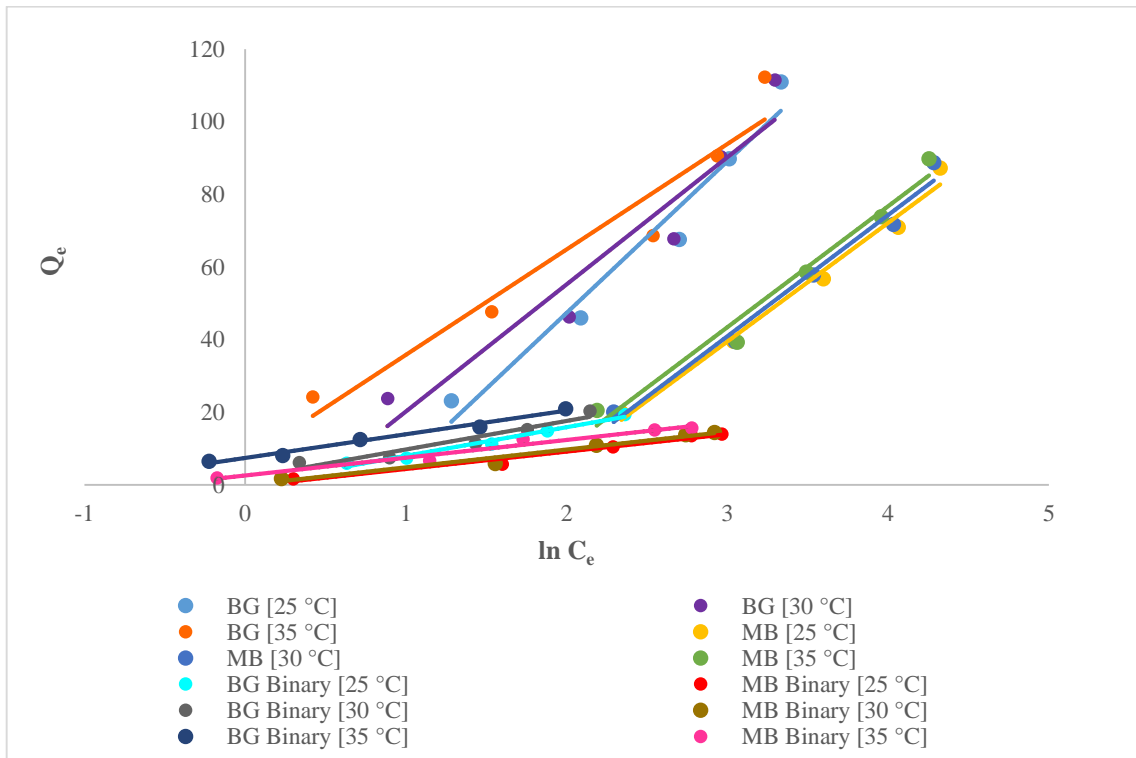


Figure 4.2.15 (c): Temkin adsorption isotherm for single and binary dye system

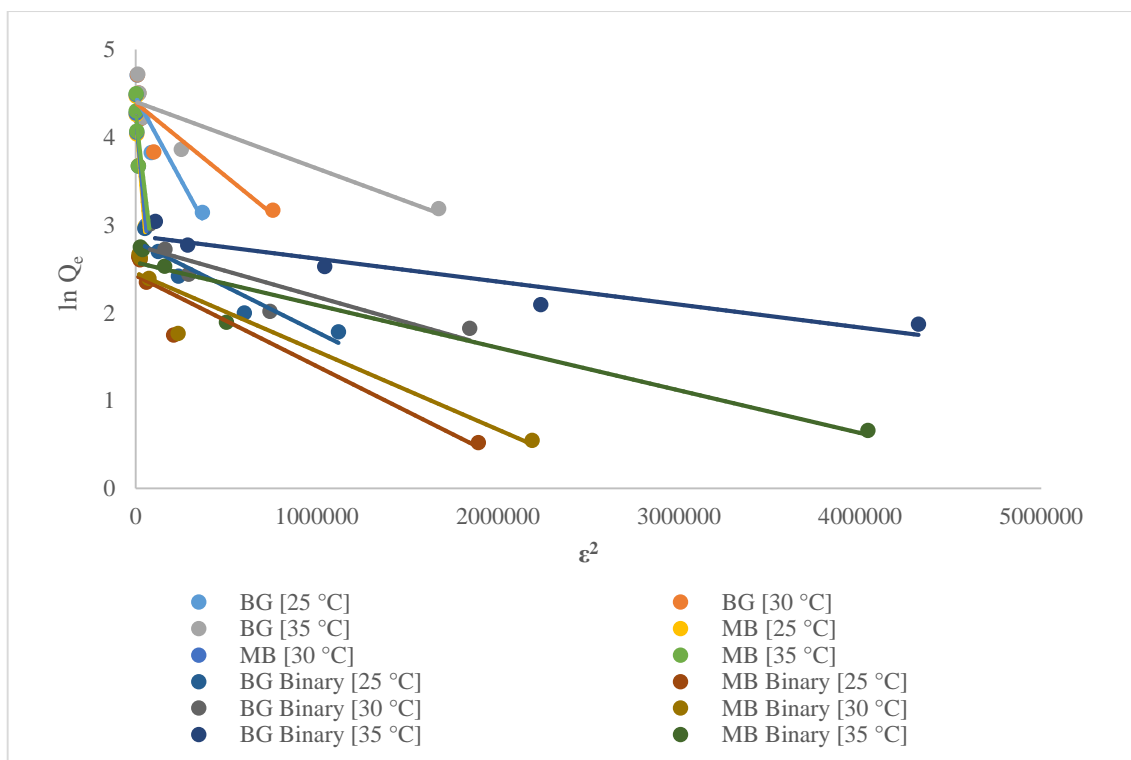


Figure 4.2.15 (d): D-R adsorption isotherm for single and binary dye system

Among the other models of adsorption isotherm, the Langmuir model demonstrated the highest R^2 (correlation coefficient) value. Therefore, according to calculations, the Langmuir model exhibited best fit. These findings suggested that the surface of NFPC composite contains uniform active sites. The maximum capacities of adsorption calculated in single system, for BG and MB were 112.36 and 163.93 mg/g, respectively. However, for binary dye, the maximum adsorption capacity for dyes BG and MB obtained were 26.66 and 38.76 mg/g, respectively.

Further, the separation factor (R_L) is the parameter associated to Langmuir isotherm which was utilized to characterize the nature of adsorption process. As shown in table 4.2.3, the R_L factor values calculated for various dyes in both the dye systems ranged between 0 and 1 which indicated that the process of adsorption is favourable for adsorption of dyes in both the dye system using NFPC composite.^{157,158}

In addition, the Adsorption Energy (E) of the adsorbent related to D-R isotherm was calculated to study the type of adsorption process. The process is considered physical, if the obtained value of 'E' is below 8 KJ/mol, otherwise, the process appeared to be chemical in nature. Table

4.2.3 illustrates the calculated values of ‘E’ for both single and binary dye systems. The resultant values exceeded 100 KJ/mol which indicates chemisorption.¹⁹⁶

Table 4.2.3: Calculated values of adsorption isotherm constants for single and binary dye system

System		Single BG			Single MB			Binary BG			Binary MB		
Isotherm model	Constant	25°C	30°C	35°C	25°C	30°C	35°C	25°C	30°C	35°C	25°C	30°C	35°C
		Langmuir model	Q	222.23	129.87	112.360	200	192.307	163.935	35.335	26.882	26.666	41.153
b	0.033		0.090	0.178	0.010	0.011	0.015	0.105	0.197	0.390	0.032	0.035	0.064
R ²	0.998		0.982	0.987	0.994	0.998	0.997	0.989	0.930	0.982	0.999	0.999	0.995
R _L	0.377		0.182	0.101	0.666	0.645	0.572	0.323	0.203	0.114	0.609	0.588	0.438
Freundlich model	K _f	8.968	13.128	19.930	3.977	4.020	4.380	3.772	4.520	7.543	1.428	1.565	2.616
	1/n	0.760	0.640	0.520	0.722	0.728	0.718	0.705	0.682	0.528	0.814	0.807	0.716
	R ²	0.997	0.995	0.990	0.981	0.985	0.993	0.995	0.976	0.976	0.985	0.980	0.936
Temkin model	b _T	60.315	71.967	86.733	77.034	75.465	75.600	318.573	321.434	387.536	522.753	511.792	514.646
	A	0.420	0.655	1.264	0.166	0.170	0.184	1.005	1.270	3.120	0.905	0.977	1.680
	R ²	0.957	0.920	0.934	0.985	0.980	0.974	0.980	0.923	0.983	0.972	0.968	0.964
D-R model	Q _m	85.935	80.947	81.736	71.015	71.115	70.302	16.608	15.950	17.802	11.298	11.625	13.113
	K	4X10 ⁻⁶	2X10 ⁻⁶	8X10 ⁻⁷	3X10 ⁻⁵	2X10 ⁻⁵	2X10 ⁻⁵	1X10 ⁻⁸	6X10 ⁻⁷	3X10 ⁻⁷	1X10 ⁻⁶	9X10 ⁻⁷	5X10 ⁻⁷
	R ²	0.862	0.796	0.818	0.905	0.886	0.850	0.875	0.760	0.893	0.902	0.897	0.916
	E	353.55	500	790.57	129.10	158.11	158.11	707.11	912.87	1290.99	707.11	745.36	1000

4.2.2.7. Adsorption Thermodynamics

The adsorption behaviour of dyes BG and MB in both single and binary dye systems was examined at different temperatures: 25°C, 30°C and 35°C. The adsorption of dye increased with the increasing temperature, indicating an endothermic nature of the adsorption process. A number of thermodynamic parameters such as the entropy change (ΔS°), enthalpy change (ΔH°) and the free energy change (ΔG°) associated with adsorption were calculated using the thermodynamic equations given in section 3.12 of chapter 3. The values for ΔH° , ΔS° and ΔG° were determined by analysing the intercept and slope of linear plot of $\ln K_d$ vs $1/T$ (Figure 4.2.16 for single dye systems and figure 4.2.17 for binary dye systems, respectively). Table 4.2.4 represents the calculated values of different thermodynamic parameters. The endothermic character of adsorption process was determined by the positive ΔH° values. Similarly, positive values of ΔS° suggest more randomization on the surface of adsorbent, whereas the negative values of ΔG° suggested the spontaneous nature of adsorption process.^{4,142}

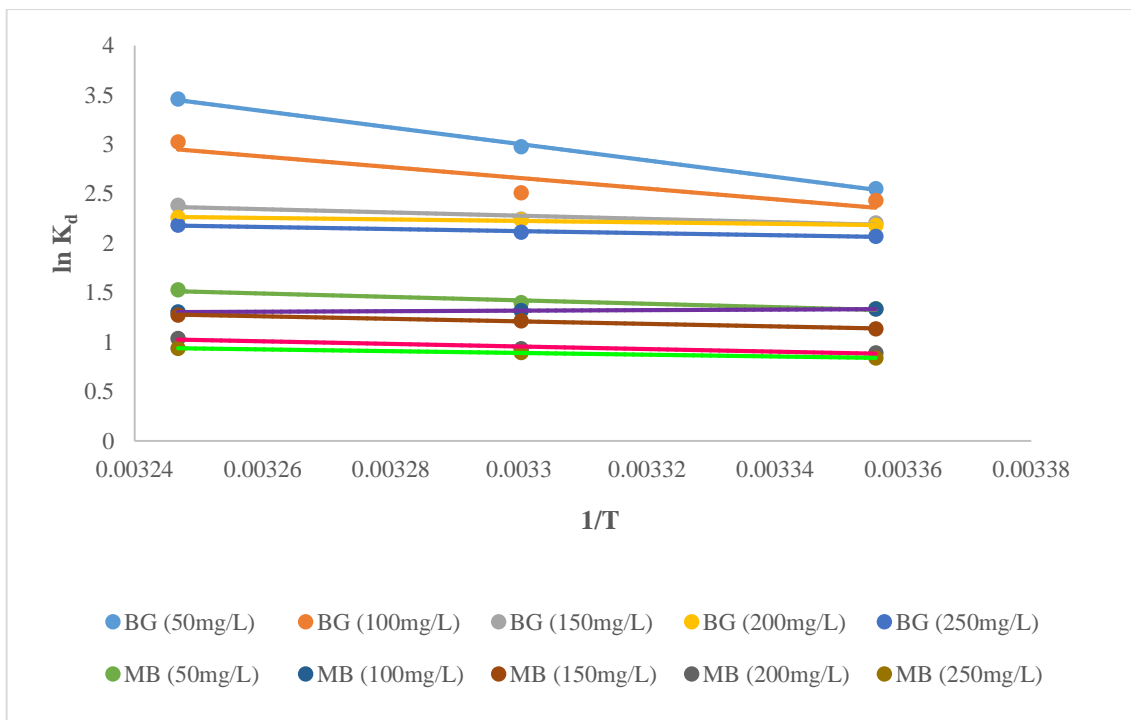


Figure 4.2.16: Adsorption thermodynamic plot for BG and MB in single dye system

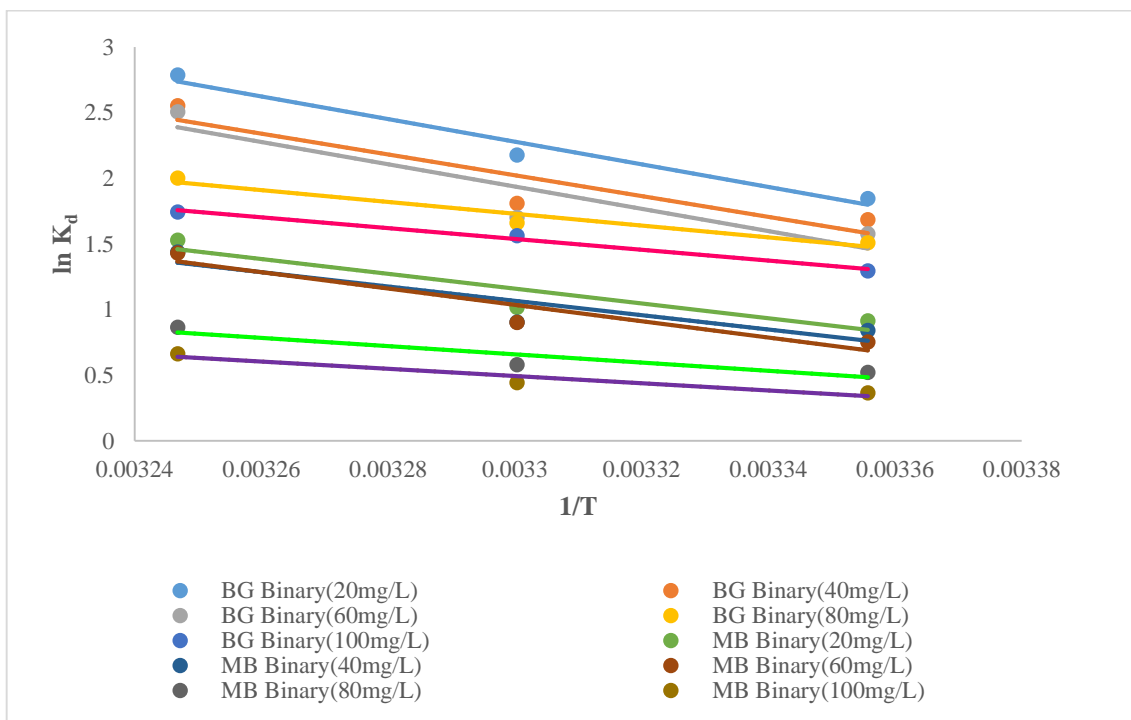


Figure 4.2.17: Adsorption thermodynamic plot for BG and MB in binary dye system

The adsorption thermodynamic studies for both the dye systems was plotted against $\ln K_d$ and $1/T$ whereas the calculated values of different thermodynamic parameters are shown in table 4.2.4.

Table 4.2.4: Calculated values of thermodynamic parameters in single and binary dye system

System	Concentration (mg/L)	ΔS° (KJ/mol/K)	ΔH° (KJ/mol)	ΔG° [25°C] (KJ/mol)	ΔG° [30°C] (KJ/mol)	ΔG° [35°C] (KJ/mol)
Single BG	50	0.254	69.183	-6.327	-7.500	-8.863
	100	0.170	44.986	-6.030	-6.327	-7.747
	150	0.064	13.585	-5.466	-5.655	-6.107
	200	0.040	6.305	-5.400	-5.635	-5.794
	250	0.046	8.608	-5.127	-5.322	-5.590
Single MB	50	0.060	14.468	-3.315	-3.524	-3.913
	100	0.003	-2.255	-3.305	-3.324	-3.342
	150	0.045	10.508	-2.814	-3.064	-3.260
	200	0.045	11.065	-2.212	-2.353	-2.657
	250	0.033	7.490	-2.077	-2.254	-2.398
Binary BG	20	0.255	71.717	-4.576	-5.492	-7.140
	40	0.235	65.914	-4.180	-4.563	-6.540
	60	0.250	70.592	-3.914	-4.288	-6.424
	80	0.138	37.502	-3.745	-4.187	-5.133
	100	0.125	34.293	-3.210	-3.940	-4.467
Binary MB	20	0.165	46.777	-2.268	-2.565	-3.920
	40	0.158	45.484	-2.084	-2.278	-3.686
	60	0.180	51.724	-1.866	-2.275	-3.670
	80	0.092	26.133	-1.294	-1.462	-2.217
	100	0.080	22.763	-0.905	-1.118	-1.702

4.2.3. Regeneration of Adsorbent

The adsorbent's regeneration is significant for assessing the efficacy of an adsorbent subsequent to adsorption studies and to ensure its cost-effectiveness. For analysing the adsorption capacity of different dyes using NFPC composite, the regeneration procedure was conducted using HCl (0.1N) as the desorbing agent for both the dye systems (single and binary dye).^{158,196} The regeneration efficiency of NFPC was calculated for up to five cycles. The findings of the study suggest that the prepared NFPC composite exhibits effective reusability and may work as economically feasible adsorbent for removing cationic dyes. Table 4.2.5

represents the regeneration efficiency of NFPC for both single as well as binary dye system. The results demonstrated that the NFPC composite retained high regeneration efficiency in both the dye systems even after five adsorption-desorption cycles. The regeneration efficiency for dyes BG and MB in single dye system was calculated to be 86.6% and 83.2%, respectively while in ternary dye system, the values calculated were 80.1% and 79.4% for BG and MB respectively. According to above findings, the NFPC composite has good reusability and may serve as an economical adsorbent.

Table 4.2.5: Regeneration efficiency of nickel ferrite pine cone composite for single and binary dye system

Regeneration cycle	Single dye (50 mg/L)		Binary dye (20 mg/L)	
	BG (%)	MB (%)	BG (%)	MB (%)
1	100	100	100	100
2	98.4	96.7	94.7	93.1
3	94.0	92.1	90.4	89.9
4	90.8	88.3	86.4	85.2
5	86.6	83.2	80.1	79.4

4.3. Walnut Shell Zinc Ferrite (WSZF) Composite

4.3.1. Characterization and Morphology

4.3.1.1. Fourier Transform Infrared Spectroscopy

The Fourier Transform Infrared spectra of walnut shell (WS), zinc ferrite (ZF) and walnut shell zinc ferrite (WSZF) are presented in figure 4.3.1. The synthesis of spinel zinc ferrite was confirmed by the presence of two distinct peaks found below 600 cm^{-1} in pure ZF and WSZF. These peaks reflected the bands of M-O (Metal Oxygen) at two distinct positions. In the tetrahedral site, the M-O band was represented by the peak found at around $500\text{-}600\text{ cm}^{-1}$. In the octahedral site, the M-O band was identified by an additional peak that was observed in range of $450\text{-}400\text{ cm}^{-1}$.¹¹²

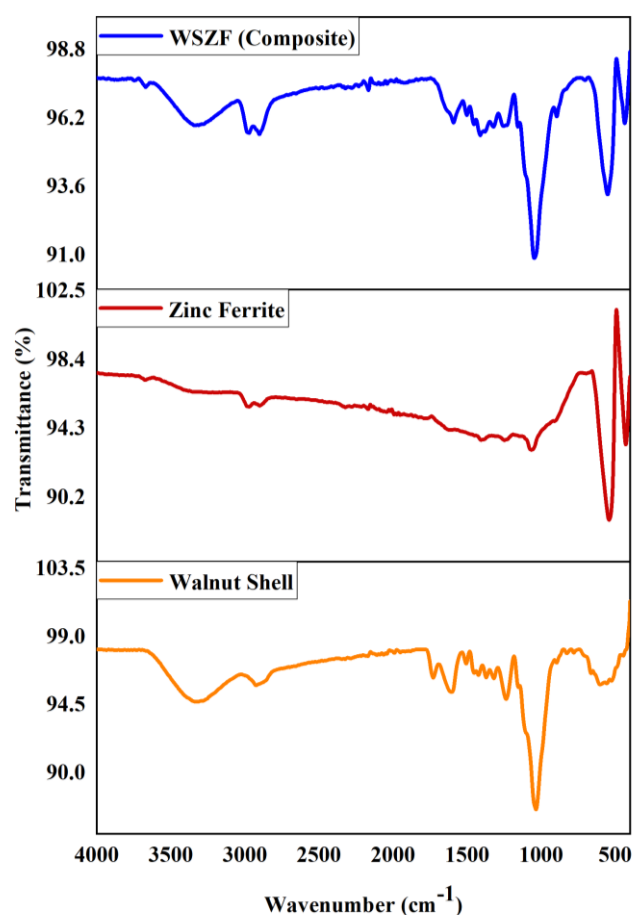


Figure 4.3.1: FTIR spectra of walnut shell, zinc ferrite and walnut shell zinc ferrite composite

The peaks observed in spectra of walnut shell at 3312.07 cm^{-1} and 2913.37 cm^{-1} were due to stretching of O-H and C-H bonds, respectively. An additional peak found at 1725.41 cm^{-1}

corresponds the stretching vibration of C=O of the carboxyl group. The presence of peak at 1604.76 cm^{-1} might be due to C=C bond of the ester.^{199–201} At 1237.15 cm^{-1} and 1035.08 cm^{-1} , there is an additional peak that corresponds to stretching of carbon-oxygen (C-O) bond in alcohol, carboxylic acid, ester and ether.^{60,159} It was found that the prepared WSZF composite showed characteristic peaks of NF and WS with slight shifts as shown in figure 4.3.1 which confirmed the successful formation of composite.

4.3.1.2. X-Ray Diffraction

The X-ray diffraction (XRD) pattern of ZF and WSZF is presented in figure 4.3.2. The XRD peaks for ZF are observed at $2\theta \sim 35.51, 70.4, 62.27, 56.63, 53.15, 49.40, 42.8, 35.24$ and 29.98 which corresponds to Miller indices pattern (533), (620), (440), (511), (422), (331), (400), (311) and (220) respectively.^{58,157} Higher phase purity and crystallinity of ZF are shown by the peaks. However, in WSZF composite, the XRD pattern showed slight different peaks having same Bragg's reflection pattern.

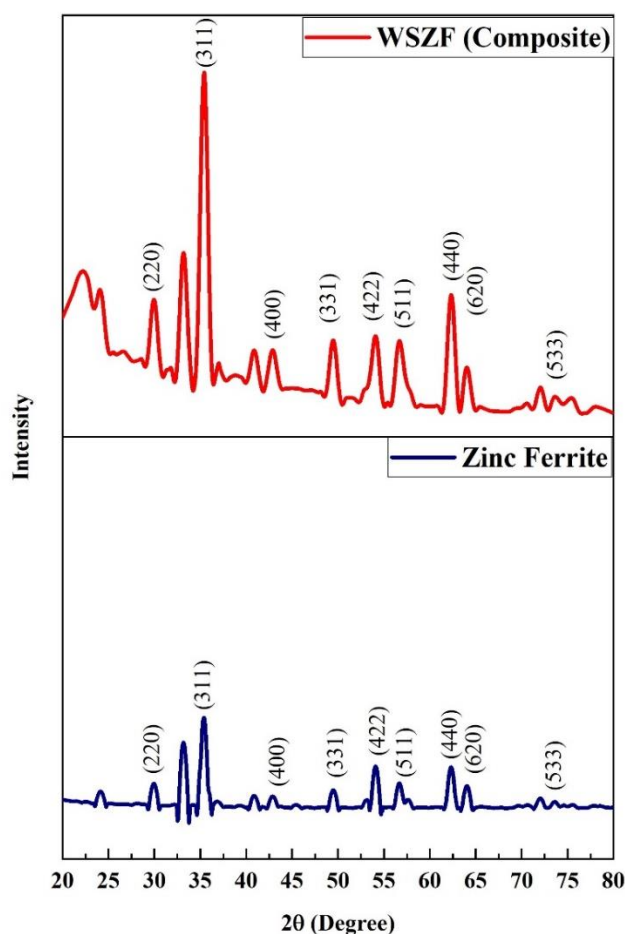


Figure 4.3.2: XRD spectra of zinc ferrite and walnut shell zinc ferrite composite

The results demonstrated that the prepared WSZF composite maintained its spinel characteristics even after the modification of surface. The Scherrer formula (equation 3.1) was used for calculating the average crystallite size of ZF and WSZF. The crystallite size calculated for ZF and WSZF was 29.50 nm and 38.67 nm respectively. The hkl plane values were indexed from JCPDS card number 00-022-1012.

4.3.1.3. Field Emission Scanning Electron Microscope

The FESEM images presenting the surface morphology of WS, ZF and WSZF are illustrated in figure 4.3.3. It is evident from figure, that ZF shows granular structure with non-uniform shape and varied particle size. The surface of WS is rough and flaky whereas the WSZF composite exhibited an identical morphology with the appearance of adhered ferrite particles on the surface of the walnut shell. This provides evidence that surface of spinel nickel ferrite has been modified successfully with walnut shell.¹⁷³

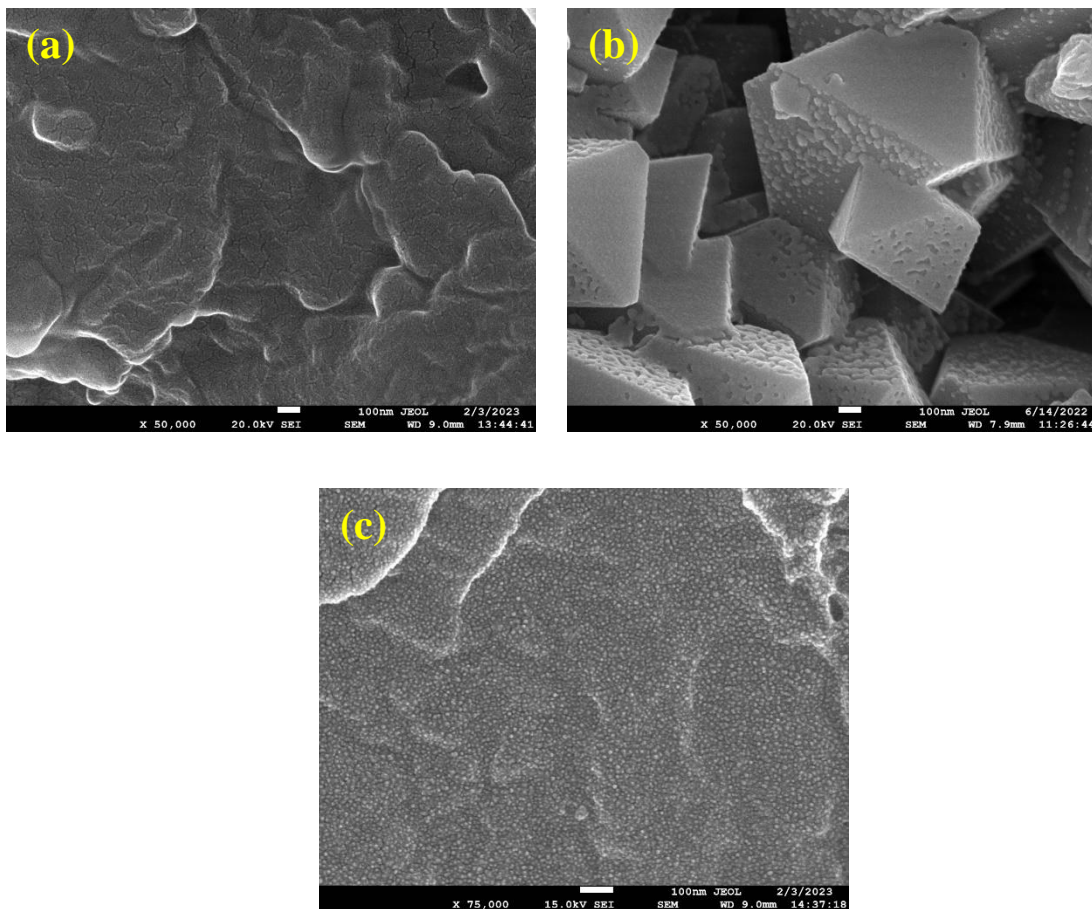


Figure 4.3.3: SEM image (a)Walnut shell (b) Zinc ferrite (c) Walnut shell zinc ferrite composite

4.3.1.4. Energy Dispersive Spectra

The Energy Dispersive Spectra of ZF and WSZF composite are shown in figure 4.3.4 along with the peaks indicative of their elemental compositions. The atomic percentages and weight percentages of the components present in ZF and WSZF are presented in table 4.3.1. It is evident from the data that the amount of carbon in WSZF composite is more in comparison to pure ZF. The presence of carbon demonstrated the fact that the walnut shell had been successfully modified with zinc ferrite to form a magnetic composite.^{58,158}

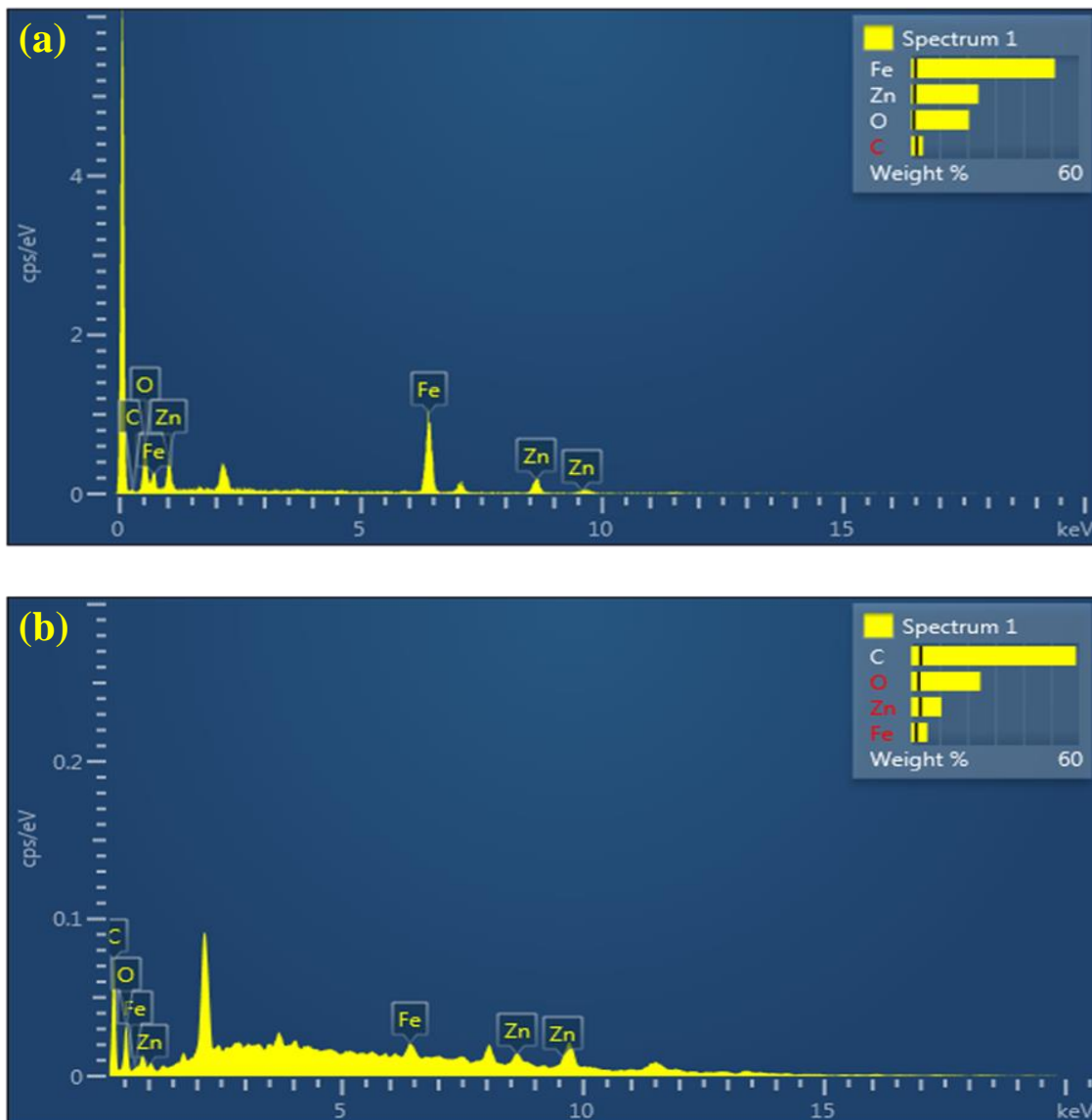


Figure 4.3.4: EDS image (a) Zinc ferrite (b) Walnut shell zinc ferrite composite

Table 4.3.1: Elemental composition of zinc ferrite and walnut shell zinc ferrite composite

Element	Zinc Ferrite		Walnut Shell zinc ferrite composite	
	Weight %	Atomic %	Weight %	Atomic %
C	4.13	11.81	58.86	73.05
O	20.54	44.06	24.65	22.96
Fe	51.31	31.53	5.72	1.53
Zn	24.02	12.61	10.77	2.45
Total	100.00	100.00	100.00	100.00

4.3.1.5. Thermogravimetric Analysis

The thermal stability of prepared WSZF composite was determined using Thermogravimetric Analysis. The TGA plot is presented in figure 4.3.5. The TGA analysis was conducted in an air atmosphere, with temperature ranging from 28 to 600°C and a consistent heat rate of 10°C/minute.

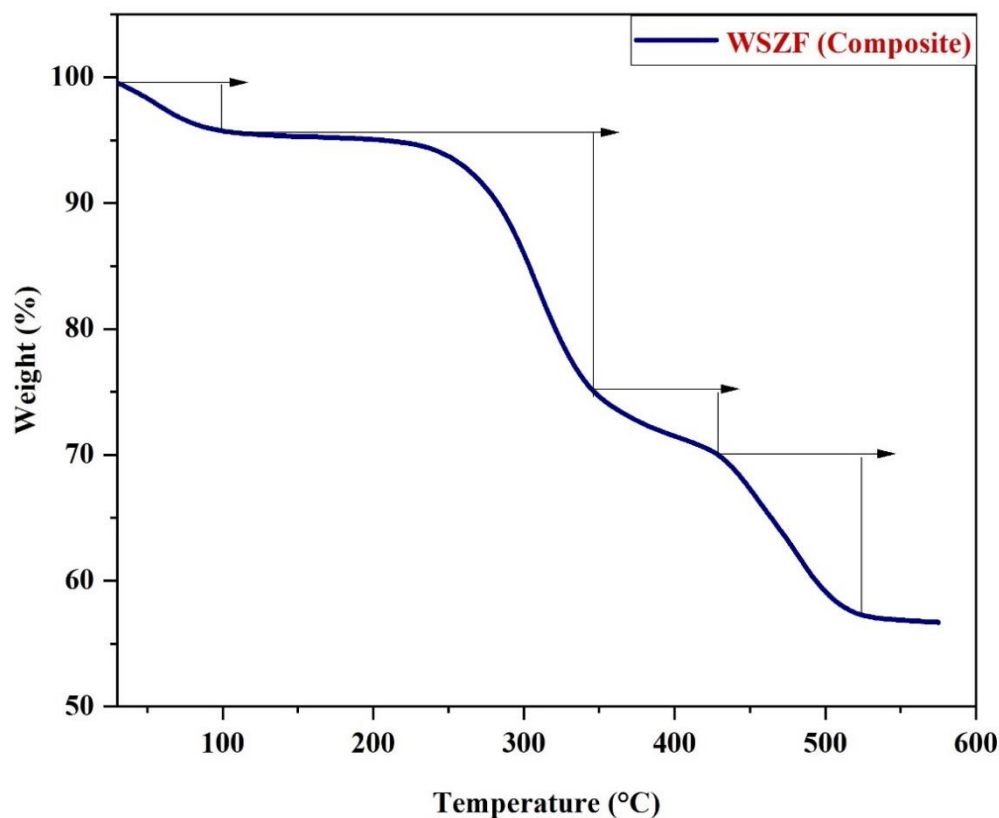


Figure 4.3.5: TGA curve of walnut shell zinc ferrite composite

It was observed that, a loss in weight of 4.4% was observed from 35.1°C to 100.4°C, which may be due to the vaporisation of sample's retained moisture content. At around 100.4°C to 345.9°C, weight loss of 20.3% was observed. An additional loss in weight of about 5% was again noticed from 345.9°C to 425.4°C. This loss of weight might be attributed to the breakdown of functional groups. As the temperature further increased, an abrupt weight loss of approximately 12.8% was observed from 425.4°C to 521.7°C which demonstrated the complete decomposition of organic matter present in the composite. According to the calculations, it was found that about 0.398 g of walnut shell powder has been attached into 1 g of WSZF composite.

4.3.1.6. Brunauer-Emmett-Teller Analysis

The specific surface area of pure ZF and WSZF composite was determined using Brunauer-Emmett-Teller analysis. The results of BET analysis clearly demonstrate that the surface area of pure nickel ferrite is smaller than that of the composite. The BET specific surface area calculated for pure ZF and WSZF composite was 1.683m²/g and 3.761 m²/g respectively. It occurred because, in comparison to pure ZF, the particle size of composite increased on surface modification of ZF with WS. The surface porosity of the composite increased due to surface modification, leading to an increase in specific surface area.^{153,200}

4.3.1.7. pH of Point Zero Charge Analysis

The solid addition method was employed to determine the pH_{zpc} of WSZF. Nine 250 mL Erlenmeyer flasks were taken and 50 mL 0.1M KNO₃ solution along with 0.1 g WSZF composite was added. The pH of the solution was initially adjusted to a range of 3 to 11 using hydrochloric acid (0.1N) and sodium hydroxide (0.1M). The flasks were placed in a thermostatic shaker and allowed to shake for a period of twenty-four hours. After removing the flasks, the solution of each flask was filtered into separate beakers. The last step was to record the pH (final pH) of the filtered solution and the calculations were done using equation 3.2.^{58,158}

Using the above calculations, a graph was plotted between the initial pH and Δ pH as seen in figure 4.3.6. From the graph, the pH_{zpc} value obtained for WSZF composite was 6.1 indicating that there was no net electric charge on composite's surface of composite at that specific pH. Therefore, the surface of composite will have a positive charge below pH 6.1 and a negative charge above pH 6.1.

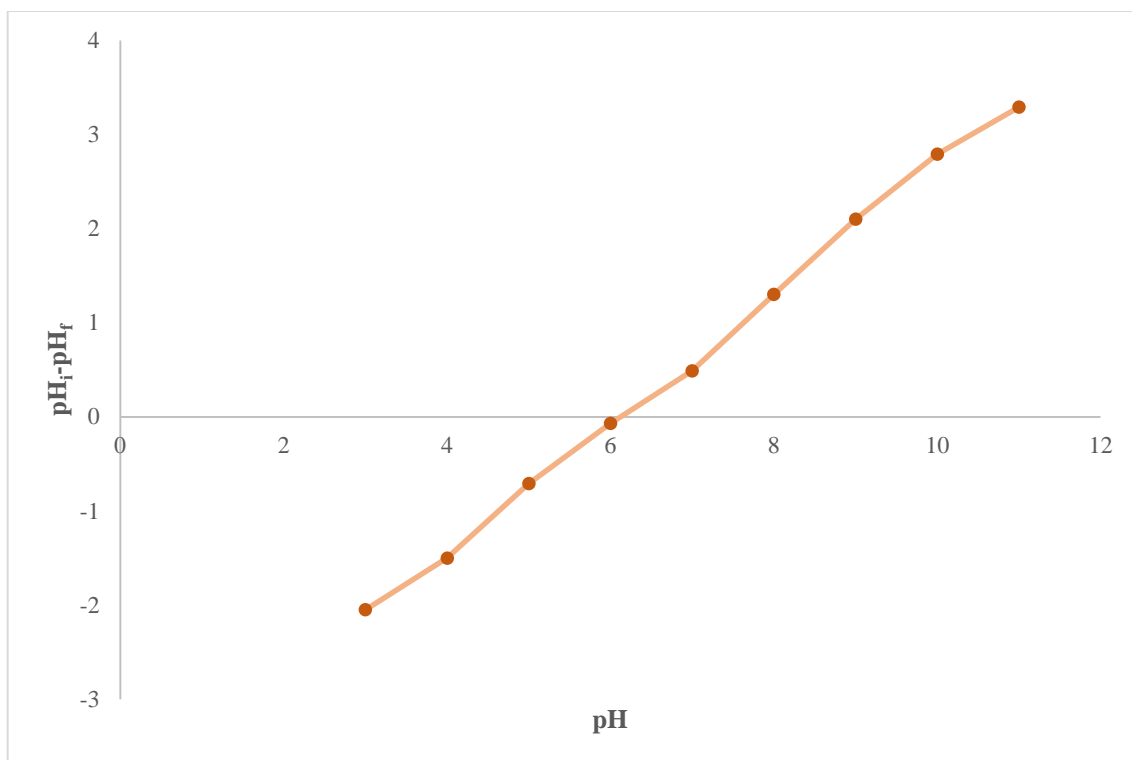


Figure 4.3.6: pH_{zpc} of walnut shell zinc ferrite composite

4.3.2. Adsorption Study in Single and Binary Dye System

The batch adsorption method was utilized for studying the dye adsorption behavior with WSZF composite. The selectivity of the cationic dyes towards prepared composite is evidenced by pilot scale studies described in chapter 3. The adsorption characteristics of the prepared composite were examined with several dyes but the dyes MG and MB showed remarkable results. So the adsorption behaviour of WSZF composite was further explored using MG and MB dye in single as well as binary system. The effect of adsorption parameters like contact time, adsorbent dosage, pH, temperature and dye concentration were examined.

4.3.2.1. Effect of Contact Time

The effect of contact time on WSZF composite was determined for both single as well as binary dye systems using predetermined dye solution concentrations i.e.; 50 mg/L for the single dye system and 20 mg/L for the binary dye system. The process of adsorption study is time-dependent. Erlenmeyer flasks containing specified dye solution volume (50 mL) and 0.1 g adsorbent dosage were placed in thermostatic shaker at 25°C for the time period of 3 hours.^{157,196} The flasks were removed at predetermined intervals and reduced dye concentration

was measured. Figure 4.3.7 shows the contact time effect on the removal of MG and MB in single as well as binary dye system. The graph showed that the dye removal was fast initially in both the systems but as the time increased, it slowed down and eventually reached equilibrium. Initially the adsorption process exhibited a significant number of unoccupied sites on its surface, to which the dye molecules got attached quickly. However, after a specific duration, each of these sites became occupied and a state of equilibrium was attained between the molecules of adsorbate and adsorbent. It was determined that the equilibrium time obtained for MG (Single), MG (Binary) and MB (Binary) was 100 minutes; whereas, the time obtained for MB (Single) was 120 minutes. The percentage of dyes MG and MB removed in single dye system were 90.7% and 93.6%, respectively, whereas in binary dye system the percentage removed were 85.4% and 75.8% for MG and MB respectively. The results also shown that the percentage removal was higher for the single dye system compared to binary dye system which could occur because the dye molecules in binary system are more competitive with one another.⁵⁸

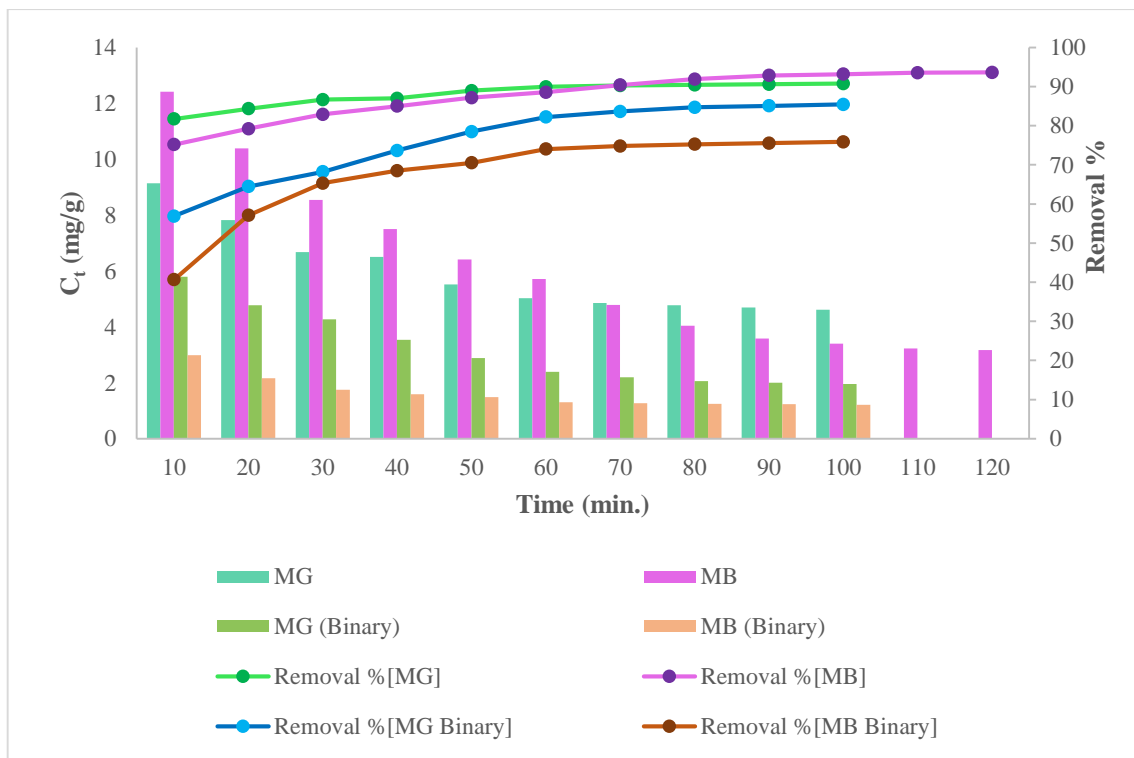


Figure 4.3.7: Effect of contact time for single and binary dye system

4.3.2.7. Adsorption Kinetics

The kinetics of adsorption is applied in order to study the behavior of adsorption in proportion to the passage of time. The Lagergren pseudo-first order, pseudo-second order and Elovich models were applied for studying the adsorption kinetics in both the dye system. The time study data was graphically represented by applying general linear equations to the kinetic models. The graphs representing the models of kinetics are illustrated in figure 4.3.8, 4.3.9 and 4.3.10 respectively for single and binary dye system. The physical and chemical nature of adsorption process was determined by kinetic studies. The possibility of physisorption is indicated when the data of adsorption demonstrate an accurate fit to pseudo first order with value of R^2 (regression coefficient) close to 1. Similarly, if the reaction has a strong correlation with the pseudo second order model, then this might be an indication that chemisorption is taking place. Therefore, for this experimental study, the pseudo second order model emerged as the most appropriate, exhibiting the highest R^2 value suggesting the chemical nature of adsorption process.

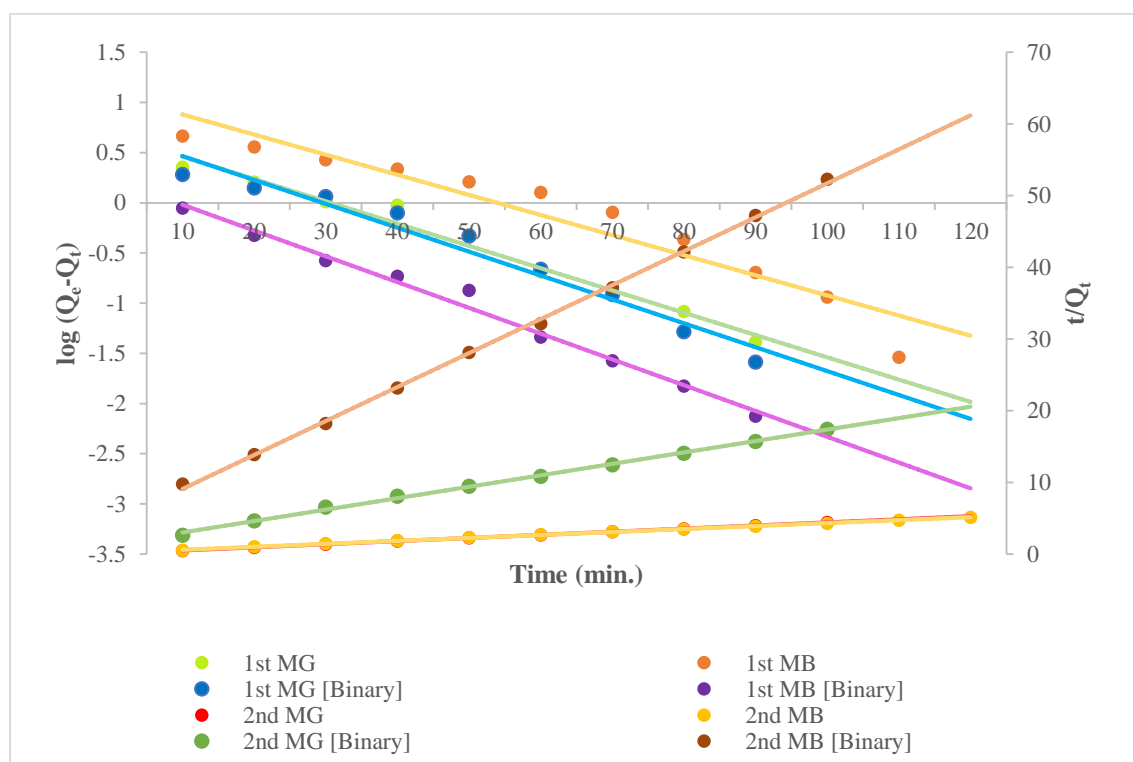


Figure 4.3.8: Lagergren pseudo first order and pseudo second order kinetics for single and binary dye system

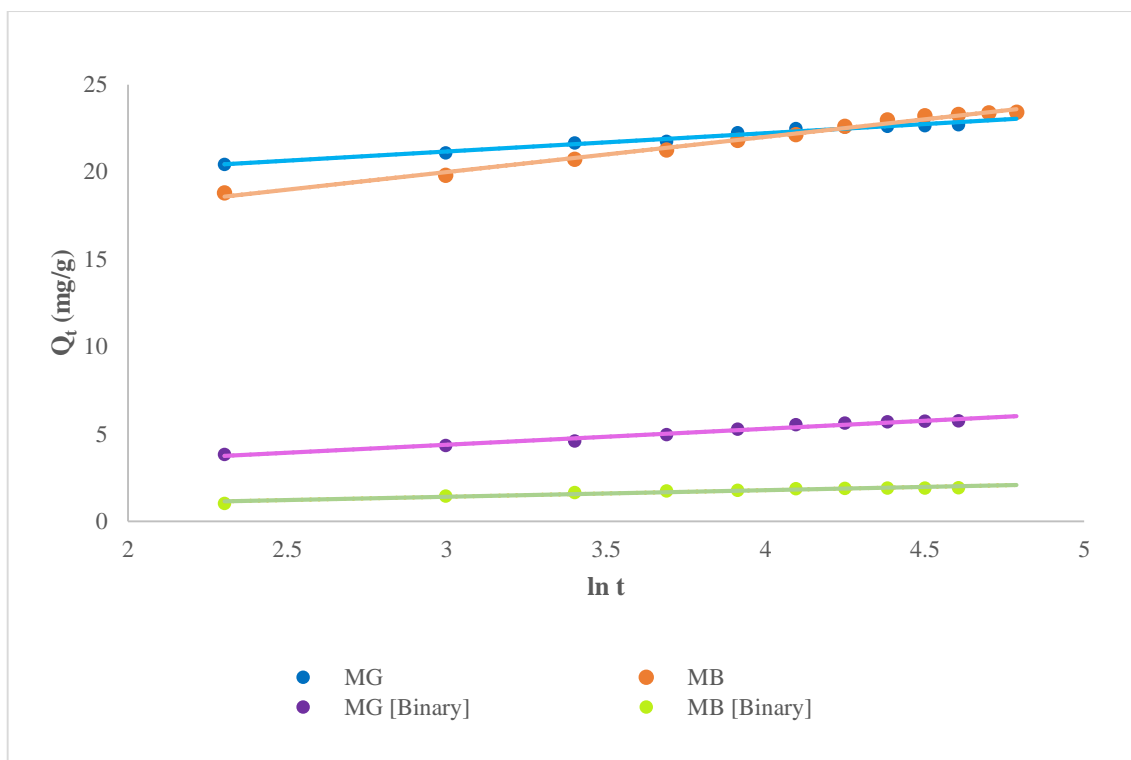


Figure 4.3.9: Elovich model for single and binary dye system

Table 4.3.2: Calculated values of different kinetic constants for single and binary dye system

KINETIC MODEL	SYSTEM				
	Parameter	Single MG	Single MB	Binary MG	Binary MB
Lagergren Pseudo first order	Q_{e1}	4.816	12.105	5.066	1.727
	K_1	0.512	0.462	0.548	0.592
	R^2	0.980	0.920	0.964	0.989
Pseudo second order	Q_{e2}	2.312	2.432	0.627	0.211
	h	12.532	5.047	0.707	0.230
	K_2	2.346	0.854	1.796	5.156
	R^2	0.999	0.999	0.998	0.999
Elovich model	α	3.386	2.61	5.511	1.063
	β	0.958	0.496	1.094	3.554
	R^2	0.978	0.991	0.978	0.937

In order to get an understanding of adsorbent's intra-particle diffusion characteristics, the Weber-Morris model was utilized to fit kinetic data enabling the comparison of dye diffusion mechanisms across various dye systems including single and binary dye systems. A graph

showing the relationship between Q_t and $t^{0.5}$ illustrates the adsorbent's diffusion behavior as K_{int} representing the rate limiting step and intra particle (IP) diffusion rate constant. A straight line should pass from the point of origin for rate-limiting step to be successful. However, the line in figure 4.3.10 does not pass through the origin, and the plot is not linear in either the single or binary dye system. This indicated that along with IP diffusion, additional variables impact the rate of adsorption in both single as well as binary dye system. The steep slope appeared in the plot of single dye system suggested that there was fast adsorption at the beginning of the process, but that it eventually got flattened as time passed on and ultimately equilibrium was achieved. On the other hand, in binary dye system, this pattern of adsorption rate was found absent. In a binary dye system, the decline in adsorption revealed that the dyes MG and MB have an antagonistic effect on one another. Dye molecules form strong bonds in aqueous solution due to several attractive factors, such as π - π and electrostatic interactions. As a consequence of this, the efficacy of the dye removal process in binary system was noticeably lesser compared to the single dye system.^{58,158}

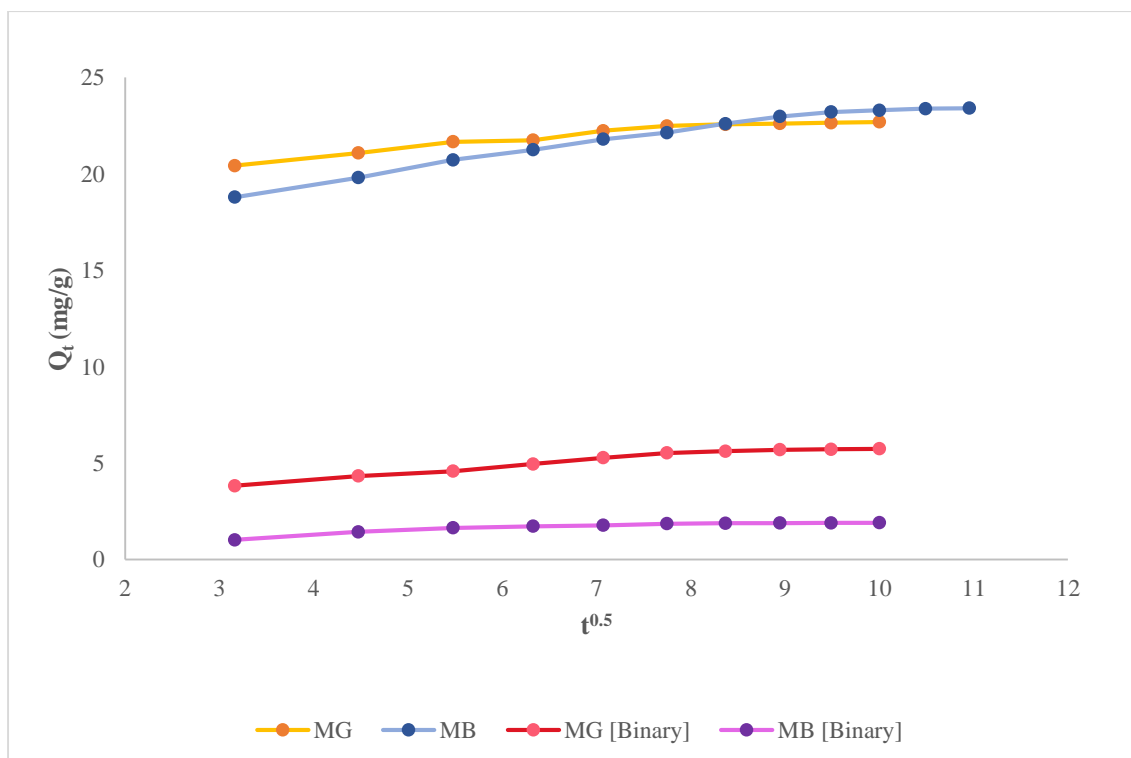


Figure 4.3.10: Intra particle diffusion model for single and binary dye system

4.3.2.8. Effect of pH

The adsorption process is significantly influenced by the pH of solution since it regulates the surface charge of adsorbent. In order to evaluate this effect, the process of adsorption in a single dye system with MG and MB was investigated at various pH levels. With a fixed dye concentration of 50 mg/L and adsorbent amount 0.1 g, the pH of solution was adjusted between 3 and 11. The glass flasks were placed in orbital shaker at 110 revolutions per minute for a period of three hours to reach equilibrium. The effect of pH on the removal of dyes is shown in figure 4.3.11. From the graph, it was found that the dye removal efficiency steadily increased with increasing pH of the solution and reached maximum at 7, after which it began to decrease further. At pH 7, the highest percentage of MG and MB that could be removed was 91.4% and 93.6%, respectively.¹⁵⁷

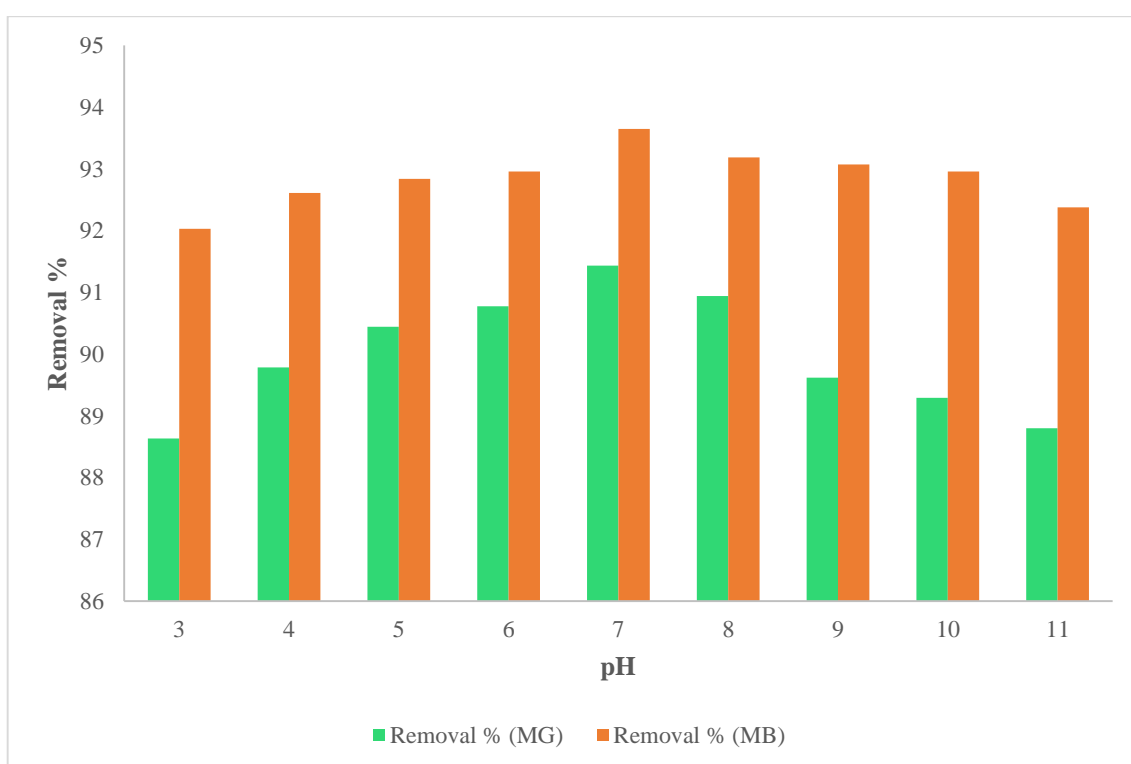


Figure 4.3.11: Effect of pH for single dye system

4.3.2.9. Effect of Adsorbent Dosage

The effect of adsorbent dose was examined by adjusting the quantity of WSZF composite from 0.1 g - 0.5 g for single and binary dye system. Figure 4.3.12 represents that the percentage of dye removal increased with increase in the composite dosage in both the dye systems. This increasing dye removal trend was observed because of increase in adsorption sites on the adsorbent's surface with increased adsorbent dosage. However, as the quantity of adsorbent

increased, the adsorbate adsorbed per gram of adsorbent (Q_e) decreased. This decrease could be attributed to the increased active sites availability on adsorbent's surface, which remained unoccupied as the adsorbent amount increased. Results showed that the binary dye systems achieved removal efficiencies of 85.5% for MG and 84.9% for MB, whereas single dye systems obtained removal efficiency of 94.3% and 95.9% for MG and MB respectively.¹⁵⁸

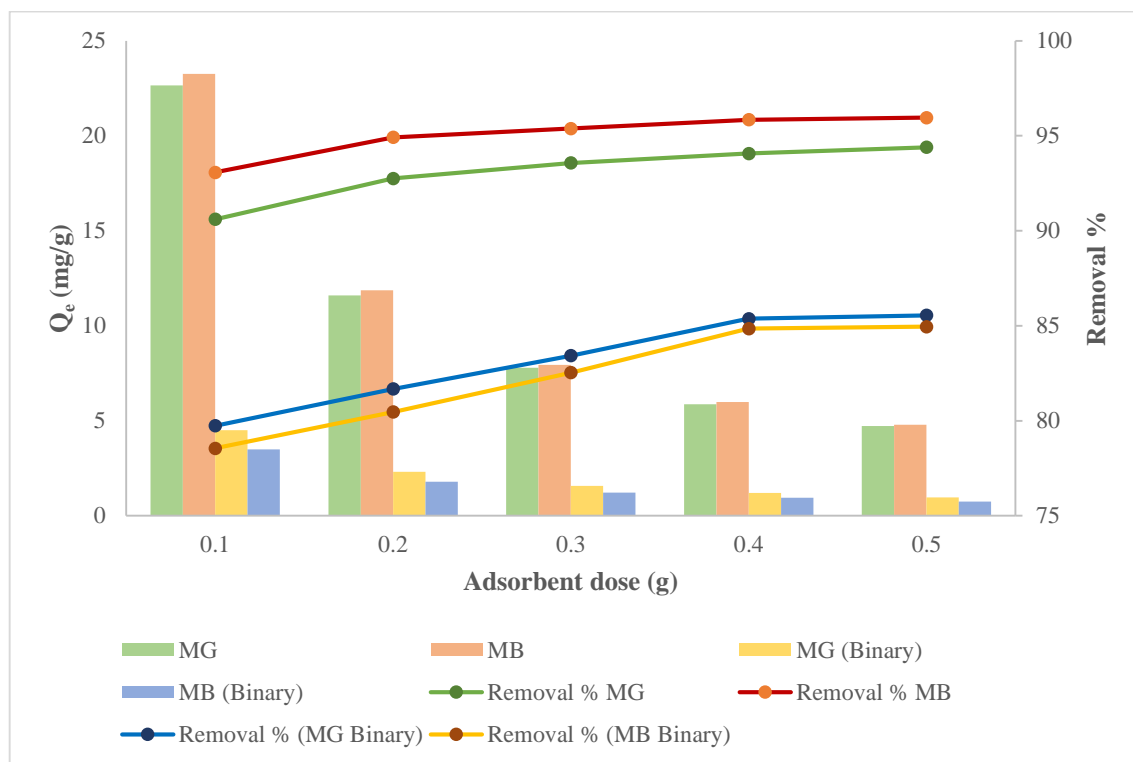


Figure 4.3.12: Effect of adsorbent dosage for single and binary dye system

4.3.2.10. Effect of Concentration and Temperature

The effect of dye concentration as well as temperature was studied using WSZF composite on MG and MB in single as well as binary systems. For the single system, initial dye concentration was adjusted between 50 and 250 mg/L, whereas for binary dye system, it was adjusted between 20 and 100 mg/L. Additionally, the impact of temperature was examined by adjusting the temperatures at 25°C, 30°C and 35°C. Figures 4.3.13 and 4.3.14 depict that the adsorption capacity ' Q_e ' of dyes increased with rising dye concentration in both systems. This may take place due to the availability of additional dye molecules for a specific amount of active sites on adsorbent's surface as well as the stronger interactions which takes place between the molecules of the adsorbate and the adsorbent which leads to more frequent collisions. To the contrary, in both the dye system, the removal percentage of MG and MB declined as the dye concentration increased which occur because the increasing number of dye molecules exceeds

with the constant number of active sites available on the adsorbent's surface in comparison to increasing dye concentration.

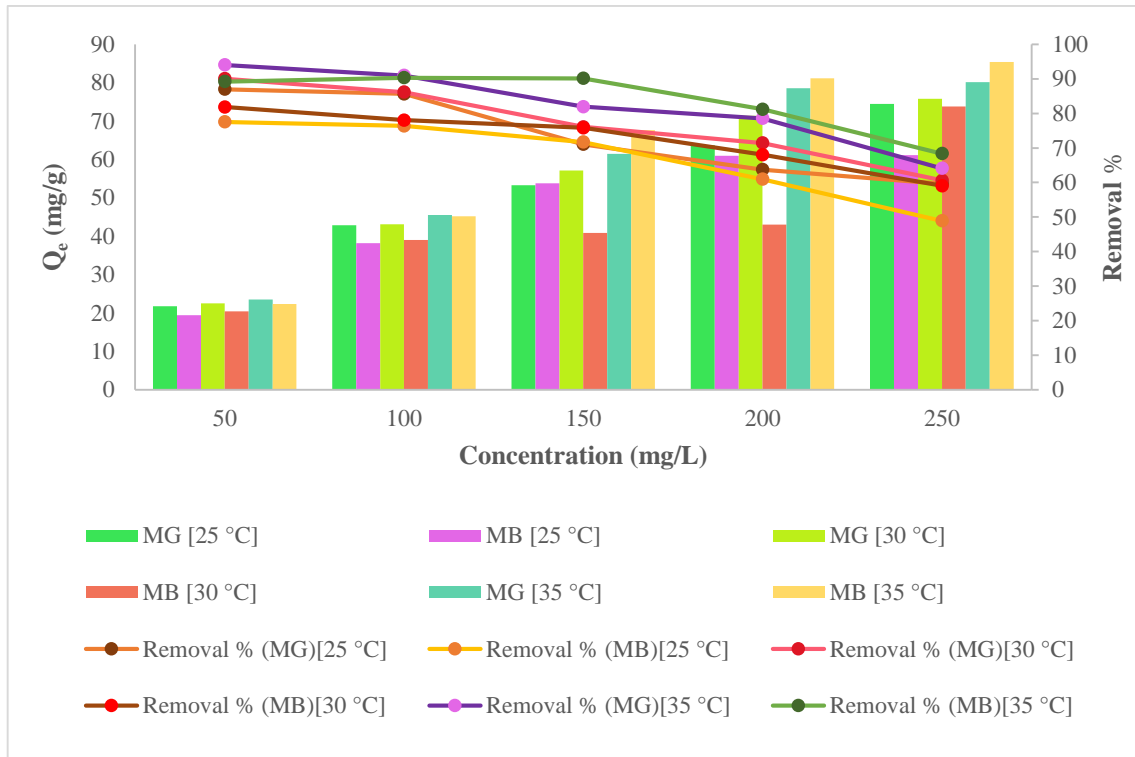


Figure 4.3.13: Effect of concentration for single dye system

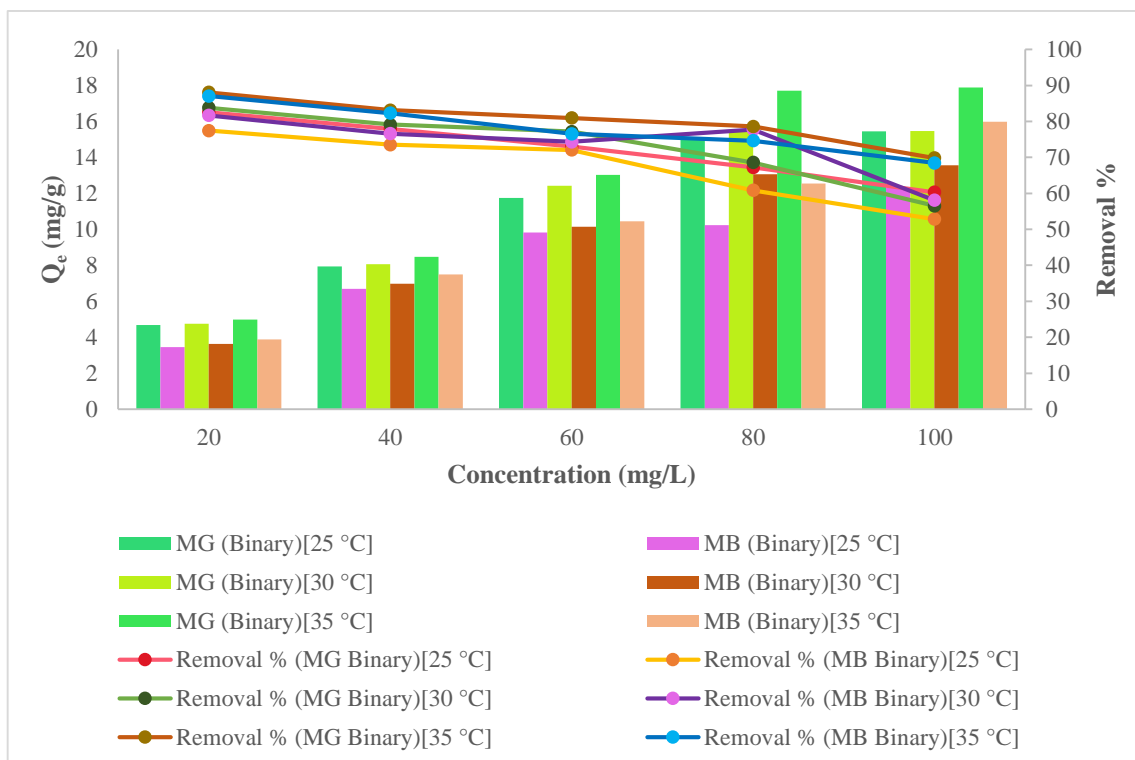


Figure 4.3.14: Effect of concentration for binary dye system

The dye adsorption capacity also showed an increase with the increasing temperature, indicated the endothermic nature. The increased adsorption capacity with respect to temperature could be because of the enhanced interaction between the adsorbate and adsorbent molecules. As the temperature increases, the pores of adsorbent may enlarge and provide greater surface area for dye molecules adsorption.

The percent removal of each dye in ternary system was lower compared to single system, probably due to the antagonistic effect of dyes. The 'Q_e' of dyes in a ternary dye system decrease as a consequence of the formation of stronger bonds caused by the different attraction forces among molecules of the dyes in the system.^{58,158}

4.3.2.11. Adsorption Isotherms

The term "adsorption isotherm" refers to the interaction occur between the molecules of adsorbate and adsorbent when they are at a state of equilibrium in an aqueous medium. The equilibrium behaviour of malachite green (MG) and methylene blue (MB) using WSZF composite in both single as well as binary dye systems at various temperatures, several adsorption isotherm models were employed. These models include the Langmuir model, Freundlich model, Temkin model, and Dubinin-Raduskevich (D-R) model. The adsorption data calculated for both the dye system at varying temperatures were fitted to various isotherm models. The isotherm plots for Langmuir, Freundlich, Temkin and Dubinin-Raduskevich (D-R) model are depicted in figure 4.3.15 (a-d) respectively.^{58,142}

Different constants associated with adsorption isotherms were calculated from the plots which are presented in table 4.3.3. Among the different models, the R² value for the Langmuir isotherm model was the most significant followed by Freundlich, Temkin and D-R model. The calculated values indicated that Langmuir model offered the most precise fit to the obtained data. Moreover, the results indicated that the active sites are uniformly distributed across the surface of the prepared composite. The highest adsorption capacity for MG and MB dyes in single system was calculated to be 86.20 and 169.5 mg/g, respectively. Conversely, in the binary dye system, the adsorption capacities were observed to be 23.92 and 18.7 mg/g, respectively. With increasing temperature, the maximum adsorption capacity (Q_{max}) of also increased which may be due to increased interaction between dyes and the adsorbent.

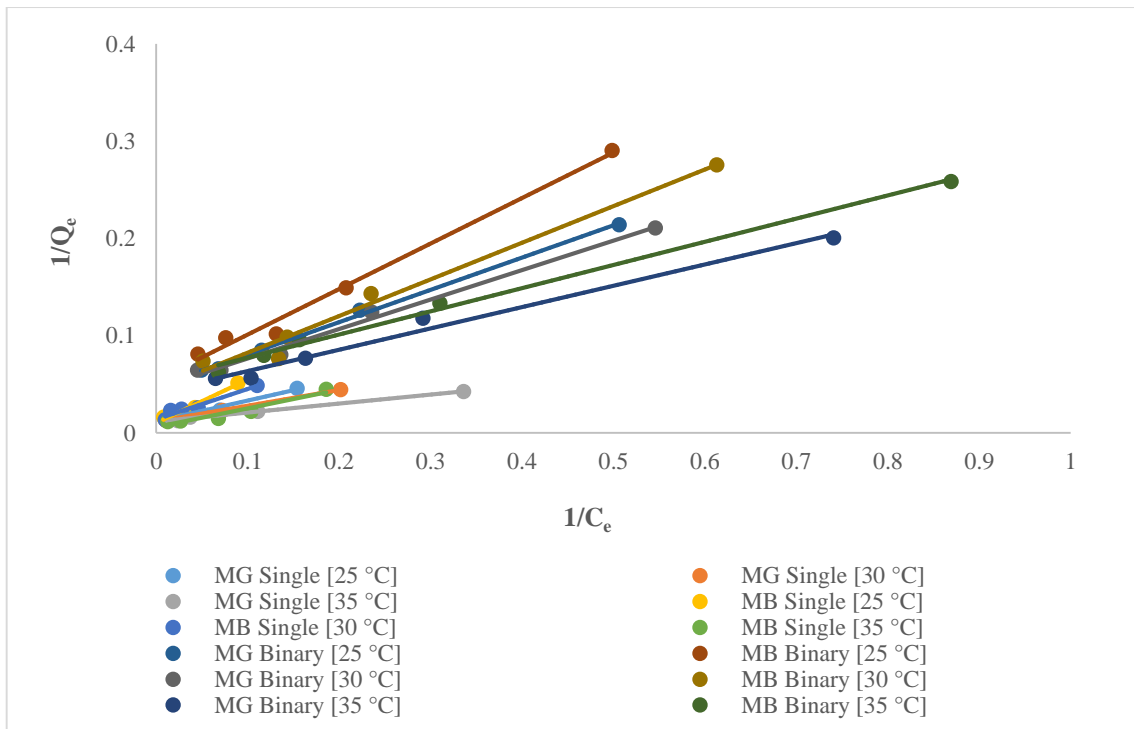


Figure 4.3.15 (a): Langmuir adsorption isotherm for single and binary dye system

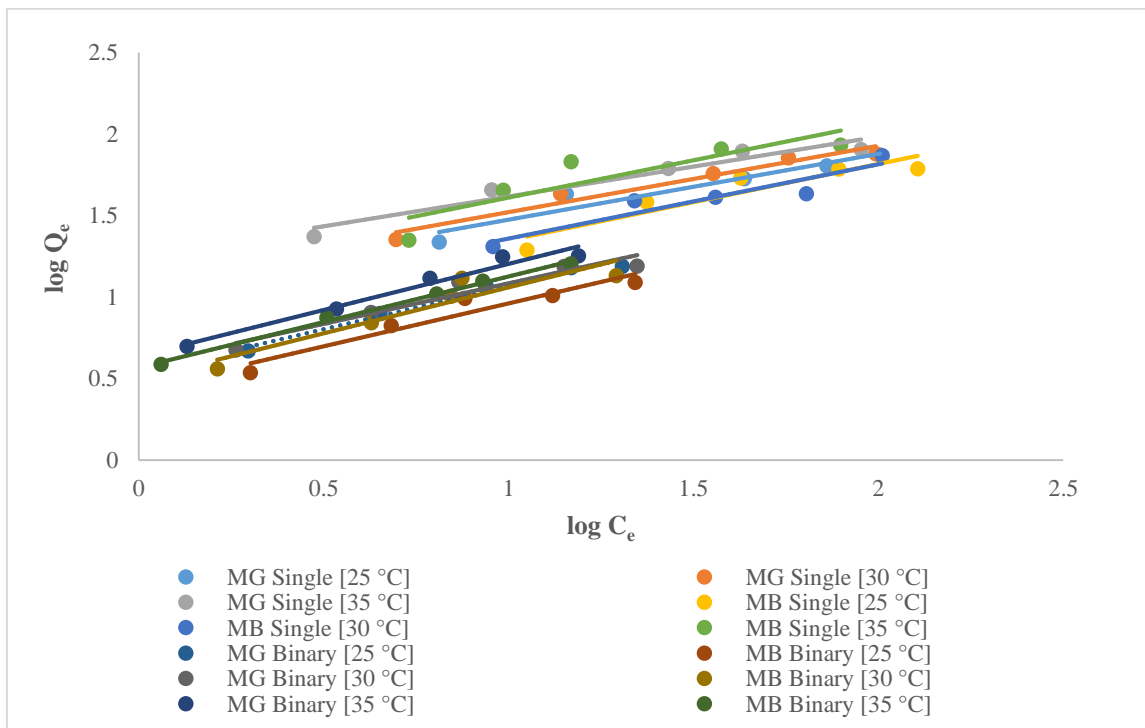


Figure 4.3.15 (b): Freundlich adsorption isotherm for single and binary dye system

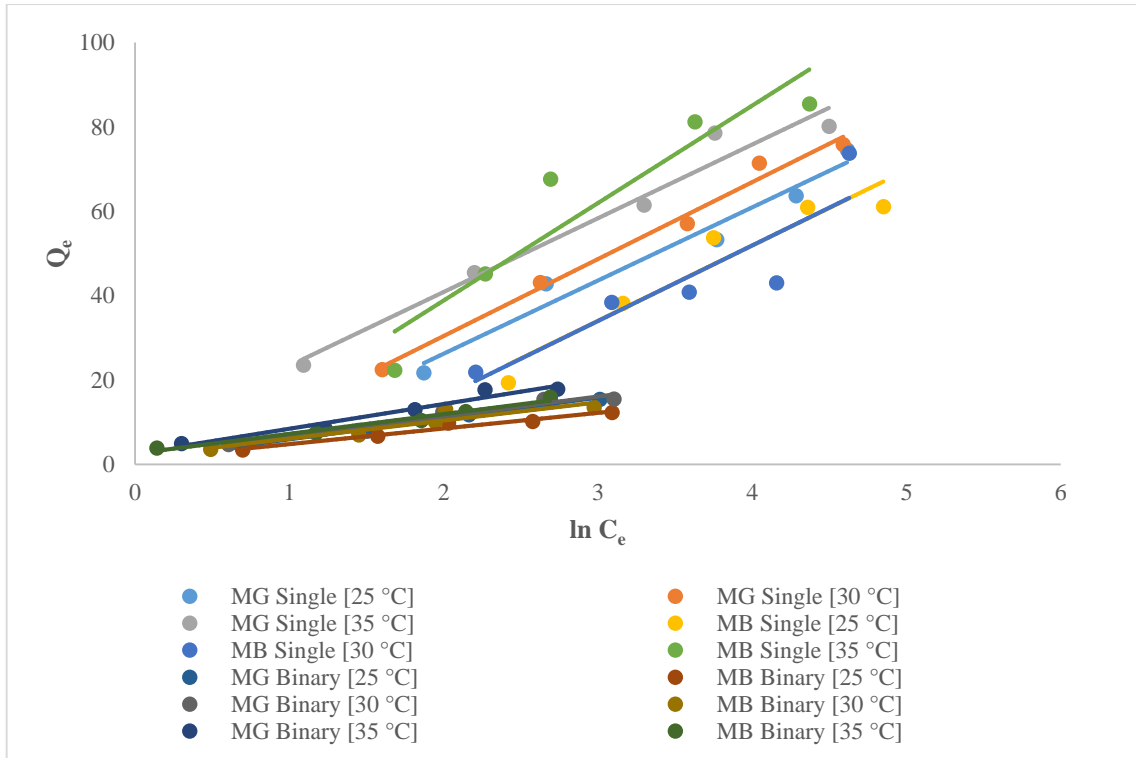


Figure 4.3.15 (c): Temkin adsorption isotherm for single and binary dye system

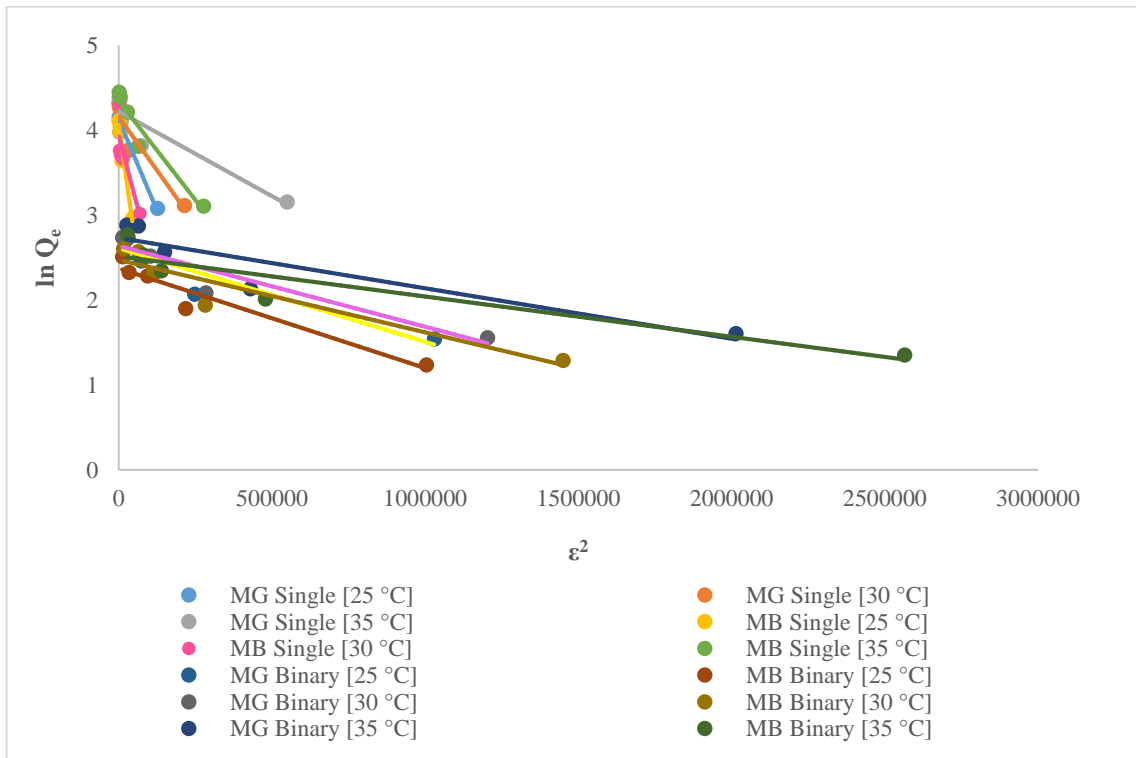


Figure 4.3.15 (d): D-R adsorption isotherm for single and binary dye system

Table 4.3.3: Calculated values of adsorption isotherm constants for single and binary dye system

System		Single MG			Single MB			Binary MG			Binary MB		
Isotherm Model	Constant	25°C	30°C	35°C	25°C	30°C	35°C	25°C	30°C	35°C	25°C	30°C	35°C
Langmuir model	Q	84.034	84.745	86.206	99.0	70.922	169.5	21.142	21.598	23.924	18.383	22.223	18.691
	b	0.055	0.073	0.125	0.023	0.045	0.030	0.143	0.153	0.190	0.116	0.120	0.225
	R ²	0.974	0.997	0.995	0.975	0.938	0.930	0.997	0.991	0.984	0.989	0.980	0.995
	R _L	0.267	0.215	0.137	0.465	0.307	0.400	0.259	0.246	0.208	0.301	0.294	0.181
Freundlich model	K _f	11.825	12.996	17.807	7.577	8.0121	14.194	3.443	3.877	4.348	2.724	3.140	3.706
	1/n	0.403	0.407	0.366	0.468	0.455	0.458	0.533	0.496	0.565	0.526	0.564	0.557
	R ²	0.925	0.957	0.986	0.858	0.887	0.780	0.977	0.933	0.966	0.919	0.872	0.995
Temkin model	b _T	145.280	138.088	144.165	141.074	140.585	109.135	510.424	537.074	430.395	681.992	582.5	539.535
	A	0.615	0.720	1.405	0.335	0.333	0.7301	1.242	1.544	1.568	1.363	1.516	1.744
	R ²	0.965	0.987	0.966	0.920	0.805	0.880	0.986	0.956	0.953	0.964	0.872	0.976
D-R model	Q _m	62.035	63.950	68.184	58.470	51.045	76.968	13.637	13.996	15.364	10.710	11.862	12.350
	K	9×10 ⁻⁶	5×10 ⁻⁶	2×10 ⁻⁶	3×10 ⁻⁵	1×10 ⁻⁵	5×10 ⁻⁶	1×10 ⁻⁶	1×10 ⁻⁶	6×10 ⁻⁷	1×10 ⁻⁶	9×10 ⁻⁷	5×10 ⁻⁷
	R ²	0.924	0.886	0.880	0.965	0.760	0.938	0.884	0.890	0.842	0.930	0.886	0.864
	E	235.70	316.23	500	129.10	223.61	316.23	707.11	707.11	912.87	707.11	745.36	1000

Separation factor ‘R_L’ is another parameter associated to the Langmuir isotherm was also calculated to ascertain the nature of adsorption process. Based on the results shown in table 4.3.3, it can be concluded that the WSZF composite is favourable for the adsorption of dyes as the R_L values for single as well as binary dye system ranged from 0 to 1.¹⁶²

Furthermore, the Adsorption Energy ‘E’ of the adsorbent related to D-R isotherm was calculated to study the type of adsorption process. If the obtained value of ‘E’ is below 8 KJ/mol, the process is typically considered physical; otherwise, it is supposed to be of chemical nature.⁴² The ‘E’ was determined using the Dubinin-Raduskevich constant ‘K’. According to the calculations, the adsorption energy for both the dye systems was greater than 100 KJ/mol, suggesting that the process of adsorption for the experimental study was of chemical nature.

4.3.2.12. Adsorption Thermodynamics

The adsorption characteristics of dyes MG and MB were examined in single as well as binary dye systems at three distinct temperatures i.e.; 25°C, 30°C, and 35°C. The endothermic nature of adsorption process was evident as the dye adsorption increased with increasing temperature. The thermodynamic parameters related to adsorption were derived by using different thermodynamic equations which are given in section 3.12. The parameters of thermodynamics include free energy change (ΔG°), entropy change (ΔS°) and the enthalpy change (ΔH°).

Values for ΔS° and ΔH° were determined by analysing the intercept and slope of linear plots of $\ln K_d$ against $1/T$. Additionally, the calculated values for various thermodynamic parameters are shown in table 4.3.4. The linear graphs for MG and MB in both single as well as binary dye system are presented in figure 4.3.16 and 4.3.17, respectively.

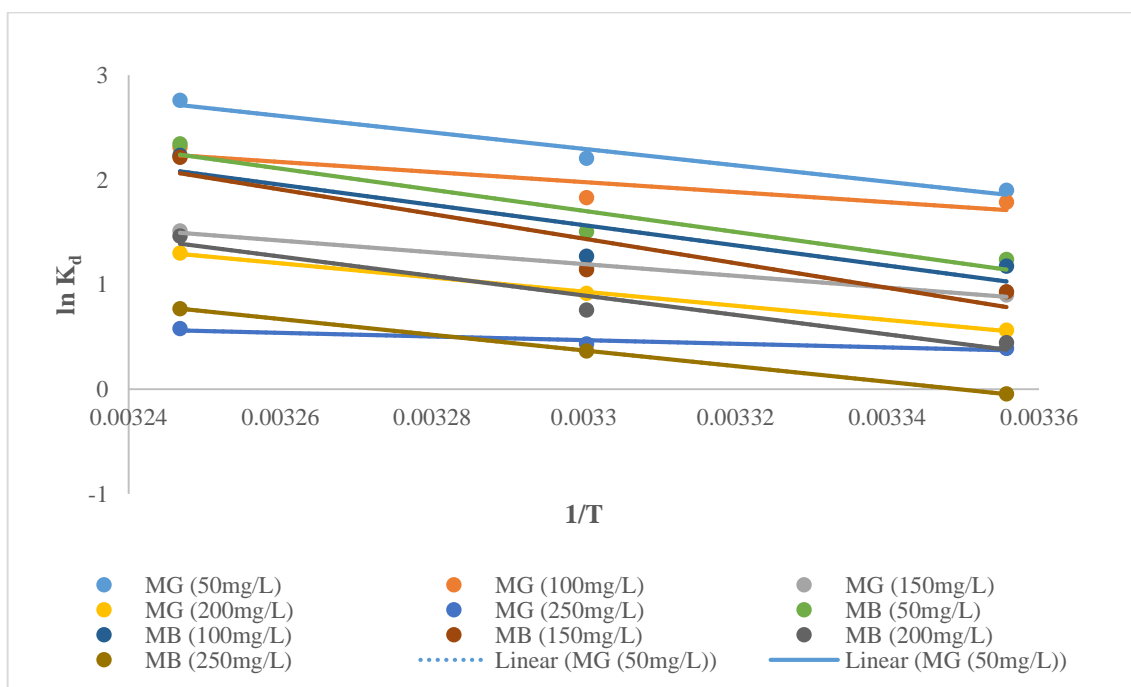


Figure 4.3.16: Adsorption thermodynamic plot for MG and MB in single dye system

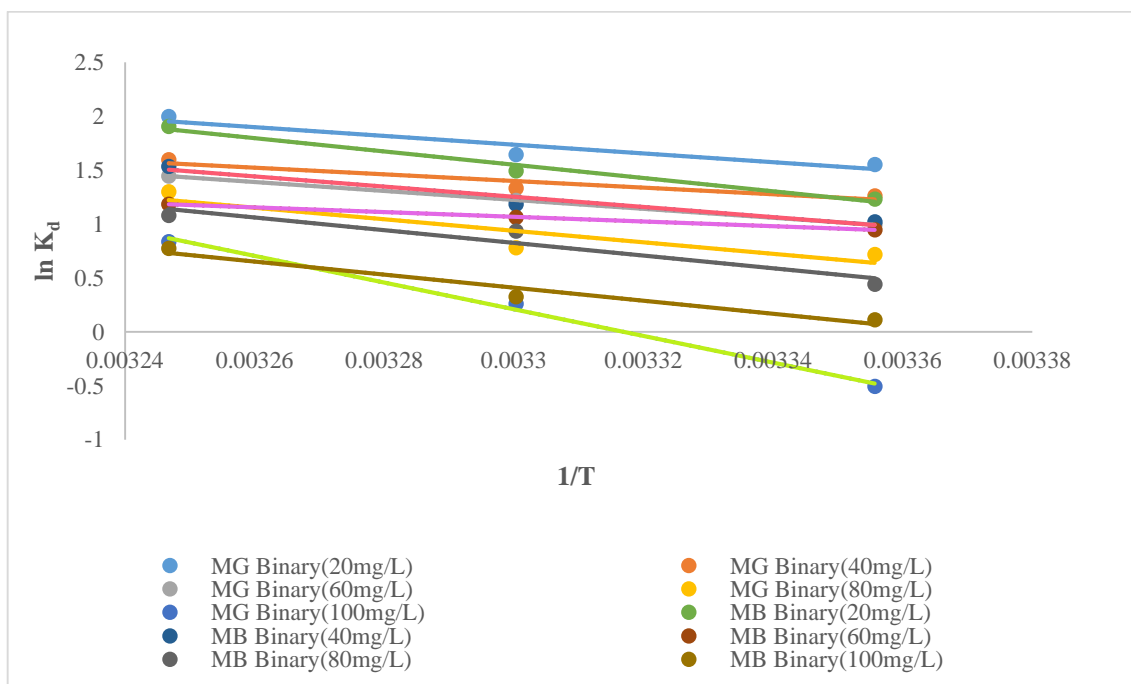


Figure 4.3.17: Adsorption thermodynamic plot for MG and MB in binary dye system

The calculated ΔH° values were found positive, confirming the endothermic character of the adsorption process. Similarly, positive ΔS° values signified increased level of randomness on the surface of adsorbent, while negative ΔG° values indicated that the adsorption process occurred spontaneously.^{153,156}

Table 4.3.4: Calculated values of thermodynamic parameters in single and binary dye system

System	Concentration (mg/L)	ΔS° (KJ/mol/K)	ΔH° (KJ/mol)	ΔG° [25°C] (KJ/mol)	ΔG° [30°C] (KJ/mol)	ΔG° [35°C] (KJ/mol)
Single MG	50	0.235	65.36	-4.710	-5.555	-7.065
	100	0.147	39.847	-4.427	-4.608	-5.920
	150	0.165	46.846	-2.226	-2.920	-3.875
	200	0.194	56.166	-1.394	-2.305	-3.326
	250	0.052	14.502	-0.962	-1.087	-1.484
Single MB	50	0.292	83.955	-3.070	-3.790	-5.999
	100	0.278	80.522	-2.908	-3.197	-5.720
	150	0.335	97.690	-2.303	-2.878	-5.670
	200	0.264	77.444	-1.103	-1.902	-3.744
	250	0.208	62.098	0.108	-0.920	-1.972
Binary MG	20	0.126	33.857	-3.850	-4.143	-5.120
	40	0.095	25.522	-3.125	-3.360	-4.088
	60	0.125	34.516	-2.464	-3.070	-3.705
	80	0.154	44.304	-1.776	-1.967	-3.330
	100	0.340	102.636	-1.037	-0.658	-2.147
Binary MB	20	0.183	51.277	-3.055	-3.760	-4.880
	40	0.140	39.125	-2.533	-2.986	-3.933
	60	0.068	17.987	-2.348	-2.680	-3.030
	80	0.168	48.887	-1.094	-2.355	-2.766
	100	0.169	50.308	-0.282	-0.823	-1.984

4.3.3. Regeneration of Adsorbent

Adsorbent's regeneration is important for assessing the performance of material after the adsorption studies. The reusability of adsorbent defines its efficacy in terms of the cost-

efficiency and its reliability. After analysing the dye adsorption capacities with WSZF composite, a regeneration process was conducted using HCl (0.1 N) as the desorbing agent for both the dye system. The regenerability of the WSZF was evaluated for up to five cycles. The regeneration efficiency of WSZF is presented in table 4.3.5 for both the dye systems. It has been found that after five adsorption-desorption cycles, the WSZF composite still showed a good regenerability. In single dye system, the regeneration efficiency calculated for MG and MB was 80.2% and 83.2% respectively whereas, in ternary dye system, the regeneration efficiency calculated was 76.9% and 80.6% for MG and MB respectively. So, the findings suggest that the prepared adsorbent showed good reusability and may be utilized several times for removing different dyes.

Table 4.3.5: Regeneration efficiency of walnut shell zinc ferrite composite for single and binary dye system

Regeneration cycle	Single dye (50 mg/L)		Binary dye (20 mg/L)	
	MG (%)	MB (%)	MG (%)	MB (%)
1	98.1	98.6	96.5	97.1
2	96.4	97.0	93.2	94.0
3	91.7	93.4	90.1	91.7
4	84.3	88.6	82.4	86.4
5	80.2	83.2	76.9	80.6

4.4. Walnut Shell Cobalt Ferrite (WCoF) Composite

4.4.1. Characterization and Morphology

4.4.1.1. Fourier Transform Infrared Spectroscopy

The Fourier Transform Infrared spectrum of pure walnut shell (WS), cobalt ferrite (CoF) and walnut shell cobalt ferrite (WCoF) is shown in figure 4.4.1. The spectra of CoF and WCoF composite exhibit two different absorption peaks below 600 cm^{-1} , which serve as confirmation for the synthesis of spinel ferrite. These peaks are specifically related with the metal oxygen (M-O) bands at two distinct points. The peak seen at around $500\text{-}600\text{ cm}^{-1}$ represents the M-O band at the tetrahedral site, whereas the peak observed near $450\text{-}400\text{ cm}^{-1}$ belongs to the M-O band at octahedral site.¹⁴²

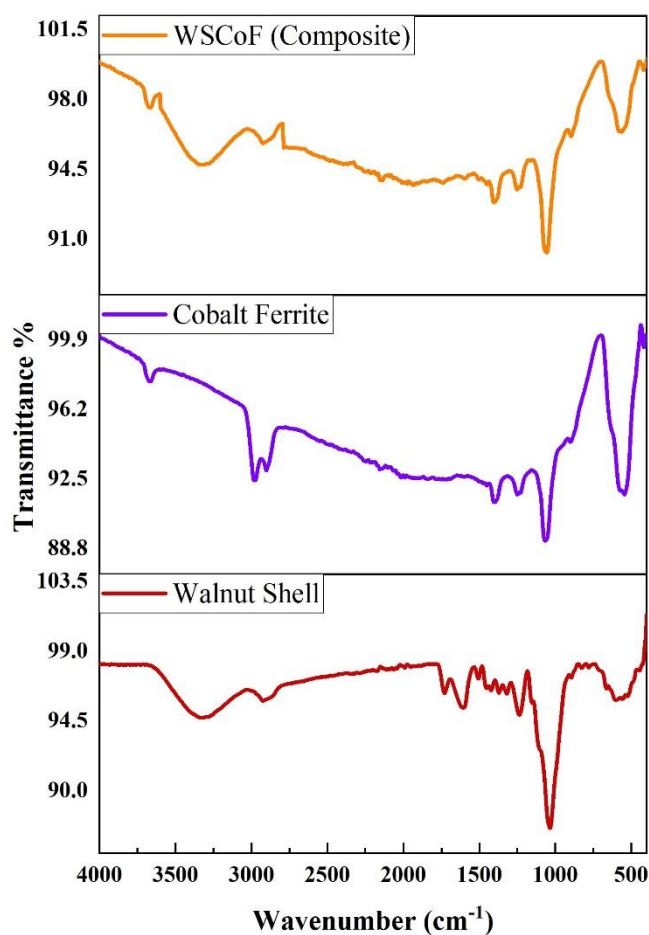


Figure 4.4.1: FTIR spectra of walnut shell, cobalt ferrite and walnut shell cobalt ferrite composite

The walnut shell spectrum has a peak at 3329.76 cm^{-1} , which corresponds to O-H bond stretching. Additionally, a peak at 2916.37 cm^{-1} was seen, indicated the stretching of C-H

bonds. Another peak at 1737.45 cm^{-1} indicated the occurrence of C=O stretching vibration in the carboxyl group. The peak seen at around 1607.02 cm^{-1} in the walnut shell corresponds to the presence of the carbon-carbon double bond (C=C) in the ester compound. The presence of an extra peak at 1237.79 cm^{-1} and 1048.16 cm^{-1} indicates the C-O bond stretching in alcohol, carboxylic acid, ester, and ether.^{159,173,200} The peak seen at around 3600 cm^{-1} in cobalt ferrite and the composite material is due to the stretching of O-H bonds. At 2984.61 cm^{-1} and 2972.96 cm^{-1} , the stretching of C-H bonds can be seen.^{142,202} The spectra of the composite showed almost similar peaks that were identical to walnut shell and cobalt ferrite with the existence of specific functional groups that may shifted to some extent. This verified that the WSCoF had been formed successfully.

4.4.1.2. X-Ray Diffraction

The X-ray diffraction pattern of WS and WSCoF are presented in figure 4.4.2. The X-ray diffraction (XRD) analysis of CoF revealed distinct peaks at specific diffraction angles: 30.117° , 35.474° , 37.108° , 43.113° , 47.205° , 53.487° , 57.018° , 62.613° , 64.534° , 71.034° , 74.075° , 75.078° , and 79.047° . These peaks correspond to the Miller indices (220), (311), (222), (400), (331), (422), (511), (440), (531), (620), (533), (622) and (444) respectively.^{142,203,204} The lattice had an apparent cubic structure. The presence of sharp peaks indicates a greater degree of crystalline structure and phase purity in the material. The composite exhibits a slight change in the diffraction peaks at certain angles: 30.087° , 35.439° , 36.671° , 43.070° , 47.157° , 53.431° , 56.958° , 62.545° , 64.763° , 70.955° , 73.991° , 74.993° , and 78.956° . It has been confirmed that the composite WSCoF exhibited the same pattern as the Miller indices of CoF. The findings indicate that even after surface modification, the composite has maintained its crystalline structure. The information pertaining to the hkl plane has been indexed by utilizing the JCPDS file number 01-074-6403 (Cobalt ferrite) and 01-079-0416 (Composite). The average crystallite size determined by using the Scherrer formula (equation 3.1) for cobalt ferrite was 22.4 nm, whereas for the composite, it was calculated to be 34.7 nm.

4.4.1.3. Field Emission Scanning Electron Microscopy

The FE-SEM images of WS, CoF and WSCoF are presented as figure 4.4.3 which describes the surface morphology. The WS exhibited a rough and flaky surface, while the prepared CoF showed an uneven shape and variable particle size. However, the WSCoF composite showed a distinct morphology with granular structures attached on the surface of walnut shell, which confirmed the proper binding of cobalt ferrite with the walnut shell.^{113,132,200}

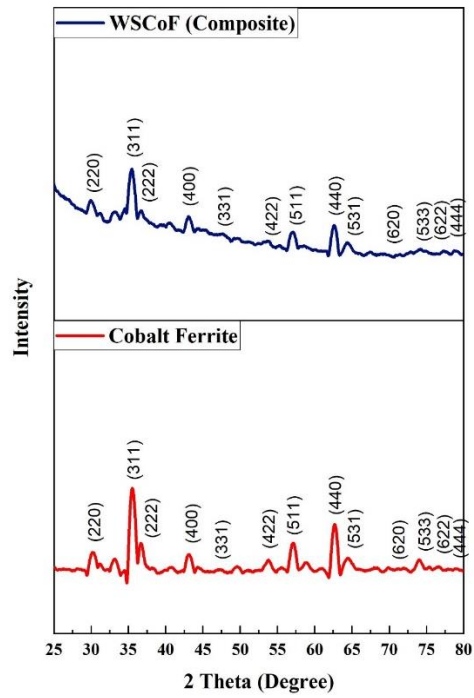


Figure 4.4.2: XRD spectra of cobalt ferrite and walnut shell cobalt ferrite composite

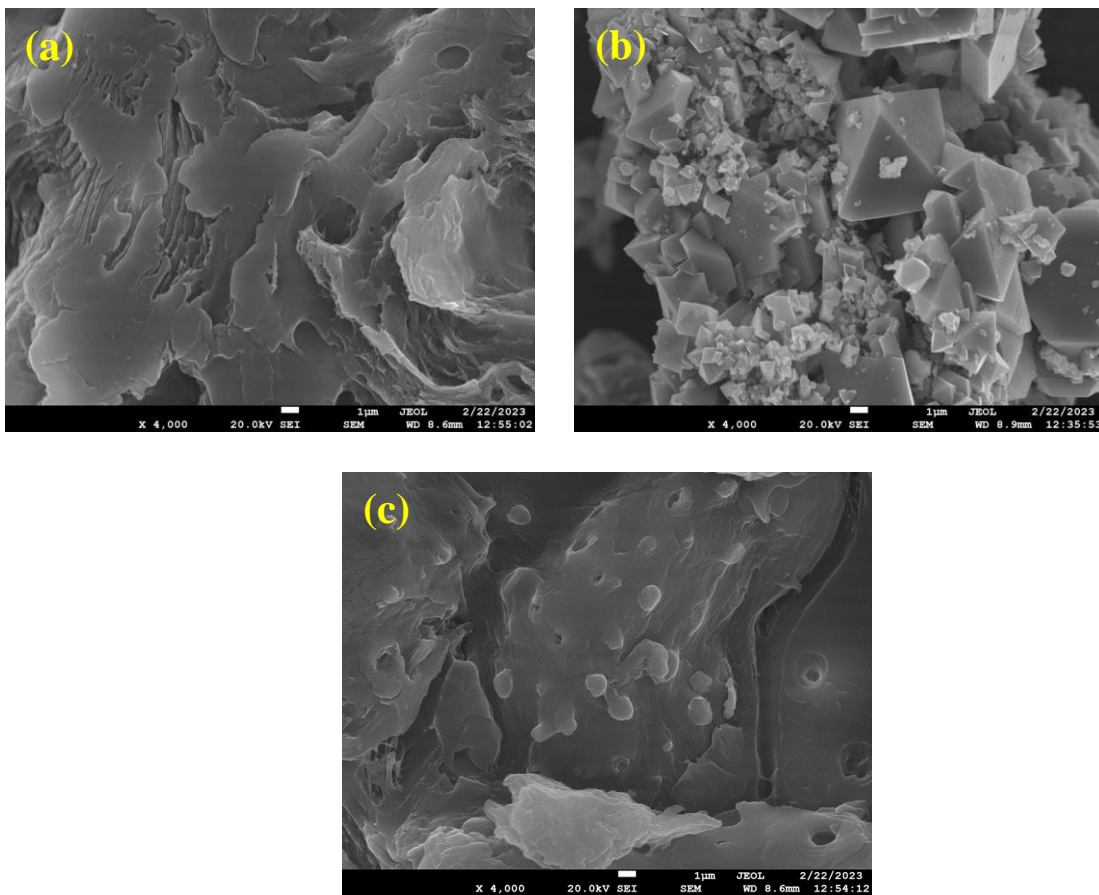


Figure 4.4.3: SEM image (a) Walnut shell (b) Cobalt ferrite (c) Walnut shell cobalt ferrite composite

4.4.1.4. Energy Dispersive Spectra

The Energy Dispersive Spectra of CoF and WSCoF along with the peaks that indicate the elemental constituents of cobalt ferrite and walnut shell cobalt ferrite composite are shown in figure 4.4.4. Table 4.4.1 illustrates the chemical composition of the compounds, including their respective weight and atomic percentages. It is evident that the percentage of carbon content in WSCoF composite is consistently higher than that of pure CoF, which indicated the effective modification of cobalt ferrite with walnut shell.¹⁴²

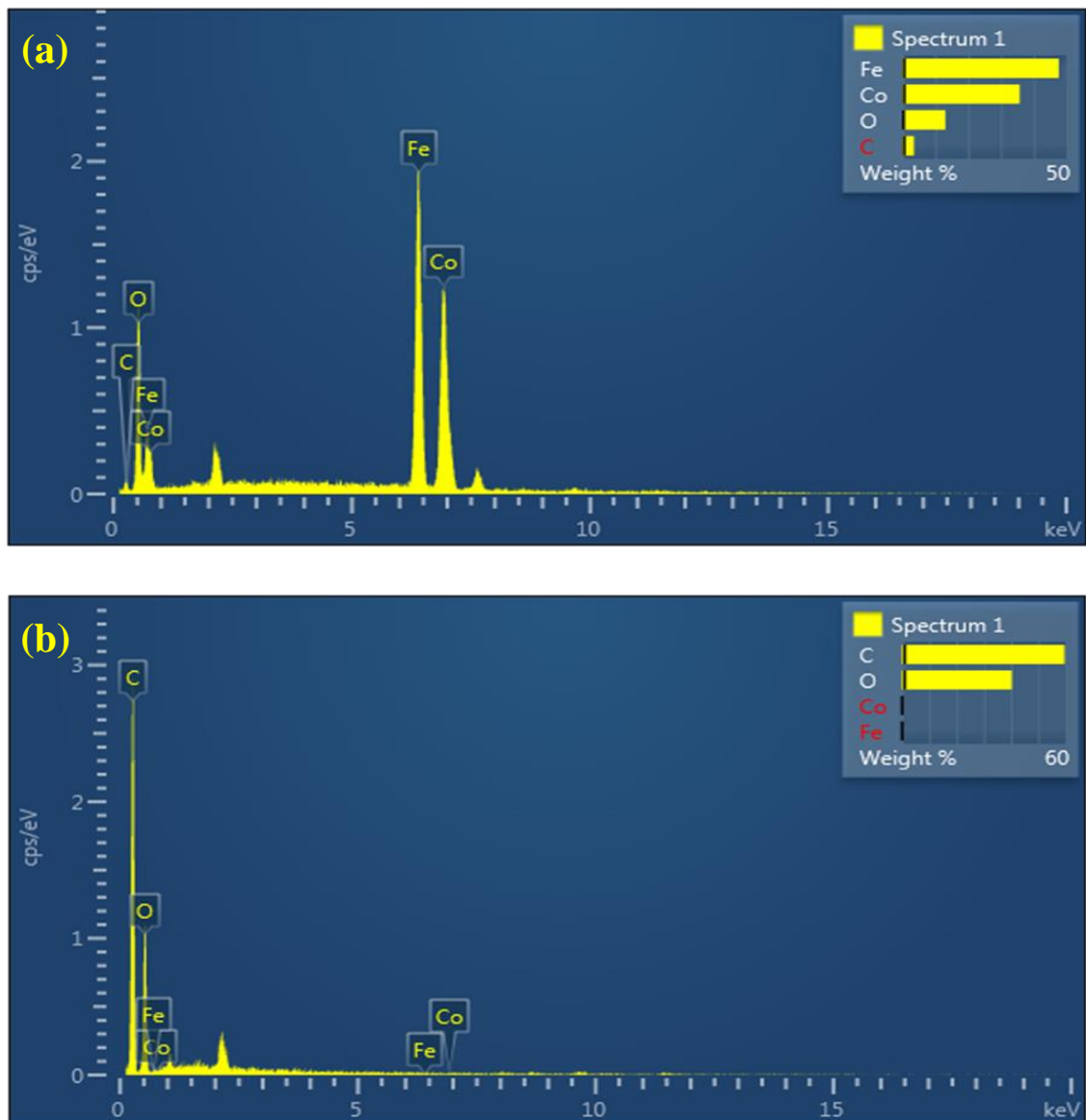


Figure 4.4.4: EDS image (a) Cobalt ferrite (b) Walnut shell cobalt ferrite composite

Table 4.4.1: Elemental composition of cobalt ferrite and walnut shell cobalt ferrite composite

Element	Cobalt Ferrite		Walnut Shell Cobalt Ferrite composite	
	Weight %	Atomic %	Weight %	Atomic %
C	3.52	11.40	49.63	56.33
O	13.10	31.84	35.30	23.66
Co	35.71	23.57	10.04	10.01
Fe	47.67	33.19	5.03	10.00
Total	100.00	100.00	100.00	100.00

4.4.1.5. Thermogravimetric Analysis

Thermogravimetric analysis was performed to assess the thermal stability of WSCoF composite. The TGA study was conducted over temperature 30 to 600°C, using a heat rate of 10°C/minute under an air atmosphere. The TGA graph of WSCoF is shown in figure 4.4.5.

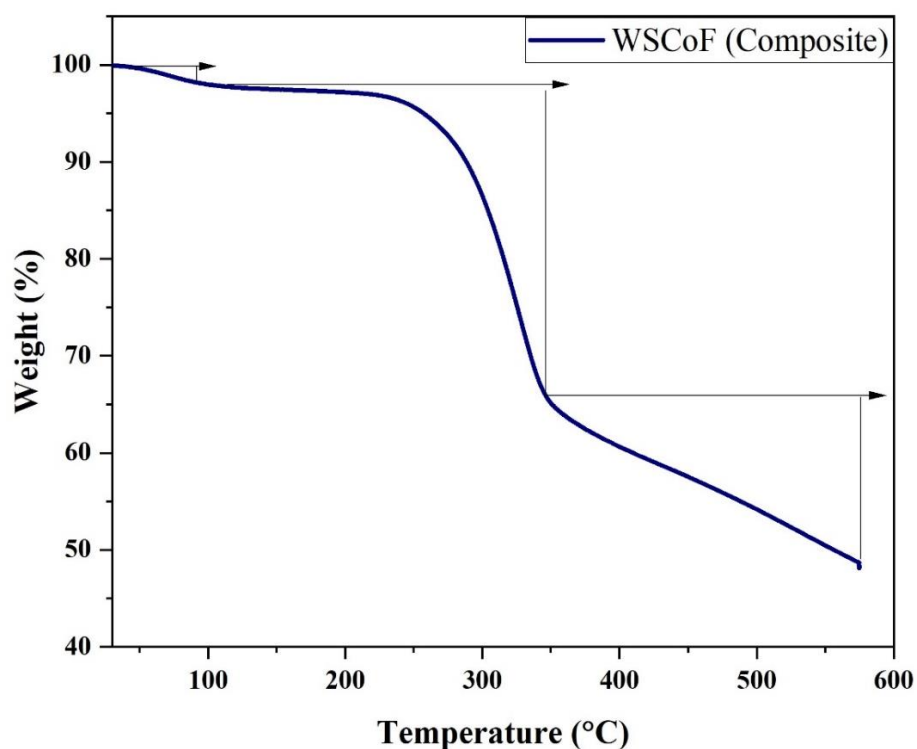


Figure 4.4.5: TGA curve of walnut shell cobalt ferrite composite

A decrease in weight of approximately 2.1% was seen from temperature 31.9°C to 98.2°C as illustrated by the graph. This drop in weight may be attributed to the vaporization of the sample's moisture. The sample lost another 32% of its weight from 98.2°C to 346.9°C which might have been attributed to the decomposition of organic functional groups present within the sample. As the temperature further increased, a consistent fall in weight of about 17.1% was noticed again from approximately 346.9°C to 575.8°C. After that no further weight loss observed which demonstrated the complete decomposition of organic matter present in the composite. As per the aforementioned calculations, 0.481 g of WS walnut shell has been attached in 1 g of WSCoF composite.^{142,158}

4.4.1.6. Brunauer-Emmett-Teller Analysis

The BET analysis was used to study the distribution of specific surface area. The results of BET analysis of WSCoF composite and pure CoF make it clear that the surface area of the pure cobalt ferrite is smaller than that of the composite. The specific surface area calculated for WSCoF was 3.592 m²/g, whereas the surface area obtained for pure CoF was 1.864 m²/g. This occurred as a result of WS modified CoF surface exhibits a greater particle size than pure CoF surface. As a result of surface modification, the porosity of the composite's surface increased, leading to a rise in its specific surface area.^{153,162}

4.4.1.7. pH of Point Zero Charge Analysis

The pH_{zpc} of WSCoF composite was determined using a solid addition method. Nine Erlenmeyer flasks, each having volume 250 mL were filled with 50 mL of a solution having 0.1M KNO₃. The pH of these solutions was adjusted to a range between pH 3 and 11 by using HCl (0.1N) and NaOH (0.1M). Subsequently, 0.1 g of WSCoF composite was added to each flask. The glass flasks were thereafter placed in shaker for the duration of 24 hours. Subsequently, the conical flasks were removed and the contents of each flask were filtered into separate beakers. The pH (final) of the solution in each beaker was noted. Further, the calculations were performed using the equation 3.2.^{121,173}

The pH_{zpc} graph of WSCoF was plotted between initial pH (on x-axis) and Δ pH (on y-axis) which is shown in figure 4.4.6. The pH_{zpc} value of composite calculated was 5.78. As a result, the material's surface will possess negative charge above pH 5.78 and positive charge below pH 5.78.

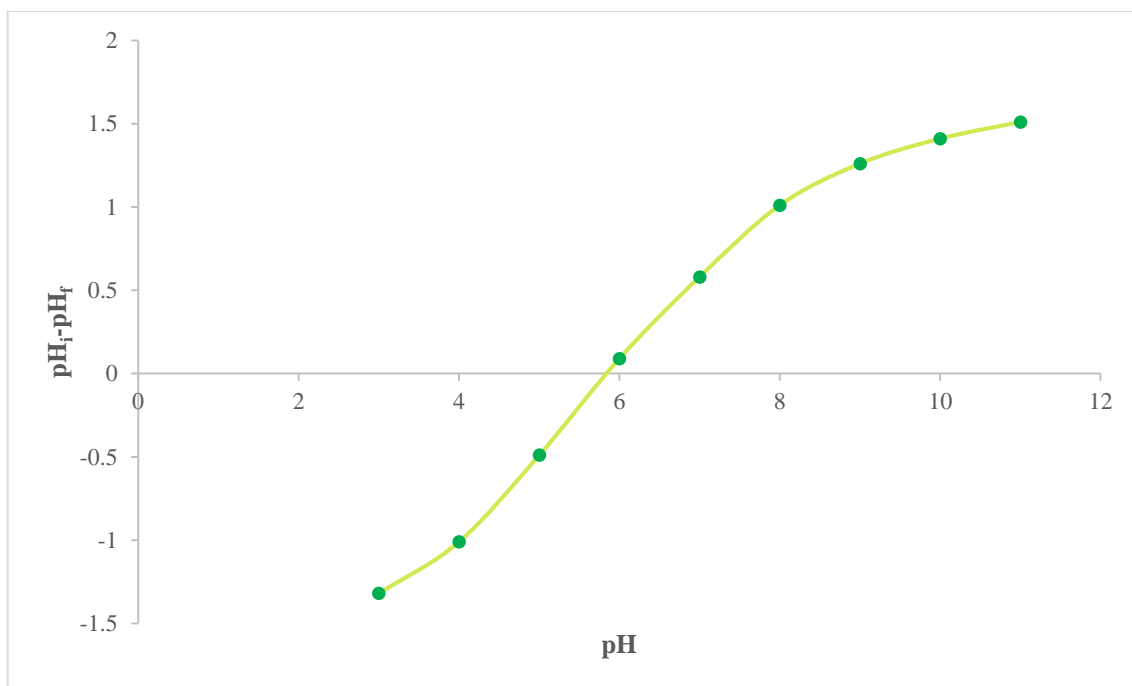


Figure 4.4.6: pH_{zpc} of walnut shell cobalt ferrite composite

4.4.2. Adsorption Study in Single and Ternary Dye System

The batch adsorption method was utilized for studying the behavior of CV, BG and MB in single as well as ternary dye systems using a WSCoF composite. Different parameters studied were contact time, adsorbent dose, pH, temperature and adsorbate concentration.

4.4.2.1. Effect of Contact Time

The effect of contact time for both single as well as ternary dye system was examined using a known concentration of single and ternary dye solution (50 mg/L and 20 mg/L respectively) along with the addition of a 0.1 g adsorbent and a fixed dye solution volume (50 mL). These flasks were then placed in thermostatic shaker for the time duration of 3 hours at 25°C. The flasks were removed from the shaker at specified regular intervals and UV-VIS Spectrophotometer (SHIMADZU-1900I) was used to measure residual dye concentration. The effect of contact time on removal of CV, BG and MB in single and ternary dye system is presented in figure 4.4.7. From the graph, it was found that percentage removal of dyes increased initially with an increase in contact time. But, the rate of adsorption slowed down after sometime and after approximately 120 minutes for BG and MB and 130 minutes for CV, the adsorption reached a constant level and equilibrium had been achieved. The graph clearly shows that the adsorption rate was initially high, leading to rapid dye elimination, then eventually stabilized and attained equilibrium. This may have occurred because an initial

stage offered a substantial number of active adsorption sites, to which the dye molecules rapidly attached. However, after a certain period of time, the unoccupied sites got occupied, the rate of adsorption slowed down and the residual concentration became constant with respect to time. The stage was referred to as equilibrium stage where the adsorption rate and the rate of desorption are equivalent to one another. The maximum percentage removal achieved for CV, BG and MB was 88%, 70% and 76.2% respectively in single dye system and in ternary dye system, the maximum removal percentage obtained was 74.4%, 58.2% and 61% for CV, BG and MB respectively.

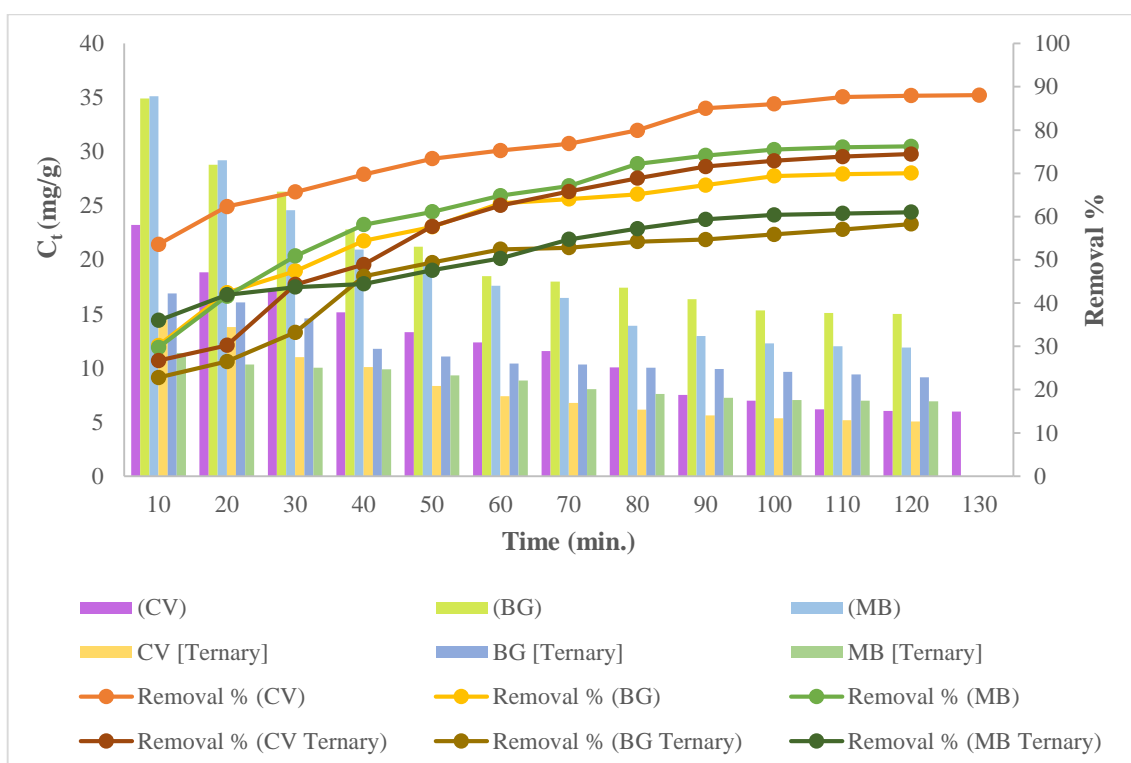


Figure 4.4.7: Effect of contact time for single and ternary dye system

4.4.2.2. Adsorption Kinetics

The kinetic behavior of WSCoF was studied for both single and ternary dye system using several model including the Lagergren pseudo first order model, pseudo second order model, Elovich model and Intra particle diffusion model. The time study was graphically represented using the kinetic models. Plot of Lagergren pseudo first order and pseudo second order model for single as well as ternary dye systems are shown in figure 4.4.8 while the plot of Elovich model is illustrated in figure 4.4.9. Table 4.4.2 represents the calculated values of different constants associated with kinetic models. The degree of model stability can be assessed by examining the value of R^2 (correlation coefficient). Therefore, the pseudo-second order model

exhibited higher R^2 for both single and ternary dye system which suggested that the pseudo-second order kinetic model was the most appropriate among other models. So, the process of adsorption for this experimental study followed chemisorption.^{58,158}

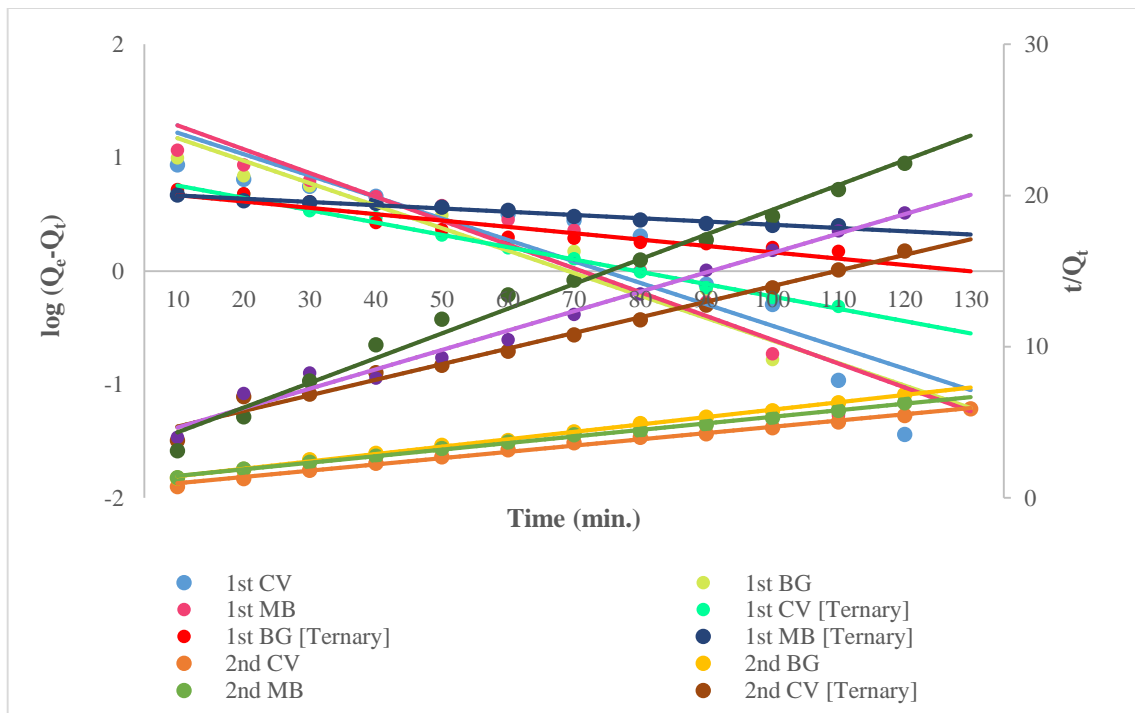


Figure 4.4.8: Lagergren pseudo first order and pseudo second order kinetics for single and ternary dye system

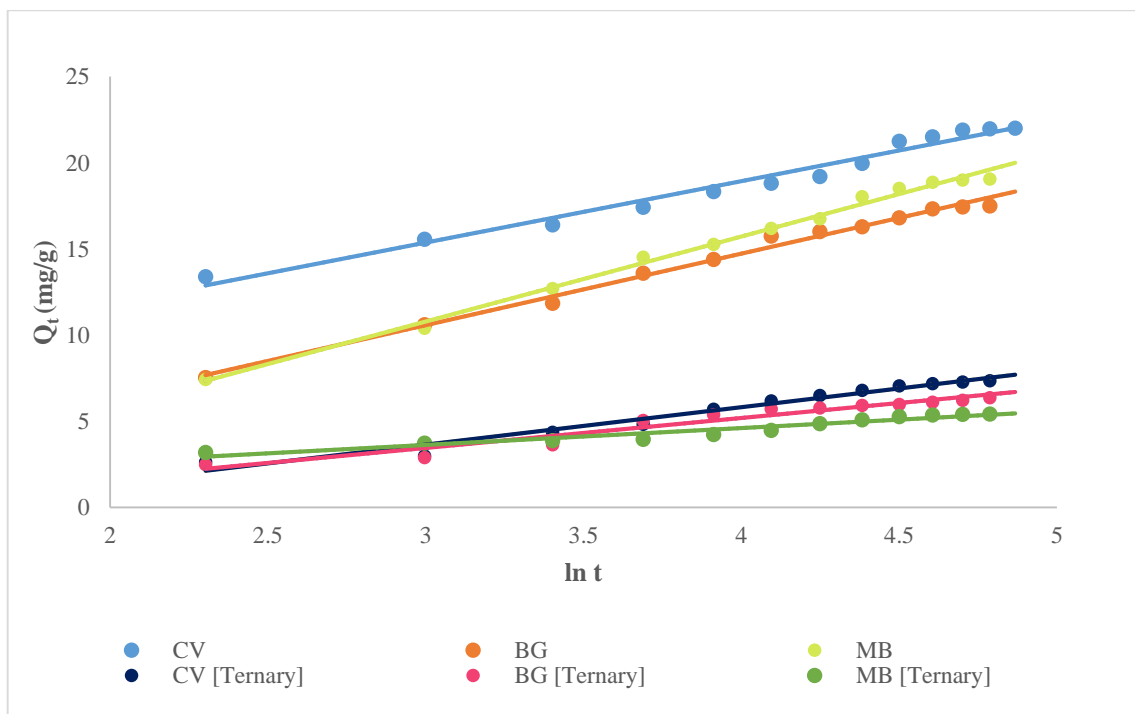


Figure 4.4.9: Elovich model for single and ternary dye system

Table 4.4.2: Calculated values of different kinetic constants for single and ternary dye system

KINETIC MODEL	Parameter	SYSTEM					
		Single CV	Single BG	Single MB	Ternary CV	Ternary BG	Ternary MB
Pseudo first order	Q_{e1}	25.686	23.447	31.275	7.316	5.307	4.957
	K_1	0.435	0.456	0.484	0.250	0.128	0.066
	R^2	0.837	0.899	0.903	0.995	0.899	0.978
Pseudo second order	Q_{e2}	2.410	2.040	2.300	0.969	0.779	0.661
	h	1.795	1.062	0.975	0.303	0.296	0.371
	K_2	0.309	0.255	0.185	0.284	0.180	0.138
	R^2	0.995	0.998	0.997	0.985	0.985	0.987
Elovich model	α	13.185	2.633	2.190	0.575	0.630	1.977
	β	0.280	0.240	0.203	0.459	0.576	1.021
	R^2	0.976	0.992	0.994	0.964	0.941	0.932

Weber-Morris model was used to describe the mechanism of adsorption for different dyes using WSCoF composite. The graph between Q_t and $t^{0.5}$ is shown in figure 4.4.10 and K_{int} which is the rate constant of intra-particle diffusion and the rate-limiting step can be calculated from the slope. This rate limiting step suggests that the straight line must pass through the origin. But, the graph shows that the plot formed a non-linear curve and the line do not pass through the origin suggested that, apart from intra-particle diffusion, the additional factors may present which influence the adsorption rate in both the dye systems. The graph shows a steep initial slope, indicating fast dye adsorption in single dye system. After a certain interval, the slope becomes more gradual and eventually reached equilibrium. But this trend was not observed in the case of ternary dye system. The reduction in ternary dye systems adsorption rate may be attributed to the antagonistic effects of various dyes. The reduced adsorption of dyes could be attributed to the influence of forces like π - π and electrostatic interaction among the CV, BG and MB molecules. As a consequence of these interactions, strong bonds were formed between distinct dye molecules. Because of this, the percentage of various dyes removed from the ternary dye system was much lower when compared to the percentage removed from a single dye system.¹¹²

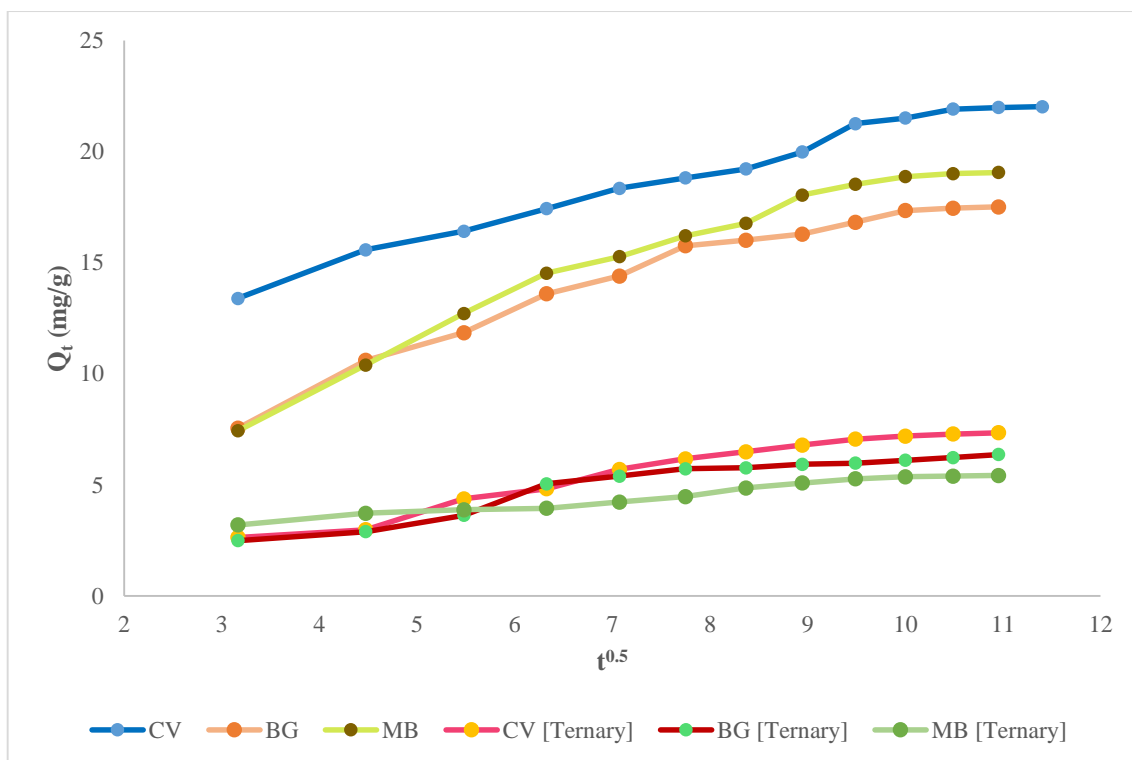


Figure 4.4.10: Intra particle diffusion model for single and ternary dye system

4.4.2.3. Effect of pH

The solution's pH plays a crucial role in the process of adsorption by influencing the surface charge of the adsorbent which in turn, changes the degree of affinity between the molecules adsorbate and adsorbent.

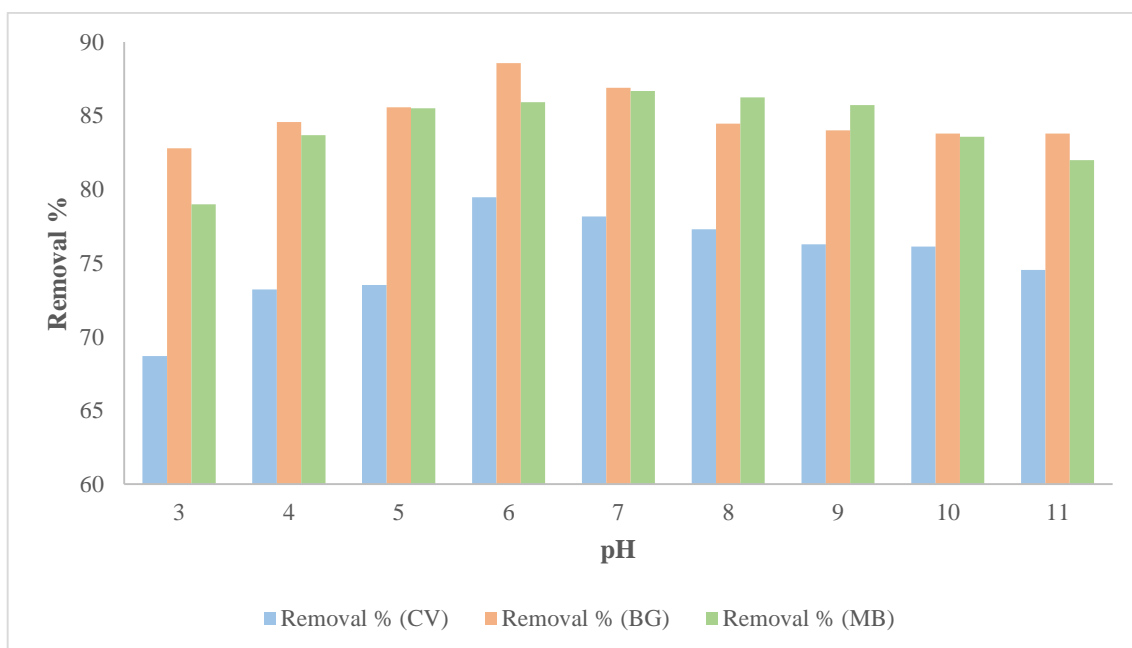


Figure 4.4.11: Effect of pH for single dye system

The effect of pH was studied to know the adsorption behavior of WSCoF composite with different dyes in single dye system at pH values ranging from 3 to 11. The prepared solution having dye concentration 50 mg/L was poured into conical flasks along with the adsorbent dosage 0.1 g. All flasks were then placed in an orbital shaker for 3 hours at 25°C. The effect of pH on CV and BG removal in single dye system is shown in figure 4.4.11. From the graph, it is clear that, the removal percent of dye increased with increase in pH till pH 6 and then further decreased. For dyes CV and BG, the maximum removal percentages obtained at pH 6 were 79.5% and 88.5%, respectively. On the other hand, for dye MB, the highest removal percentage calculated was 86.6% at pH 7.¹⁵⁸

4.4.2.4. Effect of Adsorbent Dosage

The adsorbent dosage effect was studied by altering the dosage of prepared WSCoF from 0.1 g to 0.5 g in single and ternary dye system. The experimental study was conducted using 50 mL dye solution volume having a specific concentration and at constant temperature 25°C. The effect of adsorbent dose on the quantity of dye adsorbed per gram of adsorbent (Q_e) and removal percentage is shown in figure 4.4.12.

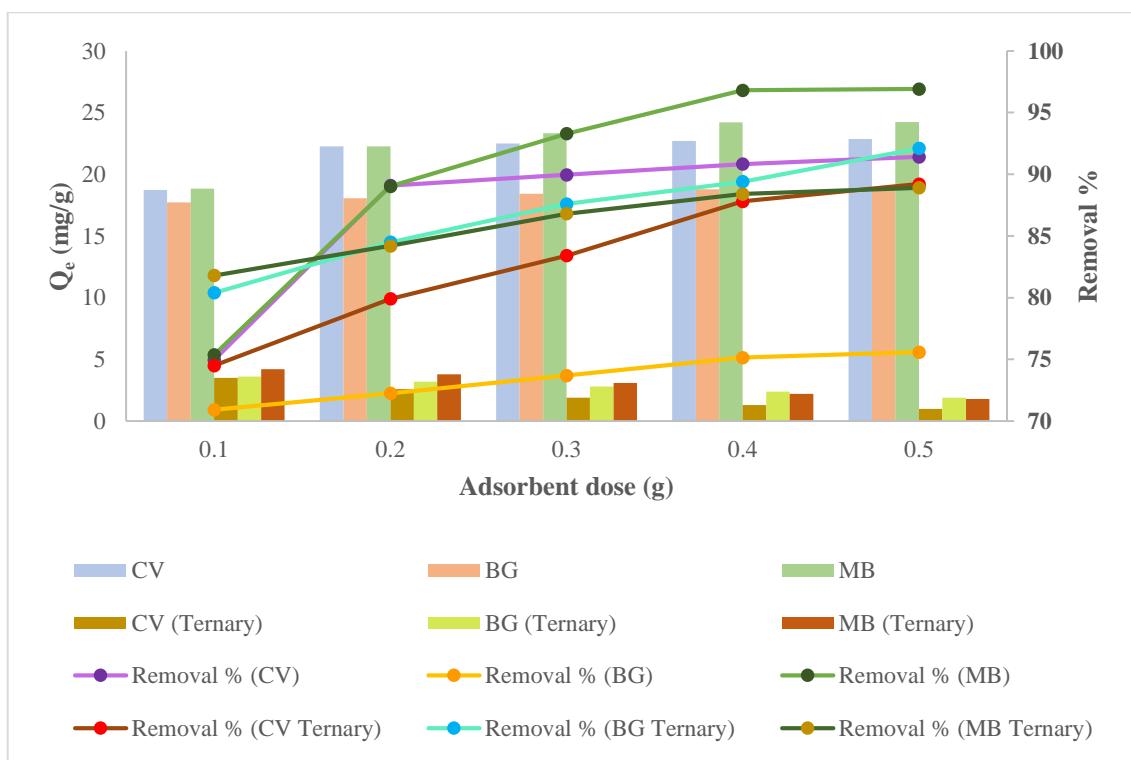


Figure 4.4.12: Effect of adsorbent dosage for single and ternary dye system

It is evident from the graph that as the dosage of the composite increased, there has been a corresponding rise in the percentage of dye removal. This trend of increasing dye removal was

seen in both the dye systems which was noticed due to more unoccupied sites on the composite's surface with an increasing adsorbent amount. However, on increasing adsorbent amount, the quantity of adsorbate adsorbed per gram of adsorbent (Q_e) decreased. This may occur due to the presence of more active sites on the surface of WSCoF which remained unoccupied on increasing adsorbent amount.^{126,142} In single dye system, the removal percent achieved for dyes CV, BG and MB was 91.4%, 75.5% and 96.9% respectively. However, in ternary dye system, the removal percentage obtained for CV, BG and MB was 89.2%, 92.1% and 88.9% respectively.

4.4.2.5. Effect of Concentration and Temperature

The effect of concentration on dye removal using WSCoF composite was studied with initial dye concentration ranged from 50 - 250 mg/L for the single dye system and 20 to 100 mg/L for ternary dye system. Along with concentration, the effect of temperature at 25°C, 30°C and 35°C was also studied. The effect of concentration and temperature in both single and ternary dye system is represented in figure 4.4.13 and 4.4.14 respectively. It was seen from the graph that the adsorption capacity ' Q_e ' of dyes in both single as well as ternary dye system increased with increased concentration of dye. This increase in the adsorption capacity occur because of the stronger interaction between the molecules of dye and adsorbents as the quantity of dye molecules increased for a given amount of adsorbent leading to more frequent collisions. The percentage removal however, decreased when the dye concentration in both the systems increased. This observation may be attributed to the consistent number of active sites available on the surface of the adsorbent, in contrast to the increasing concentration of dye molecules. Additionally, it was noted that the adsorption capacity of various dyes increased with rising temperature, indicating an endothermic adsorption process.^{58,87} The rise in adsorption capacity with respect to temperature could takes place due to the strong interaction between the molecules of adsorbent and adsorbate. As the temperature increases, certain pores within the adsorbent may expand, thereby providing a larger surface area for the adsorption of different dye molecules. Furthermore, increased temperature boosts kinetic energy, resulting in more effective collisions.

In case of ternary dye system, the percent removal was lower compared to the single dye system which may be because of the dye's antagonistic effect. In ternary dye system, dyes experience several forces of attraction among their molecules, leading to the formation of stronger bonds and consequently reducing the adsorption capacities of dyes.

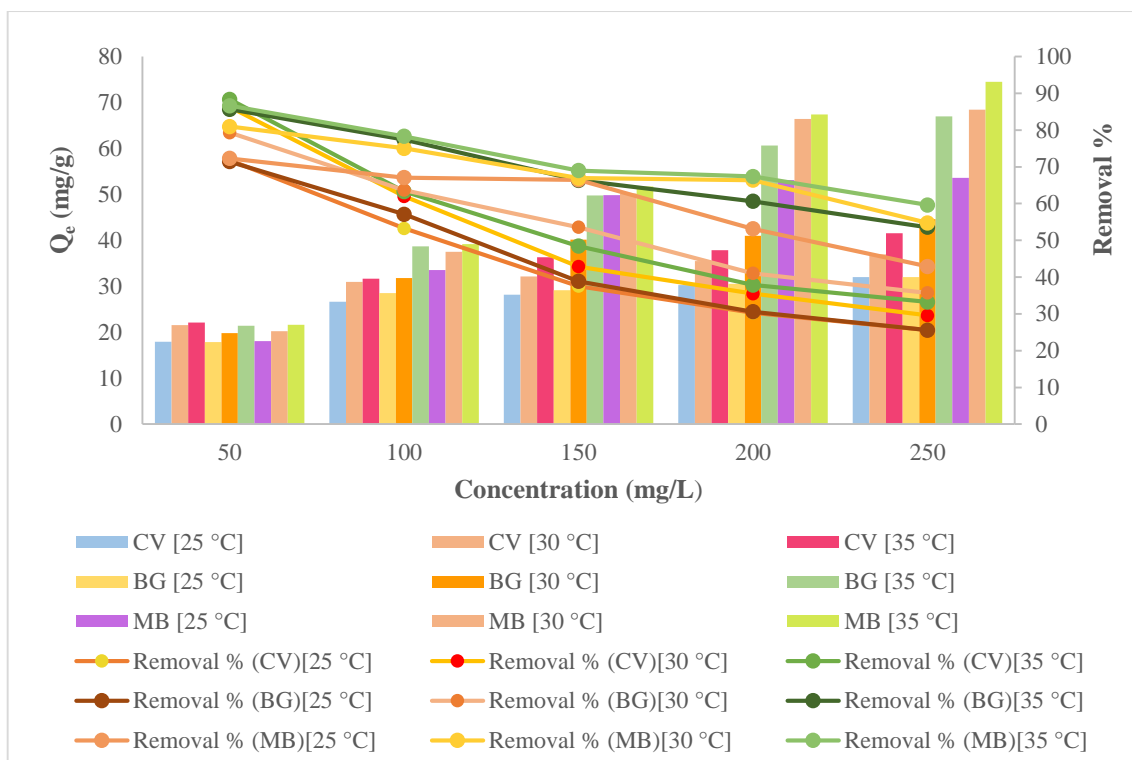


Figure 4.4.13: Effect of concentration for single dye system

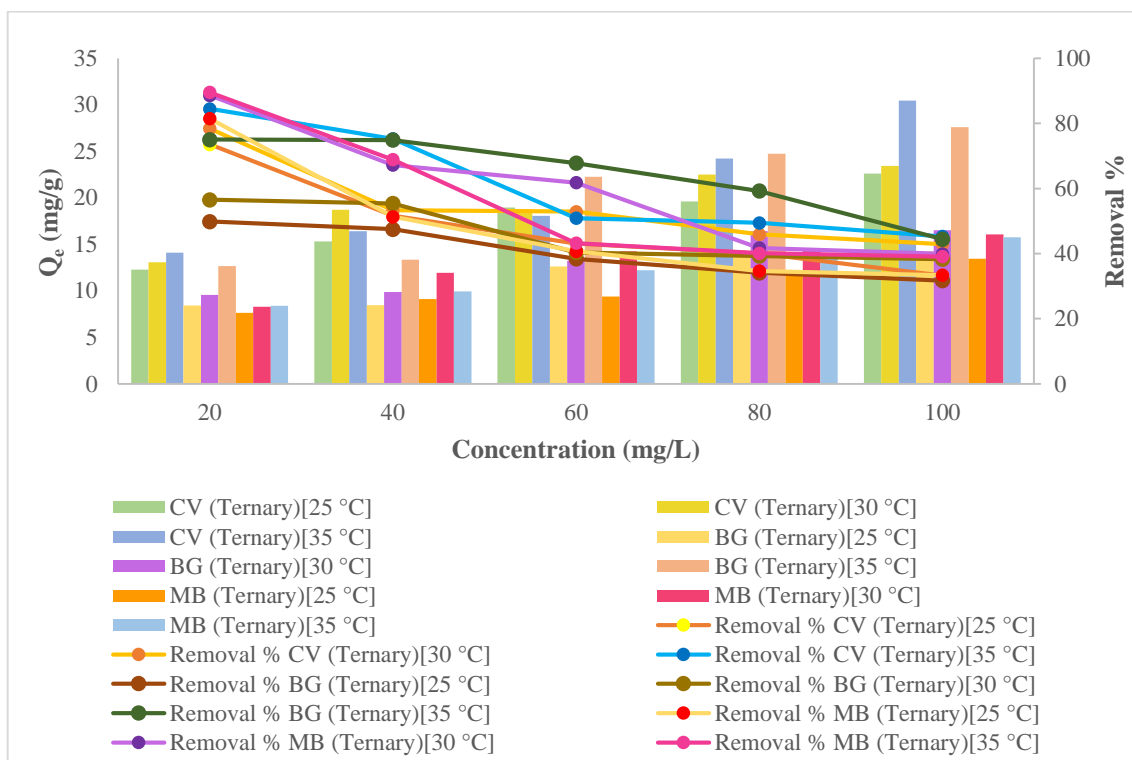


Figure 4.4.14: Effect of concentration for ternary dye system

4.4.2.6. Adsorption Isotherms

Adsorption isotherms were studied to know the behavior of adsorption under equilibrium conditions. These adsorption isotherm describes the equilibrium distribution of the adsorbate molecules between the solid and liquid phase. Different isotherm models including Langmuir, Freundlich, Temkin and Dubinin-Radushkevich (D-R) model were applied to study the behavior of adsorption for CV, BG and MB in the single as well as ternary systems at three temperatures i.e.; 25°C, 30°C and 35°C.

Different adsorption isotherms employed for both single and ternary dye systems at three temperatures and varying concentrations are presented in figure 4.4.15 (a-d). The values of different isotherm constants for both the dye systems were determined using plots of the adsorption isotherm. Among all adsorption models studied, the Langmuir model emerged as the most appropriate fit for the experimental data based on the highest R^2 (correlation coefficient) value. The findings suggested that the surface of prepared composite was found to have active adsorption sites that were distributed evenly over its surface. The Langmuir adsorption capacities obtained for dyes CV, BG and MB in single system were 38.9, 70.4 and 78.1 mg/g, respectively. However, in ternary system, the maximum adsorption capacities obtained were 23.8, 37.7 and 13.3 mg/g for CV, BG and MB respectively.

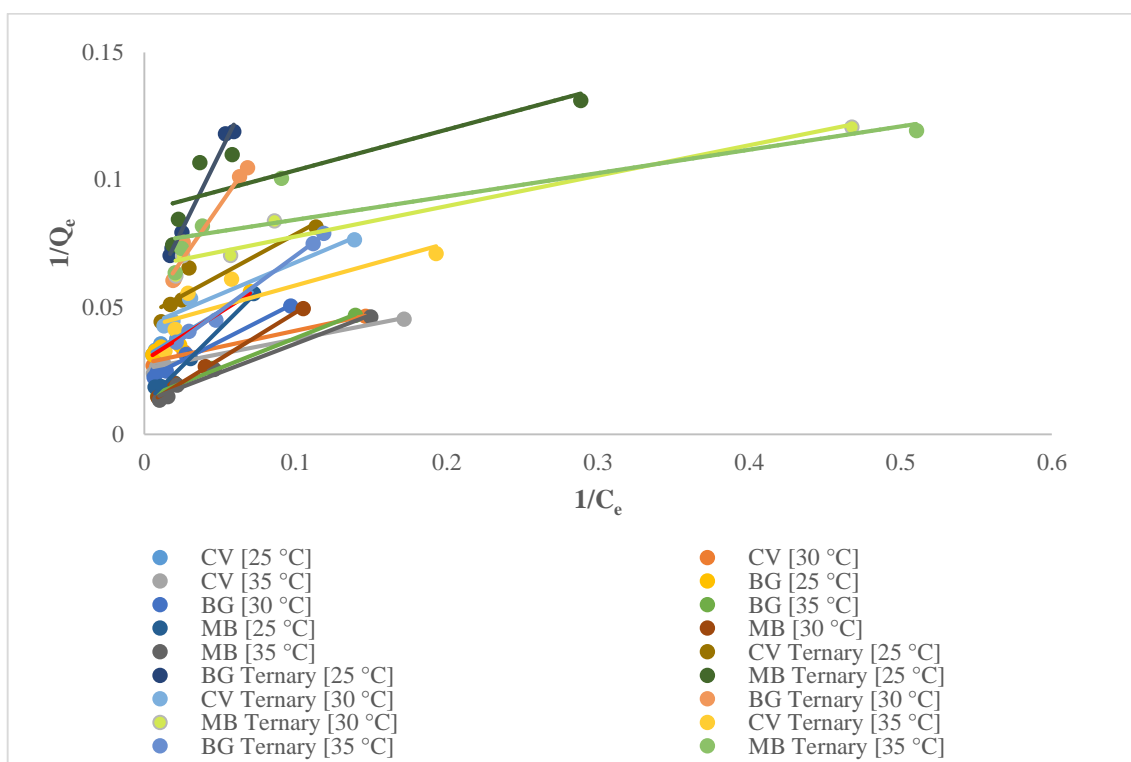


Figure 4.4.15 (a): Langmuir adsorption isotherm for single and ternary dye system

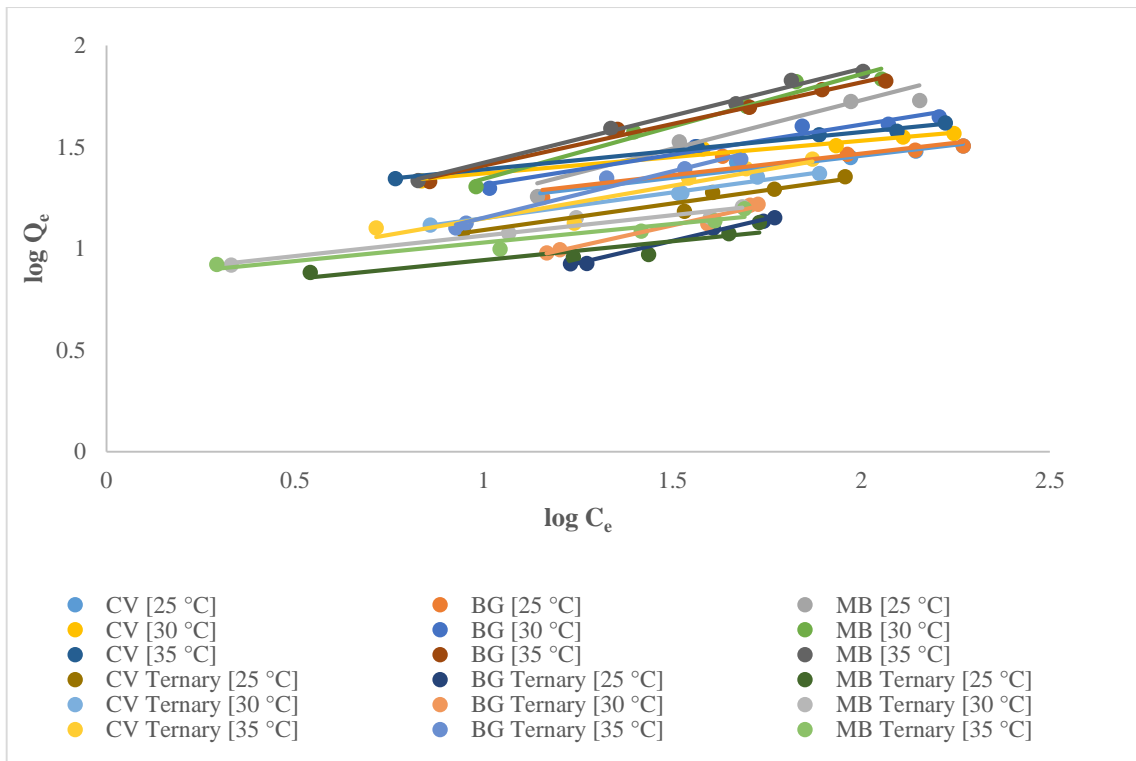


Figure 4.4.15 (b): Freundlich adsorption isotherm for single and ternary dye system

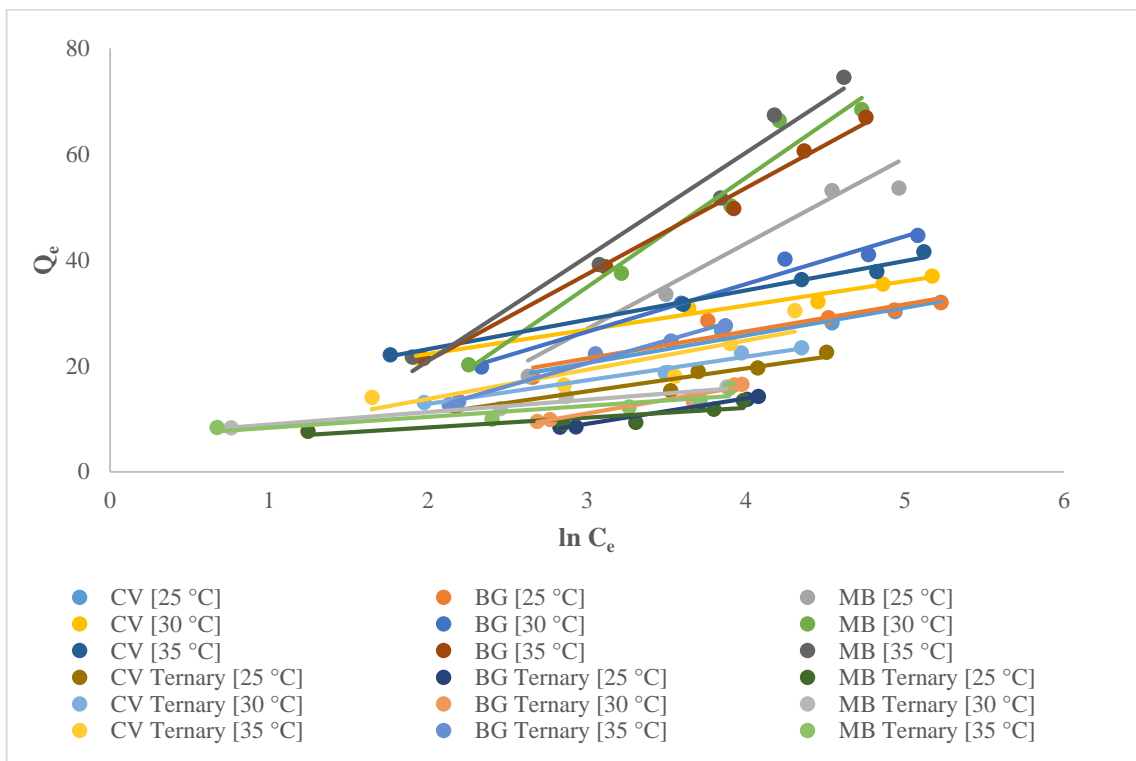


Figure 4.4.15 (c): Temkin adsorption isotherm for single and ternary dye system

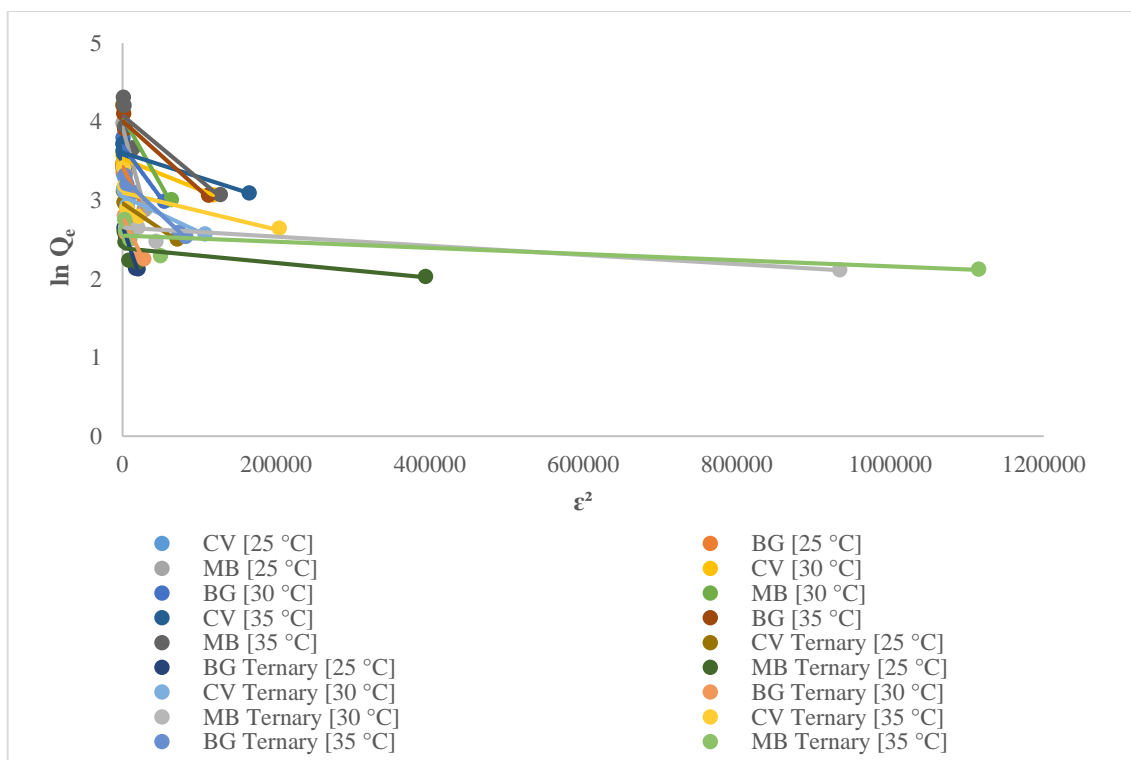


Figure 4.4.15 (d): D-R adsorption isotherm for single and ternary dye system

Further, the separation factor ' R_L ' associated with Langmuir isotherm model was computed to describe the nature of adsorption process. The obtained R_L values for single and ternary dye system were found between 0 to 1 as shown in table 4.4.3 which indicated that the prepared WSCoF composite is favorable for the dye's adsorption in single as well as ternary dye system.

An additional factor, Adsorption Energy ' E ' related to D-R isotherm was calculated to determine the type of adsorption. Adsorption is classified as physical if the calculated ' E ' value is below 8 KJ/mol; otherwise, it is regarded as chemical in nature. The D-R constant variable ' K ' was used to calculate adsorption energy ' E '. Table 4.4.3 shows that the calculated value of ' E ' for both the systems exceeded 100 KJ/mol, suggesting the process was chemical in nature.^{158,162}

Table 4.4.3: Calculated values of adsorption isotherm constants for single and ternary dye system

Adsorption		Single system									Ternary system								
Isotherm model	Constant	CV			BG			MB			CV			BG			MB		
		25°C	30°C	35°C	25°C	30°C	35°C	25°C	30°C	35°C	25°C	30°C	35°C	25°C	30°C	35°C	25°C	30°C	35°C
Langmuir	Q_e	33.003	35.714	38.910	34.364	46.728	70.422	83.333	88.495	78.125	21.598	23.529	23.866	19.841	21.276	37.735	11.389	15.220	13.315
	b	0.084	0.220	0.221	0.077	0.070	0.060	0.020	0.030	0.056	0.143	0.169	0.252	0.041	0.054	0.060	0.550	0.550	0.819
	R^2	0.992	0.970	0.953	0.975	0.991	0.992	0.979	0.994	0.981	0.852	0.945	0.658	0.991	0.967	0.995	0.670	0.951	0.745
	R_L	0.192	0.083	0.082	0.206	0.222	0.25	0.5	0.4	0.263	0.259	0.228	0.165	0.549	0.480	0.454	0.083	0.083	0.057
Freundlich	K_f	10.616	16.173	16.095	11.076	10.471	10.034	5.997	6.742	9.126	6.771	7.874	6.722	2.409	3.104	4.967	5.720	7.282	7.040
	$1/n$	0.215	0.161	0.183	0.211	0.295	0.408	0.476	0.514	0.463	0.261	0.253	0.321	0.437	0.415	0.456	0.186	0.202	0.182
	R^2	0.947	0.969	0.993	0.851	0.958	0.987	0.864	0.964	0.991	0.927	0.986	0.864	0.991	0.975	0.969	0.824	0.947	0.912
Temkin	b_T	483.260	550.523	453.058	492.799	279.538	154.491	156.148	121.603	128.096	581.680	566.328	456.002	528.133	481.055	292.138	1355.981	1080.392	1223.121
	A	2.564	17.472	8.706	3.267	0.937	0.490	0.265	0.267	0.392	1.651	2.410	1.623	0.332	0.407	0.537	12.147	16.897	20.857
	R^2	0.968	0.976	0.989	0.880	0.977	0.992	0.894	0.961	0.965	0.899	0.968	0.754	0.994	0.954	0.988	0.763	0.941	0.857
D-R model	Q_m	29.755	34.021	36.888	20.707	40.133	55.179	51.024	58.119	59.098	19.348	21.128	22.146	14.452	16.264	26.575	10.903	14.206	12.839
	K	2×10^{-5}	4×10^{-6}	3×10^{-6}	2×10^{-5}	1×10^{-5}	9×10^{-6}	4×10^{-5}	2×10^{-5}	8×10^{-6}	7×10^{-6}	5×10^{-6}	2×10^{-6}	3×10^{-5}	2×10^{-5}	9×10^{-6}	9×10^{-7}	6×10^{-7}	4×10^{-7}
	R^2	0.942	0.902	0.858	0.984	0.902	0.857	0.928	0.863	0.815	0.708	0.835	0.446	0.974	0.917	0.986	0.510	0.856	0.587
	E	158.11	353.55	408.25	158.11	223.61	235.70	111.80	158.11	250	267.26	316.23	500	129.10	158.11	235.70	745.36	912.87	1118.03

4.4.2.7. Adsorption Thermodynamics

The adsorption behavior of dyes CV, BG and MB for single as well as ternary dye system were studied at distinct temperatures i.e.; 25°C, 30°C and 35°C. A rise in dye adsorption was noticed with increase in temperature, suggesting an endothermic adsorption process.

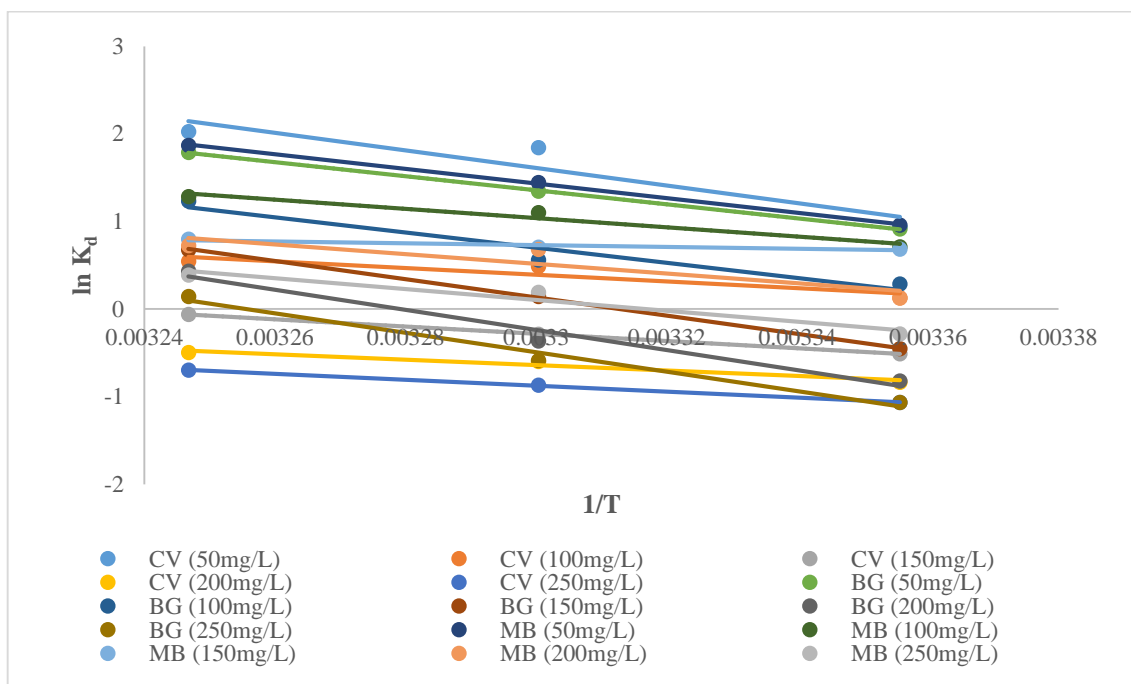


Figure 4.4.16: Adsorption thermodynamic plot for CV, BG and MB in single dye system

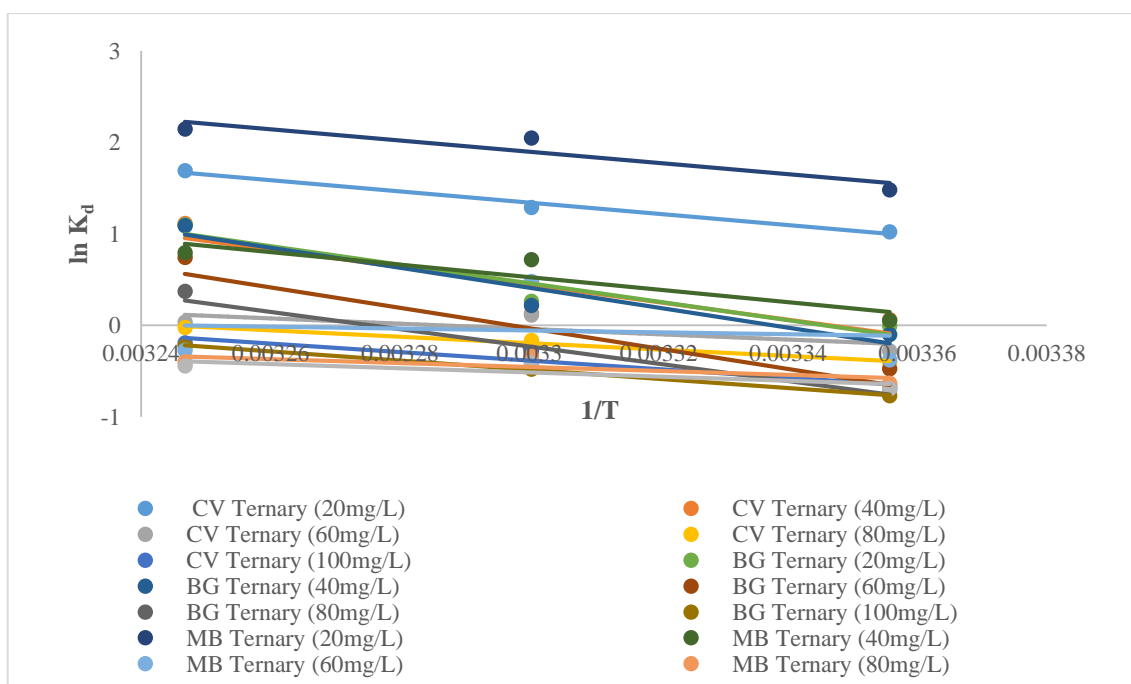


Figure 4.4.17: Adsorption thermodynamic plot for CV, BG and MB in ternary dye system

For determining various parameters including free energy change (ΔG°), enthalpy change (ΔH°) and entropy change (ΔS°), several thermodynamic equations (given in section 3.12) were applied. The calculation of ΔS° and ΔH° was conducted by plotting $\ln K_d$ against $1/T$ as illustrated in figure 4.4.16 and 4.4.17. Table 4.4.4 presents the calculated values of thermodynamic parameters. The positive ΔH° values affirmed the endothermic characteristic of adsorption process. Similarly, positive values of ΔS° indicated an increased level of randomness on the adsorbent's surface. However, the negative ΔG° value calculated signified the adsorption process was spontaneous in nature.^{142,153}

Table 4.4.4: Calculated values of thermodynamic parameters in single and ternary dye system

System	Concentration (mg/L)	ΔH° (KJ/mol)	ΔS° (KJ/mol/K)	ΔG° (25°C) (KJ/mol)	ΔG° (30°C) (KJ/mol)	ΔG° (35°C) (KJ/mol)
Single CV	50	83.497	0.288	-2.317	-4.639	-5.187
	100	31.706	0.107	-0.323	-1.229	-1.393
	150	34.086	0.110	1.261	0.724	0.159
	200	25.797	0.079	2.065	1.504	1.271
	250	28.211	0.085	2.643	2.185	1.785
Single BG	50	66.476	0.230	-2.268	-3.387	-4.575
	100	72.049	0.243	-0.709	-1.412	-3.156
	150	86.382	0.286	1.123	-0.359	-1.736
	200	95.369	0.312	2.031	0.913	-1.105
	250	92.326	0.300	2.645	1.480	-0.368
Single MB	50	69.422	0.240	-2.374	-3.643	-4.783
	100	43.784	0.153	-1.762	-2.775	-3.287
	150	8.780	0.035	-1.693	-1.777	-2.046
	200	46.046	0.156	-0.311	-1.715	-1.859
	250	51.591	0.171	0.707	-0.479	-0.996
Ternary CV	20	50.986	0.179	-2.536	-3.248	-4.334
	40	79.627	0.266	-0.160	-0.332	-2.850
	60	23.999	0.078	0.685	-0.290	-0.090
	80	29.229	0.094	1.001	0.413	0.055
	100	38.707	0.124	1.720	0.716	0.484

System	Concentration (mg/L)	ΔH° (KJ/mol)	ΔS° (KJ/mol/K)	ΔG° (25°C) (KJ/mol)	ΔG° (30°C) (KJ/mol)	ΔG° (35°C) (KJ/mol)
Ternary BG	20	84.187	0.281	0.016	-0.663	-2.816
	40	90.664	0.302	0.248	-0.547	-2.794
	60	92.493	0.304	1.172	0.984	-1.906
	80	78.556	0.257	1.631	1.095	-0.958
	100	41.532	0.133	1.902	1.199	0.573
Ternary MB	20	50.916	0.183	-3.671	-5.160	-5.496
	40	56.852	0.192	-0.132	-1.809	-2.036
	60	8.529	0.027	0.930	-1.213	0.697
	80	17.919	0.055	1.569	0.838	1.025
	100	18.993	0.058	1.711	1.031	1.136

4.4.3. Regeneration of Adsorbent

Adsorbent regeneration and reuse are essential for ensuring the performance after adsorption studies. After analyzing the capacity of adsorption for dyes CV, BG and MB in single dye as well as ternary dye system using WSCoF composite, the regeneration process was carried using HCl (0.1 N) as desorbing agent. The composite's regeneration efficiency was calculated over six cycles.

Table 4.4.5: Regeneration efficiency of walnut shell cobalt ferrite composite in single and ternary dye system

Regeneration Cycle	Single dye (50 mg/L)			Ternary dye (20 mg/L)		
	CV (%)	BG (%)	MB (%)	CV (%)	BG (%)	MB (%)
1	100	100	100	100	100	100
2	97.4	97.0	96.6	98.2	97.6	97.2
3	94.8	93.2	89.6	95.3	94.3	92.4
4	90.6	91.7	85.5	90.6	93.4	88.7
5	88.7	88.9	82.1	85.4	89.5	83.4
6	85.4	86.4	76.4	80.7	88.6	80.2

Table 4.4.5 presents the regenerable efficiency for both the dye systems. The data clearly indicates that, even after six adsorption-desorption cycles, the WSCoF composite showed good regenerability. In single dye system, the regeneration efficiency calculated for CV, BG and MB was 85.4%, 86.4% and 76.4% respectively while in ternary dye system, the regeneration efficiency calculated was 80.7%, 88.6% and 80.2% respectively. The findings suggested that the WSCoF showed good reusability and can serve as economic adsorbent for removing cationic dyes.^{58,165}

PART-II

(Metal ion adsorption using bio-waste metal ferrite composite)

Nickel ferrite pistachio shell (NFPS) composite had been selected as an efficient adsorbent for removing Cu(II) ion. The subsequent sections describe the comprehensive findings of surface characterization, morphology and adsorption studies conducted using nickel ferrite pistachio shell composite.

4.5. Nickel Ferrite Pistachio Shell (NFPS) Composite

4.5.1. Characterization and Morphology

4.5.1.1. Fourier Transform Infrared Spectroscopy

Fourier transform infrared spectra of pistachio shell (PS), nickel ferrite (NF) and nickel ferrite pistachio shell (NFPS) is shown in figure 4.5.1. The spectra of NF and NFPS composite exhibit two different peaks located below 600 cm^{-1} . These peaks serve as evidence for the synthesis of spinel ferrite and are attributed to the M-O (metal oxygen) bands at two separate locations. The peak observed between 500 and 600 cm^{-1} is due to the M-O band at tetrahedral site, while the peak seen near 450 and 400 cm^{-1} is indicative of the octahedral site.¹⁹⁶

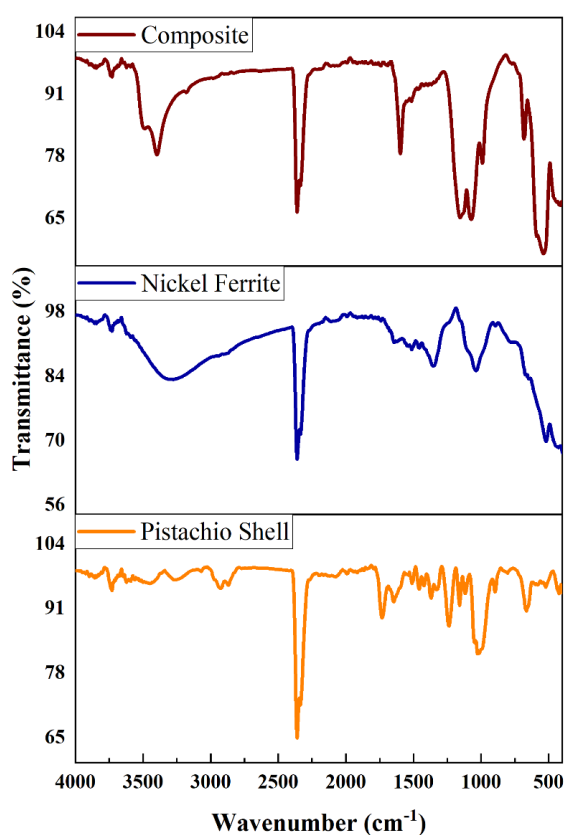


Figure 4.5.1: FTIR spectra of pistachio shell, nickel ferrite and nickel ferrite pistachio shell composite

The peak at 3449.06 cm^{-1} represents the presence of an alcoholic ($-\text{OH}$) or phenolic ($-\text{OH}$) group. The existence of CH_2 or CH_3 groups is confirmed by a peak at 2927.41 cm^{-1} , due to the stretching vibrations of $\text{C}-\text{H}$ bonds in aliphatic groups and another peak at 2360.44 cm^{-1} occurs because of the CO_2 presence. The presence of esters of lignin or ketones is discerned by a peak at 1646 cm^{-1} . The presence of aromatic groups ($\text{C}=\text{C}$ stretching) are identified by a peak at 1511.92 cm^{-1} . Peak at 1458.89 cm^{-1} corresponds the CH_2 bending vibration. Additionally, peak at 1369.21 cm^{-1} signifies $-\text{C}-\text{H}$ bending vibration of alkane groups and peak at 1238.08 cm^{-1} may appear due to the ester groups ($\text{C}-\text{O}$ stretch). A peak at 1159.01 cm^{-1} results from alcoholic $\text{C}-\text{O}$ stretch while a distinct peak at 1026.91 cm^{-1} indicates glycosidic $\text{C}-\text{H}$ deformation along with OH bending and ring vibration, signifying the linkage of cellulose and glucose.²⁰⁵⁻²⁰⁷ The prepared NFPS showed characteristic peaks of both the NF and PS with slight shifts as illustrated in figure 4.5.1. which confirmed the successful modification of NFPS composite.

4.5.1.2. X-Ray Diffraction

The X-ray diffraction pattern of NF and NFPS is illustrated in figure 4.5.2. The X-ray diffraction (XRD) spectrum of NF revealed peak diffraction angles at 33.3° , 36.3° , 43.6° , 52.5° , 54.3° , 57.8° and 62.9° . These peaks correspond to the Miller indices (220), (311), (400), (422), (333), (511) and (440) respectively. The lattice exhibited a cubic spinel structure. The material's increased crystallinity and phase purity are indicated by the stated peaks. In contrast, the diffraction peaks of the NFPS composite exhibit a slight displacement in the 2θ angles which verified that the composite exhibited a similar trend to that of the Miller indices of NF. The findings indicated that despite undergoing surface modification; the composite had maintained its crystalline structure.^{90,195} The average size of crystallite calculated by using Scherrer formula (equation 3.1) for pure NF was 32.9 nm whereas the average size obtained for NFPS was 47.4 nm .

4.5.1.3. Field Emission Scanning Electron Microscope

The material's surface morphology was determined using SEM. The SEM images of NF, PS and NFPS composite are presented in figure 4.5.3. The PS exhibit a rugged, flaky surface while the NF showed granular structures with varied particle size and irregular shape. The NFPS composite showed a unique surface morphology characterized by granular structures of NF adhering to the PS surface which confirmed the successful modification of spinel NF with pistachio shell.

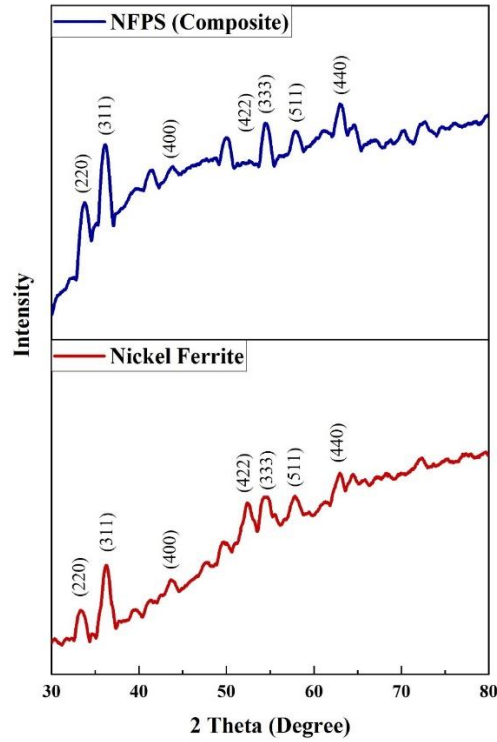


Figure 4.5.2: XRD spectra of nickel ferrite and nickel ferrite pistachio shell composite

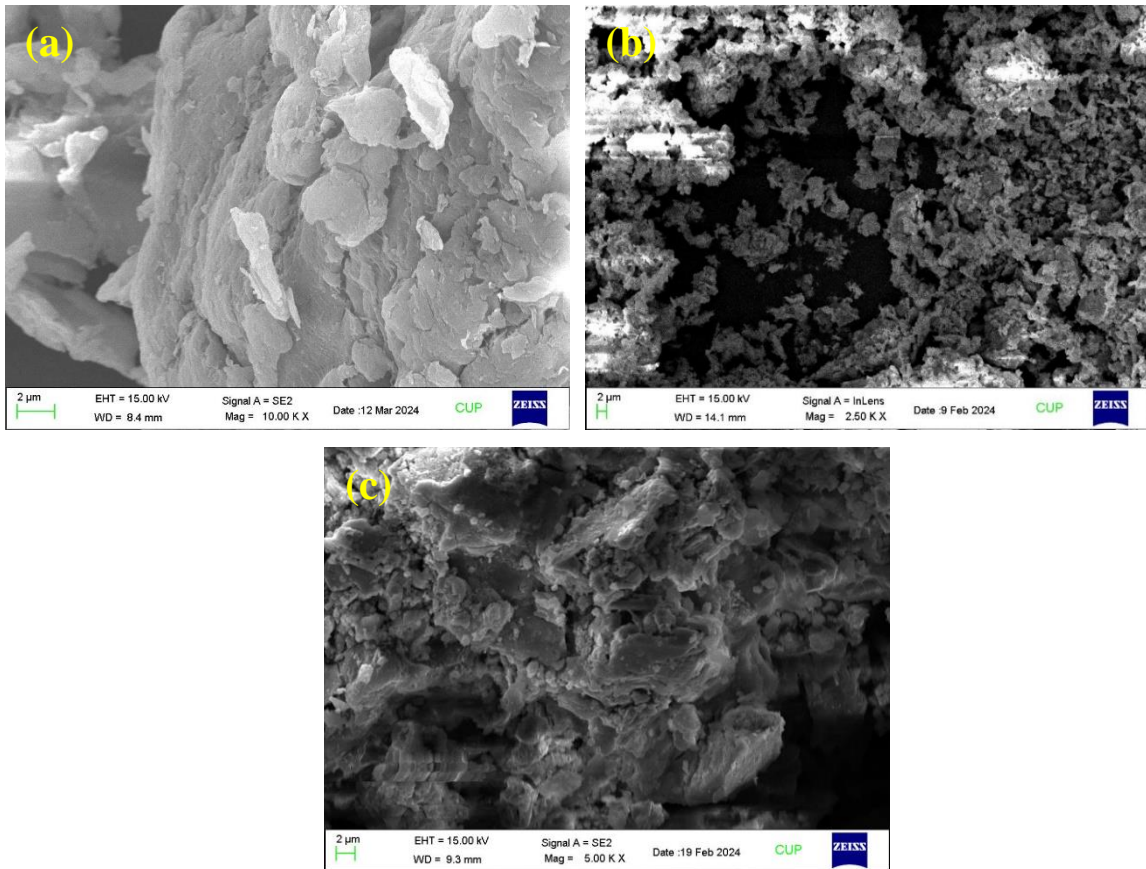


Figure 4.5.3: SEM image (a) Pistachio shell (b) Nickel ferrite (c) Nickel ferrite pistachio shell composite

4.5.1.4. Energy Dispersive Spectra

The Energy Dispersive Spectra of NF and NFPS composite showing peaks corresponding to their constituent elements is illustrated in figure 4.5.4. The weight and atomic percentage of various elemental components present in NF and NFPS are presented in table 4.5.1. Analysis of the element composition reveals a consistent increase in the percentage of carbon in the NFPS composite in comparison to pure NF. This suggests the effective modification of NF with PS resulting in the formation of a magnetic composite.^{42,196}

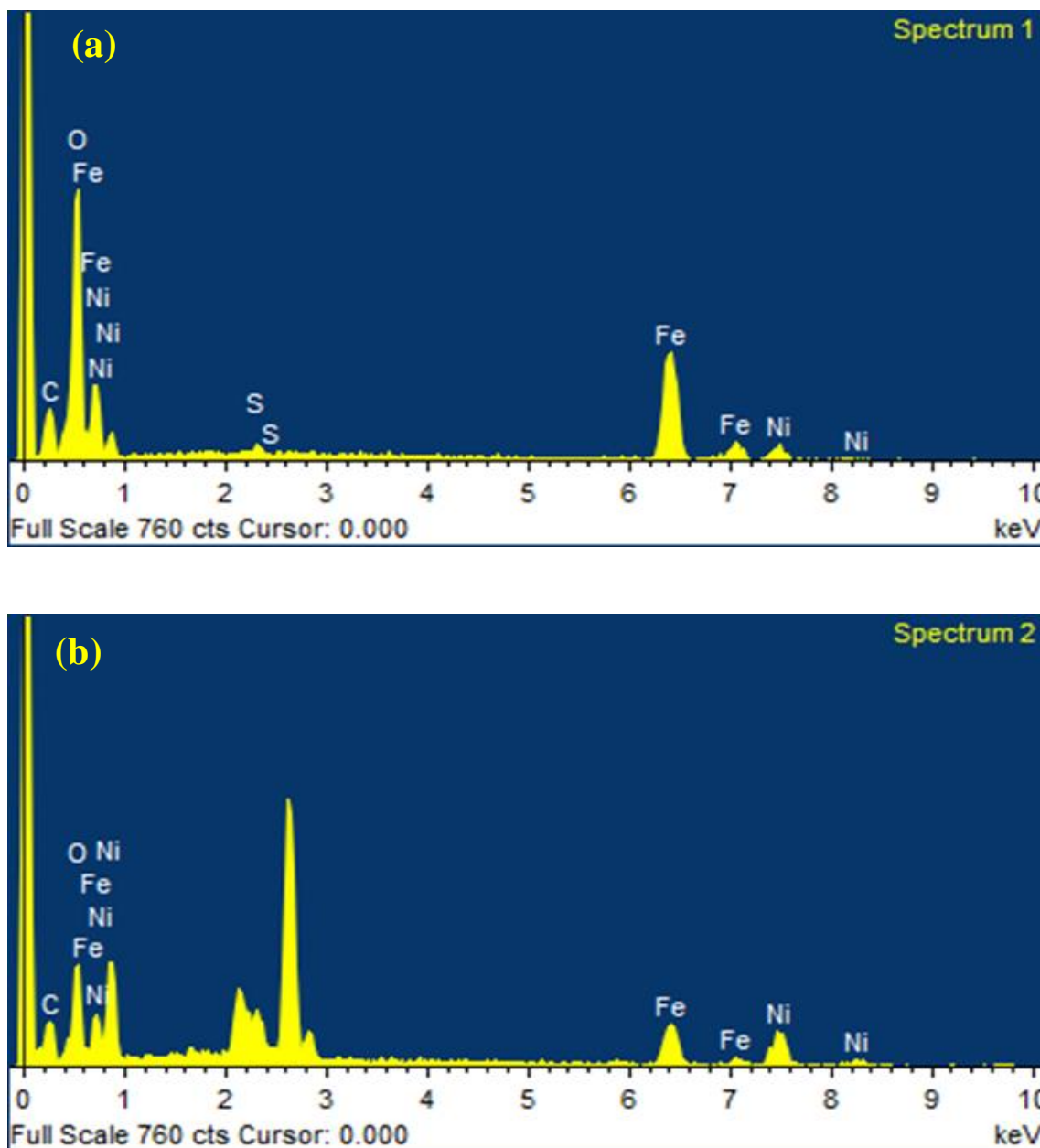


Figure 4.5.4: EDS image (a) Nickel ferrite (b) Nickel ferrite pistachio shell composite

Table 4.5.1: Elemental composition of nickel ferrite and nickel ferrite pistachio shell composite

Element	Nickel ferrite		Nickel Ferrite Pistachio Shell composite	
	Weight %	Atomic %	Weight %	Atomic %
C	10.17	22.23	16.11	37.24
O	27.56	47.34	17.74	30.79
Fe	53.69	26.42	27.83	13.84
Ni	8.58	4.01	38.32	18.13
Total	100.00	100.00	100.00	100.00

4.5.1.5. Thermogravimetric Analysis

For assessing the thermal stability of the prepared NFPS composite, thermogravimetric analysis was conducted at temperature ranging between 30-600°C with 10°C/minute heat transfer rate in the air atmosphere. Figure 4.5.5 illustrates the TGA graph of NFPS.

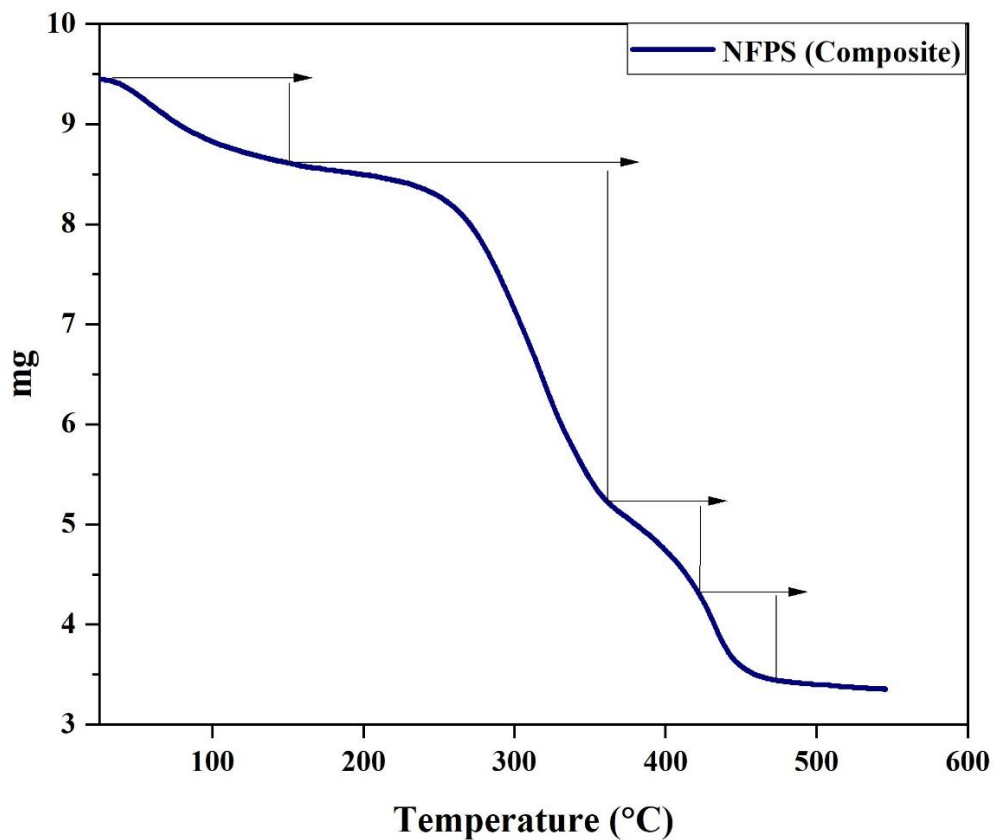


Figure 4.5.5: TGA curve of nickel ferrite pistachio shell composite

Based on the graph, a decrease in weight of around 1.4 mg was observed from temperature 31.4°C to 149.5°C which could be because of moisture evaporation from the sample. Further weight loss of 3.4 mg and 1 mg was observed in the sample from approximately 149.5°C to 359.3°C and 359.3°C to 423.9°C which could be due to the breakdown of organic functional groups present in the sample. As the temperature further increased, a consistent weight loss of approximately 0.9 mg was observed from 423.9°C to 473.1°C, once more in response to the rising temperature which demonstrated that the compound had undergone complete decomposition. As per the aforementioned observation, it was calculated that 0.616 grams of PS has been attached in 1 gram of NFPS composite.^{42,158}

4.5.1.6. pH of Point Zero Charge Analysis

For NFPS composite, the pH_{zpc} was determined using solid addition method. For the experimental procedure, nine Erlenmeyer flasks, each with a volume 250 mL was taken and filled with 50 mL 0.1M KNO_3 solution. The solution's pH was adjusted between pH 3 and 11 using HCl (0.1N) and NaOH (0.1M). Subsequently, 0.1 g of the NFPS composite was added to each conical flask. These flasks were placed in an orbital shaker at 110 rpm for 24 hours. Afterward, the flasks were taken out from shaker and the contents were filtered in different beakers. The final pH of the solution present in each beaker was noted and the calculation was performed using equation 3.2.^{121,155}

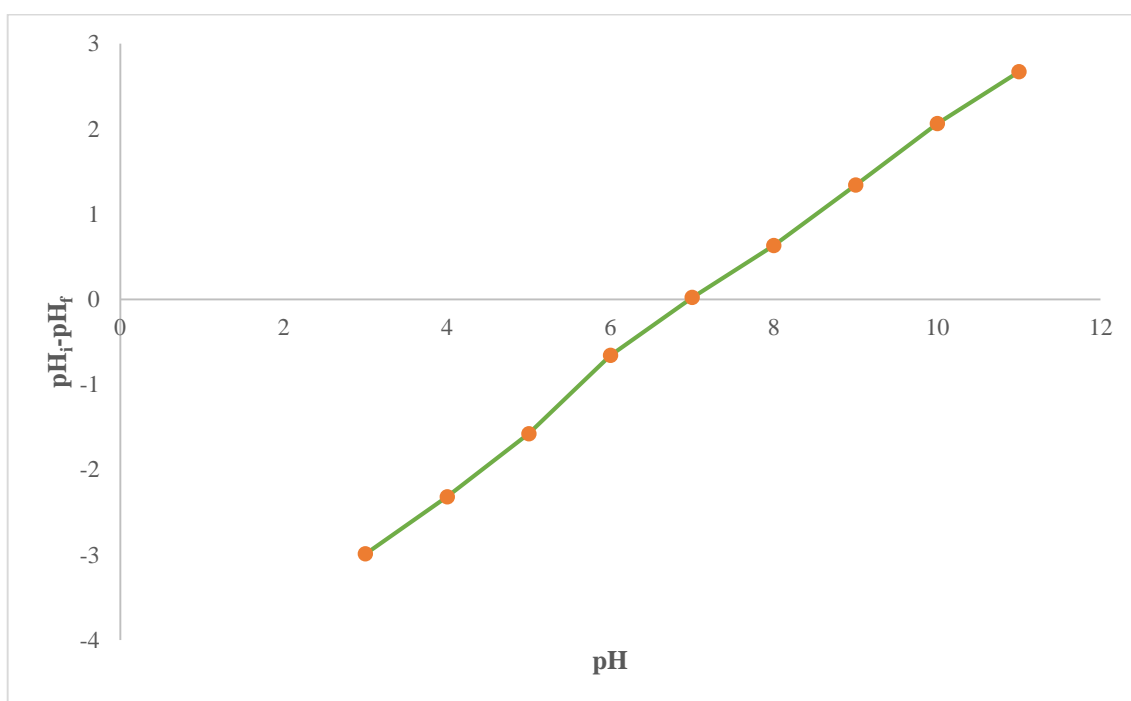


Figure 4.5.6: pH_{zpc} of nickel ferrite pistachio shell composite

By using the above calculated values, the graph for pH_{zpc} was plotted between initial pH (x-axis) and ΔpH (y-axis) which is shown in figure 4.5.6. The calculated pH_{zpc} of NFPS was 6.98 which indicated that at pH 6.98, the electric charge on composite's surface becomes neutral. Consequently, below pH 6.98, the surface of NFPS carries a positive charge, whereas above pH 6.98, it bears a negative charge.

4.5.2. Adsorption Study of Metal Ion

The adsorption behaviour of NFPS composite was studied using Batch adsorption method. The NFPC composite exhibits specific selectivity towards Cu(II) ion as evidenced in pilot scale studies (Chapter-3). The study investigated the effect of adsorption parameters including contact time, pH, adsorbent dosage, concentration of adsorbate and temperature.

4.5.2.1. Effect of Contact Time

For studying the effect of contact time, a known concentration of Cu(II) ion (50 mg/L) and adsorbent dose 0.1 g with an appropriate metal ion solution volume (50 mL) had been poured in Erlenmeyer flask and shaken at 110 rpm. At fixed interval, the flasks were taken out followed by the appropriate procedure given in chapter 3. UV-VIS spectrophotometer (SHIMADZU-1900I) was used to measure residual metal ion concentration. Figure 4.5.7 illustrates the contact time effect on removal of Cu(II) ion.

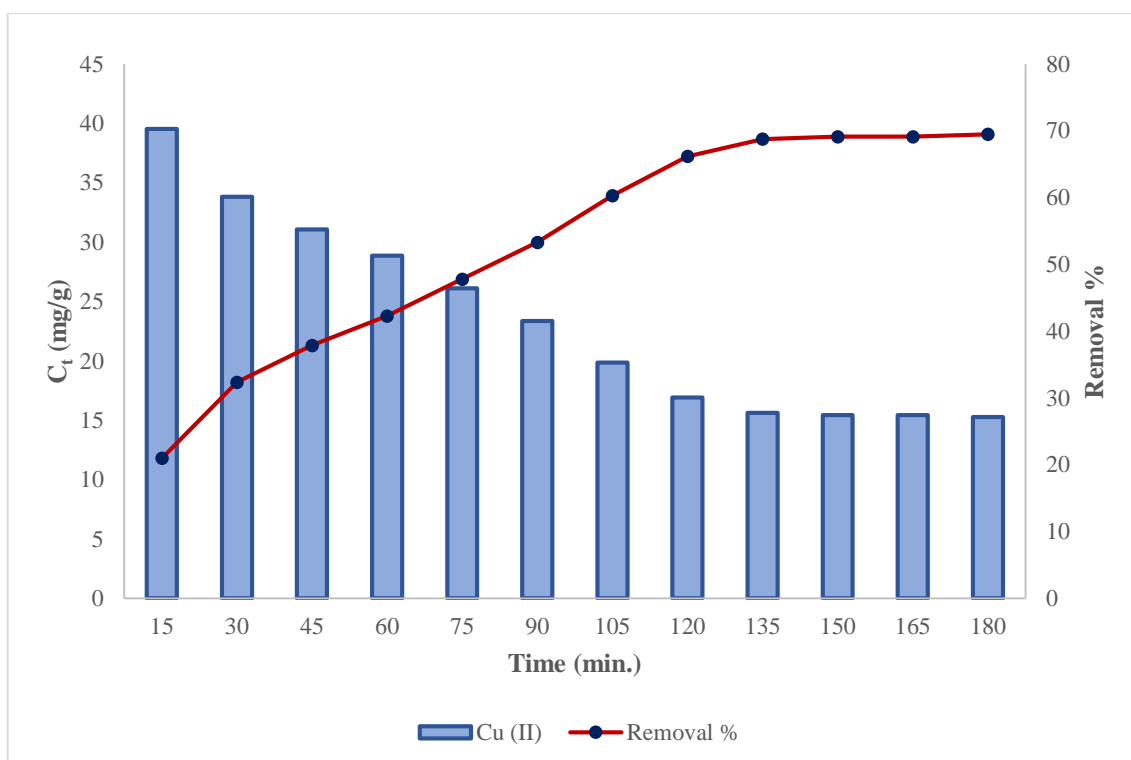


Figure 4.5.7: Effect of contact time for the removal of Cu(II) ions

From the graph, it was found that in initial phase, the removal of metal ion was extremely rapid but as the time increased, rate of adsorption gradually slowed down and eventually, after approximately 150 minutes it flattened out and reached equilibrium. This behavior suggests an abundance of active adsorption sites on NFPS surface in the initial phase, facilitating quick attachment of metal ion molecules to vacant sites. However, over time, these unoccupied sites gradually became occupied, the adsorption rate slowed down and the residual concentration with respect to time became constant which marked the attainment of equilibrium. The equilibrium signifies when the adsorption rate becomes equal to rate of desorption. The maximum removal percentage obtained for Cu(II) ion was 69.4%.

4.5.2.2. Adsorption Kinetics

The kinetic behaviour of NFPS composite with Cu(II) ion was studied using several models including the Lagergren pseudo first-order model, pseudo second-order model, Elovich model and Weber-Morris model. The data of contact time study was graphically represented using kinetic models. Figure 4.5.8 shows the plot of Lagergren pseudo first order and pseudo second order kinetic models for Cu(II) metal ion, while figure 4.5.9 illustrates the plot with respect to Elovich model.

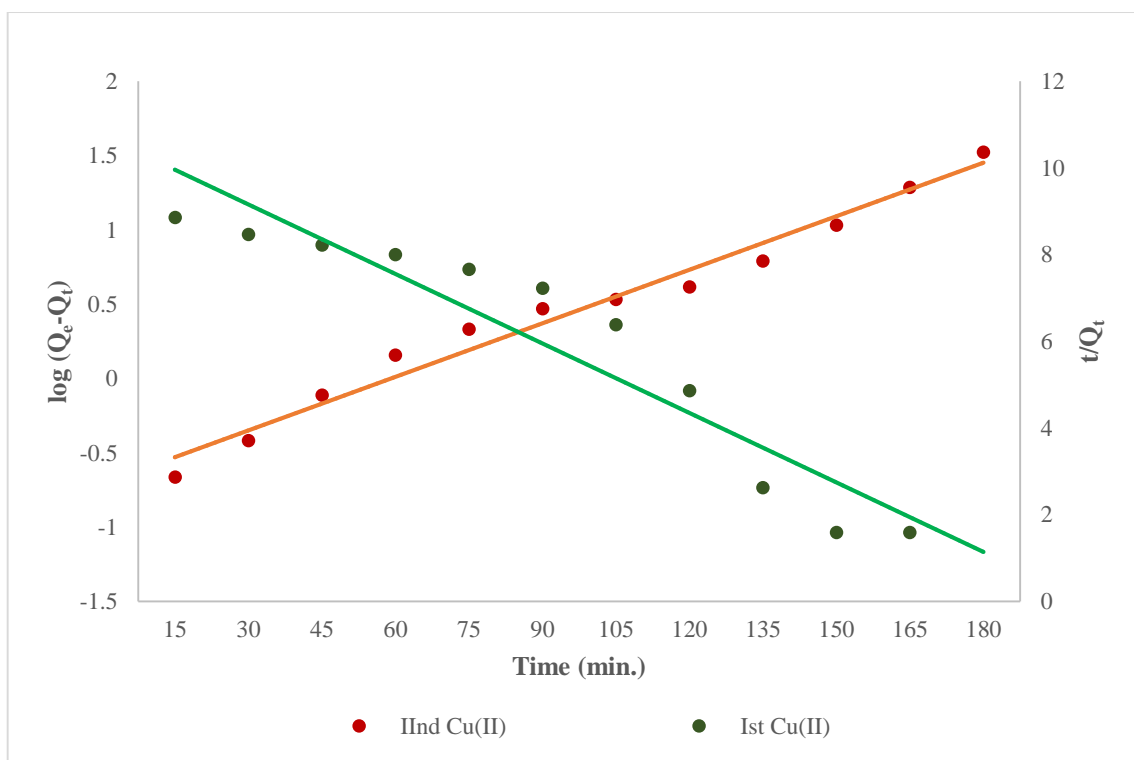


Figure 4.5.8: Lagergren pseudo first order and pseudo second order kinetic model for Cu(II) ions

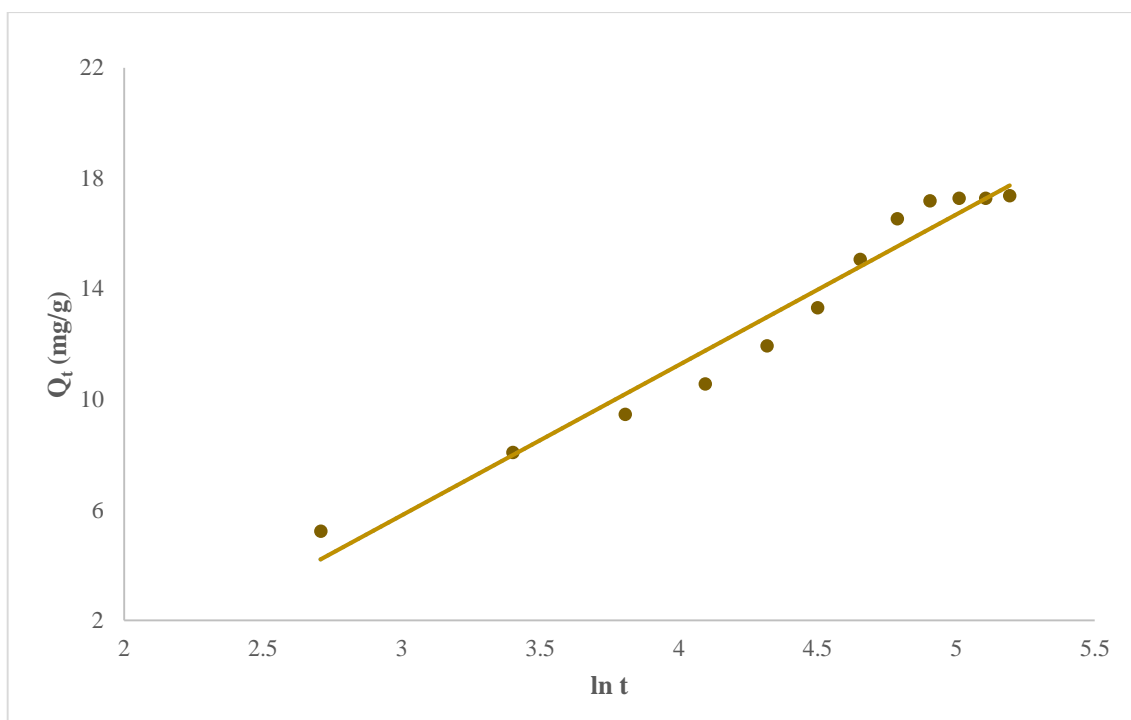


Figure 4.5.9: Elovich model for Cu(II) ions

The calculated values of different kinetic constants are presented in table 4.5.2. The degree of suitability of any model can be assessed by examining the value of regression coefficient (R^2). For this study, the pseudo second order model exhibited the highest R^2 value, followed by the Elovich and the Lagergren pseudo first order model. Hence, the pseudo second order model was determined to be the best fit with experimental data, suggesting the chemical nature of adsorption.⁵⁸

Table 4.5.2: Calculated values of different kinetic constants for Cu(II) ion

KINETIC MODEL	Parameter	Cu(II)
Lagergren Pseudo first order	Q_{e1}	43.531
	K_1	0.538
	R^2	0.893
Pseudo second order	Q_{e2}	1.619
	h	0.368
	k_2	0.140
	R^2	0.976
Elovich model	α	0.787
	β	0.183
	R^2	0.963

The Weber-Morris model of intraparticle diffusion was applied to study the mechanism of adsorption for Cu(II) metal ion using NFPS composite. The plot between Q_t versus $t^{0.5}$ is shown in figure 4.5.10. ' K_{int} ', the intraparticle diffusion rate constant and the rate-limiting step can be calculated from the slope of line if it passes through the origin. However, as indicated in graph, the plot does not show linearity and the line does not pass from the origin. This suggests that apart from intraparticle diffusion, there may be additional factors affecting the rate of adsorption in metal ion system. Moreover, in figure 4.5.10, the initial slope is steep, indicating rapid metal ion adsorption but after a certain period of time, the slope flattened out and reached equilibrium.¹⁹⁶

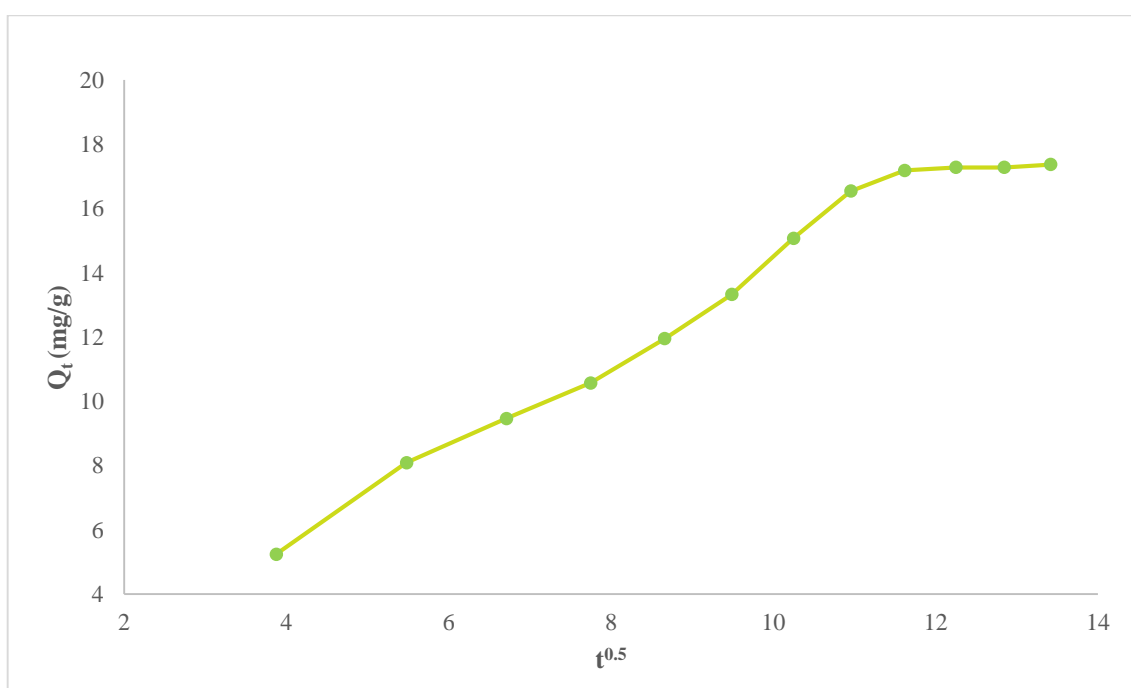


Figure 4.5.10: Weber-Morris model for Cu(II) ions

4.5.2.3. Effect of pH

The solution's pH is crucial in the process of adsorption as it influences the surface charge of material, consequently impacting the affinity between the adsorbate and the adsorbent. The pH effect on the adsorption of Cu(II) ion using NFPS was determined by varying the value of pH from 3-11. Flasks containing the prepared metal ion solution having concentration 50 mg/L and an adsorbent dosage 0.1 g, were placed in an orbital shaker at 25 °C. The effect of pH on removal of Cu(II) ion is illustrated in figure 4.5.11. The graph illustrates that the removal efficiency of Cu(II) ion increased with an increase in pH of the solution, reaching maximum at 7, then further decreased. So, the pH 7 has been determined as the optimal pH for the removal

of Cu(II) ion. As per the results, the maximum percentage of Cu(II) ion removed is 69.85%.^{42,196}

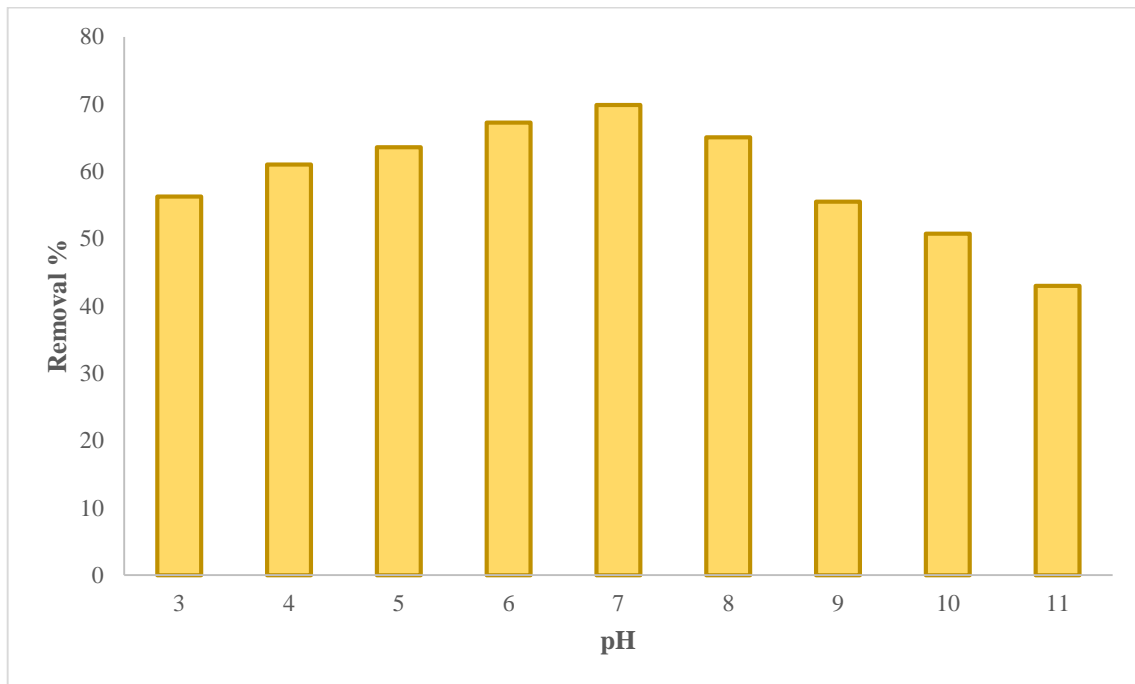


Figure 4.5.11: Effect of pH for the removal of Cu(II) ion

4.5.2.4. Effect of Adsorbent Dosage

The effect of adsorbent dose for Cu(II) ion was studied by varying the dose of NFPS from 0.1 g - 0.5 g and poured in 50 mL Cu(II) ion solution having fixed concentration 50mg/L at a constant temperature. Figure 4.5.12 illustrates the effect of adsorbent dose for the removal of Cu(II) ion from aqueous solution.

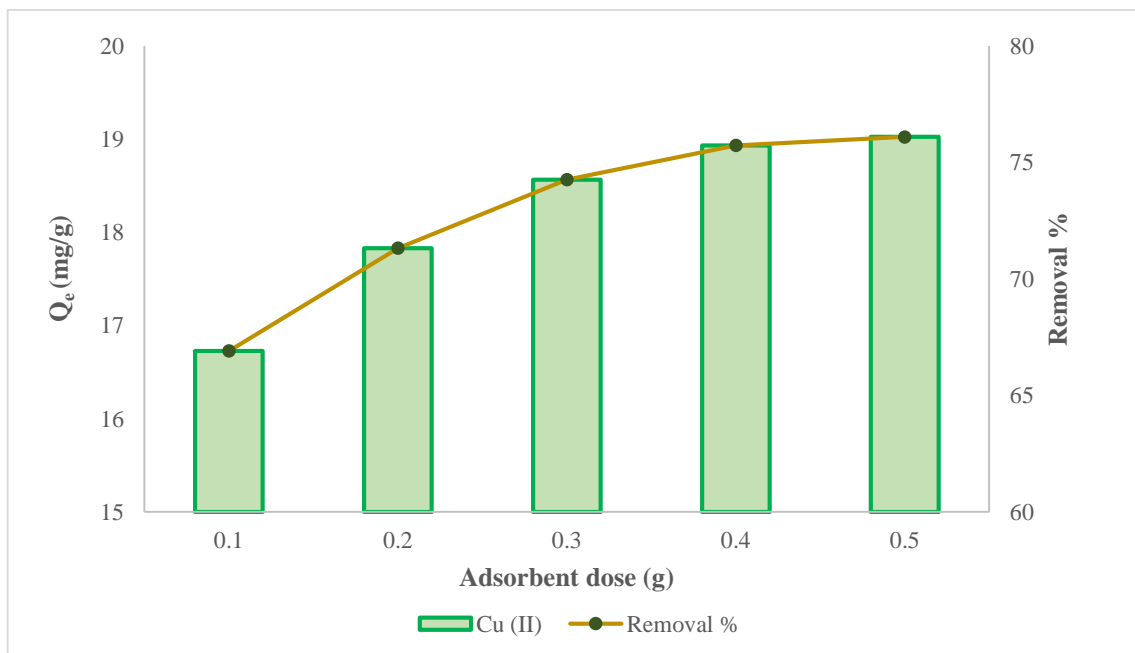


Figure 4.5.12: Effect of adsorbent dosage for the removal of Cu(II) ion

It is evident from the graph that, as the dosage of NFPS composite increased, the percentage removal of metal ion also increased. This trend of increasing metal ion solution was observed due to more vacant sites on the surface of NFPS composite with increasing adsorbent dosage. However, the amount of adsorbate adsorbed per gram of the adsorbent decreased with increasing adsorbent amount. This decrease may be due to the presence of more active sites on the NFPS surface which remained unoccupied when the adsorbent amount was increased.^{42,163}

4.5.2.5. Effect of Concentration and Temperature

The effect of concentration on metal ion removal was studied using initial concentration 50 to 250 mg/L. Additionally, the temperature effect was explored at 25°C, 30°C and 35°C. The effect of initial dye concentration and temperature on the removal of Cu(II) is illustrated in figure 4.5.13. It was seen that as the concentration of metal ion increased, the ‘ Q_e ’ adsorption capacity of the metal ion also increased. This increasing adsorption capacity may occur because the rate of interaction between metal ion molecules and the adsorbent strengthened as the quantity of metal ions increased for a fixed amount of adsorbents, leading to frequent collisions. However, the percentage removal of metal ion decreased as the concentration increased. This trend could be attributed to the constancy of active sites on the adsorbent's surface compared to the increasing concentration of Cu(II) ions. Furthermore, it was noted that with increasing temperature, the adsorption capacity of Cu(II) ion also increased, demonstrating the endothermic adsorption process.¹⁹⁶

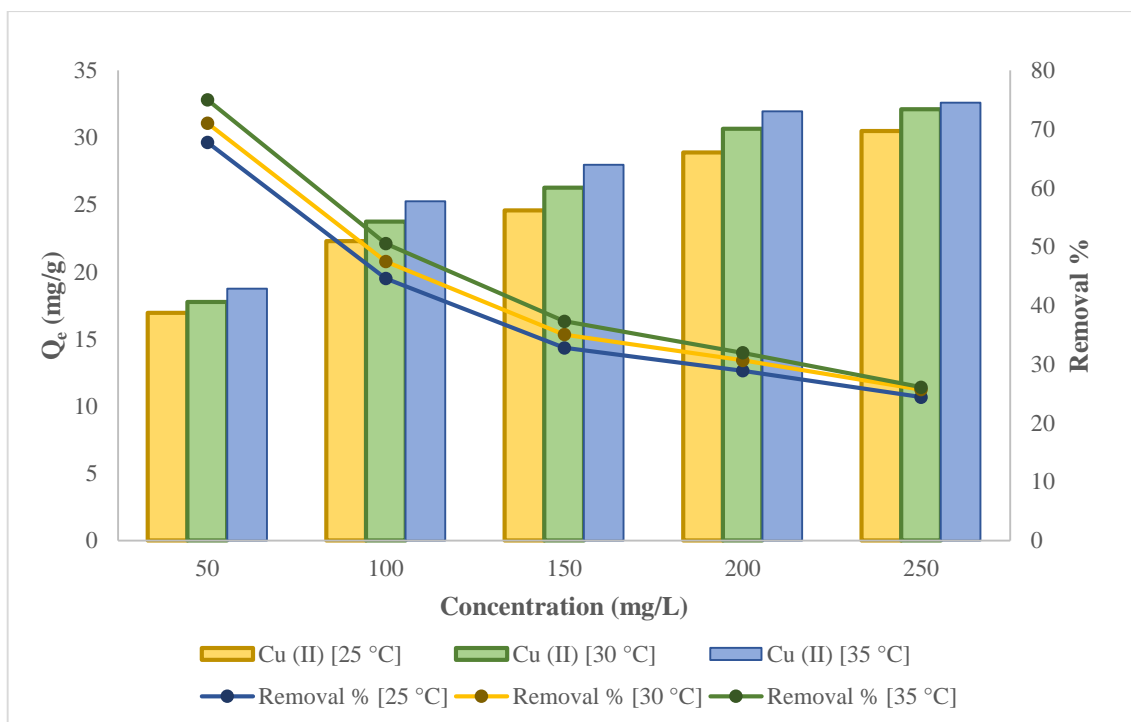


Figure 4.5.13: Effect of concentration for the removal of Cu(II) ion

The observed relationship between temperature and adsorption capacity could be attributed to an increased interaction between the molecules of adsorbate and adsorbent. As the temperature rises, specific pores inside the adsorbent may expand, resulting in a larger surface area for the adsorption of Cu(II) ion. As the temperature increased, the kinetic energy also increased leading to more efficient collisions.

4.5.2.6. Adsorption Isotherms

Adsorption isotherms were employed to study the adsorption behaviour at equilibrium. They depict the distribution pattern of adsorbate molecules between solid and liquid phase under such conditions. The adsorption behaviour of Cu(II) metal ion was examined at three temperatures which were 25°C, 30°C and 35°C by applying several isotherm models such as Langmuir, Freundlich, Temkin and Dubinin-Radushkevich (D-R) model. Figure 4.5.14 (a-d) illustrate the graphs of different adsorption isotherms utilized for removing Cu(II) ions at three distinct temperatures and varying concentrations.

From the plots of different isotherms, the values of different constants were calculated which are presented in table 4.5.3. From the various isotherms, the Freundlich model of isotherm provided the best fit with the experimental data, as evidenced by its highest R^2 (correlation coefficient) value. This implies that the surface of prepared NFPS composite contains non-uniform adsorption sites distributed across its surface and Cu(II) metal ion form multilayer on the surface of adsorbent. The maximum adsorption capacity for Cu(II) metal ion was found to be 32.15 mg/g.

Further, Separation factor ' R_L ' associated with the Langmuir isotherm was studied to describe the nature of adsorption. Table 4.5.3 shows that the calculated R_L values ranged from 0 to 1, indicating that the process of adsorption using NFPS is favourable for adsorption of Cu(II) ion.¹⁵⁸

The adsorption energy 'E' is an additional parameter associated with the D-R isotherm utilized to study the type of adsorption. If the measured value of 'E' is found below 8 kJ/mol, the process is considered physical, otherwise, it is classified as chemical. The calculated 'E' value for Cu(II) ions was found to exceed 100 kJ/mol, as demonstrated in Table 4.5.3, suggesting the chemical nature of adsorption process.¹⁹⁶

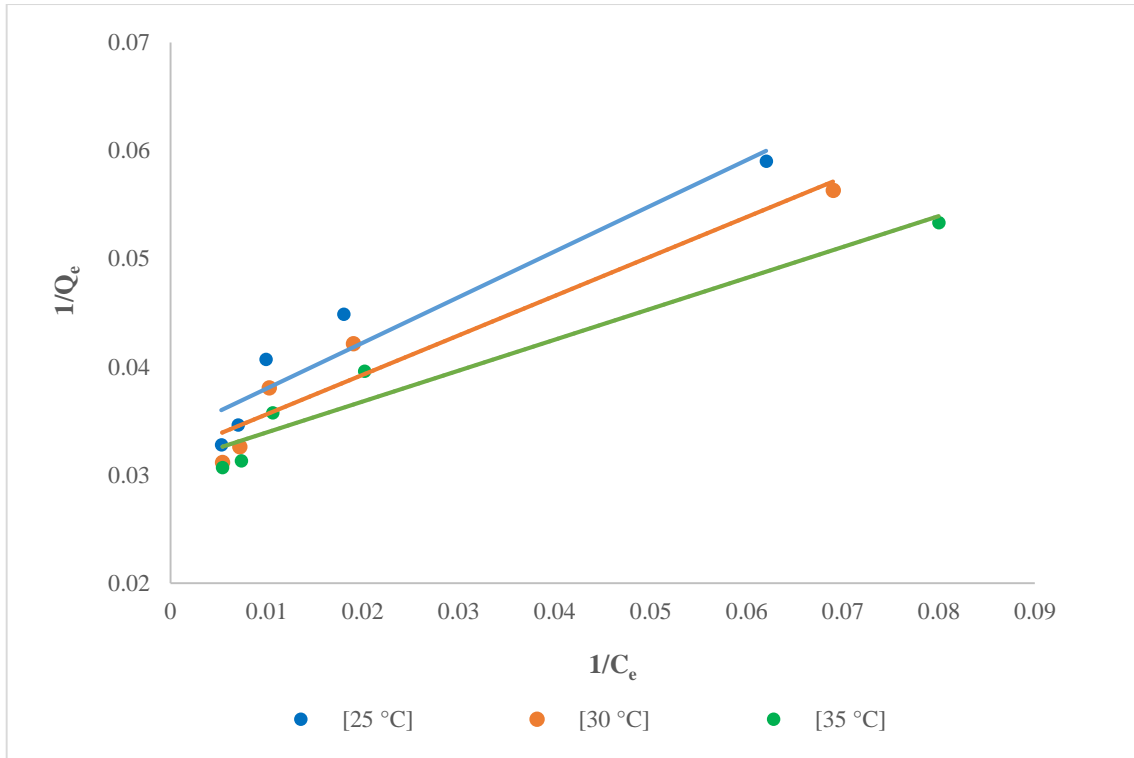


Figure 4.5.14 (a): Langmuir isotherm for the removal of Cu(II) ion

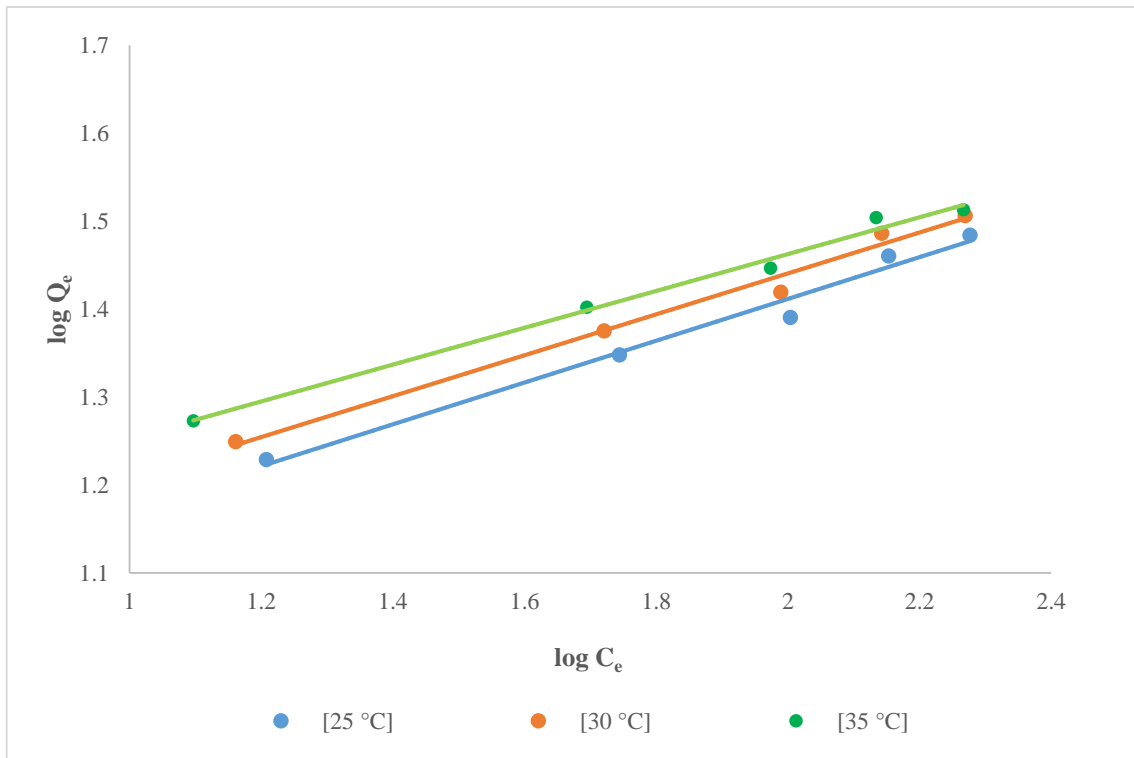


Figure 4.5.14 (b): Freundlich isotherm for the removal of Cu(II) ion

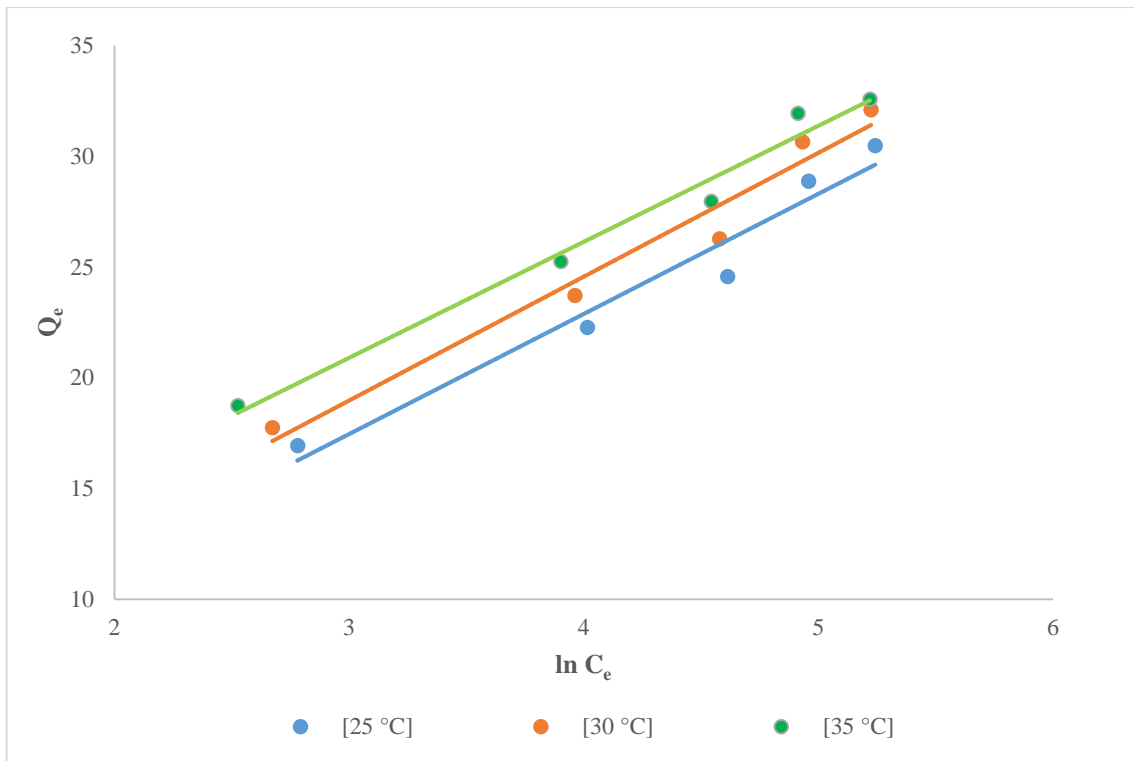


Figure 4.5.14 (c): Temkin isotherm for the removal of Cu(II) ion

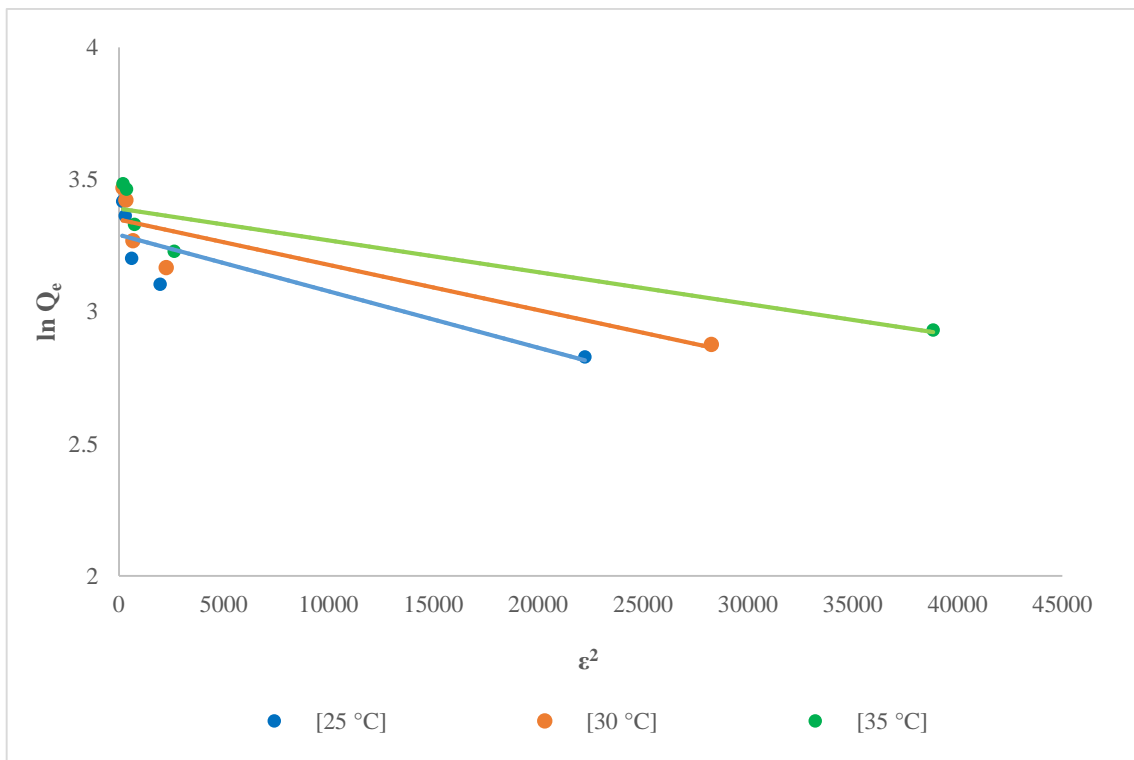


Figure 4.5.14 (d): D-R isotherm for the removal of Cu(II) ion

Table 4.5.3: Calculated values of adsorption isotherm constants for the removal of Cu(II) ion

ISOTHERM MODEL	Parameter	Cu(II)		
		25°C	30°C	35°C
Langmuir	Q_e	29.585	31.25	32.154
	b	0.079	0.087	0.108
	R^2	0.919	0.930	0.947
	R_L	0.202	0.170	0.156
Freundlich	K_f	8.635	9.453	11.058
	$1/n$	0.237	0.232	0.209
	R^2	0.982	0.987	0.991
Temkin	b_T	464.280	450.820	481.330
	A	1.243	1.486	2.704
	R^2	0.957	0.967	0.981
D-R Model	Q_m	26.864	28.477	29.689
	K	2×10^{-5}	2×10^{-5}	1×10^{-5}
	R^2	0.770	0.790	0.828
	E	158.11	158.11	223.61

4.5.2.7. Adsorption Thermodynamics

The adsorption behaviour of Cu(II) ion was studied at 25°C, 30°C and 35°C. It was observed that with increasing temperature, the adsorption of Cu(II) ion increased, indicated the adsorption process was endothermic in nature. The thermodynamic equations related to adsorption process given in section 3.12 of chapter 3 were employed to determine different thermodynamic parameters including change in enthalpy (ΔH°), change in free energy (ΔG°) and change in entropy (ΔS°). The ΔH° and ΔS° values were obtained from the intercept and slope of linear plot of $\ln K_d$ versus $1/T$. Figure 4.5.15 shows the linear graph of adsorption thermodynamics for Cu(II) ion. The various thermodynamic parameters calculated are presented in table 4.5.4.

The calculated values of ΔH° were positive, which confirmed the endothermic nature of adsorption process. Similarly, positive ΔS° values indicated increased randomization on the adsorbent's surface, while the positive ΔG° values indicated the non-spontaneous nature of adsorption process.^{42,76,208}

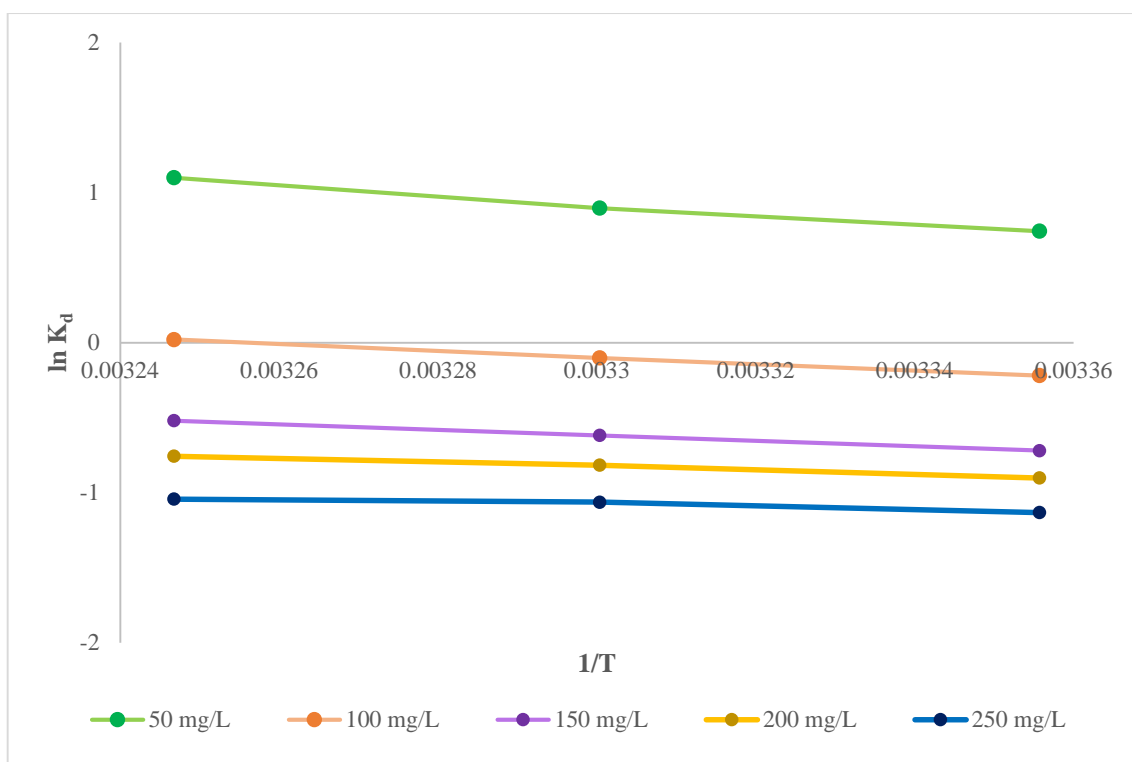


Figure 4.5.15: Adsorption thermodynamic plot for the removal of Cu(II) ion

Table 4.5.4: Calculated values of thermodynamic parameters used for the removal of Cu(II) ion

System	Concentration (mg/L)	ΔH° (KJ/mol)	ΔS° (KJ/mol/K)	ΔG° [25°C] (KJ/mol)	ΔG° [30°C] (KJ/mol)	ΔG° [35°C] (KJ/mol)
Cu(II)	50	27.153	0.097	-1.839	-2.257	-2.813
	100	18.230	0.059	0.541	0.257	-0.052
	150	15.170	0.044	1.780	1.556	1.331
	200	11.040	0.029	2.232	2.056	1.937
	250	6.807	0.013	2.803	2.677	2.669

4.5.3. Regeneration of Adsorbent

The regeneration and reuse of the adsorbent are essential for assessing the stability of the material after adsorption studies. The efficiency of adsorbent after recycling is the primary factor in determining the cost-effectiveness. To regenerate the NFPS composite, HCl (0.1N) was utilized as a desorbing agent. The regenerable efficiency of NFPS was determined up to 5 cycles which is presented in table 4.5.5. The findings suggested that NFPS composite exhibit good reusability and may serve as economic adsorbent for Cu(II) ion removal. After five adsorption-desorption cycles, the regeneration efficiency calculated for Cu(II) ion was 69.2%.

The results suggested that the NFPS composite shows good reusability and serve as a cost effective adsorbent for removing metal ions from aqueous solution.^{42,158}

Table 4.5.5: Regeneration efficiency of nickel ferrite pistachio shell composite for the removal of Cu(II) ion

Regeneration Cycle	Regeneration efficiency (%)
1	93.2
2	86.9
3	81.0
4	75.4
5	69.2

CHAPTER-5

SUMMARY AND CONCLUSION



5.1. Summary and Conclusion

The present research study includes the synthesis of various spinel metal ferrites (ZF, NF, CoF and CuF) and modification of their surface with bio-wastes such as pine-cone, walnut shell and pistachio shell. This modification results in the formation of ZFPC, NFPC, CuFPC, CoFPC, WSZF, WSNF, WSCuF, WSCoF, ZFPS, NFPS, CoFPS and CoFPS (Composite). These materials are being explored for their potential application as adsorbents for removing dyes and Cu(II) metal ion from the aqueous solution. Several analytical techniques including Fourier Transform Infrared (FT-IR) spectroscopy, X-ray diffraction (XRD), Scanning Electron Microscope (SEM), Energy Dispersive Spectra (EDS), Brunauer-Emmett-Teller (BET) analysis, Thermogravimetric Analysis (TGA) and the determination of point zero charge (pH_{pzc}) were used to characterize the different magnetic ferrite composites. The study draws significant conclusions which are outlined below:

- The FTIR spectra of pure metal ferrites exhibit two peaks below 600 cm^{-1} , which confirmed the formation of spinel metal ferrites. Additionally, in the FTIR spectra of metal ferrite bio-waste composites, supplementary peaks are observed, such as a peak at $3400\text{-}3200\text{ cm}^{-1}$ indicating the presence of hydroxyl groups and peaks at $3000\text{-}2850\text{ cm}^{-1}$ correspond to the alkanes etc. These diverse peaks indicated the presence of specific functional groups in various metal ferrite bio-waste composites. Thus, the presence of these peaks confirmed the successful modification of different metal ferrites with bio-wastes like pine cone, walnut shell and pistachio shell.
- The XRD analysis demonstrated that the various metal ferrites exhibit phase purity characterized by a spinel structure. According to calculations using the Scherrer formula, the average crystallite sizes of different metal ferrites and their corresponding bio-waste composites are as follows: 28-40 nm for ZF, 22.4 nm for CoF, 30-36 nm for NF, 54.9 nm for ZFPC, 49.6 nm for NFPC, 38.67 nm for WSZF, 34.7 nm for WSCoF and 47.4 nm for NFPS. The comparison between the XRD patterns of metal ferrite bio-waste composites and pure metal ferrite reveals that the composites maintain their phase purity and spinel character even after surface modification. Moreover, a comparison between the crystallite sizes of pure metal ferrites and their bio-waste based composites indicated an increase in the sizes of the composites, thus confirmed the modification of surface.
- The SEM analysis revealed the difference between the surface of bio-waste, spinel ferrite and the surface of metal ferrite bio-waste composite. The surface morphology

of spinel metal ferrite exhibits a non-uniform shape with granular structure and varied particle size whereas, the bio-wastes have rough surface. The metal ferrite bio-waste composites however, showed an uneven surface with ferrites attached on the surface. These findings provide evidence that the spinel metal ferrite have been successfully modified with bio-wastes.

- The EDS analysis was utilized to describe the elemental composition of pure metal ferrites and their bio-waste based composites. These findings indicated a rise in the carbon percentage in metal ferrite bio-waste composites compared to pure metal ferrites, validating the successful modification of different spinel metal ferrites with pine cone, walnut shell and pistachio shell respectively.
- The thermal stability assessment of various metal ferrite bio-waste composites was conducted through TGA analysis. Results from the TGA studies indicated that the prepared ZFPC, NFPC, WSZF, WSCoF and NFPS exhibited thermal stability up to 600°C. By using TGA analysis, the average quantity of bio-waste attached to the surface of metal ferrites was calculated. The findings revealed that in 1 gram of the respective metal ferrite-bio-waste composite, ZFPC contained 0.420 grams of pine cone, NFPC contained 0.479 grams of pine cone, WSZF contained 0.398 grams of walnut shell, WSCoF contained 0.481 grams of walnut shell and NFPS contained 0.616 grams of pistachio shell.
- BET analysis was studied to ascertain the surface area distribution of different spinel metal ferrites including ZF, NF and CoF yielding values of 0.749, 0.443 and 1.864 m²/g, respectively. The surface areas calculated for ZFPC, NFPC, WSZF and WSCoF were 1.463, 1.823, 3.761 and 3.592 m²/g, respectively. The increase in surface area of the prepared magnetic bio-waste composites provided evidence of bio-waste attachment onto the surface of the different pure metal ferrites. On surface modification, porosity increased at the surface of composite resulting in increased specific surface area.
- The pH of material is said to be at its point of zero charge when the material's surface electric charge density becomes zero. The pH_{zpc} was determined using the solid addition method. The pH_{zpc} of various metal ferrite bio-waste composites such as ZFPC, NFPC, WSZF, WSCoF and NFPS were calculated to be 7.50, 7, 6.1, 5.78 and 6.98 respectively. The pH_{zpc} value signifies that below this, there will be a net positive charge, while above it, there will be a net negative charge on the surface of material.

❖ **Adsorption of dyes and Cu(II) metal ions with metal ferrite bio-waste composites**

- In preliminary studies, it was observed that the ZFPC, NFPC, WSZF and WSCoF composites exhibited notably higher removal rates for CV, BG, MG and MB cationic dyes compared to their pure metal ferrite. In case of metal ions, NFPS demonstrated good efficiency in eliminating Cu(II) ions. Pine cone, walnut shell and pistachio shells contain various reactive functional groups like hydroxyl and carboxylic groups. Upon surface modification, the functional groups adhere to the surfaces of different metal ferrites, serving as active sites for the effective adsorption of cationic dyes and metal ions compared to pure metal ferrites. However, the anionic dye CR, showed almost negligible removal efficiency with metal ferrite bio-waste composites due to the similar anionic charge on the surface of composite and CR dye molecules. This decline indicates the selective nature of different metal ferrite bio-waste composites.
- The adsorption study represents the selective nature of different metal ferrite bio-waste composites for specific dyes and metal ions. The experimental study confirmed that ZFPC composite exhibits highest affinity for removing CV, MG and MB in both single and ternary dye system while the NFPC showed selectivity towards BG and MB dye in both single and binary dye system. Similarly, the WSZF composite demonstrates selectivity towards dye MG and MB in single dye and binary dye system, whereas WSCoF is effective for the removal of CV, BG and MB dyes in single and ternary dye system. The adsorption characteristics of NFPS were examined for Cu(II) ions.
- From the adsorption experiments, it was noticed that various metal ferrite bio-waste composites with different dyes in binary as well as ternary dye systems showed reduced adsorption compared to their respective single dye systems. This decrease in adsorption capacities could be attributed to the antagonistic effect of dyes. Various forces of attraction including electrostatic and π - π interactions, took place among the different dye molecules leading to the formation of stronger bonds in an aqueous solution. Consequently, the removal efficiency of single dye was hindered in binary as well as ternary systems.
- The kinetics studies demonstrated that among various adsorption models including Lagergren pseudo first order, pseudo second order and the Elovich model, the data

obtained from different dyes in single and multi-component systems and Cu(II) ion were most accurately represented by the pseudo second order model. This suggested that the adsorption behavior of different dyes and Cu(II) metal ion followed chemisorption. Moreover, studies using the Weber Morris intraparticle diffusion model revealed that the plots were not linear in single, binary and ternary dye systems which suggested that, apart from intraparticle diffusion, there might be other factors which influence the rate of adsorption in single, binary and ternary dye system.

- The adsorption study of different dyes under different pH conditions revealed that the highest percentage removal occurred at pH 6 and 7, while for Cu(II) ion, the optimal removal was found at pH 7. Moreover, the percent removal of dyes and Cu(II) ion increased with higher dosage of adsorbent in single, binary and ternary system, suggesting an increased availability of active adsorption sites with varying amount of adsorbent. Conversely, the removal percentage of dyes and Cu(II) ion decreased with increasing concentration of adsorbate in both single and multi-component systems, possibly due to the constant number of available active sites present on the adsorbent's surface in comparison to the increasing concentration of dye molecules. Furthermore, the adsorption behavior of dyes (in single, binary, ternary system) and Cu(II) metal ion was examined at varying temperatures i.e.; 25°C, 30°C and 35°C, while maintaining other experimental conditions constant. The removal percentage of dyes and Cu(II) ion using metal ferrite bio-waste composites in different dye system increased with increasing temperature. As temperature increases, certain pores within the adsorbent may enlarge, leading to a greater surface area availability for the adsorption of different dyes and Cu(II) metal ion.
- Adsorption isotherm models including the Langmuir, Freundlich, Temkin and Dubinin-Radushkevich (D-R) model were applied to the data obtained from single, binary and ternary system of dyes and Cu(II) metal ion using ZFPC, NFPC, WSZF, WSCoF and NFPS composites. Among these models, the Langmuir model provided the best fit for all types of dye systems studied in this research whereas, the Freundlich isotherm provided the best fit data with Cu(II) ion. According to the Langmuir assumptions, the different metal ferrite bio-waste composites possess a homogeneous surface with evenly distributed active sites. Adsorption occurs uniformly, forming a monolayer on the surface of composite.

- The adsorption thermodynamic parameters were determined using ZFPC, NFPC, WSZF, WSCoF and NFPS composites for single, binary, ternary dye system and Cu(II) ion. It was found that the calculated values of ΔH° were positive in single as well as multi-component systems which confirmed the endothermic nature of adsorption process for various dyes and Cu(II) metal ion with different metal ferrite bio-waste composites. Similarly, the positive ΔS° values indicated a rise in randomness on the adsorbent's surface. However, the negative ΔG° values calculated for ZFPC, NFPC, WSZF and WSCoF composites in single, binary and ternary dye system suggested that the adsorption behavior was spontaneous. The calculated values of ΔG° obtained for NFPS composite with Cu(II) ion were positive, confirming the non-spontaneity of adsorption process.
- The various metal ferrite bio-waste composites were subjected to recycling for up to five to six cycles in different dye systems and Cu(II) ion. Results from the regeneration studies after consequent cycles revealed that composites maintained a good regeneration efficiency for dyes (single, binary and ternary systems) and Cu(II) ion. The results indicated that the prepared magnetic bio-waste composites exhibit good reusability and can serve as cost-effective adsorbents.

CHAPTER 6

REFERENCES



Reference:

- (1) Ali, K.; Javaid, M. U.; Ali, Z.; Zaghum, M. J. Biomass-Derived Adsorbents for Dye and Heavy Metal Removal from Wastewater. *Adsorpt. Sci. Technol.* **2021**, *2021*, 1–14. <https://doi.org/10.1155/2021/9357509>.
- (2) Punia, P.; Kumar, M.; Chalia, S.; Dhar, R.; Ravelo, B.; Thakur, P.; Thakur, A. Recent Advances in Synthesis , Characterization , and Applications of Nanoparticles for Contaminated Water Treatment- A Review. *Ceram. Int.* **2020**. <https://doi.org/10.1016/j.ceramint.2020.09.050>.
- (3) Bharti, M. K.; Gupta, S.; Chalia, S.; Garg, I.; Thakur, P.; Thakur, A. Potential of Magnetic Nanoferrites in Removal of Heavy Metals from Contaminated Water: Mini Review. *J. Supercond. Nov. Magn.* **2020**, *33* (12), 3651–3665. <https://doi.org/10.1007/s10948-020-05657-1>.
- (4) Kaya, N.; Yıldız, Z.; Ceren, U.; Harun, A. Adsorption of Congo Red from Aqueous Solution onto KOH - Activated Biochar Produced via Pyrolysis of Pine Cone and Modeling of the Process Using Artificial Neural Network. *Biomass Convers. Biorefinery* **2021**. <https://doi.org/10.1007/s13399-021-01856-5>.
- (5) Madhura, L.; Singh, S.; Kanchi, S.; Sabela, M.; Bisetty, K.; Inamuddin. *Nanotechnology-based Water Quality Management for Wastewater Treatment*; Environmental Chemistry Letters, 2019; Vol. 17. <https://doi.org/10.1007/s10311-018-0778-8>.
- (6) Water and Sanitation for All. *Water Sanit. All* **1998**, *24*. <https://doi.org/10.3362/9781780446363>.
- (7) Weststrate, J.; Dijkstra, G.; Eshuis, J.; Gianoli, A. The Sustainable Development Goal on Water and Sanitation : Learning from the Millennium Development Goals. *Soc. Indic. Res.* **2019**, *143* (2), 795–810. <https://doi.org/10.1007/s11205-018-1965-5>.
- (8) Milan, B. F. Clean Water and Sanitation for All: Interactions with Other Sustainable Development Goals. *Sustain. Water Resour. Manag.* **2017**. <https://doi.org/10.1007/s40899-017-0117-4>.
- (9) Darwesh, O. M.; El-Latief, A. H. A.; Abuarab, M. E.; Kasem, M. A. Enhancing the Efficiency of Some Agricultural Wastes as Low-Cost Absorbents to Remove Textile

- Dyes from Their Contaminated Solutions. *Biomass Convers. Biorefinery* **2021**.
<https://doi.org/10.1007/s13399-020-01142-w>.
- (10) Yusuf, A.; Al, S.; Garlisi, C.; Palmisano, G. A Review of Recent and Emerging Antimicrobial Nanomaterials in Wastewater Treatment Applications. *Chemosphere* **2021**, 278 (130440), 1–20. <https://doi.org/10.1016/j.chemosphere.2021.130440>.
- (11) Zulu, C. B.; Onyango, M. S.; Ren, J.; Lwesifi, T. Y. Modified Pine Cone for Dye Pollutants Removal from Aqueous. *Proc. Sustain. Res. Innov. Conf.* **2017**.
- (12) Varma, S.; Sarode, D.; Wakale, S.; Bhanvase, B. a; Deosarkar, M. P. Removal of Nickel from Waste Water Using Graphene Nanocomposite. *Int. J. Chem. Phys. Sci.* **2013**, 2, 132–139.
- (13) P. S. Kumar, G. J. Joshiba, C. C. Femina, P. Varshini, S. Priyadharshini, M.S. Arun Karthick, R. J. A Critical Review on Recent Developments in the Low-Cost Adsorption of Dyes from Wastewater. *Desalin. Water Treat.* **2019**, 172, 395–416. <https://doi.org/10.5004/dwt.2019.24613>.
- (14) Ziajahromi, S.; Neale, P. A.; Rintoul, L.; Leusch, F. D. L. Wastewater Treatment Plants as a Pathway for Microplastics: Development of a New Approach to Sample Wastewater-Based Microplastics. *Water Res.* **2017**, 112, 1–29. <https://doi.org/10.1016/j.watres.2017.01.042>.
- (15) Tripathi, A.; Rawat Ranjan, M. Heavy Metal Removal from Wastewater Using Low Cost Adsorbents. *J. Bioremediation Biodegrad.* **2015**, 06 (06), 1–5. <https://doi.org/10.4172/2155-6199.1000315>.
- (16) Kesari, K. K.; Soni, R.; Mohammad, Q.; Tripathi, P.; Lal, J. A.; Kumar, N.; Siddiqui, M. H.; Kumar, P.; Tripathi, V.; Ruokolainen, J. Wastewater Treatment and Reuse: A Review of Its Applications and Health Implications. *Water Air Soil Pollut.* **2021**, 232 (208), 1–28. <https://doi.org/10.1007/s11270-021-05154-8>.
- (17) Rashid, R.; Shafiq, I.; Akhter, P.; Iqbal, M. J.; Hussain, M. A State-of-the-Art Review on Wastewater Treatment Techniques: The Effectiveness of Adsorption Method. *Environ. Sci. Pollut. Res.* **2021**, 28 (8), 9050–9066. <https://doi.org/10.1007/s11356-021-12395-x>.
- (18) Singh, S.; Wasewar, K. L.; Kansal, S. K. *Low-Cost Adsorbents for Removal of Inorganic*

- Impurities from Wastewater; Inorganic Pollutants in Water*, 2020. <https://doi.org/10.1016/b978-0-12-818965-8.00010-x>.
- (19) Zaim, M.; Zaimee, A.; Sarjadi, M. S. Heavy Metals Removal from Water by Efficient Adsorbents. *Water* **2021**, *13* (2659), 1–22. <https://doi.org/10.3390/w13192659>.
- (20) Zhang, Y.; Wang, Y.; Zhang, Z.; Cui, W.; Zhang, X.; Wang, S. Removing Copper and Cadmium from Water and Sediment by Magnetic Microspheres - MnFe₂O₄/Chitosan Prepared by Waste Shrimp Shells. *J. Environ. Chem. Eng.* **2021**, *9* (1), 104647. <https://doi.org/10.1016/j.jece.2020.104647>.
- (21) Katheresan, V.; Kansedo, J.; Lau, S. Y. Efficiency of Various Recent Wastewater Dye Removal Methods: A Review. *J. Environ. Chem. Eng.* **2018**, *6* (4), 4676–4697. <https://doi.org/10.1016/j.jece.2018.06.060>.
- (22) Velusamy, S.; Roy, A.; Sundaram, S.; Kumar Mallick, T. A Review on Heavy Metal Ions and Containing Dyes Removal Through Graphene Oxide-Based Adsorption Strategies for Textile Wastewater Treatment. *Chem. Rec.* **2021**, *21* (7), 1570–1610. <https://doi.org/10.1002/tcr.202000153>.
- (23) Madima, N.; Mishra, S. B.; Inamuddin, I.; Mishra, A. K. Carbon-Based Nanomaterials for Remediation of Organic and Inorganic Pollutants from Wastewater. A Review. *Environ. Chem. Lett.* **2020**, *18* (4), 1169–1191. <https://doi.org/10.1007/s10311-020-01001-0>.
- (24) Liang, L.; Xi, F.; Tan, W.; Meng, X.; Hu, B.; Wang, X. Review of Organic and Inorganic Pollutants Removal by Biochar and Biochar-Based Composites. *Biochar* **2021**, *3* (3), 255–281. <https://doi.org/10.1007/s42773-021-00101-6>.
- (25) Baruah, S.; Najam Khan, M.; Dutta, J. Perspectives and Applications of Nanotechnology in Water Treatment. *Environ. Chem. Lett.* **2016**, *14* (1), 1–14. <https://doi.org/10.1007/s10311-015-0542-2>.
- (26) Abolhassan, S.; Vossoughi, M.; Mohammad, N. Clay-Based Electrospun Nano Fibrous Membranes for Colored Wastewater Treatment. *Appl. Clay Sci.* **2019**, *168*, 77–86. <https://doi.org/10.1016/j.clay.2018.11.003>.
- (27) Jayalakshmi, R.; Jeyanthi, J.; Aswin Sidhaarth, K. R. Versatile Application of Cobalt Ferrite Nanoparticles for the Removal of Heavy Metals and Dyes from Aqueous

- Solution. *Environ. Nanotechnology, Monit. Manag.* **2022**, *17*, 100659. <https://doi.org/10.1016/j.enmm.2022.100659>.
- (28) Saleem, F.; Khan, A.; Mujawar, N.; Hua, Y. A Comprehensive Review on Magnetic Carbon Nanotubes and Carbon Nanotube-Based Buckypaper for Removal of Heavy Metals and Dyes. *J. Hazard. Mater.* **2021**, *413*, 1–32. <https://doi.org/10.1016/j.jhazmat.2021.125375>.
- (29) Zhao, X.; Baharinikoo, L.; Farahani, M. D.; Mahdizadeh, B.; Farizhandi, A. A. Experimental Modelling Studies on the Removal of Dyes and Heavy Metal Ions Using ZnFe₂O₄ Nanoparticles. *Sci. Rep.* **2022**, *12* (5987), 1–15. <https://doi.org/10.1038/s41598-022-10036-y>.
- (30) Afroze, S.; Sen, T. K. A Review on Heavy Metal Ions and Dye Adsorption from Water by Agricultural Solid Waste Adsorbents. *Water Air Soil Pollut.* **2018**, *229* (225), 1–50. <https://doi.org/10.1007/s11270-018-3869-z>.
- (31) Kavci, E. Malachite Green Adsorption onto Modified Pine Cone : Isotherms , Kinetics and Thermodynamics Mechanism. *Chem. Eng. Commun.* **2020**, 1–10. <https://doi.org/10.1080/00986445.2020.1715961>.
- (32) Mekuria, D.; Diro, A.; Melak, F.; Asere, T. G. Adsorptive Removal of Methylene Blue Dye Using Biowaste Materials: Barley Bran and Enset Midrib Leaf. *J. Chem.* **2022**, *2022*, 1–13. <https://doi.org/10.1155/2022/4849758>.
- (33) Alhogbi, B. G.; Altayeb, S.; Bahaidarah, E. A.; Zawrah, M. Removal of Anionic and Cationic Dyes from Wastewater Using Activated Carbon from Palm Tree Fiber Waste. *processes* **2021**, *9* (416), 1–20. <https://doi.org/10.3390/pr9030416>.
- (34) Kant, R. Textile Dyeing Industry an Environmental Hazard. *Nat. Sci.* **2012**, *04* (01), 22–26. <https://doi.org/10.4236/ns.2012.41004>.
- (35) Bharathi, K. .; Ramesh, S. . Removal of Dyes Using Agricultural Waste as Low-Cost Adsorbents : A Review. *Appl. Water Sci.* **2013**, *3*, 773–790. <https://doi.org/10.1007/s13201-013-0117-y>.
- (36) Al-Tohamy, R.; Ali, S. S.; Li, F.; Okasha, K. M.; Mahmoud, A. G.; Elsamahy, T.; Jiao, H.; Fu, Y.; Sun, J. A Critical Review on the Treatment of Dye-Containing Wastewater: Ecotoxicological and Health Concerns of Textile Dyes and Possible Remediation

- Approaches for Environmental Safety. *Ecotoxicol. Environ. Saf.* **2022**, *231* (113160), 1–17. <https://doi.org/10.1016/j.ecoenv.2021.113160>.
- (37) Attallah, M. F.; Ahmed, I. M.; Hamed, M. M. Treatment of Industrial Wastewater Containing Congo Red and Naphthol Green B Using Low-Cost Adsorbent. *Environ. Sci. Pollut. Res.* **2013**, *20*, 1106–1116. <https://doi.org/10.1007/s11356-012-0947-4>.
- (38) Ferdous, M.; Khandaker, S.; Sarker, F.; Islam, A.; Tamzid, M.; Rabiul, M. Current Treatment Technologies and Mechanisms for Removal of Indigo Carmine Dyes from Wastewater: A Review. *J. Mol. Liq.* **2020**, *318* (114061), 1–20. <https://doi.org/10.1016/j.molliq.2020.114061>.
- (39) Azimi, A.; Azari, A.; Rezakazemi, M.; Ansarpour, M. Removal of Heavy Metals from Industrial Wastewaters: A Review. *ChemBioEng Rev.* **2017**, *4* (1), 37–59. <https://doi.org/10.1002/cben.201600010>.
- (40) Renu; Agarwal, M.; Singh, K. Heavy Metal Removal from Wastewater Using Various Adsorbents: A Review. *J. Water Reuse Desalin.* **2017**, *7* (4), 387–419. <https://doi.org/10.2166/wrd.2016.104>.
- (41) Arora, R. Adsorption of Heavy Metals-a Review. *Mater. Today Proc.* **2019**, *18* (1), 4745–4750. <https://doi.org/10.1016/j.matpr.2019.07.462>.
- (42) Kumar, M.; Dosanjh, H. S.; Singh, H. Removal of Lead and Copper Metal Ions in Single and Binary Systems Using Biopolymer Modified Spinel Ferrite. *J. Environ. Chem. Eng.* **2018**, *6* (5), 6194–6206. <https://doi.org/10.1016/j.jece.2018.09.054>.
- (43) Naushad, M.; Alqadami, A. A.; Al-kehtani, A. A.; Ahamad, T.; Awual, R.; Tatarchuk, T. Adsorption of Textile Dye Using Para-Aminobenzoic Acid Modified Activated Carbon: Kinetic and Equilibrium Studies. *J. Mol. Liq.* **2019**. <https://doi.org/10.1016/j.molliq.2019.112075>.
- (44) Tamjidi, S.; Esmaili, H.; Kamyab Moghadas, B. Application of Magnetic Adsorbents for Removal of Heavy Metals from Wastewater: A Review Study. *Mater. Res. Express* **2019**, *6* (102004), 1–17. <https://doi.org/10.1088/2053-1591/ab3ffb>.
- (45) Qasem, N. A. A.; Mohammed, R. H.; Lawal, D. U. Removal of Heavy Metal Ions from Wastewater: A Comprehensive and Critical Review. *npj Clean Water* **2021**, *4* (1), 1–15. <https://doi.org/10.1038/s41545-021-00127-0>.

- (46) Zaim, M.; Zaimee, A.; Sarjadi, M. S. Heavy Metals Removal from Water by Efficient Adsorbents. *Water* **2021**, *13* (2659), 1–22. <https://doi.org/10.3390/w13192659>.
- (47) Segovia-Sandoval, S. J.; Ocampo-Pérez, R.; Berber-Mendoza, M. S.; Leyva-Ramos, R.; Jacobo-Azuara, A.; Medellín-Castillo. Walnut Shell Treated with Citric Acid and Its Application as Biosorbent in the Removal of Zn(II). *J. Water Process Eng.* **2018**, *25*, 45–53. <https://doi.org/10.1016/j.jwpe.2018.06.007>.
- (48) Younas, F.; Mustafa, A.; Farooqi, R.; Wang, X.; Younas, S.; Mohy-ud-din, W.; Hameed, M. A.; Abrar, M. M.; Maitlo, A. A.; Noreen, S.; Hussain, M. M. Current and Emerging Adsorbent Technologies for Wastewater Treatment: Trends, Limitations, and Environmental Implications. *Water* **2021**, *13* (215), 1–25. <https://doi.org/10.3390/w13020215>.
- (49) Crini, G.; Lichtfouse, E. Advantages and Disadvantages of Techniques Used for Wastewater Treatment. *Environ. Chem. Lett.* **2019**, *17* (1), 145–155. <https://doi.org/10.1007/s10311-018-0785-9>.
- (50) Crini, G.; Lichtfouse, E.; Wilson, L. D.; Morin-Crini, N. Conventional and Non-Conventional Adsorbents for Wastewater Treatment. *Environ. Chem. Lett.* **2019**, *17* (1), 195–213. <https://doi.org/10.1007/s10311-018-0786-8>.
- (51) Odoemelam, S. A.; Emeh, U. N.; Eddy, N. O. Experimental and Computational Chemistry Studies on the Removal of Methylene Blue and Malachite Green Dyes from Aqueous Solution by Neem (*Azadirachta Indica*) Leaves. *J. Taibah Univ. Sci.* **2018**, *12* (3), 255–265. <https://doi.org/10.1080/16583655.2018.1465725>.
- (52) Ida, S.; Eva, T. Removal of Heavy Metals during Primary Treatment of Municipal Wastewater and Possibilities of Enhanced Removal : A Review. *Water* **2021**, *13* (1121), 1–26. <https://doi.org/10.3390/w13081121> Academic.
- (53) Okoro, H. K.; Pandey, S.; Ogunkunle, C. O.; Ngila, C. J.; Zvinowanda, C.; Jimoh, I.; Lawal, I. A.; Orosun, M. M.; George, A. Nanomaterial-Based Biosorbents : Adsorbent for Efficient Removal of Selected Organic Pollutants from Industrial Wastewater. *Emerg. Contam.* **2022**, *8*, 46–58. <https://doi.org/10.1016/j.emcon.2021.12.005>.
- (54) Wang, X.; Jiang, J.; Gao, W. Reviewing Textile Wastewater Produced by Industries: Characteristics , Environmental Impacts , and Treatment Strategies. *Water Sci. Eng.*

- 2022**, 85 (7), 2076–2096. <https://doi.org/10.2166/wst.2022.088>.
- (55) Sukmana, H.; Bellahsen, N.; Pantoja, F.; Hodur, C. Adsorption and Coagulation in Wastewater Treatment – Review. *Prog. Agric. Eng. Sci.* **2021**, 17 (1), 49–68. <https://doi.org/10.1556/446.2021.00029>.
- (56) Xu, W.; Yang, T.; Liu, S.; Du, L.; Chen, Q.; Li, X.; Dong, J. Insights into the Synthesis, Types and Application of Iron Nanoparticles : The Overlooked Significance of Environmental Effects. *Environ. Int.* **2022**, 158, 1–24. <https://doi.org/10.1016/j.envint.2021.106980>.
- (57) Mpongwana, N.; Rathilal, S. A Review of the Techno-Economic Feasibility of Nanoparticle Application for Wastewater Treatment. *Water* **2022**, 14 (1550), 1–19. <https://doi.org/10.3390/w14101550>.
- (58) Kumar, M.; Singh, H.; Harminder, D. Magnetic Zinc Ferrite – Chitosan Bio-Composite : Synthesis , Characterization and Adsorption Behavior Studies for Cationic Dyes in Single and Binary Systems. *J. Inorg. Organomet. Polym. Mater.* **2018**, 28 (3), 880–898. <https://doi.org/10.1007/s10904-017-0752-0>.
- (59) Kumar, M.; Singh Dosanjh, H.; Sonika; Singh, J.; Monir, K.; Singh, H. Review on Magnetic Nanoferrites and Their Composites as Alternatives in Waste Water Treatment: Synthesis, Modifications and Applications. *Environ. Sci. Water Res. Technol.* **2020**, 6 (3), 491–514. <https://doi.org/10.1039/c9ew00858f>.
- (60) Albatrni, H.; Qiblawey, H.; Al-marri, M. J. Walnut Shell Based Adsorbents : A Review Study on Preparation , Mechanism , and Application. *J. Water Process Eng.* **2022**, 45, 1–19. <https://doi.org/10.1016/j.jwpe.2021.102527>.
- (61) Singh, N. B.; Nagpal, G.; Agrawal, S. Water Purification by Using Adsorbents : A Review. *Environ. Technol. Innov.* **2018**, 11, 187–240. <https://doi.org/10.1016/j.eti.2018.05.006>.
- (62) Gregorio, C. Non-Conventional Low-Cost Adsorbents for Dye Removal : A Review. *Bioresour. Technol.* **2006**, 97 (9), 1061–1085. <https://doi.org/10.1016/j.biortech.2005.05.001>.
- (63) Almeida-Naranjo, C. E.; Guerrero, V. H.; Villamar-Ayala, C. A. Emerging Contaminants and Their Removal from Aqueous Media Using Conventional / Non-

- Conventional Adsorbents : A Glance at the Relationship between Materials , Processes ,. *Water* **2023**, *15* (8). <https://doi.org/10.3390/w15081626>.
- (64) Amit, B.; Minocha, A. K. Conventional and Non-Conventional Adsorbents for Removal of Pollutants from Water – A Review. *Indian J. Chem. Technol.* **2006**, *13*, 203–217.
- (65) Vidu, R.; Matei, E.; Predescu, A. M.; Alhalaili, B.; Cristian, P.; Claudia, T.; Cristian, P. Removal of Heavy Metals from Wastewaters : A Challenge from Current Treatment Methods to Nanotechnology Applications. *Toxics* **2020**, *8* (101), 1–37. <https://doi.org/10.3390/toxics8040101>.
- (66) Tan, K. B.; Vakili, M.; Horri, B. A.; Poh, P. E.; Abdullah, A. Z.; Salamatinia, B. Adsorption of Dyes by Nanomaterials: Recent Developments and Adsorption Mechanisms. *Sep. Purif. Technol.* **2015**, *150*, 229–242. <https://doi.org/10.1016/j.seppur.2015.07.009>.
- (67) Yaqoob, A. A.; Parveen, T.; Umar, K.; Nasir, M. Role of Nanomaterials in the Treatment of Wastewater: A Review. *Water* **2020**, *12* (495), 1–30. <https://doi.org/10.3390/w12020495>.
- (68) Wong, J. K. H.; Tan, H. K.; Lau, S. Y.; Yap, P. S.; Danquah, M. K. Potential and Challenges of Enzyme Incorporated Nanotechnology in Dye Wastewater Treatment: A Review. *J. Environ. Chem. Eng.* **2019**, *7* (4), 103261. <https://doi.org/10.1016/j.jece.2019.103261>.
- (69) Mohmood, I.; Lopes, C. B.; Lopes, I. Nanoscale Materials and Their Use in Water Contaminants Removal - A Review. *Environ. Sci. Pollut. Res.* **2013**, *20*, 1239–1260. <https://doi.org/10.1007/s11356-012-1415-x>.
- (70) Baig, N.; Kammakam, I.; Falath, W.; Kammakam, I. Nanomaterials: A Review of Synthesis Methods, Properties, Recent Progress, and Challenges. *Mater. Adv.* **2021**, *2* (6), 1821–1871. <https://doi.org/10.1039/d0ma00807a>.
- (71) Bethi, B.; Sonawane, S. H.; Bhanvase, B. A.; Gumfekar, S. Nanomaterials Based Advanced Oxidation Processes for Waste Water Treatment : A Review. *Chem. Eng. Process. Process.* **2016**. <https://doi.org/10.1016/j.cep.2016.08.016>.
- (72) Tolani, S. C.; Golhar, A. R.; Rewatkar, K. G. A Review of Morphological, Structural Behaviour and Technological Applications of Ferrites. *AIP Conf. Proc.* **2019**, *2104*.

<https://doi.org/10.1063/1.5100459>.

- (73) Giusto, L. A. R.; Pissetti, F. L.; Castro, T. S.; Magalhães, F. Preparation of Activated Carbon from Sugarcane Bagasse Soot and Methylene Blue Adsorption. *Water. Air. Soil Pollut.* **2017**, *228* (7). <https://doi.org/10.1007/s11270-017-3422-5>.
- (74) Reddy, D. H. K.; Yun, Y. S. Spinel Ferrite Magnetic Adsorbents: Alternative Future Materials for Water Purification? *Coord. Chem. Rev.* **2016**, *315*, 90–111. <https://doi.org/10.1016/j.ccr.2016.01.012>.
- (75) Nayeri, D.; Mousavi, S. A. Dye Removal from Water and Wastewater by Nanosized Metal Oxides - Modified Activated Carbon: A Review on Recent Researches. *J. EEnvironmental Heal. Sci. Eng.* **2020**. <https://doi.org/10.1007/s40201-020-00566-w>.
- (76) Patil, D. J.; Behera, S. N. Synthesis and Characterization of Nanoparticles of Cobalt and Nickel Ferrites for Elimination of Hazardous Organic Dyes from Industrial Wastewater. *Environ. Sci. Pollut. Res.* **2023**, *30* (18), 53323–53338. <https://doi.org/10.1007/s11356-023-26059-5>.
- (77) Vedrtnam, A.; Kalauni, K.; Dubey, S.; Kumar, A. A Comprehensive Study on Structure , Properties , Synthesis and Characterization of Ferrites. *Mater. Sci.* **2020**, *7* (6), 800–835. <https://doi.org/10.3934/matetsci.2020.6.800>.
- (78) Garg, V. K.; Sharma, V. K.; Kuzmann, E. Purification of Water by Ferrites - Mini Review. *Ferrites Ferrates Chem. Appl. Sustain. Energy Environ. Remediat.* **2016**, 137–143.
- (79) Kumari, N.; Kour, S.; Singh, G.; Sharma, R. K. A Brief Review on Synthesis, Properties and Applications of Ferrites. *AIP Conf. Proc.* **2020**, *2220*, 1–5. <https://doi.org/10.1063/5.0001323>.
- (80) Dutta, S. K.; Ahmed, J. Synthesis and Catalytic Activity of Spinel Ferrites : A Brief Review. *Biointerface Res. Appl. Chem.* **2022**, *12* (4), 4399–4416. <https://doi.org/10.33263/BRIAC124.43994416>.
- (81) Kefeni, K. K.; Mamba, B. B.; Msagati, T. A. M. Application of Spinel Ferrite Nanoparticles in Water and Wastewater Treatment: A Review. *Sep. Purif. Technol.* **2017**, *188*, 399–422. <https://doi.org/10.1016/j.seppur.2017.07.015>.
- (82) Zhang, L.; Zhang, Y.; Yang, L.; Jiang, X.; Yang, Q. A Rapid Method for the Removal

- of Methyl Blue Dye from Wastewater by Magnetic Nanoparticles Mn-Ferrites. *Desalin. Water Treat.* **2015**, *54* (8), 2259–2269. <https://doi.org/10.1080/19443994.2014.902331>.
- (83) Liu, X.; An, S.; Wang, Y.; Yang, Q.; Zhang, L. Rapid Selective Separation and Recovery of a Specific Target Dye from Mixture Consisted of Different Dyes by Magnetic Ca-Ferrites Nanoparticles. *Chem. Eng. J.* **2015**, *262*, 517–526. <https://doi.org/10.1016/j.cej.2014.10.002>.
- (84) Asadi, R.; Abdollahi, H.; Gharabaghi, M.; Boroumand, Z. Effective Removal of Zn (II) Ions from Aqueous Solution by the Magnetic MnFe₂O₄ and CoFe₂O₄ Spinel Ferrite Nanoparticles with Focuses on Synthesis, Characterization, Adsorption, and Desorption. *Adv. Powder Technol.* **2020**, *31* (4), 1480–1489. <https://doi.org/10.1016/j.appt.2020.01.028>.
- (85) Mishra, S.; Sahoo, S. S.; Debnath, A. K.; Muthe, K. P.; Das, N.; Parhi, P. Cobalt Ferrite Nanoparticles Prepared by Microwave Hydrothermal Synthesis and Adsorption Efficiency for Organic Dyes: Isotherms, Thermodynamics and Kinetic Studies. *Adv. Powder Technol.* **2020**, *31* (11), 4552–4562. <https://doi.org/10.1016/j.appt.2020.10.001>.
- (86) Tatarchuk, T.; Myslin, M.; Lapchuk, I.; Shyichuk, A.; Murthy, A. P.; Gargula, R.; Kurzydło, P.; Bogacz, B. F.; Pędziwiatr, A. T. Magnesium-Zinc Ferrites as Magnetic Adsorbents for Cr(VI) and Ni(II) Ions Removal: Cation Distribution and Antistructure Modeling. *Chemosphere* **2021**, *270*, 1–14. <https://doi.org/10.1016/j.chemosphere.2020.129414>.
- (87) Jasrotia, R.; Singh, J.; Mittal, S.; Singh, H. Synthesis of CTAB Modified Ferrite Composite for the Efficient Removal of Brilliant Green Dye Removal of Brilliant Green Dye. *Int. J. Environ. Anal. Chem.* **2022**, 1–17. <https://doi.org/10.1080/03067319.2022.2098485>.
- (88) Hua, M.; Zhang, S.; Pan, B.; Zhang, W.; Lv, L.; Zhang, Q. Heavy Metal Removal from Water/Wastewater by Nanosized Metal Oxides: A Review. *J. Hazard. Mater.* **2012**, *211–212*, 317–331. <https://doi.org/10.1016/j.jhazmat.2011.10.016>.
- (89) Gupta, S.; Sireesha, S.; Sreedhar, I.; Patel, C. M.; Anitha, K. L. Latest Trends in Heavy Metal Removal from Wastewater by Biochar Based Sorbents. *J. Water Process Eng.* **2020**, *38*. <https://doi.org/10.1016/j.jwpe.2020.101561>.

- (90) Mahmoodi, N. M. Nickel Ferrite Nanoparticle: Synthesis, Modification by Surfactant and Dye Removal Ability. *Water, Air, Soil Pollut.* **2013**, *224* (1419), 1–11. <https://doi.org/10.1007/s11270-012-1419-7>.
- (91) Velasco Perez, M.; Sotelo Navarro, P. X.; Vazquez Morillas, A.; Espinosa Valdemar, R. M.; Hermoso Lopez Araiza, J. P. Waste Management and Environmental Impact of Absorbent Hygiene Products: A Review. *Waste Manag. Res.* **2021**, 767–783. <https://doi.org/10.1177/0734242X20954271>.
- (92) Wassel, A. R.; El-Naggar, M. E.; Shoueir, K. Recent Advances in Polymer/Metal/Metal Oxide Hybrid Nanostructures for Catalytic Applications: A Review. *J. Environ. Chem. Eng.* **2020**, *8* (5), 104175. <https://doi.org/10.1016/j.jece.2020.104175>.
- (93) Ali, L. I. A.; Ismail, H. K.; Alesary, H. F.; Aboul-Enein, H. Y. A Nanocomposite Based on Polyaniline, Nickel and Manganese Oxides for Dye Removal from Aqueous Solutions. *Int. J. Environ. Sci. Technol.* **2021**, *18* (7), 2031–2050. <https://doi.org/10.1007/s13762-020-02961-0>.
- (94) Liu, R.; Fu, H.; Yin, H.; Wang, P.; Lu, L.; Tao, Y. A Facile Sol Combustion and Calcination Process for the Preparation of Magnetic Ni_{0.5}Zn_{0.5}Fe₂O₄ Nanopowders and Their Adsorption Behaviors of Congo Red. *Powder Technol.* **2015**, *274*, 418–425. <https://doi.org/10.1016/j.powtec.2015.01.045>.
- (95) Afkhami, A.; Aghajani, S.; Mohseni, M.; Madrakian, T. Effectiveness of Ni_{0.5}Zn_{0.5}Fe₂O₄ for the Removal and Preconcentration of Cr(VI), Mo(VI), V(V) and W(VI) Oxyanions from Water and Wastewater Samples. *J. Iran. Chem. Soc.* **2015**, *12*, 2007–2013. <https://doi.org/10.1007/s13738-015-0675-z>.
- (96) Palmer, M.; Hatley, H. The Role of Surfactants in Wastewater Treatment: Impact, Removal and Future Techniques: A Critical Review. *Water Res.* **2018**, *147*, 60–72. <https://doi.org/10.1016/j.watres.2018.09.039>.
- (97) Rashid, T. U.; Kabir, S. M. F.; Biswas, M. C.; Bhuiyan, M. A. R. Sustainable Wastewater Treatment via Dye-Surfactant Interaction: A Critical Review. *Ind. Eng. Chem. Res.* **2020**, *59* (21), 9719–9745. <https://doi.org/10.1021/acs.iecr.0c00676>.
- (98) Rasheed, T.; Shafi, S.; Bilal, M.; Hussain, T.; Sher, F.; Rizwan, K. Surfactants-Based Remediation as an Effective Approach for Removal of Environmental Pollutants—A

- Review. *J. Mol. Liq.* **2020**, *318*, 1–76. <https://doi.org/10.1016/j.molliq.2020.113960>.
- (99) Singh, M.; Dosanjh, H. S.; Singh, H. Surface Modified Spinel Cobalt Ferrite Nanoparticles for Cationic Dye Removal : Kinetics and Thermodynamics Studies. *J. Water Process Eng.* **2016**, *11*, 152–161. <https://doi.org/10.1016/j.jwpe.2016.05.006>.
- (100) Zhang, P.; Lo, I.; O'Connor, D.; Pehkonen, S.; Cheng, H.; Hou, D. High Efficiency Removal of Methylene Blue Using SDS Surface-Modified ZnFe₂O₄ Nanoparticles. *J. Colloid Interface Sci.* **2017**, *508*, 39–48. <https://doi.org/10.1016/j.jcis.2017.08.025>.
- (101) Adel, M.; Ahmed, M. A.; Mohamed, A. A. Effective Removal of Indigo Carmine Dye from Wastewaters by Adsorption onto Mesoporous Magnesium Ferrite Nanoparticles. *Environ. Nanotechnology, Monit. Manag.* **2021**, *16*, 1–10. <https://doi.org/10.1016/j.enmm.2021.100550>.
- (102) Ophardt, C. Polymer Fundamentals. *Virtual Chemb.* **2020**, 8–10.
- (103) Saldivar-Guerra, E.; Vivaldo-lima, E. *INTRODUCTION TO POLYMERS AND POLYMER TYPES*; 1920.
- (104) Khodakarami, M.; Bagheri, M. Recent Advances in Synthesis and Application of Polymer Nanocomposites for Water and Wastewater Treatment. *J. Clean. Prod.* **2021**, *296*, 1–35. <https://doi.org/10.1016/j.jclepro.2021.126404>.
- (105) Lofrano, G.; Carotenuto, M.; Libralato, G.; Domingos, R. F.; Markus, A.; Dini, L.; Gautam, R. K.; Baldantoni, D.; Rossi, M.; Sharma, S. K.; Chattopadhyaya, M. C.; Giugni, M.; Meric, S. Polymer Functionalized Nanocomposites for Metals Removal from Water and Wastewater: An Overview. *Water Res.* **2016**, *92*, 1–64. <https://doi.org/10.1016/j.watres.2016.01.033>.
- (106) Mignon, A.; De Belie, N.; Dubruel, P.; Van Vlierberghe, S. Superabsorbent Polymers: A Review on the Characteristics and Applications of Synthetic, Polysaccharide-Based, Semi-Synthetic and ‘Smart’ Derivatives. *Eur. Polym. J.* **2019**, *117*, 165–178. <https://doi.org/10.1016/j.eurpolymj.2019.04.054>.
- (107) Pandey, N.; Shukla, S. K.; Singh, N. B. Water Purification by Polymer Nanocomposites : An Overview. *Nanocomposites* **2017**, *3* (2), 47–66. <https://doi.org/10.1080/20550324.2017.1329983>.
- (108) Noamani, S.; Niroomand, S.; Rastgar, M.; Sadrzadeh, M. Carbon-Based Polymer

- Nanocomposite Membranes for Oily Wastewater Treatment. *npj Clean Water* **2019**, 2 (1), 1–14. <https://doi.org/10.1038/s41545-019-0044-z>.
- (109) Ahalya, K.; Suriyanarayanan, N.; Ranjithkumar, V. Effect of Cobalt Substitution on Structural and Magnetic Properties and Chromium Adsorption of Manganese Ferrite Nano Particles. *J. Magn. Magn. Mater.* **2014**, 372, 208–213. <https://doi.org/10.1016/j.jmmm.2014.07.030>.
- (110) Narian, E.; Arami, M.; Bahrami, H.; Pajootan, E. Modification of Nickel Ferrite with Cationic Surfactant: Dye Removal from Textile Wastewater Using Magnetic Separation. *J. Environ. Eng.* **2015**, 141 (2), 1–10. [https://doi.org/10.1061/\(asce\)ee.1943-7870.0000888](https://doi.org/10.1061/(asce)ee.1943-7870.0000888).
- (111) Muthukumar, C.; Sivakumar, V. M.; Thirumarimurugan, M. Adsorption Isotherms and Kinetic Studies of Crystal Violet Dye Removal from Aqueous Solution Using Surfactant Modified Magnetic Nanoadsorbent. *J. Taiwan Inst. Chem. Eng.* **2016**, 63, 354–362. <https://doi.org/10.1016/j.jtice.2016.03.034>.
- (112) Kumar, M.; Dosanjh, H. S.; Singh, H. Synthesis of Spinel ZnFe₂O₄ Modified with SDS via Low Temperature Combustion Method and Adsorption Behaviour of Crystal Violet Dye. *Asian J. Chem.* **2017**, 29 (9), 2057–2064. <https://doi.org/10.14233/ajchem.2017.20827>.
- (113) Homayonfard, A.; Miralinaghi, M.; Seyed Mohammad Shirazi, R. H.; Moniri, E. Efficient Removal of Cadmium (II) Ions from Aqueous Solution by CoFe₂O₄/Chitosan and NiFe₂O₄/Chitosan Composites as Adsorbents. *Water Sci. Technol.* **2018**, 78 (11), 2297–2307. <https://doi.org/10.2166/wst.2018.510>.
- (114) Thi, D.; Nguyen, C.; Tran, T. Van; Senthil, P.; Azam, K.; Mohd, T. *Invasive Plants as Biosorbents for Environmental Remediation: A Review*; Springer International Publishing, 2022; Vol. 20. <https://doi.org/10.1007/s10311-021-01377-7>.
- (115) Hamad, H. N.; Syazwani, I. Recent Developments in the Application of Bio-Waste-Derived Adsorbents for the Removal of Methylene Blue from Wastewater: A Review. *Polymers (Basel)*. **2022**, 14 (4). <https://doi.org/10.3390/polym14040783>.
- (116) Nakum, J.; Bhattacharya, D. Various Green Nanomaterials Used for Wastewater and Soil Treatment: A Mini-Review. *Front. Environ. Sci.* **2022**, 9, 1–9.

<https://doi.org/10.3389/fenvs.2021.724814>.

- (117) Hakim, H. M. A.; Supartono, W. Equilibrium and Kinetic Studies of Methylene Blue Biosorption by Sugar Palm Dregs. *IOP Conf. Ser. Earth Environ. Sci.* **2021**, *653* (1). <https://doi.org/10.1088/1755-1315/653/1/012026>.
- (118) Premkumar, M. P.; Kumar, V. V.; Kumar, P. S.; Baskaralingam, P.; Sathyaselvabala, V.; Vidhyadevi, T.; Sivanesan, S. Kinetic and Equilibrium Studies on the Biosorption of Textile Dyes onto Plantago Ovata Seeds. *Korean J. Chem. Eng.* **2013**, *30* (6), 1248–1256. <https://doi.org/10.1007/s11814-013-0049-0>.
- (119) Yagub, M. T.; Sen, T. K.; Ang, H. M. Equilibrium, Kinetics, and Thermodynamics of Methylene Blue Adsorption by Pine Tree Leaves. *Water. Air. Soil Pollut.* **2012**, *223* (8), 5267–5282. <https://doi.org/10.1007/s11270-012-1277-3>.
- (120) Sen, T. K.; Afroze, S.; Ang, H. M. Equilibrium, Kinetics and Mechanism of Removal of Methylene Blue from Aqueous Solution by Adsorption onto Pine Cone Biomass of Pinus Radiata. *Water. Air. Soil Pollut.* **2011**, *218*, 499–515. <https://doi.org/10.1007/s11270-010-0663-y>.
- (121) Litefti, K.; Freire, M. S.; Stitou, M.; González-Álvarez, J. Adsorption of an Anionic Dye (Congo Red) from Aqueous Solutions by Pine Bark. *Sci. Rep.* **2019**, *9* (1), 1–11. <https://doi.org/10.1038/s41598-019-53046-z>.
- (122) Senthil Kumar, P. Removal of Congo Red from Aqueous Solutions by Neem Saw Dust Carbon. *Colloid J.* **2010**, *72* (5), 703–709. <https://doi.org/10.1134/S1061933X10050182>.
- (123) Georjina, J.; Drumm, F. C.; Grassi, P.; Franco, D.; Allasia, D.; Dotto, G. L. Potential of Araucaria Angustifolia Bark as Adsorbent to Remove Gentian Violet Dye from Aqueous Effluents. *Water Sci. Technol.* **2018**, *78* (8), 1693–1703. <https://doi.org/10.2166/wst.2018.448>.
- (124) Dawood, S.; Sen, T. K. Removal of Anionic Dye Congo Red from Aqueous Solution by Raw Pine and Acid-Treated Pine Cone Powder as Adsorbent: Equilibrium, Thermodynamic, Kinetics, Mechanism and Process Design. *Water Res.* **2012**, *46* (6), 1933–1946. <https://doi.org/10.1016/j.watres.2012.01.009>.
- (125) Kumar, P. S.; Ramalingam, S.; Sathishkumar, K. Removal of Methylene Blue Dye from

- Aqueous Solution by Activated Carbon Prepared from Cashew Nut Shell as a New Low-Cost Adsorbent. *Korean J. Chem. Eng.* **2011**, *28* (1), 149–155. <https://doi.org/10.1007/s11814-010-0342-0>.
- (126) Singh, H.; Tshering, D. Removal of Methylene Blue Using Lemon Grass Ash as an Adsorbent. *Carbon Lett.* **2014**, *15* (2), 105–112. <https://doi.org/10.5714/CL.2014.15.2.105>.
- (127) Singh, S.; Sidhu, G. K.; Singh, H. Removal of Methylene Blue Dye Using Activated Carbon Prepared from Biowaste Precursor. *Indian Chem. Eng.* **2017**, 1–12. <https://doi.org/10.1080/00194506.2017.1408431>.
- (128) Namasivayam, C.; Kavitha, D. Removal of Congo Red from Water by Adsorption onto Activated Carbon Prepared from Coir Pith, an Agricultural Solid Waste. *Dye. Pigment.* **2002**, *54*, 47–58.
- (129) Suyamboo, B. K.; Perumal, R. S. Equilibrium, Thermodynamic and Kinetic Studies on Adsorption of a Basic Dye by Citrullus Lanatus Rind. *Iran. J. Energy Environ.* **2012**, *3* (1), 23–34. <https://doi.org/10.5829/idosi.ijee.2012.03.01.0130>.
- (130) Malik, P. K. Use of Activated Carbons Prepared from Sawdust and Rice-Husk for Adsorption of Acid Dyes: A Case Study of Acid Yellow 36. *Dye. Pigment.* **2003**, *56* (3), 239–249. [https://doi.org/10.1016/S0143-7208\(02\)00159-6](https://doi.org/10.1016/S0143-7208(02)00159-6).
- (131) Li, W.; Yang, X.; Doshmanziari, M.; Esmaeili, H. Elimination of Methyl Violet 2B Dye from Water Using Citrus Limetta Leaves-Activated Carbon Modified by Copper-Ferrite Nanoparticles. *Sep. Sci. Technol.* **2021**, 1–14. <https://doi.org/10.1080/01496395.2021.1919143>.
- (132) Karthikeyan, P.; Vigneshwaran, S.; Preethi, J.; Meenakshi, S. Preparation of Novel Cobalt Ferrite Coated-Porous Carbon Composite by Simple Chemical Co-Precipitation Method and Their Mechanistic Performance. *Diam. Relat. Mater.* **2020**, *108*, 107922. <https://doi.org/10.1016/j.diamond.2020.107922>.
- (133) Güzel, F.; Yilmaz, C. On the Performance of Wild Plant-Derived Biochar @ MnFe₂O₄ Composite in Remediation of Synthetic Aqueous Copper Solution. *Biomass Convers. Refin.* **2021**. <https://doi.org/10.1007/s13399-021-01508-8>.
- (134) Hardian, A.; Rosidah, R.; Budiman, S.; Gustaman, D. Preparation of Composite Derived

- from Banana Peel Activated Carbon and MgFe_2O_4 as Magnetic Adsorbent for Methylene Blue Removal. *J. Sci. Appl. Chem.* **2020**, *23* (12), 440–448. <https://doi.org/10.14710/jksa.23.12.440-448>.
- (135) Hoang, L. P.; Van, H. T.; Nguyen, H.; Nguyen, V. Q.; Thang, P. Q. Coconut Shell Activated Carbon/ CoFe_2O_4 Composite for the Removal of Rhodamine B from Aqueous Solution. *J. Chem.* **2020**, *2020*, 1–12. <https://doi.org/10.1155/2020/9187960> Research.
- (136) Sirajudheen, P.; Karthikeyan, P.; Ramkumar, K.; Nisheetha, P.; Meenakshi, S. Magnetic Carbon-Biomass from the Seeds of Moringa Oleifera @ MnFe_2O_4 Composite as an Effective and Recyclable Adsorbent for the Removal of Organic Pollutants from Water. *J. Mol. Liq.* **2021**, *327*, 114829. <https://doi.org/10.1016/j.molliq.2020.114829>.
- (137) Thangamani, K. S.; Andal, N. M.; Kumar, E. R.; Saravanabhavan, M. Utilization of Magnetic Nano Cobalt Ferrite Doped Capra Aegagrus Hircus Dung Activated Carbon Composite for the Adsorption of Anionic Dyes. *J. Environ. Chem. Eng.* **2017**, 1–34. <https://doi.org/10.1016/j.jece.2017.05.030>.
- (138) Foroutan, R.; Mohammadi, R.; Ramavandi, B.; Bastanian, M. Removal Characteristics of Chromium by Activated Carbon/ CoFe_2O_4 Magnetic Composite and Phoenix Dactylifera Stone Carbon. *Korean J. Chem. Eng.* **2018**, *35* (11), 2207–2219. <https://doi.org/10.1007/s11814-018-0145-2>.
- (139) Karthikeyan, P.; Sirajudheen, P.; Raja, M.; Meenakshi, S. Removal of Phosphate and Nitrate via a Zinc Ferrite@activated Carbon Hybrid Composite under Batch Experiments : Study of Isotherm and Kinetic Equilibriums. *Environ. Nanotechnology, Monit. Manag.* **2020**, *14*, 1–9. <https://doi.org/10.1016/j.enmm.2020.100378>.
- (140) Suba, V.; Ranjith, G. R. E.; Saravanabhavan, K. M.; Nayak, V.; Thangamani, B. K. S. Enhanced Adsorption and Antimicrobial Activity of Fabricated Apocynaceae Leaf Waste Activated Carbon by Cobalt Ferrite Nanoparticles for Textile Effluent Treatment. *J. Inorg. Organomet. Polym. Mater.* **2019**, *29* (2), 550–563. <https://doi.org/10.1007/s10904-018-1030-5>.
- (141) Perveen, S.; Nadeem, R.; Nosheen, F.; Asjad, M. I.; Awrejcewicz, J.; Anwar, T. Biochar-Mediated Zirconium Ferrite Nanocomposites for Tartrazine Dye Removal from Textile Wastewater. *Nanomaterials* **2022**, *12* (16), 1–22. <https://doi.org/10.3390/nano12162828>.

- (142) Kumar, M.; Dosanjh, H. S.; Singh, H. Surface Modification of Spinel Ferrite with Biopolymer for Adsorption of Cationic and Anionic Dyes in Single and Ternary Dye System. *Fibers Polym.* **2019**, *20* (4), 739–751. <https://doi.org/10.1007/s12221-019-8462-6>.
- (143) Ivanets, A. I.; Srivastava, V.; Roshchina, M. Y.; Sillanpää, M.; Prozorovich, V. G.; Pankov, V. V. Magnesium Ferrite Nanoparticles as a Magnetic Sorbent for the Removal of Mn²⁺, Co²⁺, Ni²⁺ and Cu²⁺ from Aqueous Solution. *Ceram. Int.* **2018**, *44* (8), 9097–9104. <https://doi.org/10.1016/j.ceramint.2018.02.117>.
- (144) Podder, M. S.; Majumder, C. B. Studies on the Removal of As (III) and As (V) through Their Adsorption onto Granular Activated Carbon/MnFe₂O₄ Composite: Isotherm Studies and Error Analysis. *Compos. Interfaces* **2016**, *23* (4), 327–372. <https://doi.org/10.1080/09276440.2016.1137715>.
- (145) Venkateswarlu, S.; Natesh, B.; Prathima, B.; Subbarao, Y.; Venkata, N.; Jyothi, V. A Novel Green Synthesis of Fe₃O₄ Magnetic Nanorods Using Punica Granatum Rind Extract and Its Application for Removal of Pb(II) from Aqueous Environment. *Arab. J. Chem.* **2019**, *12* (4), 588–596. <https://doi.org/10.1016/j.arabjc.2014.09.006>.
- (146) Niu, Z.; Feng, W.; Huang, H.; Wang, B.; Chen, L.; Miao, Y.; Su, S. Green Synthesis of a Novel Mn-Zn Ferrite/Biochar Composite from Waste Batteries and Pine Sawdust for Pb²⁺ Removal. *Chemosphere* **2020**, *252*, 1–9. <https://doi.org/10.1016/j.chemosphere.2020.126529>.
- (147) Tul, K.; Salman, S.; Hasan, N.; Islam, A.; Hasan, M.; Awual, R. Utilizing an Alternative Composite Material for Effective Copper(II) Ion Capturing from Wastewater. *J. Mol. Liq.* **2021**, *336*, 1–11. <https://doi.org/10.1016/j.molliq.2021.116325>.
- (148) Din, M. I.; Jabbar, S.; Najeeb, J.; Khalid, R.; Ghaffar, T.; Arshad, M.; Khan, S. A.; Ali, S. Green Synthesis of Zinc Ferrite Nanoparticles for Photocatalysis of Methylene Blue. *Int. J. Phytoremediation* **2020**, 1–9. <https://doi.org/10.1080/15226514.2020.1781783>.
- (149) Zhang, W.; Zhang, Y. Development of ZnFe₂O₄ Nanoparticle Functionalized Baker's Yeast Composite for Effective Removal of Methylene Blue via Adsorption and Photodegradation. *J. Water Process Eng.* **2020**, *37*, 1–8. <https://doi.org/10.1016/j.jwpe.2020.101234>.

- (150) Nadeem, N.; Zahid, M.; Rehan, Z. A.; Hanif, M. A.; Yaseen, M. Improved Photocatalytic Degradation of Dye Using Coal Fly Ash-Based Zinc Ferrite (CFA/ZnFe₂O₄) Composite. *Int. J. Environ. Sci. Technol.* **2021**, 1–17. <https://doi.org/10.1007/s13762-021-03255-9>.
- (151) Tu, Y. J.; Chang, C. K.; You, C. F.; Wang, S. L. Treatment of Complex Heavy Metal Wastewater Using a Multi-Staged Ferrite Process. *J. Hazard. Mater.* **2012**, 209–210, 379–384. <https://doi.org/10.1016/j.jhazmat.2012.01.050>.
- (152) Keyhanian, F.; Shariati, S.; Faraji, M.; Hesabi, M. Magnetite Nanoparticles with Surface Modification for Removal of Methyl Violet from Aqueous Solutions. *Arab. J. Chem.* **2016**, 9, S348–S354. <https://doi.org/10.1016/j.arabjc.2011.04.012>.
- (153) Periyaraman, P. M.; Karan, S.; Ponnusamy, S. K.; Vaidyanathan, V.; Vasanthakumar, S.; Dhanasekaran, A.; Subramanian, S. Adsorption of an Anionic Dye onto Native and Chemically Modified Agricultural Waste. *Environ. Eng. Manag. J.* **2019**, 18 (1), 257–270. <https://doi.org/10.30638/eemj.2019.025>.
- (154) A. M. Babakir, B.; Abd Ali, L. I.; Ismail, H. K. Rapid Removal of Anionic Organic Dye from Contaminated Water Using a Poly(3-Aminobenzoic Acid/Graphene Oxide/Cobalt Ferrite) Nanocomposite Low-Cost Adsorbent via Adsorption Techniques. *Arab. J. Chem.* **2022**, 15 (12), 104318. <https://doi.org/10.1016/j.arabjc.2022.104318>.
- (155) Meghana, C.; Juhi, B.; Rampal, N.; Vairavel, P. Isotherm, Kinetics, Process Optimization and Thermodynamics Studies for Removal of Congo Red Dye from Aqueous Solutions Using Nelumbo Nucifera (Lotus) Leaf Adsorbent. *Desalin. Water Treat.* **2020**, 207, 373–397. <https://doi.org/10.5004/dwt.2020.26389>.
- (156) Yalvaç, G. M.; Bayrak, B. Use of Natural and Effective Mandarin Peel in Elimination of Malachite Green from the Aqueous Media: Adsorption Properties, Kinetics and Thermodynamics. *Desalin. Water Treat.* **2020**, 177, 176–185. <https://doi.org/10.5004/dwt.2020.24876>.
- (157) Kumar, M.; Singh, H.; Harminder, D. Magnetic Zinc Ferrite – Alginic Biopolymer Composite : As an Alternative Adsorbent for the Removal of Dyes in Single and Ternary Dye System. *J. Inorg. Organomet. Polym. Mater.* **2018**, 28 (5), 1688–1705. <https://doi.org/10.1007/s10904-018-0839-2>.

- (158) Sharma, D.; Jasrotia, R.; Singh, J.; Singh, H. Removal of Cationic Dyes in Single as Well as Binary Dye Systems from Aqueous Solution Using Zinc Ferrite-Rice Husk Silica Composite. *Int. J. Environ. Anal. Chem.* **2022**, 1–22. <https://doi.org/10.1080/03067319.2022.2140416>.
- (159) Tang, R.; Dai, C.; Li, C.; Liu, W.; Gao, S.; Wang, C. Removal of Methylene Blue from Aqueous Solution Using Agricultural Residue Walnut Shell : Equilibrium , Kinetic , and Thermodynamic Studies. *J. Chem.* **2017**, 2017, 1–10. <https://doi.org/10.1155/2017/8404965>.
- (160) Jayalakshmi, R.; Jeyanthi, J. Simultaneous Removal of Binary Dye from Textile Effluent Using Cobalt Ferrite-Alginate Nanocomposite : Performance and Mechanism. *Microchem. J.* **2019**, 145, 791–800. <https://doi.org/10.1016/j.microc.2018.11.047>.
- (161) Khan, M. A.; Otero, M.; Kazi, M.; Alqadami, A. A.; Wabaidur, S. M.; Siddiqui, M. R.; Alothman, Z. A.; Sumbul, S. Unary and Binary Adsorption Studies of Lead and Malachite Green onto a Nanomagnetic Copper Ferrite/Drumstick Pod Biomass Composite. *J. Hazard. Mater.* **2018**. <https://doi.org/10.1016/j.jhazmat.2018.11.072>.
- (162) Jasrotia, R.; Singh, J.; Mittal, S.; Singh, H. Robust Removal of Cationic Dyes by Zinc Ferrite Composites in Single and Ternary Dye Systems. *Inorg. Chem. Commun.* **2023**, 153, 1–19. <https://doi.org/10.1016/j.inoche.2023.110756>.
- (163) Singh, H.; Rattan, V. K. Adsorption of Nickel from Aqueous Solutions Using Low Cost Biowaste Adsorbents. *Water Qual. Res. J. Canada* **2011**, 46 (3), 239–249. <https://doi.org/10.2166/wqrjc.2011.024>.
- (164) Kolluru, S. S.; Agarwal, S.; Sireesha, S.; Sreedhar, I.; Kale, S. R. Heavy Metal Removal from Wastewater Using Nanomaterials-Process and Engineering Aspects. *Process Saf. Environ. Prot.* **2021**, 150, 323–355. <https://doi.org/10.1016/j.psep.2021.04.025>.
- (165) Mine, Z.; Serap, Ş.; Hasan, Ç. Recycling of Labada (Rumex) Biowaste as a Value - Added Biosorbent for Rhodamine B (Rd-B) Wastewater Treatment : Biosorption Study with Experimental Design Optimisation. *Biomass Convers. Biorefinery* **2023**, 13, 2413–2425. <https://doi.org/10.1007/s13399-022-02324-4>.
- (166) Sud, D.; Mahajan, G.; Kaur, M. P. Agricultural Waste Material as Potential Adsorbent for Sequestering Heavy Metal Ions from Aqueous Solutions - A Review. *Bioresour.*

- Technol.* **2008**, *99* (14), 6017–6027. <https://doi.org/10.1016/j.biortech.2007.11.064>.
- (167) Wakkal, M.; Khiari, B.; Zagrouba, F. Textile Wastewater Treatment by Agro-Industrial Waste: Equilibrium Modelling, Thermodynamics and Mass Transfer Mechanisms of Cationic Dyes Adsorption onto Low-Cost Lignocellulosic Adsorbent. *J. Taiwan Inst. Chem. Eng.* **2019**, *96*, 439–452. <https://doi.org/10.1016/j.jtice.2018.12.014>.
- (168) Dawood, S.; Sen, T. K.; Phan, C. Synthesis and Characterisation of Novel-Activated Carbon from Waste Biomass Pine Cone and Its Application in the Removal of Congo Red Dye from Aqueous Solution by Adsorption. *Water. Air. Soil Pollut.* **2014**, *225* (1). <https://doi.org/10.1007/s11270-013-1818-4>.
- (169) Güzel, F.; Yılmaz, C. On the Performance of Wild Plant-Derived Biochar@MnFe₂O₄ Composite in Remediation of Synthetic Aqueous Copper Solution. *Biomass Convers. Biorefinery* **2021**. <https://doi.org/10.1007/s13399-021-01508-8>.
- (170) Humelnicu, I.; Baiceanu, A.; Ignat, M. E.; Dulman, V. The Removal of Basic Blue 41 Textile Dye from Aqueous Solution by Adsorption onto Natural Zeolitic Tuff: Kinetics and Thermodynamics. *Process Saf. Environ. Prot.* **2017**, *105*, 274–287. <https://doi.org/10.1016/j.psep.2016.11.016>.
- (171) Mane, V. S.; Deo Mall, I.; Chandra Srivastava, V. Kinetic and Equilibrium Isotherm Studies for the Adsorptive Removal of Brilliant Green Dye from Aqueous Solution by Rice Husk Ash. *J. Environ. Manage.* **2007**, *84* (4), 390–400. <https://doi.org/10.1016/j.jenvman.2006.06.024>.
- (172) Hariani, P. L.; Desneli, D.; Hermansyah, H.; Salni, S. CoFe₂O₄ Modified with Polyethylene Glycol (PEG) for Removal of Chromium (VI) Ion from Electroplating Wastewater. *EnvironmentAsia* **2018**, *11* (1), 15–30. <https://doi.org/10.14456/ea.2018.2>.
- (173) Ojo, T. A.; Ojedokun, A. T.; Bello, O. S. Functionalization of Powdered Walnut Shell with Orthophosphoric Acid for Congo Red Dye Removal. *Part. Sci. Technol.* **2017**, 1–14. <https://doi.org/10.1080/02726351.2017.1340914>.
- (174) Soltani, A.; Faramarzi, M.; Mousavi, S. A. A Review on Adsorbent Parameters for Removal of Dye Products from Industrial Wastewater. *Water Qual. Res. J.* **2021**, *56* (4), 181–193. <https://doi.org/10.2166/wqrj.2021.023>.
- (175) Chong, M. Y.; Tam, Y. J. Bioremediation of Dyes Using Coconut Parts via Adsorption:

- A Review. *SN Appl. Sci.* **2020**, 2 (2), 1–16. <https://doi.org/10.1007/s42452-020-1978-y>.
- (176) Fan, C.; Li, K.; Li, J.; Ying, D.; Wang, Y.; Jia, J. Comparative and Competitive Adsorption of Pb(II) and Cu(II) Using Tetraethylenepentamine Modified Chitosan/CoFe₂O₄ Particles. *J. Hazard. Mater.* **2017**, 326, 211–220. <https://doi.org/10.1016/j.jhazmat.2016.12.036>.
- (177) Sukla Baidya, K.; Kumar, U. Adsorption of Brilliant Green Dye from Aqueous Solution onto Chemically Modified Areca Nut Husk. *South African J. Chem. Eng.* **2021**, 35, 33–43. <https://doi.org/10.1016/j.sajce.2020.11.001>.
- (178) Dod, R.; Banerjee, G.; Saini, S. Adsorption of Methylene Blue Using Green Pea Peels (*Pisum Sativum*): A Cost-Effective Option for Dye-Based Wastewater Treatment. *Biotechnol. Bioprocess Eng.* **2012**, 17 (4), 862–874. <https://doi.org/10.1007/s12257-011-0614-5>.
- (179) Hayati, B.; Mahmoodi, N. M.; Maleki, A. Dendrimer-Titania Nanocomposite: Synthesis and Dye-Removal Capacity. *Res. Chem. Intermed.* **2015**, 41, 3743–3757. <https://doi.org/10.1007/s11164-013-1486-4>.
- (180) Imessaoudene, A.; Cheikh, S.; Bollinger, J.; Belkhiri, L.; Tiri, A.; Bouzaza, A.; Jery, A. El; Assadi, A.; Amrane, A.; Mouni, L. Zeolite Waste Characterization and Use as Low-Cost, Ecofriendly, and Sustainable Material for Malachite Green and Methylene Blue Dyes Removal: Box-Behnken Design, Kinetics, and Thermodynamics. *Appl. Sci.* **2022**, 12 (15), 1–18. <https://doi.org/10.3390/app12157587>.
- (181) Zein, R.; Purnomo, J. S.; Ramadhani, P.; Alif, M. F. Lemongrass (*Cymbopogon Nardus*) Leaves Biowaste as an Effective and Low-Cost Adsorbent for Methylene Blue Dyes Removal: Isotherms, Kinetics, and Thermodynamics Studies. *Sep. Sci. Technol.* **2022**, 57 (15), 2341–2357. <https://doi.org/10.1080/01496395.2022.2058549>.
- (182) Mahmoodi, N. M.; Bashiri, M.; Moeen, S. J. Synthesis of Nickel – Zinc Ferrite Magnetic Nanoparticle and Dye Degradation Using Photocatalytic Ozonation. *Mater. Res. Bull.* **2012**, 47 (12), 4403–4408. <https://doi.org/10.1016/j.materresbull.2012.09.036>.
- (183) Khoso, W. A.; Haleem, N.; Baig, M. A.; Jamal, Y. Synthesis, Characterization and Heavy Metal Removal Efficiency of Nickel Ferrite Nanoparticles (NFN's). *Sci. Rep.* **2021**, 11 (3790), 1–10. <https://doi.org/10.1038/s41598-021-83363-1>.

- (184) Tianci, Z.; Xiaolong, M.; Hao, C.; Zichuan, M.; Huifeng, L. Study on the Adsorption of CuFe₂O₄-Loaded Corncob Biochar for Pb(II). *molecules* **2020**, *25* (3456), 1–16. <https://doi.org/10.3390/molecules25153456>.
- (185) Li, X.; Wang, Y.; Li, Y.; Zhou, L.; Jia, X. Biosorption Behaviors of Biosorbents Based on Microorganisms Immobilized by Ca-Alginate for Removing Lead (II) from Aqueous Solution. *Biotechnol. Bioprocess Eng.* **2011**, *16*, 808–820. <https://doi.org/10.1007/s12257-010-0434-z>.
- (186) Narkiewicz, U.; Konicki, W.; Sibera, D.; Mijowska, E.; Lendzion-bielun, Z. Equilibrium and Kinetic Studies on Acid Dye Acid Red 88 Adsorption by Magnetic ZnFe₂O₄ Spinel Ferrite Nanoparticles. *J. Colloid Interface Sci.* **2013**, *398*, 152–160. <https://doi.org/10.1016/j.jcis.2013.02.021>.
- (187) Adeogun, A. I. Removal of Methylene Blue Dye from Aqueous Solution Using Activated Charcoal Modified Manganese Ferrite (AC-MnFe₂O₄): Kinetic, Isotherms, and Thermodynamics Studies. *Part. Sci. Technol.* **2019**, 1–13. <https://doi.org/10.1080/02726351.2019.1626516>.
- (188) Ratan, J. K.; Kaur, M.; Adiraju, B. Synthesis of Activated Carbon from Agricultural Waste Using a Simple Method: Characterization, Parametric and Isotherms Study. *Mater. Today Proc.* **2018**, *5* (2), 3334–3345. <https://doi.org/10.1016/j.matpr.2017.11.576>.
- (189) Laskar, N.; Kumar, U. Removal of Brilliant Green Dye from Water by Modified Bambusa Tulda: Adsorption Isotherm, Kinetics and Thermodynamics Study. *Int. J. Environ. Sci. Technol.* **2019**, *16* (3), 1649–1662. <https://doi.org/10.1007/s13762-018-1760-5>.
- (190) Ahmed, H. A.; Mubarak, M. F. Adsorption of Cationic Dye Using A Newly Synthesized CaNiFe₂O₄/Chitosan Magnetic Nanocomposite: Kinetic and Isotherm Studies. *J. Polym. Environ.* **2021**, *29* (6), 1835–1851. <https://doi.org/10.1007/s10924-020-01989-0>.
- (191) Sareban, Z.; Javanbakht, V. Preparation and Characterization of a Novel Nanocomposite of Clinoptilolite/Maghemite/Chitosan/Urea for Manganese Removal from Aqueous Solution. *Korean J. Chem. Eng.* **2017**, *34* (11), 2886–2900. <https://doi.org/10.1007/s11814-017-0216-9>.

- (192) Mahmoodi, N. M.; Abdi, J. Surface Modified Cobalt Ferrite Nanoparticles with Cationic Surfactant: Synthesis, Multicomponent Dye Removal Modeling and Selectivity Analysis. *Prog. Color. Color. Coatings* **2019**, *12* (3), 163–177.
- (193) Sharma, A.; Rasheed, S.; Mangla, D.; Choudhry, A.; Shukla, S.; Chaudhry, S. A. Cobalt Ferrite Incorporated *Ocimum Sanctum* Nanocomposite Matrix as an Interface for Adsorption of Organic Dyes: A Sustainable Alternative. *ChemistrySelect* **2023**, *8* (5). <https://doi.org/10.1002/slct.202203709>.
- (194) GUR, T.; DEMIR, C.; Kul, A. R. REMOVAL of METHYLENE BLUE FROM AQUEOUS SOLUTIONS USING PINE CONE and STATISTICAL COMPARISON of ADSORBED MATERIAL. *J. Sci. Reports-A* **2021**, No. 47, 235–245.
- (195) Zeraatkar Moghaddam, A.; Ghiamati, E.; Pourashuri, A.; Allahresani, A. Modified Nickel Ferrite Nanocomposite/Functionalized Chitosan as a Novel Adsorbent for the Removal of Acidic Dyes. *Int. J. Biol. Macromol.* **2018**, *120*, 1714–1725. <https://doi.org/10.1016/j.ijbiomac.2018.09.198>.
- (196) Singh, R.; Jasrotia, R.; Sharma, D.; Singh, J.; Mittal, S.; Singh, H. Recyclable Magnetic Nickel Ferrite–Carboxymethyl Cellulose–Sodium Alginate Bio-Composite for Efficient Removal of Nickel Ion from Water. *J. Dispers. Sci. Technol.* **2024**, 1–12. <https://doi.org/10.1080/01932691.2024.2320302>.
- (197) Meigoli Boushehrian, M.; Esmaeili, H.; Foroutan, R. Ultrasonic Assisted Synthesis of Kaolin/CuFe₂O₄nanocomposite for Removing Cationic Dyes from Aqueous Media. *J. Environ. Chem. Eng.* **2020**, *8* (4), 103869. <https://doi.org/10.1016/j.jece.2020.103869>.
- (198) Chandra, M.; Pawan, A.; Bafila, S.; Mishra, D.; Negi, K.; Kumar, R.; Bughani, A. Adsorptive Removal of Remazol Brilliant Blue R Dye from Its Aqueous Solution by Activated Charcoal of Thuja Orientalis Leaves : An Eco-Friendly Approach. *SN Appl. Sci.* **2020**, *2* (2), 1–10. <https://doi.org/10.1007/s42452-020-2063-2>.
- (199) Shao, Q.; Li, Y.; Wang, Q.; Niu, T.; Li, S.; Shen, W. Preparation of Copper Doped Walnut Shell-Based Biochar for Efficiently Removal of Organic Dyes from Aqueous Solutions. *J. Mol. Liq.* **2021**, *336*, 116314. <https://doi.org/10.1016/j.molliq.2021.116314>.
- (200) Li, X.; Qiu, J.; Hu, Y.; Ren, X.; He, L.; Zhao, N.; Ye, T.; Zhao, X. Characterization and

- Comparison of Walnut Shells-Based Activated Carbons and Their Adsorptive Properties. *Adsorpt. Sci. Technol.* **2020**, 38 (9–10), 450–463. <https://doi.org/10.1177/0263617420946524>.
- (201) Dahri, M. K.; Raziq, M.; Kooh, R.; Lim, L. B. L. Water Remediation Using Low Cost Adsorbent Walnut Shell for Removal of Malachite Green : Equilibrium , Kinetics , Thermodynamic and Regeneration Studies. *J. Environ. Chem. Eng.* **2014**. <https://doi.org/10.1016/j.jece.2014.07.008>.
- (202) Liaskovska, M.; Tatarchuk, T.; Kotsyubynsky, V.; Ersteniuk, H. Zn-Doped CoFe₂O₄ Nanoparticles Synthesized Using Ginkgo Biloba Extract : Cation Distribution , Mossbauer Studies and Application for Water Treatment. *Phys. Chem. Solid State* **2021**, 22 (4), 792–803. <https://doi.org/10.15330/pcss.22.4.792-803>.
- (203) Chakhtouna, H.; Benzeid, H.; Zari, N.; Qaiss, A. el kacem; Bouhfid, R. Functional CoFe₂O₄-Modified Biochar Derived from Banana Pseudostem as an Efficient Adsorbent for the Removal of Amoxicillin from Water. *Sep. Purif. Technol.* **2021**, 266, 1–12. <https://doi.org/10.1016/j.seppur.2021.118592>.
- (204) Cruz, D. R. S.; Santos, B. T. J.; Cunha, G. C.; Romão, L. P. C. *Green Synthesis of a Magnetic Hybrid Adsorbent (CoFe₂O₄/NOM): Removal of Chromium from Industrial Effluent and Evaluation of the Catalytic Potential of Recovered Chromium Ions*; Elsevier B.V., 2017; Vol. 334. <https://doi.org/10.1016/j.jhazmat.2017.03.062>.
- (205) Banerjee, M.; Kumar, R.; Kumar, S. Adsorptive Removal of Cu(II) by Pistachio Shell: Isotherm Study , Kinetic Modelling and Scale-up Designing - Continuous Mode. *Environ. Technol. Innov.* **2019**, 15, 100419. <https://doi.org/10.1016/j.eti.2019.100419>.
- (206) Adaobi, C.; Joshua, I.; Ghosh, S.; Ahmadi, S.; Ugonabo, V. I. Pistachio (Pistacia Vera) Waste as Adsorbent for Wastewater Treatment : A Review. *Biomass Convers. Biorefinery* **2023**, 13, 8793–8811. <https://doi.org/10.1007/s13399-021-01739-9>.
- (207) Turan, N. G.; Mesci, B. Use of Pistachio Shells as an Adsorbent for the Removal of Zinc (II) Ion. *Clean- Soil, Air, Water* **2011**, 39 (5), 475–481. <https://doi.org/10.1002/clen.201000297>.
- (208) Sherlala, A. I. A.; Raman, A. A. A.; Bello, M. M.; Buthiyappan, A. Adsorption of Arsenic Using Chitosan Magnetic Graphene Oxide Nanocomposite. *J. Environ.*

Manage. **2019**, 246, 547–556. <https://doi.org/10.1016/j.jenvman.2019.05.117>.

LIST OF PUBLICATIONS

1. **Rimzim**, Jandeep Singh and Harminder Singh*, “**A Review of Bio Waste Based Ferrite Composites for the Wastewater Treatment**”, AIP Conference Proceedings, vol. 2800, no. 1, 2023, doi: [10.1063/5.0162761](https://doi.org/10.1063/5.0162761)
2. **Rimzim**, Jandeep Singh, Sunil Mittal and Harminder Singh*, “**Synthesis of CTAB modified ferrite Composite for the efficient removal of Brilliant Green Dye,**” International Journal of Environmental Analytical Chemistry, p. 1-7, 2022, doi: [10.1080/03067319.2022.2098485](https://doi.org/10.1080/03067319.2022.2098485).
3. **Rimzim**, Jandeep Singh, Sunil Mittal and Harminder Singh*, “**Robust removal of cationic dyes by zinc ferrite composites in single and ternary dye systems,**” Inorganic Chemistry Communications, vol. 153, 2023, doi: [10.1016/j.inoche.2023.110756](https://doi.org/10.1016/j.inoche.2023.110756).
4. **Rimzim**, Rajinder Singh, Dimple Sharma, Jandeep Singh, Sunil Mittal and Harminder Singh*, “**A Sustainable Approach for Enhancing Cationic Dyes Adsorption in Single and Multiple Systems Using Novel Nano Ferrites Modified with Walnut Shell,**” Chemistry Select, vol. 9, 2024, doi: [10.1002/slct.202304810](https://doi.org/10.1002/slct.202304810).
5. **Rimzim**, Dimple Sharma, Rajinder Singh, Jandeep Singh, Sunil Mittal and Harminder Singh*, “**Fabrication of Walnut Shell Cobalt Ferrite Green Composite for the Removal of Cationic Dyes in Single and Ternary Dye System: Kinetic, Isotherm and Thermodynamic Studies,**” Heliyon (Under Review)
6. Dimple Sharma, **Rimzim Jasrotia**, Jandeep Singh and Harminder Singh*, “**Removal of cationic dyes in single as well as binary dye systems from aqueous solution using Zinc ferrite-rice husk silica composite,**” International Journal of Environmental Analytical Chemistry, p. 1-22, 2022, doi: [10.1080/03067319.2022.2140416](https://doi.org/10.1080/03067319.2022.2140416)
7. Dimple Sharma, **Rimzim Jasrotia**, Jandeep Singh, Sunil Mittal and Harminder Singh*, “**Novel Zinc Ferrite Composite with Starch and Carboxy Methyl Starch for the**

Removal of Ni (II) Ion from Aqueous Solutions,” Journal of Dispersion Science and Technology, vol. 45, no. 8, 2024, doi: 10.1080/01932691.2023.2222809.

8. Rajinder Singh, **Rimzim**, Jandeep Singh, Sunil Mittal and Harminder Singh*,
“Recyclable Magnetic Nickel Ferrite-Carboxymethyl Cellulose-Sodium Alginate Bio-Composite for Efficient Removal of Nickel Ion from water,” Journal of Dispersion Science and Technology, doi: 10.1080/01932691.2024.2320302
9. Rajinder Singh, **Rimzim**, Dimple, Jandeep Singh, Sunil Mittal and Harminder Singh*,
“Selective Removal of Cationic Dyes in Single and Multiple Dye Systems by Recyclable Spinel Ferrite-Biopolymer Based Composites,” International Journal of Environmental Analytical Chemistry (Under Review)

A Review of Bio-Waste Based Ferrite Composites for the Wastewater Treatment

Rimzim^{1,a)}, Dr. Jandeep Singh^{1,b)} and Dr. Harminder Singh^{1,c)}

Department of Chemistry, School of Chemical Engineering and Physical Sciences, Lovely Professional University, Phagwara, 144411 (India)

^{a)} rimzijasrotia1281995@gmail.com

^{b)} singhjandeep@gmail.com

^{c)} Corresponding author: harminder_env@yahoo.com

Abstract: Water that is clean and safe is a basic necessity for society's multifaceted growth and a vibrant economy. In most countries, wastewater is one of the serious concerns these days. Therefore, treatment of polluted water becomes necessary to get clean and safe water. Various methods are used to treat wastewater like coagulation, ion exchange, ozonation, adsorption etc. One such method is the usage of eco-friendly adsorbents to address the concerns of water contamination. Because the adsorption process is relatively straightforward, has become the most popular since it is cost-efficient, effective, and versatile. Nano materials are of great interest due to significant adsorption capacity. This review paper aims to bring together the disparate information of composites prepared with nano-ferrites and an extensive variety of potentially efficient adsorbents such as natural materials, industrial waste, by-products of agriculture, and so on for efficient removal of dyes and heavy metals. Furthermore, the use of bio-waste based ferrite composites is environmentally benign and have widened the horizons to tackle the problem of wastewater treatment.

Keywords: Water pollution, dyes, heavy metals, adsorption, ferrites, Nano particles, bio-waste

INTRODUCTION

We live on Earth in collaboration with our mother nature as our environment. Mother Nature provides us tremendous resources of which water is one of the precious resources that exist on Earth. Life can never be possible without water. As we all know that one-third of Earth is covered with water out of which 97% is non-portable and only 3% comes under the category of fresh water¹. According to World Health Organization (2012), approximately 780 million people worldwide have not had access to safe and clean drinking water². Water pollution worldwide emerge as the biggest problem of this century, so United Nations (2015) in their 17 Sustainable Development Goals also highlighted the issue in their Sustainable Development Goal number 6 which states “Clean water and sanitation for all” by 2030. Safe water access is essential for economic growth as well as productivity³. The continuous growth in world's population and access to improved living standard increase



Synthesis of CTAB modified ferrite composite for the efficient removal of brilliant green dye

Rimzim Jasrotia^a, Jandeep Singh^a, Sunil Mittal^b and Harminder Singh ^a

^aSchool of Chemical Engineering and Physical Science, Lovely Professional University, Phagwara, India;

^bDepartment of Environmental Science and Technology, Central University of Punjab, Bathinda, India

ABSTRACT

In the present work, magnetic nickel ferrite (NiFe₂O₄) have been synthesised using low temperature combustion method and then modified with Cetyltrimethylammonium bromide (CTAB) to form a magnetic composite. Prepared composite (CTAB-NiFe₂O₄) was used as an adsorbent for removing brilliant green dye from aqueous solution. Adsorbent was investigated by using various techniques like Fourier transform infrared spectroscopy, X-ray diffraction, field emission scanning electron microscopy, energy-dispersive spectra, thermogravimetric analysis and pH of point zero charge. Different parameters such as effect of contact time, pH, adsorbent dose and initial dye concentration were studied for the adsorption of dye. The optimum values observed were 170 minutes equilibrium time at pH 6 and adsorbent dose 0.6 g. Various adsorption kinetic models such as pseudo first-order kinetic model, pseudo second-order kinetic model and Elovich model were used to determine the nature of adsorption. Pseudo second-order kinetic model fitted better with higher R² value which indicated that the adsorption was chemical in nature. Langmuir isotherm was best fitted to experimental data for the adsorption of brilliant green dye with maximum adsorption capacity 'Q_e' 250 mg/g. It revealed that the adsorption in this study takes place on homogenous surface and follows monolayer pattern. Therefore, for the removal of Brilliant green dye from wastewater using composite (CTAB-NiFe₂O₄) can be considered as an effective adsorbent.

ARTICLE HISTORY

Received 29 May 2022

Revised 29 June 2022

Accepted 30 June 2022

KEYWORDS

Ferrites; wastewater; adsorption; Cetyltrimethylammonium bromide (CTAB); brilliant green(BG) dye

1. Introduction

Rapid economic development, population growth, increasing urbanisation, growing mega-cities, industrialisation and intensified agriculture have led to enormous environmental problems [1]. Water generally consists of hydrogen molecules having chemical formula H₂O, which is a precious natural resource [2]. One third of the world's population resides on 90% of groundwater, which is available as fresh water sources [3]. As a result of overexploitation of resources, use of hazardous substances, soil degradation and air pollution in mega-cities are increasing at alarming rates which are causing threat to ecology and living beings [4].

CONTACT Harminder Singh  harminder_env@yahoo.com

© 2022 Informa UK Limited, trading as Taylor & Francis Group



Contents lists available at ScienceDirect

Inorganic Chemistry Communications

journal homepage: www.elsevier.com/locate/inoche

Short communication

Robust removal of cationic dyes by zinc ferrite composites in single and ternary dye systems

Rimzim^a, Jandeep Singh^a, Sunil Mittal^b, Harminder Singh^{a,*}^a School of Chemical Engineering and Physical Sciences, Lovely Professional University, Phagwara, Punjab 144411, India^b Department of Environmental Science and Technology, Central University of Punjab, Bathinda, Punjab, India

ARTICLE INFO

Keywords:

Adsorption
Dyes
Pine cone
Single and Ternary Dye System
Wastewater
Zinc Ferrite

ABSTRACT

For the continuous economic growth and development of society, clean and safe water is the basic necessity. Therefore, it is necessary to treat contaminated water. Magnetic ferrite composites with bio-waste materials are less explored in the area of research, so these need to be focused. In present study, novel magnetic Zinc Ferrite Pine Cone composite was prepared and used for the efficient removal of Crystal Violet, Malachite Green and Methylene Blue (Dye) from aqueous solution in single and ternary dye system. Various characterization techniques such as FTIR (Fourier Transform Infrared Spectroscopy), XRD (X-Ray Diffraction), FE-SEM (Field Emission Scanning Electron Microscopy), EDS (Energy Dispersive Spectroscopy), TGA (Thermogravimetric Analysis) and BET (Brunauer-Emmett-Teller Analysis) are used for the structure elucidation of Zinc Ferrite and Zinc Ferrite Pine cone (Composite). Batch adsorption method was used for the removal of dyes in single and ternary dye system. Lagergren pseudo second order adsorption model fits best in the kinetic studies whereas, Langmuir adsorption isotherm showed better results with maximum adsorption capacity 76.33, 200 and 94.33 mg/g for single dye system and 9.46, 20.45 and 27.93 mg/g respectively in ternary dye system for dyes CV, MG and MB. Thermodynamic study confirmed about the spontaneous nature of adsorption process. The regeneration ability of the composite in both the systems was studied up to five cycles. So, it becomes clear that the composite (Zinc Ferrite Pine Cone) will work as best alternative for dyes removal in single and ternary dye system.

1. Introduction

Water is the basic necessity of environment and plays a key role in the smooth functioning of all ecological processes. Despite this, some regions of the population still lack safe and clean drinking water[1]. Water pollution caused by a variety of harmful chemicals emerged to be as one of the most severe global challenges[2]. Various Anthropogenic activities, increasing industries, haphazard urbanisation, sloppy natural resource management, a huge growth in population and lack of water supplies pollute the environment with a variety of hazardous substances [3,4]. Furthermore, 75% of all groundwater aquifers are contaminated. Only 3% of water is pure, with only 1% of it being pure which is available for drinking and household use[5]. Water pollution can be mainly categorized as Point and non-point sources. The first category comprises of contaminants that emits from a single source such as industrial emissions in water bodies and the second refers to contaminants having different emission sources[6]. Water contamination in general is affected by a wide range of sources but the most common among all is

Human activities[5,7]. Plasticizers, insecticides, polychlorinated biphenyls, toxic metals, dyes[8] etc. are some of the common pollutants found in wastewater as reported in various research studies[9]. Among the various contaminants, dyes are known to be the most toxic due to their ecological impacts as these pollutants show mutagenic[10] and carcinogenic effects on human health[5]. Dyes are often used in textiles [11], paint, pigment [12] and a variety of other purposes for centuries [13]. The textile dyeing sector is well known for the world's largest water-polluting as well as chemically intensive sector which affects both flora and fauna[14]. Around 100,000 distinct dye kinds are commercially available[15]. Dyes are synthesized at a rate of 1.6 million tonnes every year to meet the increasing demands, out of which 10 to 15% amount of this is disposed as wastewater. As a consequence, dyes are serious water contaminants[16]. Dyes released into aquatic habitats can have disastrous effects by lowering light penetration into water, disrupting the photosynthetic efficiency of aquatic flora and ultimately results in Eutrophication[17]. On the basis of structure, applications and origin, dyes are divided into different categories such as Reactive Dye,

* Corresponding author.

E-mail address: harminder_env@yahoo.com (H. Singh).<https://doi.org/10.1016/j.inoche.2023.110756>

Received 15 February 2023; Received in revised form 12 April 2023; Accepted 25 April 2023

Available online 2 May 2023

1387-7003/© 2023 Elsevier B.V. All rights reserved.

A Sustainable Approach for Enhancing Cationic Dyes Adsorption in Single and Multiple Systems using Novel Nano Ferrites Modified with Walnut Shell

Rimzim Jasrotia,^[a] Rajinder Singh,^[a] Dimple Sharma,^[a] Jandeep Singh,^[a] Sunil Mittal,^[b] and Harminder Singh^{*[a]}

Walnut shell has been used in various experimental studies for different dyes removal, but it is exciting to study the adsorption behaviour of bio-waste (walnut shell) in combination with spinel zinc ferrite which resulted in the formation of a novel material having magnetic properties and help in easy separation after the wastewater treatment. Novel magnetic walnut shell zinc ferrite (WSZF) composite has been synthesized and used to remove Malachite Green and Methylene Blue from aqueous solution in single and binary dye systems. Different techniques have been used to characterize the composite such as Fourier Transform Infrared Spectroscopy, X-Ray Diffraction, Field Emission Scanning Electron Microscopy, Energy Dispersive Spectroscopy, Thermogravimetric Analysis and pH-zpc. Adsorption of dyes were studied to see the effect of time, pH,

adsorbent dose, dye concentration and temperature. The Lagergren pseudo second order model fitted well among various kinetic models employed. Langmuir adsorption isotherm best fitted with maximum adsorption capacities of 86.20 and 169.5 mg/g in single dye and 23.92 and 18 mg/g respectively in binary dye system for Malachite Green and Methylene Blue. Process was spontaneous and ΔH° were found positive, confirmed endothermic process of adsorption. The composite's regeneration capacity was studied for five cycles and at the end of five cycle the efficiency of the material was found to be around 80% for both single as well as binary dye systems. It is concluded that the chosen WSZF will be the optimum solution for cationic dyes removal.

1. Introduction

Rapid increase in population growth, various industrial activities, climatic variations etc. leads to the deterioration of available fresh water resources in the whole world.^[1] Industries such as paint, plastic, leather, food processing, textile, pharmaceutical industries etc. are using dyes as colorants in their production process.^[2] Dyes are used by industries in large quantities and discharged directly into water bodies without their treatment.^[3] The discharge of harmful pollutants into water bodies can cause mutagenicity, embryo toxicity and carcinogenicity.^[4] The dyes are of basically synthetic origin which possess complex molecular structure, thus shows more stability and difficulty in biodegradation.^[1] The dyes can be categorized as cationic, anionic and non-ionic dyes.^[5] Approximately ten thousand types and about 7×10^5 tons of different dyes are produced by these industries annually.^[6] Even at very low concentration, dyes are easily visible to naked eye. Dyes contain harmful components which are toxic in nature that can damage aquatic life, human life and may also results in the

disruption of ecological balance. Therefore, presence of dyes in the water body beyond maximum permissible limits affects the quality of water and also results in the inhibition of sunlight penetration which ultimately affects the photosynthetic activity.

Different treatment methods available for the degradation of dyes from wastewater depending upon wastewater source are as- Advanced Oxidation process, Coagulation/flocculation, Adsorption, Membrane filtration, Photocatalytic degradation etc.^[7]

Adsorption techniques are effective practices that are extensively used in the industrial sector to remediate organic as well as inorganic pollutants due to their low cost, ease of operation, minimum sludge creation, regeneration ability and other benefits.^[8-11]

Nanotechnology has emerged as an excellent alternative to wastewater treatment. Because the nanoparticles show numerous advantages such as high active surface sites, increased strength, short density and so on.^[12] The size of nanoparticles ranges from diameter 1–100 nm. There are different materials which can be used as nanoparticles. In this experimental study, ferrites were chosen as efficient nano materials. Ferrites represent a type of magnetic nanoparticles that are derived from various metal oxides as well as hematite and magnetite.^[13] Ferrites have exceptional electrical and magnetic characteristics.^[14] According to literature studies, spinel ferrites are widely used for wastewater treatment. However, in some cases magnetic nanoparticles show certain disadvantages such as limited efficiency, short shelf life.^[15-17] To overcome these limitation, different materials are used to coat nano particles for

[a] R. Jasrotia, R. Singh, D. Sharma, J. Singh, H. Singh
School of Chemical Engineering and Physical Sciences, Lovely Professional University, Phagwara, Punjab, 144411, India
E-mail: harminder_env@yahoo.com

[b] S. Mittal
Department of Environmental Science and Technology, Central University of Punjab, Bathinda, Punjab, India

Supporting information for this article is available on the WWW under <https://doi.org/10.1002/slct.202304810>



Removal of cationic dyes in single as well as binary dye systems from aqueous solution using Zinc ferrite-rice husk silica composite

Dimple Sharma, Rimzim Jasrotia, Jandeep Singh and Harminder Singh 

School of Chemical Engineering and Physical Sciences, Lovely Professional University, Phagwara, India

ABSTRACT

Magnetic green adsorbents have been gaining importance in wastewater treatment field due to their versatile properties. In this study, a novel magnetic green adsorbent Zinc Ferrite-Rice Husk Silica (ZFN-RHS) composite has been prepared by extracting silica from rice husk. ZFN-RHS is characterised using variety of techniques which includes FESEM, FT-IR, XRD, BET, pH_{zpc} and EDS. Effect of various parameters like time, concentration, pH, adsorbent amount and temperature was assessed using the batch adsorption method to remove cationic dyes (Methylene Blue and Crystal Violet) from aqueous solution in single as well as binary dye solutions. Results showed that Lagergren pseudo-second order kinetic model best fitted with the adsorption data indicating chemisorption. In adsorption isotherm study, Freundlich as well as Langmuir adsorption isotherms fitted better than other isotherms. Maximum adsorption capacities for removal of CV and MB dyes in this study have been found to be 138.8 and 84.8 mg/g respectively. From the positive values of ΔH° , it has been observed that the process of removal of MB and CV from aqueous solution using ZFN-RHS was endothermic in nature and the negative ΔG° values confirmed the spontaneous nature of the process. Regeneration studies were also conducted with significant outcomes in five cycles. The research study revealed that ZFN-RHS can be used as an adsorbent to remove other cationic dyes also.

ARTICLE HISTORY

Received 25 August 2022
Accepted 18 October 2022

KEYWORDS

Binary dye system; dyes adsorption; regeneration; rice husk silica (RHS); single system; Zinc ferrite (ZFN)

1. Introduction

In the modern world, the biggest problem is deterioration of drinking water quality, which is a global problem. Textile industries are using dyes rapidly but are not concerned about their proper disposal methods. A wide range of health problems occurs as a result of dyes being disposed of without prior treatment. It also adversely affects water quality. Various diseases caused by dyes are increased heart rate, vomiting, jaundice, cyanosis, decreased spermatogenesis, altered genes, etc [1–8].

Dye removal can be accomplished with a variety of techniques like ion exchange, ozonation, membrane filtration, coagulation and flocculation, desalination, chemical dehydration, anaerobic–aerobic methods, etc [9–14]. These methods have their own advantages and disadvantages like – Ozonation method is suitable for azo dye removal

CONTACT Harminder Singh  harminder_env@yahoo.com

© 2022 Informa UK Limited, trading as Taylor & Francis Group



Novel Zinc ferrite composite with starch and carboxy methyl starch from biowaste precursor for the removal of Ni (II) ion from aqueous solutions

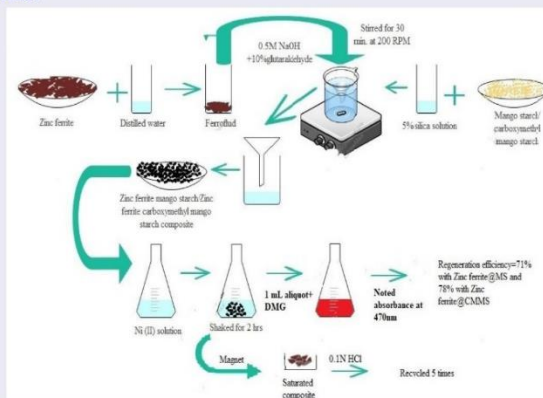
Dimple Sharma^a, Rimzim Jasrotia^a, Jandeep Singh^a, Sunil Mittal^b, and Harminder Singh^a

^aSchool of Chemical Engineering and Physical Sciences, Lovely Professional University, Phagwara, Punjab, India; ^bDepartment of Environmental Science and Technology, Central University of Punjab, Bathinda, Punjab, India

ABSTRACT

In the present work, Zinc ferrite composites with Mango starch (MS) and carboxymethyl mango starch (CMMS) were synthesized for the removal of Ni (II) ions from aqueous solutions. Composites prepared were characterized by Fourier Transform Infrared (FTIR) Spectroscopy, X-Ray Diffraction (XRD) analysis, pH of point zero charge (pH_{zpc}), Scanning Electron Microscopy (SEM), and BET. Batch adsorption technique was used to study effect of various parameters such as pH, adsorbent dose, contact time, concentration, and temperature for removal of Ni (II) ions from aqueous solutions. The optimum time, pH, adsorbent dose and temperature required for ZFN@MS and ZFN@CMMS in this study was 110 min., 7 & 8, 0.1 g and 308 K, respectively. Out of various adsorption isotherms, Freundlich isotherm model fitted best with adsorption data. Maximum adsorption capacity for removal of Ni (II) were found to be 65.3 and 208.3 mg/g, respectively by using Zinc ferrite@MS and Zinc ferrite@CMMS adsorbents. Lagergren Pseudo second order model best fitted with results which indicated that the process of adsorption was chemical in nature. The value of adsorption energy for ZFN@MS was 50 kJ/mol and for ZFN@CMMS, it was 31.62 kJ/mol. Thermodynamic study revealed that process was endothermic and non-spontaneous in nature. Regeneration studies were conducted for five cycles where Zinc ferrite@MS showed 71% regeneration efficiency and Zinc ferrite@CMMS showed 78% regeneration efficiency for nickel ion removal from aqueous solution.

GRAPHICAL ABSTRACT



ARTICLE HISTORY

Received 28 March 2023
Accepted 1 June 2023



KEYWORDS

Adsorption; bio-waste;
ferrite; waste water; nickel;
regeneration

Introduction

With increasing population, the demand of utilization of natural resources is also increasing day by day. Water is the basic amenity of every individual surviving on earth and is used for various purposes. Industries, urbanization, agriculture, etc. are the main sources of water pollution. By 2025,

half of the population of earth will face water crisis.^[1] The problem of water pollution caused by agriculture is mainly because of the use of different insecticides, herbicides, fertilizers, etc. whereas textile, electroplating, chemical industries, etc. also contribute to water pollution.^[1] Different inorganic and organic pollutants are present in effluents discharged from various industries. Heavy metals, which are inorganic


CONTACT Harminder Singh  harminder_env@yahoo.com  School of Chemical Engineering and Physical Sciences, Lovely Professional University, Phagwara, Punjab 144411, India.

 Supplemental data for this article can be accessed online at <http://dx.doi.org/10.1080/01932691.2023.2222809>

© 2023 Taylor & Francis Group, LLC



Novel magnetic metal ferrite-mango starch composite for the removal of dyes in single and ternary dye mixtures from aqueous solutions: kinetic and thermodynamic studies

Dimple Sharma^a, Rimzim Jasrotia^a, Rajinder Singh^a, Jandeep Singh^a, Sunil Mittal^b and Harminder Singh ^a

^aSchool of Chemical Engineering and Physical Sciences, Lovely Professional University, Phagwara, India;

^bDepartment of Environmental Science and Technology, Central University of Punjab, Bathinda, India

ABSTRACT

Magnetic metal ferrites attached to biowastes are proven to be promising adsorbents for the removal of dyes from water. Magnetic composites with biopolymers are gaining interest in the field of treatment of wastewater because of their selective nature, recyclability, low cost and environmental compatibility. In this work, Zinc ferrite composite with starch, extracted from mango seed kernel (ZFNMS) was synthesised. Characterisation techniques, such as FTIR, XRD, FESEM, BET, TGA and pHzpc, were used for the structural analysis of ZFNMS. ZFNMS was used to remove Methylene blue, Crystal violet and Brilliant green dyes in single and multiple (ternary) dye systems. The kinetics of adsorption by ZFNMS revealed that pseudo-second-order of kinetics was most appropriate for this study. Maximum adsorption capacities using ZFNMS for CV, BG and MB dyes were 142.9, 101.2 and 105.8 mg/g, respectively. The values of adsorption energies using ZFNMS were 200.5, 494.3 and 183.6 KJ/mol for CV, BG and MB dyes, respectively. Thermodynamic data revealed the spontaneous nature of the adsorption of dyes by ZFNMS and it was found that chemical adsorption was taking place in the present study. Regeneration of the adsorbent was done for successive five cycles and showed significant results. Thus ZFNMS is an ideal adsorbent for cationic dyes removal from water.

ARTICLE HISTORY

Received 25 June 2024
Accepted 18 September 2024

KEYWORDS

Ternary dyes; spinel ferrites; adsorption; kinetics; Langmuir



1. Introduction

With the increase in the population, industrialisation also increased proportionately, thereby increasing the use of chemicals, which cause pollution and associated effects [1]. The scarcity of clean water is the main problem which our society is facing today. Dyes have been used in various industries, such as textile industries, printing presses, drugs, etc. These used dyes have been discarded into water bodies before any treatment [2]. Their direct disposal into water bodies causes various mutagenic and carcinogenic diseases. So, there is a challenge before us to develop a sustainable method for the treatment of dye-containing water before its discharge into water bodies. Because most dyes cause various diseases in humans, their treatment before discarding them into water becomes necessary.

CONTACT Harminder Singh  harminder_env@yahoo.com  School of Chemical Engineering and Physical Sciences, Lovely Professional University, Phagwara, 144411, Punjab, India

© 2024 Indian Institute of Chemical Engineers



Recyclable magnetic nickel ferrite–carboxymethyl cellulose–sodium alginate bio-composite for efficient removal of nickel ion from water

Rajinder Singh^a, Rimzim Jasrotia^a, Dimple Sharma^a, Jandeep Singh^a, Sunil Mittal^b, and Harminder Singh^a

^aSchool of Chemical Engineering and Physical Sciences, Lovely Professional University, Phagwara, India; ^bDepartment of Environmental Science and Technology, Central University of Punjab, Bathinda, India

ABSTRACT

In waste water treatment, magnetic bio-composites are frequently investigated as an adsorbent recently due to their great capacity for adsorption and affordability. In this current work, an attempt has been made to develop spinel nickel ferrite–carboxymethyl cellulose (NiFCMC) composite and modified its surface by alginate polymer to form NiFCMC–Alg composite. Several techniques were utilized to characterize these adsorbents including Fourier transform infrared spectroscopy, x-ray diffraction, field emission scanning electron microscopy, energy-dispersive spectra, thermogravimetric analysis, vibration sample magnetometry and pH of point zero charge. These adsorbents were explored to check their potentiality to remove Ni (II) ions in aqueous medium on various parameters such as contact time, initial metal ion concentration, pH, adsorbent dose and temperature. The optimum time for establishment of equilibrium was 180 minutes at pH 8 with adsorbent dose of 0.1 g. Results of kinetic studies revealed that the best fit for the metal ion adsorption data was the Lagergren pseudo-second-order mode indicating the chemisorption nature. Likewise, the Langmuir isotherm model also showed good agreement with adsorption equilibrium data with maximum adsorption capacities 47.84 ± 2.39 and 60.24 ± 3.01 mg/g for NiFCMC and NiFCMC–Alg respectively. The calculated adsorption thermodynamic parameters confirmed the spontaneous nature of adsorption process. The regeneration efficiency of both adsorbents was studied for five cycles and showed significant results. This study has shown that NiFCMC and NiFCMC–Alg can be a good substitute for removing Ni (II) ions in aqueous medium.

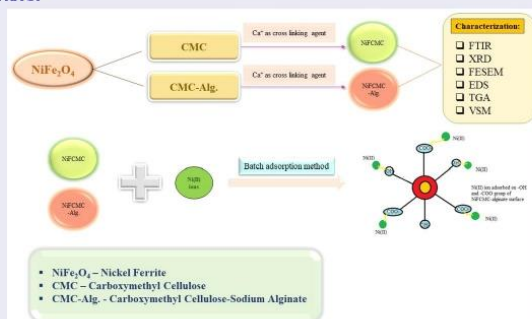
ARTICLE HISTORY

Received 17 October 2023
Accepted 13 February 2024

KEYWORDS

Spinel ferrite;
carboxymethyl cellulose;
alginate; surface
modification; adsorption;
regeneration

GRAPHICAL ABSTRACT



1. Introduction

Water pollution is one of the major environmental problems globally with the rapid industrialization, urbanization and intensified agricultural practices that need much attention of the researchers worldwide. The primary reason behind water contamination is direct disposal of effluents without treatment into water bodies by textile, dyes and tanning

industries, painting, mining, petrochemical and fertilizer/pesticides industries.^[1,2] Heavy metals are especially harmful and tend to accumulate in human bodies and pose severe health issues. Therefore, their removal from the waste water is necessary. Different traditional approaches and methodologies such as coagulation, filtration, precipitation, ion exchange, solvent extraction, reverse osmosis, electrochemical treatment and evaporation. etc. have been explored for

CONTACT Harminder Singh harminder_env@yahoo.com School of Chemical Engineering and Physical Sciences, Lovely Professional University, Phagwara, Punjab 144411, India.

Supplemental data for this article can be accessed online at <https://doi.org/10.1080/01932691.2024.2320302>.

© 2024 Taylor & Francis Group, LLC

DIVISION OF RESEARCH AND DEVELOPMENT

[Under the Aegis of Lovely Professional University, Jalandhar-Delhi G.T. Road, Phagwara (Punjab)]

Certificate No.240211

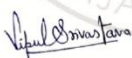
Certificate of Participation

This is to certify that **Ms. Rimzim** of **Lovely Professional University, Phagwara, Punjab, India** has presented paper on **A Review of Bio Waste Based Ferrite Composites for the Wastewater Treatment** in the **International Conference on Materials for Emerging Technologies (ICMET-21)** held on February 18-19, 2022, organized by Department of Research Impact and Outcome, Division of Research and Development, Lovely Professional University, Punjab.

Date of Issue: 16-03-2022
Place: Phagwara (Punjab), India



Prepared by
(Administrative Officer-Records)



Dr. Vipul Srivastava
Convener
(ICMET-21)



Dr. Manish Vyas
Organizing Secretary
(ICMET-21)



Dr. Chander Prakash
Co-Chairperson
(ICMET-21)



Celebrating 60 Years of Academic Excellence

Under Diamond Jubilee Celebration
International Conference



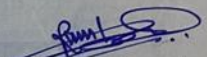
on


Molecules and Materials Technology (MMT-2023)

21st - 22nd April, 2023

Certificate of Presentation

This is to certify that Dr./Mr./Ms. RIMZIM JASROTIA
of LOVELY PROFESSIONAL UNIVERSITY has Presented POSTER
in International Conference on Molecules and Materials Technology (MMT-2023)
organized by, Department of Chemistry National Institute of Technology, Kurukshetra held in
21st - 22nd April, 2023.


Conference Secretary
MMT-2023


Chairman
MMT-2023



**LOVELY
PROFESSIONAL
UNIVERSITY**

Transforming Education Transforming India



Certificate No. 263458

Certificate of Participation

This is to certify that **Dr./Mr./Ms. Rimzim** of Lovely Professional University has given oral presentation on **Dye Containing Wastewater Treatment Using Various Bio-Waste Based Ferrite Composites** in the 4th International Conference on "Recent Advances in Fundamental and Applied Sciences" (RAFAS 2023) held on March 24-25, 2023, organized by School of Chemical Engineering and Physical Sciences, Lovely Faculty of Technology and Sciences, Lovely Professional University, Punjab.

Date of Issue: 12-04-2023
Place: Phagwara (Punjab), India

Prepared by
(Administrative Officer-Records)

Organizing Secretary
(RAFAS 2023)

Convener
(RAFAS 2023)

STUTI

This is to certify that

Ms. Rimzim

*has successfully completed the
workshop*

**On Spectroscopic, Chromatographic,
Bioanalytical & Imaging Techniques
(28th November - 04th December, 2022)**

conducted by

Central University Of Punjab

in association with


Amity University

under the auspices of

Department of Science and Technology(DST)
Government of India

under

**Synergistic Training Program Utilizing Scientific
and Technological Infrastructure (STUTI)**


Prof. Ramkrishna Wusirika
Dean Incharge Academics
Central University of Punjab


Prof. Anjana Munshi
Director R&D
Central University of Punjab


Dr. Nitin Batra
CEO,
Amity Institute of Training
& Development


Dr. W Selvamurthy
President, ASTIF
Chancellor,
Amity University Chattisgarh



CERTIFICATE OF PARTICIPATION

This acknowledges that

RIMZIM

from LOVELY PROFESSIONAL UNIVERSITY, PHAGWARA, JALANDHAR

has attended DST-PURSE sponsored three-day workshop & hands-on training on "*Spectroscopy, Separation, and Surface Characterization Techniques*", organized by Department of Chemistry and Biochemistry (DCBC), during March 04-06, 2024 at Thapar Institute of Engineering and Technology (TIET), Patiala, Punjab

Prof. Amjad Ali
Organizer of Workshop
TIET, Patiala, Punjab

Prof. Soumen Basu
Organizer of Workshop
TIET, Patiala, Punjab

Prof. Manmohan Chhiber
Head DCBC
TIET Patiala, Punjab